A Fundamental Study on Steam and Air Fluidized Bed Drying of Victorian Brown Coal

David Kee William Stokie

B.Eng. (Chemical Engineering, Honours)

A thesis submitted in fulfilment of the requirements for the degree of

Doctor of Philosophy

Department of Chemical Engineering

Monash University

Australia

2016

Declaration

This thesis contains no material which has been accepted for the award of any other degree or diploma at any university or equivalent institution and that, to the best of my knowledge and belief, this thesis contains no material previously published or written by another person, except where due reference is made in the text of the thesis.

_____

David Stokie

Department of Chemical Engineering

Monash University

2016

Acknowledgements

First and foremost, I would like to thank my primary supervisor Professor Sankar Bhattacharya for his knowledge and guidance, without him none of this would be possible.

I would also like to thank:

My other supervisors and academics – Professor Klaus Hein, Dr Meng Wai Woo, Dr Anthony Auxilio, Dr Wei Lit Choo and Dr Maggie Chen – for always being available with insight and a helping hand.

My group members – Bayzid Kazi, Kawnish Kirtania, Joanne Tanner, Adam Rady, Sunaina Dayal, and Sharmen Rajendran – for innumerable pieces of advice and help, while helping me to stay happy and sane.

I would like to acknowledge the Australian Department of Resources, Energy and Tourism Joint Coordination Group (JCG) on Coal, the Australian China Strategic Research Fund (ACSRF), the European Commission / Research Fund for Coal and Steel (collaborative project DRYLIG, Grant Number RFCR-CT-2014-00009) and Australian Research Council LIEF grant LE120100141 for funding this research.

The Department of Chemical Engineering at Monash University for the opportunity to pursue a PhD. Within the chemical engineering department I would like to thank Lilyanne Price, Jill Crisfield, Ronald Graham, Harry Bouwmeester, Kim Phu, Garry Thunder, Gamini Ganegoda, Ross Ellingham and Martin Watkins for their continual help.

Dr. Arash Tahmasebi, Ms. Yanna Han and Professor Jianglong Yu from the University of Science and Technology Liaoning (USTL) for help in both coal characterisation and data analysis of the chemical characteristics.

My friends and family patiently hearing about coal drying and the joys of student life over the last four years, and especially my parents Mr. Geoffrey Stokie and Mrs. Voon Stokie for graciously volunteering to proof read this thesis.

Abstract

Almost 50% of the world's coal resources are low rank coals. Efficiency for low rank coal utilization is reduced by high moisture contents and can decrease the conventional power plant efficiency by up to 9%. Drying coal is an effective way of increasing the efficiency of low rank coal combustion for power generation. A drying technology for use with Victorian brown coal is steam fluidized bed drying. However fundamental drying data is required for scaling up steam fluidized bed drying to a commercial scale. This study generates the data and also provides an understanding of the kinetics on fluidized bed drying in general, and steam fluidized bed drying in particular.

Water in Victorian brown coal consists mainly of non-freezable and bulk water whereas similar coals such as Chinese lignite only contains bound and non-freezable water. The structure of bound water in Chinese Shenhua lignite also differs from that in Victorian brown coals –Loy Yang, Yallourn and Morwell–, displaying two separate freezing temperatures (-36°C and -48°C) compared to Victorian brown coal's one (-47°C). When re-introducing water to dried coal, non-freezable water returns to previous levels, while the bound water is reduced. The difference in re-wetted coal-water interactions affects the energy requirements for re-wetted coals, and can impact agglomeration and slurry processes when water is added to coal. Observing different size fractions, smaller fractions exhibit lower bulk water mass, however the non-freezable and bound water mass remains relatively unchanged.

The kinetics of both air and steam fluidized bed drying of Victorian brown coal show that increasing the fluidization velocity and bed temperature or decreasing the particle size results in a lower drying time. This trend occurs regardless of the fluidization medium, with drying ratio's between drying temperatures and fluidization velocities remaining consistent between air and steam fluidization mediums. Through experiments in a 1 kg bed a drying time of 30 minutes was established to completely dry the coal and represents a practical drying time closer to commercial driers. To reconcile laboratory and larger drying kinetics a scaling co-efficient of 1.33 has been created in conjunction with a modified Page model. This model accurately describes the scaling of drying in a small steam fluidized bed to a large steam fluidized bed.

Analysis of the chemical characteristics of dried coal indicates that the oxygen functional groups change with temperature. Synchrotron infrared experiments of single particle drying in Nitrogen indicates that functional group breakdown of Victorian brown coals occur

between 140 and 250°C, while Chinese lignite's begin to break down at 160°C. The loss of functional groups was also dependent on the residence time. At 130°C longer residence times show Chinese Shenhua lignite showing faster and different functional group loss than Yallourn brown coal. At 170°C a drop in COOH dimers is seen after 15 minutes, with additional functional group loss occurring at 25 minutes. These results show Shenhua lignite is more temperature sensitive and should be dried at temperatures below 200°C to avoid major functional group loss.

During steam fluidized bed drying particle breakage occurs, with a 100 μm drop in average particle diameter observed. However a 100 μm average particle size drop occurs regardless of drying medium or method and is attributed to the transition from bulk/bound water to non-freezable water and not fluidization. At 30 and 60 minutes residence time, air fluidization decreases the average particle diameter by an additional 75 μm, while steam fluidization has no additional effect.

Moisture re-adsorption of Victorian brown coal shows steam fluidized bed dried coal re-adsorbs up to 2% less moisture than air fluidized bed dried coals (9.6% vs. 7.6% for Loy Yang brown coal), and has been attributed to the change in oxygen functional groups.

Unlike previously developed engineering models, a single particle model for steam drying has been developed for implementation into computational fluid dynamics (CFD) simulations. Using a lumped, master curve approach, a model has been developed to describe the surface temperature and moisture content of a coal particle during drying. This provided comparable results to other drying models in the literature, with a significantly simpler calculation method. The form of the equations allows for modelling of local dryer conditions and has practical applications in drier design and optimization.

The characteristics of the dried coal were investigated through the combustion and gasification reactivity along with the ignition point analysis. The change in drying temperature and fluidization medium make no observable impact on either the reactivity or ignition point. This proves steam fluidized bed drying maintains similar combustion and gasification properties of dried coal when compared to other forms of drying.

This thesis characterised the steam fluidized bed drying process, allowing for an accurate prediction of the output coal quality, from the moisture content to the resultant coal properties to the coals usability in combustion and gasification processes.

Publications

Journal Publications

David Stokie, Meng Wai Woo, and Sankar Bhattacharya, "Comparison of Steam and Air Fluidized Bed Drying Characteristics in Victorian Low Rank Coals", *Energy and Fuels*, 2013, 27(11), pp6598-6606

David Stokie, Meng Wai Woo, Sankar Bhattacharya "Attrition of Victorian Brown Coal in a Fluidized Bed Drier" *Drying Technology* DOI: 10.1080/07373937.2015.1080723

Arash Tahmasebi, Jianglong Yu, Yanna Han, Fengkui Yin, Sankar Bhattacharya, and David Stokie "Study of Chemical Structure Changes of Chinese Lignite upon Drying in Superheated Steam, Microwave, and Hot Air", *Energy and Fuels*, 2012, 26 (6), pp 3651–3660

Meng Wai Woo, David Stokie, Wei Lit Choo, and Sankar Bhattacharya "Master curve behaviour in superheated steam drying of small porous particles" *Applied Thermal Engineering*, 2012, 52 (2), pp 460-467

Publications Submitted

David Stokie, Srikanth Srivatsa, Sankar Bhattacharya "The Effect of Drying and Pyrolysis on Surface Function Group Evolution in Brown Coal and Chinese Lignite using Synchrotron In-situ Infrared Analysis" *Submitted to Spectrochimica Acta*

David Stokie, Arash Tahmasebi, Meng Wai Woo, Wei Lit Choo, Sankar Bhattacharya "Comparison of lignite-water interactions between Victorian (Australia) brown coals and Shenyang (China) lignites" *Drying Technology*

In Preparation

David Stokie and Sankar Bhattacharya "Coal Drying using Low Rank Coals – Current status, Research and Development Needs for Large Scale Fluidised Bed Drying

Conference Publications

D. Stokie, J. Yu, A. Auxilio, S. Bhattacharya, Coal Drying and Dewatering for power generation – Current Status, Research and Development Needs, *International Conference on Coal Science and Technology*, Oviedo, Spain 2011

D. Stokie, K. Hein, A. Rady, S. Bhattacharya, The Kinetics of Steam Fluidized Bed Drying of Victorian Brown Coal *The 37th International Technical Conference on Clean Coal & Fuel Systems Clearwater*, Florida, USA, 2012

D. Stokie, Steam Fluidized Bed Drying (SFBD) of Victorian Brown Coal, *1st Annual Australia-China Workshop on Novel Carbon Capture Technologies*, Anshan, China, 2012

D. Stokie, A. Tahmasebi, S. Bhattacharya, Steam Fluidized Bed Drying of Low Rank Coal, *The AIE Postgraduate Student Energy Awards*, Melbourne, Australia, 2012

D. Stokie, S. Bhattacharya, J. Tanner, Physical and Chemical Properties of Steam Fluidized Bed Dried Coal, *The 38th International Technical Conference on Clean Coal & Fuel Systems Clearwater*, Florida, USA, 2013, pp. 11

Abbreviations

Abbreviation	Full Name
AFBD	Air Fluidized Bed Drying
Ar	Archimedes Number
AUS	Australia
CCS	Carbon Capture and Storage
CHN	China
db	Dry basis
DME	Dimethyl Ether
DSC	Differential Scanning Calorimetry
FC	Fixed Carbon
FT-IR	Fourier Transfer Infra-Red spectroscopy
GCV	Gross Calorific Value
GER	Germany
GRE	Great River Energy
INA	Indonesia
LFES	Lignite Fuel Enhancement System
LY	Loy Yang
MTE	Mechanical Thermal Expression
MW	Morwell
NCV	Net Calorific Value
NMR	Nuclear Magnetic Resonance
PFBD	Pressurised Fluidised Bed Drying
Re	Reynolds Number
SFBD	Steam Fluidized Bed Drying
TGA	Thermo-gravimetric Analyser
UBC	Upgraded Brown Coal
USA	United States of America
VM	Volatile Matter
wb	Wet basis
WTA	Wirbelschicht-Trocknung mit interner Abwärmenutzung (fluidised bed drying with internal waste heat utilization)
YL	Yallourn

Nomenclature

Chapter 2 – Literature Review

Nomenclature	
m	Change in mass per second (kg/s)
ΔH	Change in enthalpy (J/g)
R_o	Radius (m)
Subscript	
vap	Vaporization
avg	Average
const	Constant
in	Initial

Due to the large number of formulas within the literature review modelling section, a separate nomenclature list can be found in Appendix A1.

Chapter 4 – Water in Coal

Nomenclature	
m	Mass (g)
h	Enthalpy (J/g)
MC	Moisture content $(\%)$
Subscript	
c	Coal
bu	Bulk
bo	Bound
NF	Non Freezable
f	Fusion

Chapter 5 – Drying Kinetics

Nomenclature	
Ar	Archimedes number $Ar = g.d^3.\rho_l(\rho - \rho_l)$
d	Diameter (m)
ρ	Density (kg/m^3)
μ	Viscosity $(kg/m\ s)$
g	Gravity (m/s^2)
u	Velocity (m/s)
Re	Reynolds Number $Re = \rho.v.L/\mu$
M	Moisture content
χ^2	Chi-square
X,k,a,c,b,L,g,n	Model variables used in specific thin layer equations
t	Time (s)
Subscript	

s	Solid
gas	Gas
mf	Minimum fluidization
p	Particle
e	equilibrium
R	Ratio
0	Initial

Chapter 6 – Chemical Characteristics

Nomenclature	
C	Carbon
H	Hydrogen
O	Oxygen
N	Nitrogen
S	Sulphur
K	Potassium
Br	Bromide
Subscript	
ar	Aromatic
al	Aliphatic

Chapter 7 – Physical Characteristics

Nomenclature	
P_d	Cumulative percentage distribution
A_1, A_2, x_o, p	Model variables used in specific experimentally defined equations
d	Particle diameter (μm)
d(0.1), d(0.5), d(0.9)	Diameter at 10%, 50% and 90% of the total sample volume distribution (μm)

Chapter 9 – Modelling

Nomenclature	
m	Mass (kg)
C_p	Specific heat capacity $(J/kg$ ℃)
dT/dt	Rate of change of particle temperature $(℃/s)$
A	Surface area (m^2)
h	Heat transfer co-efficient $(W/m^2$ ℃)
T	Temperature (℃)
X	Dry basis moisture content (kg moisture/kg dry solid)

x	Mass fraction (kg moisture/kg total)
k	Thermal conductivity (W/m ℃)
R	Radius (m)
d	Diameter (m)
ρ	Density (kg/m^3)
u	Particle steam relative velocity (m/s)
μ	Viscosity ($kg/m\ s$)
dm/dt	Rate of change of particle mass (kg/s)
Re	Reynolds number $Re = \rho.v.L/\mu$
Pr	Prandtl number $Pr = C_p.\mu/k$
Nu	Nusselt number $Nu = h.L/k$
ψ	Surface temperature multiplier
ϕ	Falling rate delineator
ΔH	Latent heat (J/kg)
	Subscript
p	Particle
a	Atmosphere
s	Steam
sat	Saturated
n	Normalised
max	Maximum
min	Minimum
evap	Evaporation
ini	Initial
eq	Equilibrium
w	Water
l	Liquid
c	Ceramic

Chapter 10 – Combustion, Gasification and Ignition Point Analysis

	Nomenclature
R_T	Reactivity (*%/min*)
w	Initial weight (*mg*)
dw/dt	Rate of weight loss (*mg/min*)
T	Temperature
	Subscript
inst	Instantaneous
max	Maximum
i	Ignition

Contents

List of Figures

List of Tables

Chapter 1. Introduction

As of 2011, 28.8% of the world's primary energy supply was from coal or peat [1]. Coal types have been defined in many ways. A definition introduced by the Economic Commission for Europe, having low rank coals classified with the Gross Calorific Value, calculated on an ash and moisture free basis, of less than 24 MJ/kg and a vitrinite mean random reflectance percentage (in oil) of less than 0.6%. This new classification system no longer uses the term brown coal due to the lack of consistent definitions and parameters [2]. However, the term 'brown coal' is currently still in use with a broader definition, comprising the categories of subbituminous coals (with a calorific value between 17.4 MJ/kg and 23.9 MJ/kg, and greater than 31% volatile content on a moisture and ash free basis) and lignite coals (with a calorific value less than 17.4 MJ/kg and greater than 31% volatile content on a moisture and ash free basis) [3]. **Figure 1.1** identifies the major countries using low rank coals, and indicates the range of moisture content, ash content and calorific values of the typically used fuels for each.

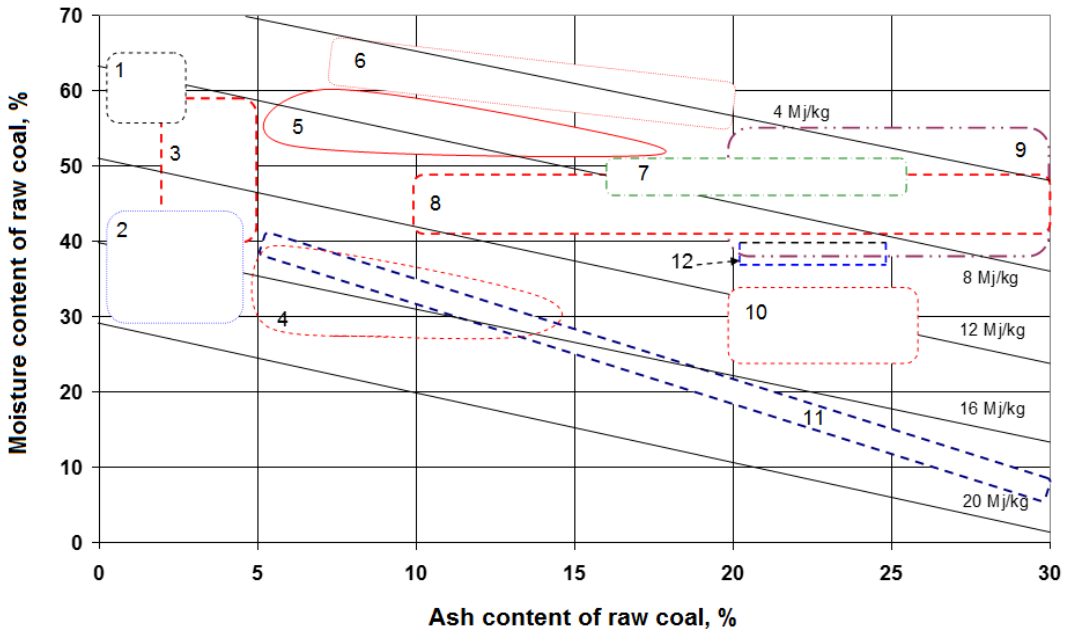

Figure 1.1 High-ash and/or high-moisture containing coals– their location, and calorific values (LHV, MJ/kg); country labels as follows: [4]

1: Australia; 2: Indonesia; 3: India; 4: USA (Texas, North Dakota); 5: Germany; 6: Greece; 7: Spain; 8: Poland; 9: Czech Republic; 10: China; 11: Turkey; 12: Romania. Compiled from various sources

Coal drying is essential for improving the efficiency of existing coal fired power plants, and when using high moisture coals is a significant factor in the approval and viability of new

coal fired power plants. The maximum efficiency of a coal combustion power station drops by up to 4 percentage points when the fuel's initial moisture content increases from 10% and 40%. At moisture contents approaching 60% a 9% percentage point efficiency drop can be assumed [4]. This is shown graphically in **Figure 1.2**. Estimates show that 20 – 25% of the fuel's heat of combustion is lost in order to remove the inherent moisture from brown coal [5-8]. With low rank coal constituting approximately half of the world's coal resources the impact of drying at this stage cannot be overlooked [9].

Recent developments in the use of low rank coal has resulted in a diversification in coal treatment and use, potentially including:

- Gasification. Coal gasification can convert carbon rich feeds, such as coal, to gaseous products – typically CO, CO_2, H_2O and H_2. This gaseous product has the capacity to be used for a wide range of applications, including power generation, liquid fuel and chemical synthesis [10, 11].
- Liquefaction. To turn coal into liquid fuel or chemical feedstock. Multiple methods for liquefaction (pyrolysis, direct or indirect) have been developed, with products including C_1 to C_4 hydrocarbons, preasphaltene, asphaltene and oil [12, 13].

However, both technologies require minimise moisture within the coal, otherwise the moisture will reduce the efficiency of the process, or provoking unintended side reactions.

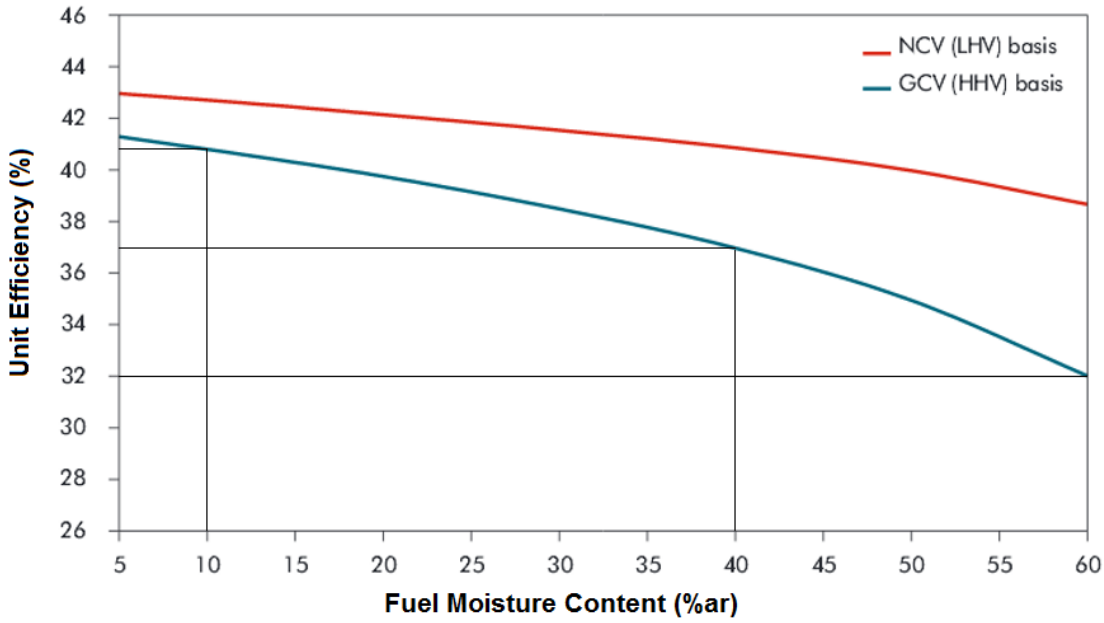

Figure 1.2 The impact of coal moisture content on unit efficiency [14]
NCV– net calorific value; GCV – gross calorific value

The Latrobe Valley, in Victoria, Australia is one region where coal drying can provide a large difference. At current consumption rates, Latrobe valley contains up to 500 years (or over 430 billion tonnes [15]) of economically recoverable Victorian brown coal. However this coal is characterised by high moisture content, reaching over 60% wt(H_2O)/wt(coal) for some coal types. The average global efficiency of coal-fired power stations is 34% on a HHV basis, in comparison to the highest possible efficiency which is approximately 45% [16]. However, Victorian brown coal fired power stations operate at significantly lower efficiencies than the global average, with reports and modelling suggesting a base efficiency of between 28% to 31% due to the use of high moisture fuels requiring additional drying energy as part of the overall process [17]. To compensate for this loss, larger quantities of coal are required, resulting in a corresponding energy penalty and increased emissions.

Approximately 75% of Victoria's 9,000 MW power capacity is generated through brown coal combustion [15]; the increase in efficiency coupled with the scale of brown coal usage means the application of drying technologies can be strongly justified. Apart from an efficiency reduction in the boiler, a high moisture content also:

- Increases the coal feed throughput for a similar power output, resulting in increased auxiliary power requirements in coal handling systems and pulverisers.
- Increases plant operating, capital and maintenance costs due to the larger boilers required [4], implying increased costs for the life of the plant.
- Increases the mass of CO_2 released per unit of electricity output. Studies suggest a 1% increase in process efficiency can result in up to a 3% reduction in CO_2 emissions [16].

Drying of the feed coal is the obvious solution to many of these issues; however drying requires additional safety considerations and has potential drawbacks, including:

- High temperatures and pressures may be required, creating an increased risk of spontaneous combustion during drying [4, 18].
- Moisture re-adsorption from the atmosphere which has the capacity to reduce the combustion efficiency.
- Many older boilers cannot accommodate a substantial reduction of feedstock moisture, as changes to the boiler design would be required.

Many different drying technologies have been successfully commercialised or are in the late stages of development, however none have succeeded in completely addressing the

environmental, economic and efficiency challenges inherent in power generation from high moisture, low rank coals. The wide range of methods is due to the heterogeneous nature of low rank coals, which vary in moisture content and physical and chemical composition [19-25]. Due to the specific nature of the drying technologies and the nature of bonding of moisture in coal, many of which have been developed for an individual fuel, an ideal drying technology for one low rank coal may be inefficient and ineffective for another.

Technologies such as densification have been discussed in the literature review (Chapter 2) with an overview of the current technologies and their state of commercial implementation. It explains that fluidized bed drying with either air or steam is an established technology in Germany and the USA, and has potential for application in other countries such as China and Australia. While other viable technologies are in development or implementation, fluidized bed drying, especially with steam, has a number of distinct advantages, such as operating in an inert atmosphere, high heat transfer and good bed mixing.

Steam fluidised bed drying with in-bed heating was proposed and pioneered by Professor Owen Potter at Monash University in the 1970s [26] and has since undergone many changes [27]. Using steam as a fluidization medium, steam fluidized bed drying has the capacity to dry large quantities of coal and has some notable advantages over traditional air fluidization, including:

- A faster drying rate than air when operated over the inversion temperature. This is due to the reduction in the mass transfer resistance when the liquid is dried in an atmosphere of its own vapour [28]. The inversion temperature is defined as the temperature where the average evaporation rates in different gas fluxes with different vapour mole fractions are equal [29]
- A greater energy recovery through vapour recompression cycles
- An inert atmosphere, limiting spontaneous combustion within the bed

The emphasis of this thesis is the development of the fundamental properties of steam fluidized bed drying, observing the drying kinetics, and chemical and physical properties during drying. This information is not currently available in the public domain and will help in scaling of steam fluidized bed drying which can be applied specifically for Victorian brown coal. The information contributes to the development of the theory and application of steam fluidized bed drying of Victorian brown coal, and to investigate the optimal operational

conditions required for the drying of Victorian brown coal. As a comparison, air fluidized bed drying and drying of Chinese lignite has also been considered in this thesis.

This has been discussed in the proceeding literature review. In conjunction with this literature review the scope of this thesis has been summarized and defined into separate objectives to find the fundamental gaps present in the current knowledge of drying Victorian brown coal.

Chapter 2. Literature Review on Drying Technologies

This literature review provides context for the current state of coal drying and defines the scope of the thesis. Individual literature reviews can also be found in each experimental chapter, to define the state of the art of individual aspects of coal drying.

Information from this chapter is presented in the keynote presentation: D. Stokie, J. Yu, A. Auxilio, S. Bhattacharya, Coal Drying and Dewatering for power generation – Current Status, Research and Development Needs, International Conference on Coal Science and Technology, Oviedo, Spain 2011

2.1. Water in Low Rank Coal

Before the drying methods can be properly analysed, the water in coal needs be investigated. Water – coal interactions change for a variety of reasons and it is important to understand as the bonding nature of the water can affect the energy requirements and moisture loss depending on the drying technology used.

Brown coal is a comparatively young fuel on the classification spectrum and as such has higher moisture content than most other coals. As coalification time (age of the coal) increases the amount of oxygen in the coal decreases, reducing the coals hydrophilicity and moisture content [5, 30, 31]. By determining how the water bonds to the coal structure and how this varies between coals, a more informed choice of the drying methods can be made.

Water in coal occurs in many different forms. According to Carr et. al. [32] and more recently Karthikeyan et. al. [8], there are five different forms of water in coal which are defined in Table 2.1:

Table 2.1 Moisture in coal and removal methods **[33]**

Category	Location	Removal Method
Inter Adsorption Water	Micro-pores and micro-capillaries within each coal particle	Thermal or Chemical
Surface Adsorption Water	Particle surface	Thermal or Chemical
Capillary Water	Capillaries in coal particles	Thermal or Chemical
Inter-particle Water	Small crevices found between two or more particles	Mechanical or Thermal
Adhesive Water	Film around the surface of individual or agglomerated particles	Mechanical or Thermal

Adhesion water and inter-particle water are known as free surface moisture and are relatively easy to remove through mechanical or thermal methods. Capillary water can be only partially removed by mechanical means, with the extent dependent on the individual structure of the coal particles. Finally, interior and surface adsorbed moisture can only be removed through thermal or chemical means. These states are further defined and summarised in Figure 2.1 and Table 2.1.

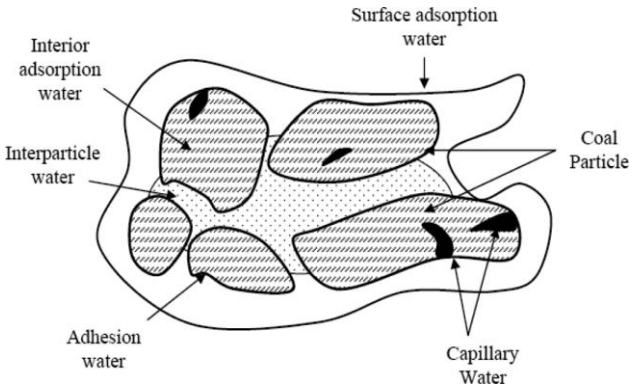

Figure 2.1 Different forms of water associated with coal, Karthikeyan et. al. [8]

A different method of defining water in coal is to observe and measure water-coal interactions through analytical techniques [34, 35]. This classification separates the forms of water through its freezing conditions in the coal particles, and designates freezable, bound and non-freezable water fractions.

For Victorian brown coals, freezable water accounts for a large proportion of the coal water and is weakly bound to the coal surface [36]. It is found in the larger pores in coal [5, 20], and characterised by freezing temperatures slightly below 0°C. Allardice et. al. [37, 38] found, for a Victorian brown coal, that the isosteric heat of desorption is equal to the heat of vaporization of bulk water for water ratios down to 60g(H_2O)/100g(Dry Coal), suggesting that water above this ratio can be classified as freezable. Bound water accounts for a significantly smaller portion of water present [36] and is typically seen to freeze at lower temperatures, approximately -45°C [36, 39, 40]. Non-freezable water cannot form a crystalline matrix either due to the water's presence in small pores or through adsorption onto the coal structure [34, 39], where it is strongly bound to the coal through hydrogen bonding with oxygen functional groups (typically carboxyl, hydroxyl and carbonyl groups) [5, 41, 42]. Table 2.2 presents the proportion of forms of water for a selection of low rank coals. This comparison indicates that the composition of the four coals (with a moisture content ranging

from 4.6% to 32.2%) is predominantly non-freezable water, with small amounts (7% to 29%) of the water within the bound region. Victorian brown coals are different because of the large quantities of free water, from 45% to 49%.

Table 2.2 Differential Scanning Calorimetry of water in coal **[36]**

Coal	Peak at higher temp.		Peak at lower temp.		Water Type		
	ΔH J/g	Temp K	ΔH J/g	Temp K	Free	Bound [% to total]	Non Freezing
BL	0	-	1.1	226.2	0	7	93
IL	0	-	5	227	0	19	81
WY	0	-	25.1	227.6	0	27	73
BZ	0	-	23	226.4	0	21	79
SB	0	-	31	(248.1,227.6)	0	29	71
YL	86.7	258.5	25.4	226.3	45	13	42
LY	93.6	258.4	18.4	227.1	49	10	41
MW	83.6	257.9	13.9	227	45	7	48

Coal Types: BL – Blind Canyon; IL – Illinois #6; WY – Wyodak; BZ – Beulah Zap; SB – South Banko; YL – Yallourn; LY – Loy Yang; MW- Morwell

Two techniques have been used to determine the breakdown of water in coal, proton nuclear magnetic resonance (NMR) and differential scanning calorimetry (DSC). A comparison between DSC and NMR results has been conducted by Allardice et. al [7] and found that DSC results typically overestimates non-freezable water by up to 12%, predominantly through calculation assumptions.

Differential scanning calorimetry has a range of purposes [43, 44], but for water in coal it can quantify the mass of freezable and bound water in a sample. This is achieved through as steady temperature change and analysis of the energy (enthalpy) release as a function of the phase change. Because the enthalpy of freezing is well know the mass can be calculated [39, 40]. NMR determines the amount of mobile and region hydrogen in coal [5] and classifies non freezable water as liquid water at -3°C. NMR has been previously applied to brown coals [45] with water coal interactions seen from 0 kg(H_2O)/100 kg(dry coal) to 26 kg(H_2O)/100 kg(dry coal) and any additional water beyond this point showing no interactions [46], suggesting that water below this ratio would be non-freezable.

2.2. Hot Air (low temperature) fluidised bed drying

Fluidization occurs when a gas is passed upwards through a bed of particles at sufficient velocity to counteract the weight of the particles under gravity. This causes the bed to increase in height and the particles to separate, allowing the particles to move freely

throughout the bed. Advantages of a fluidised bed include a high heat transfer rate, a high solid to gas contact area, and the inherent continual mixing of particles [8, 47].

Air fluidised bed drying uses preheated air as a fluidization medium, typically in conjunction with hot air in heating tubes to dry the coal particles prior to combustion. With continued investigation into the best application of the technology, the initial process has been developed in different directions. Designs such as multi-level cascade systems [33], staggered temperature beds [48, 49] and plug fluidised bed driers [50] have all been tested, and a selection of the novel fluidised bed drying patents designed specifically for coal are shown in **Table 2.3**. Air fluidised bed drying has a typical energy requirement range of 3100 to 4000 kJ/kg(H_2O removed) [8].

The kinetics of fluidised bed drying has been investigated for a range of coals under various conditions. Work with Indonesian brown coal has shown that the amount of moisture removed on drying increased at higher temperatures, and that larger particle sizes results in decreased drying times [51]. The increased drying rate for larger particles is inconsistent with other kinetic analyses, where larger particle sizes require longer drying times [52]. This discrepancy is due to the choice of fluidization velocity. If the velocity remains absolute for every particle size then the larger particles take longer to drying, however, if the fluidization velocity is varied based on the minimum fluidization velocity (in this case 1.5 times) than the drying rate becomes higher. The fluidised bed drying trends with bed height and initial moisture content were examined by Calban using Turkish coal, from the Erzurum Ispir-Karahan province, with results indicating that a shallower bed height reduces drying time, and a reduction in the initial moisture content reduces the drying rate. This result is confirmed by Levy et. al. [113, 114] using larger scale beds to test North Dakota Lignite and Powder River Basin Coal.

The overall trends for fluidised bed drying typically show that higher fluidization velocities, smaller particle sizes and higher temperatures reduce drying time [53-55]. Kim et. al. [54] investigated an additional factor, relating the relative humidity of the gas stream to the drying rate. Reducing the relative humidity from 40% to 0% at a constant bed temperature of 40°C resulted in shorter drying rates.

Despite these and other promising results, there are drawbacks to using hot air as a fluidization medium, primarily, the high propensity of some dried low rank coals for spontaneous combustion. The removal of moisture and the addition of heat and oxygen to

these fuels as part of the air fluidised bed drying process provides the ideal environment for spontaneous combustion, making air fluidised bed drying a greater safety risk when compared to other drying technologies such as steam fluidised bed drying.

Another shortcoming in fluidised bed drying is the lack of predictability as the bed size increases [56, 57]. The hydrodynamics within the bed become increasingly complex with scale, and can conceivably result in undesirable bed phenomena such as large bubble sizes, channelling or partial de-fluidization [56]. Currently, there are few reliable mathematical models for scaling up fluidised bed driers, rendering empirical data from pilot plant trials important [47].

Air fluidised bed drying is one of the most prominent drying technologies currently in use. While energy requirements can be comparably high (see **Table 2.4**) air fluidised bed drying is one of the few technologies currently implemented on an industrial scale, as discussed below and in **Table 2.5**. While air fluidised bed drying must address spontaneous combustion issues, unlike steam fluidised bed drying or any dewatering process, its ability to use waste heat and operate at low temperatures and pressures allows for greater process integration.

The most successful implementation of air fluidised bed drying of low rank coal is the Dryfining process implemented by Great River Energy (GRE), USA. Otherwise known as the Lignite Fuel Enhancement System (LFES), the process uses waste heat from the boiler to dry the fuel before being fed into the boiler exploiting otherwise unused low-grade heat (shown in **Figure 2.2**). In the LFES, low temperature hot air fluidises and heats the coal. The air stream is cooled and humidified as it flows upward through the fluidised bed removing the coal moisture. The amount of moisture that can be removed is limited by the drying capacity of the air stream, which is supplemented by an in-bed hot water coil. GRE tested a number of coals in a 2 tonne/h pilot-scale drier [17] to evaluate the drying potential of different feedstock. Currently, four individual driers are in operation in GRE's Coal Creek Power Station in North Dakota. Operational since 2009, each drier has a throughput of approximately 125 tonne/h, and is capable of reducing the coal moisture by 9% from 38% to 29% by mass. More information on the implementation of LFES is presented in **Table 2.5**.

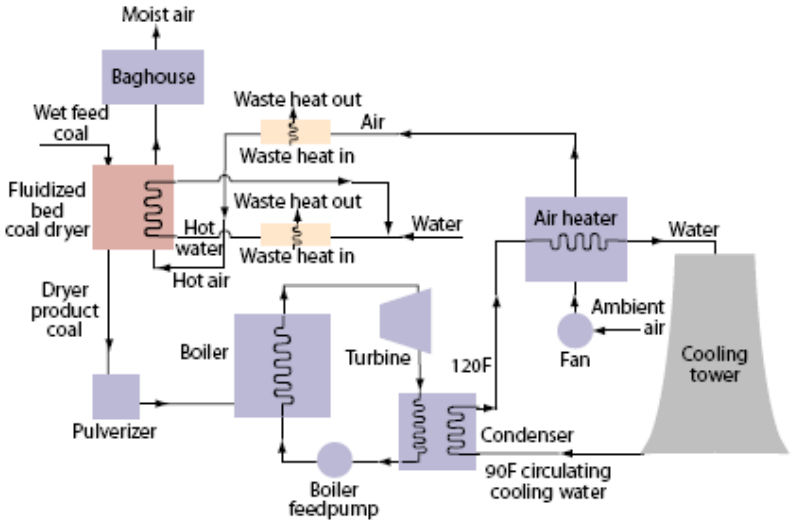

Figure 2.2 A schematic of the Lignite Fuel Enhancement System, which uses waste heat from condenser water and flue gas [58, 59]

In 2013 The Global CCS institute prepared a report on retrofitting Loy Yang A power station in Victoria, Australia with post-combustion carbon capture technology. A section of the modelling incorporated the potential impact of implementing the DryFining (GRE) technique [17]. This analysis suggests the maximum theoretical moisture reduction of the Victorian brown coal fuel used at Loy Yang A was 6% (from 60% to 54%) resulting in a boiler efficiency increase from 72% to 75.4% and a CO_2 emission reduction from 1.057 to 1.016 kg/kWh.

2.3. Steam Fluidised Bed Drying

Steam fluidised bed drying is fundamentally similar to air fluidised bed drying substituting the air for steam as the fluidization medium. Steam fluidised bed drying with in-bed heating was invented by Professor Owen Potter at Monash University in the 1970s [26], and has undergone many changes since [27]. Steam fluidised bed drying also underwent extensive testing and development in Germany with RWE first operating a 53 t/h demonstration facility in 1993. Further demonstration, prototype and production plants were commissioned in 1999, 2005 and 2008 respectively [60]. Research has also continued in Australia, with a single demonstration facility at Loy Yang A power plant operational between 1992 and 2003 [20].

A schematic representation of a steam fluidised bed drier is presented in **Figure 2.3** and indicates that two steam supplies are required; fluidisation steam at 15-25 kPag and up to 120°C, and saturated heating steam at 400-500 kPag [20]. Raw coal is thus fluidised by one

stream while additional heat is supplied through high temperature steam tubes immersed in the fluidised coal bed. A temperature gradient is deliberately induced between the heating steam and the drier bed to ensure an optimum level of drying and residence time. For drying to be accomplished at atmospheric pressure (i.e. with a saturation temperature of 100°C in the bed), the heating steam is pressurised to approximately 5 bar (152°C). This steam can potentially be supplied from low-pressure turbines in a coal-fired power plant. Variations of the process shown in **Figure 2.3** are possible, including the complete removal of vapour compression, in which case the vapour is either released into the atmosphere or used for thermal recuperation [61]. In such cases the heating steam, contained in the in-bed coil, can be sourced from the steam cycle of the plant.

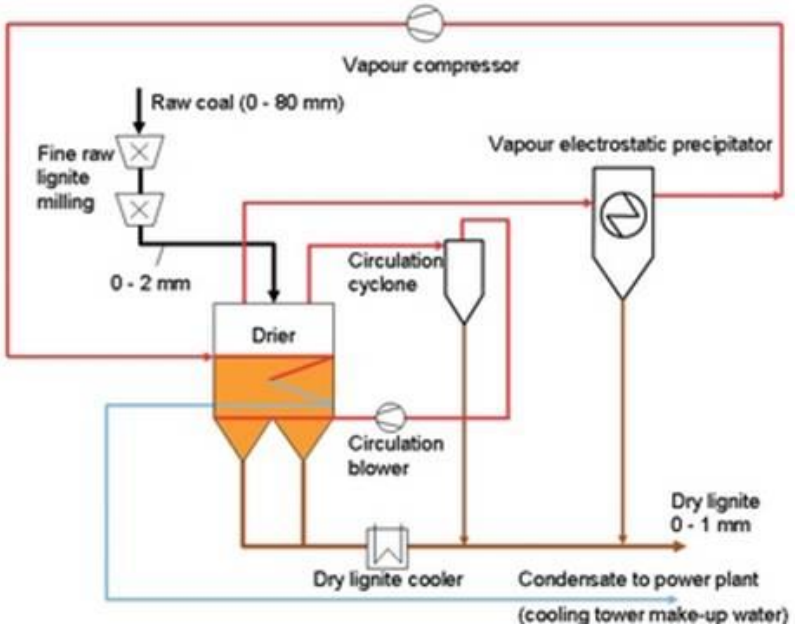

Figure 2.3 General schematic of WTA steam fluidised bed drying [59]

The volume of the vessel and the extent of moisture removal that can be achieved in a steam fluidised bed drier depend on a number of factors, including:

- The conditions of the steam used for heating
- The particle size of raw coal feed, which affects the drying time
- The fluidisation velocity, which is important to ensure maximum contact between the heating steam and the particles

There are also considerations in scaling up the capacity of a steam fluidised bed drier. For example, though a finer coal size is conducive to faster drying effective fluidisation is made

more difficult, which influences the level of drying that can be obtained within a reasonable time.

Relatively little information is publically available on the kinetics of steam fluidised bed drying of coal. One investigation was conducted into the pressure and particle size effects in a pressurised steam fluidised bed. **Figure 2.4** presents the effect of pressure and particle size on heat transfer during drying of German brown coal using this configuration [62]. Further work on pressurised steam fluidised bed drying of German lignite was conducted by Vattenfall. Higher overall heat transfer co-efficients were obtained at higher pressures and with smaller particle sizes [63].

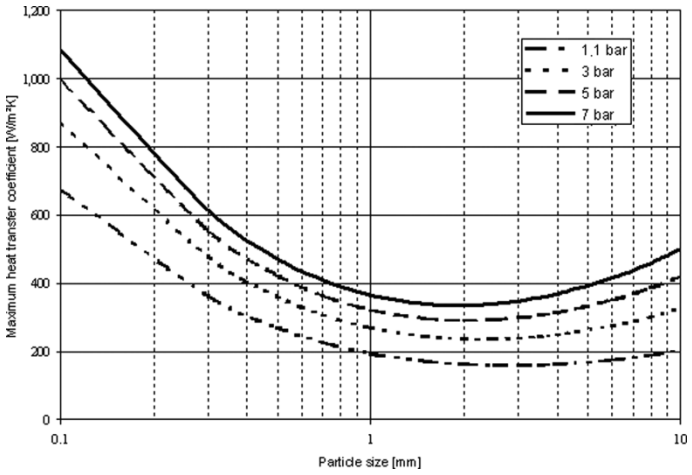

Figure 2.4 The effect of particle size and pressure on heat transfer of German brown coal during steam fluidised bed drying [64]

A study on the chemical changes to coal as a result of steam fluidised bed drying was conducted by Tahmasebi et. al. [65]. Results of this study indicate that there is a substantial difference in the composition of the oxygen functional groups before and after drying by this method, and also in comparison with air and nitrogen fluidised bed drying. Under steam conditions, a minor decrease in aliphatic hydrogen and a major decrease in carboxyl, carbonyl, phenolic and carboxylic structure was observed, this result being confirmed by comparing the oxygen to carbon ratio from the steam dried and raw coals.

One of the major advantages of steam fluidization is the negation of the risk of spontaneous combustion. With a steam atmosphere, there is no oxygen for combustion to occur, therefore the process safety is drastically increased in comparison to the analogous air-drying process [33]. This is most readily seen in the application of air fluidized bed drying and steam

fluidized bed drying in industry, with steam fluidized bed drying previously operating at 120C [20], while air fluidized bed drying has been successfully tested with conditions at approximately 70-80°C [66].

Another benefit of the steam fluidised bed drying of coal is increased heat transfer. Comparing air to steam fluidization, as gas temperature increases there comes a point where the heat transfer rate in steam exceeds that in air and is known as the inversion temperature. Chen et. al. has modelled the theoretical position of the inversion temperature for water droplets as well as coal and found that the inversion temperature decreases with the increase in gas flow rate and initial diameter. Continually, with porous particles they observed an increase of coal permeability decreases the inversion temperature [67].

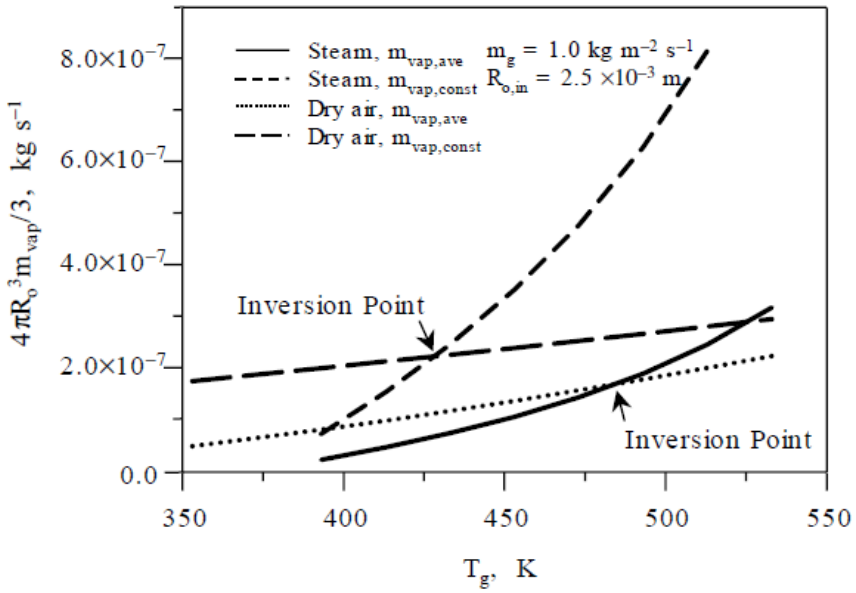

Figure 2.5 The inversion temperature of water droplets [67]

Steam fluidization also allows for greater energy recovery through steam re-compression and, when fully integrated with a power station and using low grade 'waste' steam, the energy consumption of this process can theoretically be as little as 400 kJ/kg(H_2O) [8].

Despite these advantages, there are still some drawbacks to steam fluidization. Introducing coal particles directly into a steam atmosphere can result in initial condensation of liquid water on the surface of the particle, increasing the drying time required. Additional problems include higher corrosion rates and tighter sealing requirements to prevent leaking steam to the atmosphere [68-70].

One of the most advanced steam fluidised bed drying processes was developed and implemented by RWE in Germany. Commonly known as WTA (Wirbelschicht-Trocknung mit interner Abwärmenutzung or fluidised bed drying with internal waste heat utilization) This process typically uses a nominal feed particle size of either 6 mm or 2 mm, with the fine grain driers (0 – 2 mm) resulting in a smaller vessel size and cost, and a reduction in the steam required to maintain fluidization. The temperature of the steam is also somewhat lower than that required to dry the coarser coal fraction due to the increased drying rates with the smaller particles [4]. Large-scale application of the WTA process is being carried out by RWE Niederaussem Power Station, where 25% of this supercritical unit's input fuel is being pre-dried using this technology [4], with the scale of operations outlined in **Table 2.5**.

In addition to the demonstration at Niederaussem Power Station, the WTA technology was also planned for demonstration at the Hazelwood Power Station in Victoria, Australia [71]. A WTA drier was to be retrofitted to an existing 200MWe unit to dry 50% of the high-moisture feed coal, reducing the moisture content from about 60% to 12%. The dried coal would then be co-fired with 50% high-moisture coal into the boiler. However, this plan is no longer under development due to economic considerations.

Vattenfall, in conjunction with Brandenburg Technical University, is also known to develop steam fluidised bed drying [72]. Known as Pressurised Fluidised Bed Drying (PFBD), a 5 t/h (output) pilot plant at Schwarze Pumpe has been in operation since October 2008. Using steam as a fluidization medium, drying operates at between 4-6 bar with temperatures ranging from 100°C to 160°C resulting in output coal moisture contents between 8% to 12%. An advantage of the higher pressures is the smaller fluidization velocity required. However, feeding requirements become complex due to the higher pressure. Also, high pressure steam from high or intermediate pressure turbines are required to accomplish the drying.

2.4. Other Drying Technologies

2.4.1. Entrained Flow Drying

Entrained flow drying [20, 73], otherwise known as flash mill drying, uses hot flue gas to flash dry coal with the majority of drying occurring within the first second of coal-gas contact. Created specifically for high moisture, low rank coals, the process offers high efficiencies through direct integration. Key advantages of entrained flow driers are the simplicity of operation, and low cost for implementation. However, experimental data and

modelling shows that particles larger than 0.6 mm were not substantially dried in the single second [74, 75].

The Cooperative Research Centre for Clean Power from Lignite trialled a 10 bar pressurised entrained flow drier using hot flue gas at 800°C and a maximum oxygen content of 3% by volume to minimise coal oxidation [76, 77]. A schematic of the process is shown in **Figure 2.6**. Trials resulted in a moisture reduction from 67% to 30%, however, a high attrition rate was observed. Changes to the feed variables resulted in higher moisture contents with an increased feed rate and inlet particle sizes. White Energy, Australia is currently developing this technology. Predominantly targeting sub-bituminous coals [78], they have commissioned a demonstration plant in Australia, as well as a commercial plant in Indonesia [79]. Analysis using sub-bituminous Power River Basin coals from Wyoming, America show an energy content increase from 19.5 MJ/kg to 26.4 MJ/kg [79]. A comparison of White Energy's flash drying facilities is presented in **Table 2.5**.

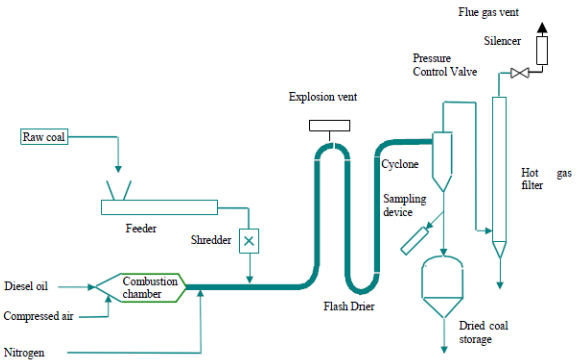

Figure 2.6 Schematic of a Pressurised Flash Drier [73, 77]

2.4.2. Mechanical Thermal Expression (MTE)

Mechanical thermal expression also referred to as mechanical thermal dewatering, removes moisture from coal without evaporation. This process builds on research undertaken at Diffenbacher and at the University of Dortmund in the late 1990s [80]. MTE works on the principle that if coal is heated to between 150 – 200°C [81, 82] the water in coal can then be 'squeezed' out by applying mechanical pressure. The process pressure is maintained at or above the saturation pressure corresponding to the process temperature in order to avoid any evaporation. Raising the temperature makes the coal easier to deform under compression and

renders the water more mobile by reducing its viscosity and surface tension. Up to 80% of the total moisture from Victorian brown coals can be removed in this way [83].

The advantages of this method of dewatering include the elimination of the latent heat energy required for evaporative procedures, as well as relatively few chemical changes to the coal. However, as the water released may be acidic, salty and / or rich in organic compounds [84], wastewater treatment and remediation must also be taken into account. This is an ongoing area of research, with many different methods still under investigation [85, 86]

While the initial conception of the technology occurred in the 1990s mechanical thermal expression has not yet been implemented beyond the pilot scale. This places it behind more established technologies such as air or steam fluidised bed drying. However, the reported energy requirements (see **Table 2.4**) suggests that mechanical thermal expression is comparable with many of the efficient coal drying techniques, with an energy requirement between 1600 and 1800 kJ/kg(H_2O) removed [87].

Research and development into mechanical thermal expression was undertaken in Australia by the Cooperative Research Centre for Clean Power from Lignite [4] including a bench scale and 1 tonne/h scale apparatus, where the effect of variables including pressure, temperature, coal type, and durations of heating and compression were correlated with throughput and extent of dewatering [4]. A 25 t/h demonstration plant was commissioned at the Niederaussem Power Station in Germany. Operating in a semi-batch configuration, the typical drying cycling ran for 12 minutes, with 6 minutes of heating included. For this reason the productivity and design of this form of MTE was considered a potential problem [88]. A 15 tonne/h plant was designed, constructed and operated by Loy Yang Power in Victoria, however no further development work at the site is planned [4].

2.4.3. Hydrothermal Dewatering

Hydrothermal dewatering [89] occurs at high temperatures and pressures, typically 200-350°C and 100 bar [58, 90], which decarboxylates the coal, removing moisture associated with these functional groups. CO_2 is also ejected as the coal is physically compressed, expelling liquid water from its interstices in the process [20, 91]. Although hydrothermal dewatering has a long history of exploratory development, several key hurdles remain, including process scalability and treatment of discharged water [92]. Hydrothermal dewatering, like mechanical thermal expression, releases organic compounds into the removed water, presenting problems for downstream effluent treatment. Therefore, while

many companies have had success with pilot scale facilities there appear to be no currently operating commercial plants (see **Table 2.5).** In relation to Victorian brown coals, hydrothermal dewatering was initially rejected due to the higher capital cost (versus Steam Fluidised Bed Drying and mechanical thermal expression) and the difficulty of separating the released water from the coal product [83].

The impact of hydrothermal dewatering on the inorganic constituents in a range of low rank coals shows a reduction in Sodium of more than 70%, whereas Potassium removal was dependent on its chemical form in the coal. Magnesium, Calcium and Sulphur were also removed in varying degrees but are dependent on coal types and drying kinetics. Removal of many of these constituents can affect the downstream treatment such as sulphur scrubbing or reduce existing problems such as slagging and fouling [91, 93, 94].

A range of companies are currently developing similar technologies based off hydrothermal dewatering. Exergen, Australia, is developing an improved hydrothermal dewatering technology using hydrostatic pressure to feed fresh coal into a vertical autoclave shaft (up to 1000 m deep) at pressures of approximately 10 MPa and temperatures of 300°C. K-Fuel technology developed by Evergreen Energy, USA [78] involves heating and pressurization of the coal at typical conditions up to 260°C and 3.4 MPa [58], with a 53.1% moisture removal. Ignite Energy Resources, Australia uses a continuous flow catalytic hydrothermal reactor [95] to quickly depolymerise coal under high temperatures (250°C to 400°C) and pressures (100 to 250 bar) [58]. The products from this process are an upgraded coal and a synthetic crude oil [96]. The pilot plants based on these technologies can be found in greater detail in **Table 2.5**.

2.4.4. Rotary Driers

Hot gas rotary drum drying was initially attempted as early as 1925, using direct contact between flue gas and coal particles, but was suspended due concerns over fire and explosion risks [20, 58]. The concept has since been diversified to include a range of different configurations such as direct, indirect, indirect-direct and special types which are applied depending on the feedstock and drying requirements.

Rotary driers are a well-established technology in a range of industries, including coal [33]. They consist generally of a rotating cylindrical vessel through which a gaseous drying medium flows in various configurations. Direct rotary driers are the simplest and the most economical, with direct gas contact with the coal [97], however they are not widely used due

to the risk of combustion [58], meaning the reactivity of the intended feed coal must be taken into account. Indirect heating units use hot fluids and tube walls to heat and dry the coal, requiring only enough gas flow to remove the water vapour generated by the process heat.

Many novel forms of the basic rotary drying technology have been researched, including the addition of internal structures in the drum such as removable flights or passive rakes [68, 98-101]. With continued development into modifications such as flighting, aeration, novel flow characteristics, indirect rotary tube driers and direct and indirect combination heating a wide range of possibilities exist for application. In-depth analysis of rotary drying technologies by Osman et. al. suggests that many of these technologies have not yet been proven independently, and may have add complexities in construction and operation [33]. Configurations in which particles are dried through flights and particle showering can increase the heat transfer in rotary drum driers as they enhance particle mixing and reduce dead zones, however these layouts often increase particle attrition and the risk of dust explosions [33].

Keith Engineering has developed a superheated steam rotary drum drier which has the capacity to reduce the moisture content from 61% to 11% operating at temperatures between 180°C and 230°C with a raw coal feed of 23-46 kg/h [3, 4, 70, 78]. Direct flue gas drum drying has seen potential growth in Xilin Gol League, with Datang International and Sunite-ZuoQi Xiaobaiyang Mining Co. reported to be adopting this technology for removing surface moisture [102]. An application of indirect steam rotary driers was used by ZEMAG. where coal is placed in a set of parallel rotating tubes and steam circulated through the drum shell to provide the necessary heat for drying [102, 103].

2.4.5. The UBC (Upgraded Brown Coal) Process

This method of drying allows for a simultaneous removal of moisture, upgrade in coal calorific value, and recovery of steam vapour for recompression Raw coal is slurried with low grade, heavy oil and pumped under elevated temperature and pressure such that the moisture is forced out of the pores and replaced with the heavier fraction of the oil components. The remaining lighter fraction of oil is then recovered.

Kobe steel has been working on a related method of upgrading low rank coal, known as the Upgraded Brown Coal (UBC) method since the early 1990s. The UBC method involves immersing crushed coal in a mixture of light and heavy oil also containing asphalt [83]. At temperatures of 130 - 160°C and pressures of 400 - 450 kPa, the water in the coal is

vaporised and removed [104]. Work at laboratory scale using Indonesian lignite a reduction in moisture content from 32% to 3.2-2% and an upgraded heating value of 12.5 MJ/kg to 25.1 MJ/kg was achieved after 10 minutes' treatment [105].

The UBC process results in essentially no chemical reaction of the coal, minimising the waste treatment required. The steam released through the drying process also has the capacity to be compressed and used as a heat source and the heavy fractions of oil have been reported to reduce the propensity for spontaneous combustion of the coal [104].

While classified as catalytic hydrothermal dewatering, Ignite Resources' process provides the best comparison to upgraded brown coal drying. Both methods result in higher calorific coal through the immersion in an oil mixture. The UBC method, however, operates at lower temperatures and pressures, and vaporises the moisture as opposed to non-thermal dewatering, enabling easier separation. Comparing the state of these two technologies, both have previously operated pilot plant facilities, however the UBC demonstration plant has much more reported information available (**Table 2.5**).

Implementation of the UBC process includes a 0.13 t/h pilot plant constructed in Java, Indonesia, operational from 2001 to 2004 and a 25 t/h plant constructed in Kalimantan, Indonesia operated from 2006 to 2009 for demonstration prior to commercialization [104].

2.4.6. Solvent Dewatering

Also known as solvent displacement, the initial forms of the solvent dewatering process began as early as 1926 [101] using oil or hydrocarbons. The solvent is required to be miscible with water at high temperatures (150°C - 200°C) but immiscible with water at low temperatures. Early results suggest that polar solvents have better water removal but prove difficult to separate, while nonpolar solvents achieve good separation but require large volumes of solvent to be effective. Solvent dewatered coals have been found to have heating values equal to subbituminous or bituminous coals [106].

Recent innovations in solvent dewatering of brown coal include the use a range of solvents to remove the moisture as a liquid [106, 107]. With a range of solvents at temperatures up 200°C Morwell coal can be dewatered, with the remaining moisture content as low as 2% based on the solvent, temperature and contact times used [20, 107]. Under the best case scenario tetralin appeared to have energy requirements less than 1000 kJ/kg(H_2O) removed [20, 107].

Another form of solvent dewatering uses liquefied dimethyl ether (DME) at 0.8 MPa, which is highly miscible with water at room temperature. The solvent is then depressurised, separating it from the water by evaporation [108]. Using this solvent, the moisture content of Loy Yang coal was reduced from 54% to 4% at an energy estimate of 948 kJ/ kg(H_2O). Further work using Indonesian sub-bituminous coal reduced the moisture content of the coal from 40.6% to 13% at a calculated energy cost of approximately 2069 kJ/kg(H_2O removed) [109].

While early analysis of this drying method suggests that the energy requirements per kilogram of water is comparable to many other forms of drying discussed, this technology is still in the very early stages of development, and an accurate comparison with industrial drying technologies cannot be made. At this time there are no public plans for commercialisation.

2.4.7. Microwave Drying

Microwave drying uses targeted heating and energy, which is preferentially transferred to the water instead of the coal [33]. As all forms of water absorb microwave energy, both bound and free moisture in coal can be released by this method [3]. In addition, by controlling the residence time and the energy wavelength, drying can be achieved without raising the temperature of the coal over 90°C [110].

Microwave drying is distinguished by its higher diffusion co-efficients and higher drying rates with larger particle sizes in comparison to more conventional technologies [111-113]. It has advantages of high process speed [112] and uniform heating [101, 113] as well as reductions in sulphur, and potentially mercury, potassium and phosphorus content in comparison to alternative technologies [110]. Conversely, it is regarded as one of the most energy intensive drying technologies and can also result in overheating during the drying process through non-uniform heating [70].

Research into various microwave designs and technology combinations is ongoing [113-117], with several companies working on methods at industrial scale. DBA Global have built a 25 t/h demonstration plant based on their Drycol process [110]. The Drycol process is a continuous system using a microwave source with a controlled power input to achieve predetermined exit moisture content. The coal is conveyed through the microwave at a maximum average bed temperature of 90°C, and the released water is taken through the air steam and condensed.

Another process developed by CoalTek uses microwave drying to remove 40% to 50% of a coal's moisture, and can remove both surface and bound water. Currently CoalTek has a 15 t/h commercial scale demonstration facility in Calvert City, and a 1250 t/h facility in construction in Inner Mongolia, China [118].

2.4.8. Solar Drying

The process of solar drying uses milled coal slurry which is pumped into open-air ponds[92]. The water is then evaporated to ambient equilibrium moisture, approximately 12% [119].

Due to the large tracts of land and labour intensive nature of this form of drying, it has never resulted in continued large scale implementation. While this was found to be unfeasible in Australia, difference in coal quality, land utilization and atmospheric conditions may make this method viable in other countries. Other options for this technology include the use of solar ponds for secondary coal recovery [120]. A single 2200 t/y plant operated at Hazelwood, Australia in 1986 [58] at an average energy cost of 400 MJ/kg(H_2O removed).

2.4.9. Densified Brown Coal

Another technology currently under consideration for the upgrading of low rank coals is the production of densified brown coal pellets [121] using various proprietary techniques, most notably the Coldry process [21].

The Coldry process was developed in the 1980s. It collapses the coal's pore structure through milling, reducing the particle size to approximately 10 microns [119]. The resultant slurry (created through the milling process) is then pelletized by extrusion and then dried at low temperatures to reduce particle shrinkage and weakening [121]. As coal densification operates at much lower temperatures than most other drying technologies, there is a reduced chance of spontaneous combustion.

After the densification process the resultant pellets have high density and a hard shell, with energy densities close to those of bituminous coals [58]. Coldry pellets derived from Victorian brown coals have an upgraded net wet specific energy increase between 8.4 MJ/kg and 21.7 MJ/kg [122] with a variable moisture reduction from 10% to 70%. The products can be used in existing black coal power stations (10% to 30% feedstock additive) or in upgraded lignite plants [123] resulting in a CO_2 emissions reduction of 5% – 15%.One drawback of coal densification is the slow heat transfer during drying. A typical temperature range of between 30°C and 60°C [121] is used due to a reduction in structural strength due to uneven

heating gradients through the pellets at higher temperatures/ Pacific Edge Holdings (which incorporates La Trobe Lignite Developments) employs a similar technique using either air or flue gas as the gaseous drying medium, while Jott Engineering describes the use of integrating plant cooling water to preheat the air drying stream [83]. Recent work has begun to re-establish a Coldry plant (initial throughput is aimed at 2 million tonnes per annum, with 2,500 t/h targeted for 2025) in Victoria, Australia with commissioning scheduled for 2014 [124].

2.4.10. High Velocity Grinding and Drying

High velocity grinding and drying, otherwise known as Vortex drying, has been independently developed by various companies, resulting in technologies such as Windhexe, DevourX and LamiFlo [83]. Windhexe uses high velocity preheated air mixed with the coal particles. The air-coal combination then enters a cyclone where a combination of drying and particle breakage occurs [3, 78, 125]. DevourX accelerates the particles from 0 to 100 km/h in a space of 1 metre during which sound frequencies break the particles and release the water [3].

LamiFlo uses preheated air in a cyclonic air stream. The particles are introduced and suspended in this stream where drying and segregation occurs. As the wet coal particles are introduced, the lighter, dried material moves outwards towards the edge of the cyclone, while the heavier, wet particles move towards the centre, allowing the wet particles to be in contact with the faster air velocities, increasing drying rate [126]. Analysis of the remaining forms of water in the dried product moisture shows that this technology removes bulk and capillary water from the coal particles after two passes through the cyclone. Inherent moisture can be partially removed but requires the use of torrefaction [126]. Trials with American lignite have achieved a moisture reduction from 30% to 7%, for a maximum particle size of 10 mm. Similar analysis of Latrobe Valley brown coal samples show a decrease from 63% to 15% [126].

In terms of the further development of these technologies, a 150 t/h DevourX plant and a 250 t/h LamiFlo module are in the demonstration phase [78, 126]. Unfortunately, little detailed information on these processes or the implementation thereof is publically available, so an accurate comparison of the technologies or coal properties cannot be made.

2.5. Modelling of the Drying Process

Modelling the kinetics for any drying process is an important step in the understanding and scaling up of a drying technology. An accurate model has the capacity to reduce the amount of experimental investigation required for reliable scaling of a drying technology occurs. Particle drying occurs in a wide range of industries and technologies, and individual models need to be generated to specifically account for the individual characteristics of the drying system. For coal drying, the specific drying technology as well as the region and rank of coal particles used can have a large effect on the drying times observed.

Currently there are many different drying models available; however the large variation in drying methods and particle materials require the careful choice of model. Single particle models can accurately describe drying conditions but are often insufficient to solely predict drying in a bed. Fluidized bed drying of coal has been previously modelled; however this has generally been conducted for air fluidization. Steam drying of coal has also been investigated; however less information on steam fluidized bed drying models are currently available [29, 127]. There is a need for an engineering model which is easy to implement without sacrificing accuracy of the drying kinetic data.

Thin-layer models are capable of generalizing drying curves and are often used to choose drying conditions, as they are simple to employ and give reasonable results. Thin layer models can be applied when a) a single product exposed to the drying air or one layer of the grains or b) a multiplayer of many grain thicknesses if the temperature and relative humidity of the drying air can be assumed to be the same at any time in the drying process [128]. However, Kucuk et. al. (2014) cautions that thin layer equations are dependent on experimental data, and may potentially be affected by experimental errors [128].

Theoretical models typically use Ficks second law and takes into account moisture conditions as well as the internal movement of moisture and as such are more complex to calculate and implement than other types of models [129, 130]. Semi-theoretical models can be derived from Ficks second law and benefit from fewer assumptions and easier implementation; however they are typically limited to the drying and product conditions the model has been developed in [131]. Empirical models are based on experimental data and have similar characteristics to semi-theoretical models but give limited information on drying behaviours [132].

Many previous models have been discussed in regards to their primary characteristics and equations. Due to the wide range of models available, those presented in **Table 2.6** and **Table 2.7** are chosen for their relevance to coal drying. Although the list is not exhaustive it highlights the diverse range of potential models which have the capacity to fit the current drying conditions. Because of the large number of different variables used, the different models often have overlapping nomenclature, to clarify this, a separate nomenclature section can be found in Appendix A1. A review paper published by Kucuk et. al. overviews many of the thin layer drying curve equations used [128]. While exhaustive, the models reviewed are primarily for food and agricultural industry and does not include coal.

2.6. A Comparison of Models

With many different modelling methods available, many of the major models in literature are overviewed in **Table 2.6** and **Table 2.7**. **Table 2.6** discusses the drying models which focus on fluidized bed models while **Table 2.7** examines the models which only apply to single particles. Typically two models for particle drying are used, one assumes the core particle temperature is the same as the surface, and one proposes a moisture front with recedes as the moisture decreases, resulting in a dynamic temperature profile across a particle. The majority of models, both a single particle and fluidized bed appear to use a shrinking core mechanism for the primary description of moisture loss. While this has the capacity to make models more accurately reflect particle conditions, the iterative analysis and the coupled differential equations may result in longer calculation times, making modelling more complex.

Models by Agarwal et. al. [133] and Komatina et. al. [134] have investigated drying of coal in a fluidized bed combustor. For both a single particle analysis and a fluidized bed analysis these models appear focused on intense particle drying. While Agarwal uses a temperature of 1100K during the parametric studies, the experimental comparison occurs at 423 K. Found to be in good agreement with experimental results, Agarwal has also linked the drying temperatures for Mississippi lignite with the devolatilization of coal particles in a fluidized bed. Agarwal has not mentioned the fluidization medium used in the evaluation, however it is most likely air or nitrogen. Komatina et. al. uses a receding core method for Kosovo and Bogovina lignite's, however the comparisons use a single particle (from 5 to 10 mm) in a fluidized bed heated to 300°C. This drying model appears closer to a single particle analysis, as the bed drying characteristics are extrapolated and compared to a single particle within an already hot bed.

Kovenskii et. al. [135] discussed the drying of biomass in a fluidized bed. Initially defining the mathematical model for a single particle, the required bed mass and residence time is calculated based on the required outlet moisture content of the particles (called the humidity of the particles). While the formulation of the model is present, as well as the experimental apparatus used for the models confirmation, little comparison of the models and the experimental data is available, and a sensitivity analysis on the impact of the models assumptions has not been made available.

Olufemi and Udefiagbon [136] discuss the use of a receding core model for particle drying by numerically solving partial differential equations. Using steam as a drying atmosphere the models matches closely for the experimental data over a range of conditions. This model shows a good accuracy however the equations complexity requires the uses of modelling software and particle tessellation in order to generate the particles moisture content and suggests that scaling for industrial processes would be difficult and computationally intensive.

Fyhr and Kemp [137] used a different method for modelling drying in a fluidized bed. To approximate the throughput of continuously fed fluidized bed, the bed was split into individual layers, with a single particle approximating each layer. The moisture within the particle is governed by the effective diffusion co-efficient, however the moisture content of the bed is determined through the combination of each 'layer' while the continuous feeding component substitutes layer of particles for fresh (wet) particles at specific intervals.

Analysing **Table 2.6**, the prevalent model appears to be used in fluidized bed systems are based on Feng [138] and used in previously in multiple papers and thesis' [138-141]. While this has appeared in multiple master's thesis's, the energy and mass balances operate as a black box over the entire fluidized bed, with the correlation for specific humidity related empirically to the outlet relative humidity and air temperature. However, this model is not been applied to a steam fluidized bed and is not applicable to the experiments in this thesis. This is due to the dependence measuring the outlet humidity and air temperature to predict the moisture content within the bed. Additionally the empirically relationship between relative humidity and air temperature has not been investigated parametrically for conditions such as particle size and coal type, which may have bearing on the relationship between humidity and temperature.

Several models have been identified for potential use in the steam fluidized bed drying of Victorian brown coal, most notably by Chen et. al. [67, 142]. Developed for water droplets and ceramic particles, the model generates drying kinetics using three simultaneous equations, based on heat transfer, mass transfer and an experimentally derived isotherm equation. The authors developed and verified this model using ceramic drying, with manipulation of particle properties enabling the transition from ceramic particles to brown coal (maintaining similar assumptions) however the Chen has not verified the accuracy of the model for coal.

Thin layer models that are applied to thin layer drying curves come in a variety of forms and is defined in Kucuk et. al. [128]. The empirical nature of the model means the equations and variables are not correlated with physical characteristics of the particle and as a result the transition between the literature analysis and individual drying conditions may vary. **Table 2.8** compares the thin layer models used in a coal drying literature.

A wide range of thin layer drying curve models currently exist, varying from a single constant to six constants. Each constant increases complexity of the model, with the Newton model considered one of the simplest (with 1 constant) while the modified Henderson or Pabis model requires six constants. An overview of a wide range of different models coupled with a wide range of particle conditions shows the Midilli-Kucuk models is mostly suitable for modelling thin layer drying processes [128]. A review article by Kucuk et. al. quantified the accuracy of thin layer models over a range of previous applications and papers, with different particles and drying conditions. Kucuk found that some models, most notably Midilli-Kucuk, Page, logarithmic, two-term, Wang and Singh, approximation of diffusion, Modified Henderson and Pabis, Modified Page, Henderson and Pabis, two-term exponential, Verma et al., and Weibull et al. fulfil the selection criteria better than the others available, with the Midilli-Kucuk model found generally the most suitable. The overview of thin layer models has only been applied to the foodstuff industry, with no comparison of the thin layer models in coal present. This can conceivably mean the conclusions drawn in Kucuk et.al. are not representative of coal drying.

Investigation into thin layer models for coal drying for coal has been studied by Tahmasebi et. al. [143]. Using a fixed bed and Chinese lignite a range of equations have been analysed describing the effect of drying temperature and sample weight on the drying kinetics. Tahmasebi investigated the best fit for Chinese lignite, and using a range of thin layer models

(similar to those identified earlier) the Midilli-Kucuk equation is found to the best fit for fixed bed lignite. This conclusion parallels the conclusion found in Kucuk et. al. [128], which suggests the Midilli-Kucuk equation best fit for biomass. Kim et. al. [54] also investigated thin layer equations for coal drying, but instead focused on fluidized bed drying of Loy Yang coal. Kim did not test a variety of models but instead used the Henderson model to model the drying characteristics, and correlates the temperature, velocity and relative humidity. While Kim finds the model fits the data well, because they have not tested a range of equations, it was not determined if the Midilli-Kucuk equation is equally applicable.

Comments and analysis from the modelling of such a wide range of models show the opportunity and need still exists for the development of a mathematical model which is accurate as well as easy to implement. From the literature discussed, many of them require the calculation of a receding front, which requires solving of simultaneous differential equations for each particle. While this method provides accuracy for the moisture content of a particle, it makes the particle population within the bed more difficult to account for. A gap exists where a semi-empirical lump model can be used to approximate the moisture content of a particle, without the need for complex differential simultaneous equations. Another gap is the use of thin layer models for Victorian brown coal. While empirical models have been used extensively for food industries, its application to coal drying has received less attention.

2.7. Drying technology comparison, R&D needs and conclusions

Comparing the current level of implementation of the discussed drying technologies, many of the larger commercial facilities use fluidized bed drying, with air fluidized bed drying applied by GRE and steam fluidized bed drying applied by RWE. Few technologies have similar levels of development, as established technologies such as rotary drying or mill drying do not have the same level of information available. Similar scale facilities currently in operation such as Beijing Cleanstar, Direct Flue Gas Drying or Flash Heat Drying (**Table 2.5)** do not have publically available information. Other technologies such as mechanical thermal expression, hydrothermal dewatering, microwave drying and coal densification are still in development or have limited commercial implementation.

The energy efficiencies in **Table 2.4** show steam fluidized bed drying as one of the lowest energy requirements for drying (energy efficiency is the energy required to remove one kg of water from coal). While not heavily discussed solar drying also has relatively low energy usage, but lack of any major implementation or commercialization, coupled with its seasonal

dependence preclude it from immediate consideration. In many cases the non-evaporative dewatering methods such as mechanical thermal expression have lower energy requirements than evaporative drying techniques such as air fluidized bed drying or rotary drying. Although not numerically reported, microwave drying is widely considered one of the most energy intensive technologies.

Comparing the downstream processing of effluent and emissions, this is mostly required in non-evaporative dewatering methods. Technologies including rotary drying, air fluidized bed drying and steam fluidized bed drying, which use evaporation, have little issue with downstream cleaning, with elutriation of particle mass the only major consideration. However, mechanical thermal expression and hydrothermal dewatering both require extensive downstream treatment due to organic and inorganic components left in the wastewater. A comparison between these technologies suggests hydrothermal dewatering has greater organic loss, and more extensive wastewater treatment may be required.

An assessment of the current level of coal drying technologies, many of the technologies available has major issues which currently exclude them from commercial scale implementation. Technologies such as solar drying, MTE and HTD have stagnated with little progress made in key areas which are essential for commercial implementation, whereas older technologies such as rotary drying have decreased due to the associated risks and relatively high energy requirements. Similarly, newer technologies such as microwave drying and vortex drying have yet to establish large scale cost and energy efficiency, in the few cases where large scale facilities exist.

Of the technologies discussed, the variations on fluidised bed drying stand out as the most prominent and well developed. It has been commercially implemented in the USA (GRE) and Germany (RWE) and renewed interest has been shown in Australia. With four facilities operating with a range of 16 to 110 t/h dry coal, RWE has proved steam fluidized bed drying to be a viable drying technology. Similarly, GRE has four 125 t/h drying operating at Coal Creek Power Station, partially drying all feed coal before combustion. Steam fluidised bed drying shows particular promise due to the higher temperatures and heating rates possible, along with the inert atmosphere and relatively low energy costs associated with integration with steam turbines.

This leads to the conclusion that steam fluidized bed drying is the technology with the greatest potential for use with Victorian brown coal. With low energy requirements, already

successful commercial implementation and operational advantages (such as an inert atmosphere and little to no effluent processing) steam fluidized bed drying removes many of the issues other drying technologies face.

Identified through the literature review, relatively little information on steam fluidized bed drying is currently publically available. While some kinetics data exists for Victorian brown coal drying, the majority of the results relate exclusively with air fluidized bed drying or at low relative humidity. The impact of pure steam and how it changes the drying kinetics is still not experimentally determined or publically available.

Continually, there is a lack in our understanding of the physical and chemical characteristics of dried Victorian brown coal. While recent work has investigated aspects of the change in chemical properties in a steam fluidized bed drier, the impact of drying variables (velocity, coal type, particle size, drying medium) on the chemical characteristics such as oxygen functional groups and hydrophobicity have yet to be determined. These characteristics have the capacity to affect downstream usage of dried coal.

Little information is present within literature about the change in physical characteristics of coal as it dries. While it is generally known that coal will undergo physical changes associated with drying, such as attrition (in a fluidized bed), mechanical strength and pore collapse the effect of drying as well as drying conditions have not been analysed. Properties such as attrition and mechanical strength can affect the requirements for elutriate gas scrubbing as well affect the stability of the dried product. The relative change in surface and porosity has the capacity to affect properties such as combustion and gasification reactivity.

These issues need addressing to further develop steam fluidized bed drying as a viable option in Victorian brown coal drying. Identified throughout the literature review this thesis fills some of these gaps in knowledge, with the projects aims and scope defined in the following chapter.

Table 2.3 Selected coal fluidized bed drier patents

Patent Number	Date	Patent Holder [1st Author]	Technology	Temperature	Pressure	Fluidization Medium	Input Moisture Content	Output Moisture Content
WO 2008/127709 A2[48]	23/10/2011	Bullinger, Charles	Using heat from either flue gas or a steam generator to dry coal in a multistage fixed and fluidized bed	200 – 300 °F [A] 92 °F [B]	Open Air Atmospheric	Air	60-39%	32% - 27% [<10 % Possible]
4324544[144]	13/04/1982	Blake, John H.	Drying of coal in a fluidized bed using partial coal combustion as a heating source	400-600 °F [A] 400-600 °F [B]	Not Available	Air	Subbituminous	5% - 10%
4571174[49]	18/02/1986	Shelton, Walter. W	Drying low rank coal particulate through variable gas temperatures in a fluidized bed	400 – 1000 °F [B]	Not Available	Air	Not Available	Not Available
4495710[145]	29/01/1985	Ottoson, Javan. D	Drying dow rank particulate coal using two beds with different gas temperatures	400-900 °F [B] 200 °F [B]	Not Available	Air / Flue Gas	Not Available	<10%
3985516	12/10/1976	Johnson, Clarence. A	Drying and pacification of low rank coal particles	250-500 °F [A] 200-400 °F [B]	0-5 psig	Inert Gas, <2% O_2 [N_2 CO_2 or flue gas]	15-50%	1% - 3%
4444129[146]	24/04/1984	Ladt, Max. A	Drying coal fines in a vibrating fluidized bed	500°F [A]	Above Atmospheric	Air	<20%	Not Given
7537622[147]	26/05/2009	Dunlop, Donald. D	Multi-staged fluidized bed coal drier	Stage 1: 150-290 °C Stage 2: 290 – 350 °C	Not Given	Air	15% - 40%	1 %
6829840[148]	14/12/2004	Stone, Lawrence. H	A multilevel vibrating fluid bed drier	Not Available	Above Atmospheric	Air	Not Available	Not Available
5087269 [50]	11/02/1992	Chang, Cha. Y	An inclined plug flow fluidized bed	<200 °C	Not Available	Flue Gas or CO_2	22% - 29%	<1.5%

[A] Bed Temperature; [B] Fluidization Gas Temperature

Table 2.4 Summary of Drying Technologies

Technology	Description of the Technology	Advantages	Disadvantages	Energy Efficiency (kJ/kg H_2O)	Drying Method
Rotary Drier [8, 20, 33, 149]	A rotating steel tube on rollers at an angle. Hot gas is passed through the drier, with 15 to 40 minutes of direct contact drying the coal	• Established technology • Variable drying configurations	• Risk of spontaneous combustion	3100 – 3700	Direct Drying
Rotary Tube Drier [20, 149]	An indirect drier using superheated steam. Coal is fed through heating tubes and slope and rotation of the tubes pushes it along the drier	• Inert atmosphere	• Not widely employed (for coal)	2950 – 3100	Indirect Drying
Pneumatic /	A vertical tube (Approximately 14 –	• Fast drying	• Spontaneous	3100	Direct

Flash Driers [149]	35 m). Coal is fed from the bottom and dried while being entrained to the top tube. Either air or combustion gases have been used	• Low outlet moisture content		combustion		Drying
Air Fluid Bed Driers [8, 33, 140, 149]	Using air, a bed of coal is fluidised to increase drying rates. Heating is supplied through the fluidization medium and through internal heating tubes	• Uniform temperature distribution • Fast heating rates	• Spontaneous combustion • Particle entrainment • Scaling issues	3100 – 4000	Direct Drying
Steam Fluidised Bed Driers [20, 26, 61, 62, 69, 84, 149-151]	Using a similar technique to air fluidized bed driers, with the substitution of steam as a fluidizing medium	• Inert atmosphere • Uniform heat distribution • Entrainment separation	• Higher corrosion rates • Scaling issues	450, 1000 – 1500	Direct and Indirect Drying
Hot Oil/Hydrocarbon Drying [20, 33, 149]	Coal is dried at high pressures with a hydrogen donor solvent, this technique results in higher quality coal as well as partially refined oil.	• Significantly upgrades calorific value	• Not Commercially Proven	Not Available	Dewatering
Hydrothermal Dewatering [8, 20, 22, 84, 149]	Moisture is removed by the expansion and expulsion of micro pores with the evolved CO_2 from the decarboxylation process	• No heat of vaporization required • High energy recovery	• Increased effluent treatment required	Not Available	Dewatering
Fleissner Process [20, 84, 149]	Drying lumps of coal under a steam atmosphere in a batch autoclave treatment, with moisture expressed as liquid water	• No heat of vaporization required • Product transportable	• Prohibitive particle size range • Continuous version not commercialised	130 –1750	Dewatering
Mechanical Thermal Expression (MTE) [20, 81, 84, 149, 152, 153]	Increasing pressure (1 to 10 MPa) at elevated temperatures cause non-thermal dehydrogenation	• No heat of vaporization required	• Increased effluent treatment required	1600 – 1800	Dewatering
Microwave Drying [20, 33, 70]	Using microwaves to preferentially excite and heat the water molecules in the coal	• Targeted energy reduces bed temperature	• Energy intensive • Not Commercially Proven	Not Available	Direct Drying
Solar Drying [20]	Direct sunlight over time allows coals to reach atmospheric equilibrium moisture content	• Low energy requirements	• Dependent on climate • Large land requirements	Not Available	Direct Drying
Densified Brown Coal [20, 33, 123]	Water-coal slurries are kneaded to 5-10 micron, releasing water from the pores. It is then dried to ambient conditions	• Low temperature • Storable • Transportable	• Product prone to breakage • Low drying rates	Not Publically Available	Direct Drying
Solvent Dewatering [20, 33, 107-109]	A solvent (such as DME) is passed over the coal, which is miscible in water. The solvent draws the water from the coal which is then separated. The water is removed together while the solvent is reused.	• Low energy requirements • Less organic contamination	• Not yet commercialised (lab scale only)	1100 – 948	Dewatering

Table 2.5 Summary and comparison of coal drying plants

Technology	Drying Company or Equipment Manufacturer	Plant Location	Maximum Product Capacity (t/h)	Final Moisture Content – kg(H_2O)/kg)	Calorific Values – initial to final (MJ/kg)	Years Operational
Steam Fluidised Bed Drying [58, 61, 71, 78] [20]	RWE Power	Frechen, GER Frechen, GER Niederaussem, GER Niederaussem, GER Hazelwood, AUS	16 t/h 28 t/h 90 t/h 110 t/h 70 t/h [P]	12% 10%	Not Available	1999 to Present 1993 to 1999 Not Available 2008 to Present Not Available
Steam Fluidised Bed Drying [20, 102]	Loy Yang Power	Loy Yang, AUS	55 t/h	10%	Not Available	1992 to 2003
Pressurized Fluidised Bed Drying [72, 154, 155]	Vattenfall	Schwarze Pumpe, GER	5 t/h	~ 6%-14%	Not Available	2008 to 2014 [P]
Low Temperature Fluidised bed Drying (DryFining) [4, 17, 78, 156-158]	Great River Energy	North Dakota, USA	2 t/h 75 t/h 4×125 t/h	Not Available 28.6% 29.5%	Not Available 14.4 to 16.5 MJ/kg	2003 to 2004 Not Available 2009 to Present
Drum Drier Indirect Steam heating Process [102]	Not Available	Indonesia (INA)	136 t/h	33%	Not Available	Not Available
Brown Coal Densification (Coldry Process) [58, 102, 122] [159]	Environmental Clean Technologies Limited	Latrobe Valley, AUS	1.2 t/h [A] 20.5 t/h [A, P]	10% 12%	8.4 to 24.6 MJ/kg	2004 to 2007 2014 [P]
Flash Heat Drying (Drying & Briquetting) [78, 102, 160-163]	White Energy Company Ltd	Cessnock, AUS Tabang, INA	11.2 t/h [A] 124.9 t/h [A]	Not Available ~ 6-7%	Not Available 18.0 to 25.6 MJ/kg (INA coal)	2008 to Present 2009 to Present
	White Energy and Datang International Power Company	East Kalimantan, INA Inner Mongolia, CHN	1000 t/h [A, P] 1250.1 t/h [A, P]	Not Available Not Available	Not Available Not Available	Not Available Not Available
Microwave Drying (DRYCOL) [58, 78]	DBA Global Australia	Powder River Basin, USA	25 t/h	12%	Not Available	2009 to Present
Microwave Drying [58]	CoalTek	Kentucky, USA	15 t/h	10%	20.45 to 25.59 MJ/kg	2007 to Present
High Velocity air grinding/drying[78]	Alligrator Mills Australia Pty Ltd	Not Available	0.15 t/h [P] 1.5 t/h [P] 3 t/h [P]	Not Available	Not Available	Not Available
High Velocity air grinding/drying[78]	LF Pumping Ltd, England	USA	250 t/h	3%	Not Available	Not Available
High velocity air grinding/drying [58, 78]	DevourX	Not Available	150 t/h	Not Available	Not Available	Not Available
Hydrothermal Dewatering[78, 164-166]	Exergen Pty Ltd	Beaconsfield, AUS	4 t/h	47% to 5% (47% to 26%) (61% to 48%)		2002 to 2005
		Latrobe Valley, AUS	50 t/h [P]	65 to 31 to 9 (<9%)	24.3 MJ/kg (Final)	2006 to 2008 2014
		AUS	200 t/h [P]	Not Available	Not Available	Not Available

			350 t/h [P] 4000 t/h [P]			
Hydrothermal Dewatering[78, 95, 167] (Micronised Coal) (UBC)	Ignite Energy Resources Pty Ltd	Somersby, AUS Not Available Not Available	0.95 t/h [A] 15.7 t/h [A] 156.2 t/h [A]	1.4% Not Available Not Available	10.0 to 32.7 MJ/kg	2009 to Present Not Available Not Available
Hydrothermal Dewatering (K-Fuel) [78] [102, 168, 169]	Evergreen Energy Inc USA	Fort Union, Wyoming, USA	93.7 t/h [A]	~ 12-13%	14.7 to 23.7 MJ/kg	2005 to 2008
Mechanical Expression [58, 78]	Aquex pty Ltd	Loy Yang, AUS	15 t/h	~50%	Not Available	Not Available
Mechanical Thermal Dewatering [58]	RWE	Niederaussem, GER	15 t/h (Dry)	Not Available	Not Available	Not Available
Mechanical Thermal Dewatering [58]	White Australia	Loy Yang, AUS	15 t/h 200 t/h [P]	Not Available	Not Available	Not Available
Mechanical Thermal Dewatering[20]	CRC	AUS	1 t/h 15 t/h [P] 100 t/h [P]	25%	Not Available	Not Available
Mechanical Thermal Dewatering	RWE	Niederaussem, GER	25 t/h	Not Available	Not Available	2002
Tube Dried Engrained Bed Direct Flue Gas Drying Process (HPU-06) [102]	Shenhua International Ltd.	Hulunbeier League, Inner Mongolia, CHN	187.5 t/h [A]	Not Available	Not Available	Not Available
Tube Dried Engrained Bed Direct Flue Gas Drying Process (HPU-06) [78]	Bayan Resources	Kalimantan, INA	125 t/h [A]	Not Available	Not Available	Not Available
Beijing Cleanstar Belt Drying Process [102]	Beijing Cleanstar Technology Development Co. Ltd	Inner Mongolia, CHN	34.2 t/h 114.2 t/h (feed) 342.5 t/h (feed) 433.8 t/h [P]	Not Available	Not Available 22.2 MJ/kg (product)	Not Available 2009 to 2010 2010 to Present Not Available
Vibratory Hot Air Belt Drying	Tangshan Shenzhou Co. Ltd.	Shenhua, CHN	450 t/h	20-50 % to 5-10% (70-80% Reduction)	4.2 to 6.3 MJ/kg	Currently in Operation
GTLE Process [58, 102, 170]	GTL Energy	Hazen	Not Available	80% Moisture Loss	Increase of Thermal Value 50%, 70% and 125% (AUS Coal)	Not Available
UBC Hot Oil Drying [102, 104, 171] [20, 104, 171]	Kobe Steel	Mataura Palimanan, INA Satui, INA	11.3 t/h [A] 0.13 t/h 25 t/h	Not Available ~ 8-0%	Not Available 18 to 25.5 /or 9.6 to 25.1 MJ/kg	Not Available 2001 to 2005 2008 to 2010
Brown coal densification and drying (LLD Process)[172, 173] [58]	La Trobe Lignite Developments (LLD) (Pacific Holdings)	Victoria, AUS	5 t/h 25 t/h [P] 50 t/h [P]	Not Available	Not Available	Not Available

[A] Converted from per annum to per hour, estimated on a 8000 hour operational year

[P] Plant is under construction or proposed, and not currently in operation

Table 2.6 Summary of fluidized bed drying models

Author	Model / Paper Name	Description	Major Characteristics	Equations
Agarwal et. al. [133, 174] **(2.1)**	Model for drying during fluidized bed combustion of wet low-rank coals	Using a receding surface model, an unsteady state heat model has been proposed using dimensionless cubic equation and solved by the Newton-Raphson method	• Drying during combustion • Fluidized bed – atmosphere not defined • Receding core model • Transient heat conduction model • Cubic equation governing drying curve, solved through the Newton-Raphson method • Can be correlated with further volatilization studies • Analysed for temperatures between 400 and 1400 K, confirmed for experimental data at 423 K	$B\phi_m^3 + (D-E-B)\phi_m^2 + (C-B-D)\phi_m + B - C + E - A \times F = 0$ $A: \left(\frac{T_e+L}{2}\right) - \frac{T_e + T_{s\,\theta=1}}{12} + \frac{Bi\phi_{ms\,\theta=1}(T_a-T_e)}{12(2\phi_{ms\,\theta=1} + Bi(1-\phi_{ms\,\theta=1})}$ $B: \frac{\phi_{ms} Bi(T_a-T_e)}{12(2\phi_{ms} + Bi(1-\phi_{ms})}$ $C: \frac{T_e+5T_s}{12}$ $D: \frac{T_e+T_s}{4}$ $E: \left(\frac{T_e+L}{2}\right)$ $F: \frac{\phi_{ms}^2 - 1}{\phi_{ms\,\theta=1}^2 - 1}$ $L: \frac{\lambda' C_0}{C_p}$ $\lambda' = \lambda + (T_e - T_0)(C_{pw} + C_p/C_0)$
Kovenskii et. al. [135] **(2.2)**	Modelling of Superheated-Steam Drying of Biofuel in a Fluidized Bed	Steam drying of biofuel using a single particle mathematical model for a using an energy and kinetic equation, and later applied to a particle bed. The model is then compared to shaped pinewood granules.	• Steam drying of biomass • Single particle drying calculated, then expanded to fluidized bed drying • Relys on three equations: Energy/Kinetic/Mass • Uses a distribution function for mean residence time in a fluidized bed	$\rho_s^2(c_s + \hat{c}_s c_{liq})\frac{\pi d^3}{6}\frac{dT_s}{dt} = \frac{\pi d^2}{4}\alpha_*(T_f - T_s) + \rho_s^0\frac{\pi d^3}{6}\left(q + (c_{liq} - c_f)(T_{cr} - T_s)\right)\frac{d\hat{c}_s}{dt}$ $\rho_s^0\frac{\pi d^3}{6}\frac{d\hat{c}_s}{dt} = \frac{\pi d^2}{4}\beta\rho_s^0\hat{c}_s$ Initial conditions: $t = 0, \hat{c}_s = \hat{c}_0 T_s = T_0$
Srinivasakannan and Balasubramanian [130] **(2.3)**	An Analysis on Modelling of Fluidized Bed Drying of Granular Material	Analysis of the use of Fick's diffusion and its role in fluidized bed drying models	• Used for an air fluidized bed, with no specific material • Fick's diffusion equation is used • The model is dependent on effective diffusivity, as the solid holdup is assumed to be a function of a simple particle opposed to bed geometry • Diffusion co-efficient on many parameters are empirical and varies by order of magnitudes • Author concludes caution is required when bases fluidized bed kinetics on the diffusion co-efficient	$\frac{C - C_e}{C_i - C_e} = \sum_{n=1}^{\infty}\frac{6Bi_m^2\exp(-\beta_n^2 D_{eff}\,t/R_s^2)}{\beta_n^2(\beta_n^2 + Bi_m(Bi_m - 1))}$ $\beta_n \cot\beta_n + Bi_m - 1 = 0$
Garnavi et. al. [175] **(2.4)**	Mathematical modelling of a continuous fluidized bed dryer	A numerical simulation based of two phase fluidization theory, this model no longer assumes bubble size uniformity	• Numerical simulation of fluidized bed drier based on two phase theory of fluidization • Influence on gas velocity, temperature, particle size and temperature reported • Numerically solved • Bubble diameter varies with bed height, changing heat and mass transfer rate • Used for an air fluidized bed, with no specific material	$\frac{dx_b}{dz} = \frac{\pi d_b}{8A_b u_b \rho_g}\{\rho_g K_{bc}(x_e - x_b)(2d_b + 4z\psi) - x_b\rho_g\psi[4(u_{in} - u_{mf}) + 3.6\sqrt{gd_b}]\}$ $x_e = \frac{\left(\frac{A_{bed}u_{mf}\rho_g}{v_{bt}}\right)x_{gin} + \rho_g K_{be}\widetilde{x_b} + \frac{6}{d_p}\delta(1 -}{\left(\frac{A_{bed}u_{mf}\rho_g}{v_{bt}}\right) + \rho_g K_{be} + \frac{6}{d_p}\delta(1 - \varepsilon_n}$

Fyhr and Kemp [137] **(2.5)**	Mathematical modelling of batch and continuous well-mixed fluidised bed dryers	A multi-particle model for a fluidized bed drier, the method divides the bed into layers with individual particles representing layers	• An air multi-particle fluidized bed model, used for zeolite and wheat • The bed is divided into discrete layers, where one particle represents an entire layer • A continuous fluidized bed replaces layers at intervals with fresh sample • A diffusion model is used for the single particle drying kinetics	$$\rho_s \frac{dx_p}{dt} = \frac{6}{d_p}\left(1 - x_p \frac{\rho_s}{\rho_w}\right)\delta\left(x_p^* - x_c\right)$$ $$\delta = \frac{h_p \rho_g D_g}{k}$$ $$\frac{dT_b}{dz} = \frac{1}{\rho_g A_b\left(u_{in} - u_{mf} + u_{br}\right)\left(Cp_g + x_b CP_{wv}\right)} \times \left(A_b + \frac{\pi}{2} z d_b \psi\right) \times \left\{\left[H_{be}(T_e - T_h) + \rho_g K_{be}\gamma(x_e - x_b)\right] - \rho_g\left(Cp_{wv}T_b + \gamma\right) \times \left(u_{in} - u_{mf} + u_{br}\right)A_b \frac{dx_b}{dz} - \rho_g\left[\frac{\pi}{2} d_b\left(u_{in} - u_{mf}\right) + \frac{5\pi}{8} u_{br} d_b^{1/6}\right]\psi\left[Cp_g T_b + x_b\left(Cp_{wv}T_b + \gamma\right)\right]\right\}$$ $$T_e = \frac{1}{\left\{\frac{A_{bed}u_{mf}\rho_g}{v_{bt}}\left(Cp_g + x_e CP_{wv}\right) + H_{be}\left(h_p - \delta\left(\bar{x}_p^* - x_e\right)Cp_{wv}\right.\right.} \left\{\frac{A_{bed}u_{mf}\rho_g}{v_{bt}}\left(Cp_g + x_{g_{in}} CP_{wv}\right)T_{g_{in}} + \left(x_{g_{in}}\right.\right. \left.\left.\left(h_p \bar{T}_p - \delta\left(\bar{x}_p^*\right.\right.\right. + \frac{S_{ex_{wall}}}{v_{bt}} h_{wall} T_{wall} + \rho_g K_t$$ $$\frac{dT_p}{dt} = \left(\frac{1}{\rho_s} - \frac{1}{\rho_w}x_p\right)\left(\frac{6}{d_p\left(Cp_p - x_p Cp_w\right)}\right)\left[h_p\left(T_e - T_p\right) - \delta\left(\bar{x}_p^* - x_e\right)\left(Cp_{wv}T_e - Cp_w T_p + \gamma\right)\right]$$ $$X_{out} = X_{in} - \frac{G(Y_{out} - Y_{in})}{\dot{m}} = X_{in} - \frac{GCp(t_{in} - t_{out})}{m}$$ $$\varphi = f(X_{out})$$ $$Y_{out} = f(\varphi, Y_{in}, t_{in})$$

Chen et. al. [67, 142] **(2.6)**	Steam-drying of coal	Modelling both a single particle and a fluidized bed fluidized bed drier under steam and air. Split into condensation phase and drying phase – with the single particle steam drying model shown	• Developed for ceramic particles, later applied to coal particles • Receding core model in a steam fluidized bed drier • 3 equations solved simultaneously: a mass balance, energy balance and moisture isotherm • Initially models a single particle, which is expanded into a fluidized bed • Has not been verified for coal • The temperature and moisture content predictions lag experimental results	$\left(\frac{Bi_h-2}{3}\right)(1-\phi_c^3)-\frac{Bi_h}{2}(1-\phi_c^2)=\frac{k_p Bi_h}{(\lambda_{vap}-W_{p,w,eq})}\int_0^t(T_{g,bed}-T_{p,c})dt$ $\frac{1}{3}(1-\phi_c^3)-\frac{1}{2}(1-\phi_c^2)=\frac{K}{v(W_{p,w,in}-W_{p,w,eq})\rho_p R_{o,p}^2}\int_0^t(P_{atm}-P_c)dt$ $P_c=P_{sat}(T_{p,c})\left(1-\exp\left[-2.53(T_{p,c}-273)^{0.47}W_{p,w,c}^{1.58}\right]\right)$ $m_{vap}=-3(W_{p,w,in}-W_{p,w,eq})\rho_p\phi_c^2\frac{d\phi_c}{dt}$ $W_{p,w,ave}=W_{p,w,in}\phi_c^3+W_{p,w,eq}(1-\phi_c^3)$ $T_{p,s}=\frac{Bi_h(1-\phi_c)T_{g,bed}+2\phi_c T_{p,c}}{Bi_h(1-\phi_c)+2\phi_c}$
Wang, Wei-Cheng [55] **(2.7)**	Laboratory investigation of drying process of Illinois coals	Calculating the coal moisture content, exit air temperature, exit relative humidity and exit specific humidity through an energy balance, mass balance and relative humidity	• Used in air fluidized bed drying • The governing equations use a conservation of mass for dry air and coal, conservative energy equations; relationship between specific humidity and relative humidity, relationship between relative humidity and coal moisture content • A Runge-Kutta method was used to calculate the drying parameters with time. • The same process is used in Gu, Feng [138] and Levy et. al. [139, 140]	$Q_{heater}-Q_{loss}=\frac{d(m_{dc}u_{sx})}{dt}+\frac{d(m_L u_L)}{dt}+(m_a h_a+m_v u_v)_2-(m_a h_a+m_v u_v)_1=m_{dc}\left[(C_c+\Gamma C_L)\frac{dT_2}{dt}+u_L\left(-\frac{\dot{m}_a}{m_{dc}}\right)(\omega_2-\omega_1)\right]+m_a\left[(T_2+\mathrm{T}_1)C_{pa}+\omega_2 h_{g2}-\omega_1 h_{g1}\right]$ $m_{dc}.\frac{d\Gamma}{dt}+m_a.(\omega_2-\omega_1)=0$ $\Gamma=\frac{m_L}{m_{dc}}$ $\omega_2=\frac{0.622\times\phi_2\times P_{g2}}{P-\phi_2\times P_{g2}}$ Coal dependent equations $\phi=f(\Gamma)$ $\phi=1162^*\Gamma^4-580.01^*\Gamma^3+61.878^*\Gamma^2+6.6736^*\Gamma-0.0855$ (Buckheart)
Gu, Feng [138] **(2.8)**	Coal drying in a bubbling fluidized bed	A good agreement between the experimental and theoretical results was seen using a method outlined in Wang, Wei-Cheng [55]	•	$Q_{heater}-Q_{loss}=\frac{d(m_{dc}u_{sx})}{dt}+\frac{d(m_L u_L)}{dt}+(m_a h_a+m_v u_v)_2-(m_a h_a+m_v u_v)_1$ $m_{dc}.\frac{d\Gamma}{dt}+m_a.(\omega_2-\omega_1)$ $\Gamma=\frac{m_L}{m_{dc}}$ $\omega_2=\frac{0.622\times\phi_2\times P_{g2}}{P-\phi_2\times P_{g2}}$ Coal dependent equations $\phi=f(\Gamma)$ $TLog(\phi)=-13227^*\Gamma^4+22882^*\Gamma^3-14723^*\Gamma^2+4336.4^*\Gamma-538.7$

Levy et. al. [139, 140] **(2.9)**	Kinetics of Coal Drying in a Bubbling Fluidized Beds	For a batch fluidized bed drier, Levy applied a model similar to Wang [55] and Feng [138]		$Q_{heater} - Q_{loss} = \frac{d(m_{dc}u_{sx})}{dt} + \frac{d(m_L u_L)}{dt} + (m_a h_a + m_v u_v)_2 - (m_a h_a + m_v u_v)_1 = m_{dc}\left[(C_c + \Gamma C_L)\frac{dT_2}{dt} + u_L\left(-\frac{\dot{m}_a}{m_{dc}}\right)(\omega_2 - \omega_1)\right] + m_a\left[(T_2 + \mathrm{T}_1)C_{pa} + \omega_2 h_{g2} - \omega_1 h_{g1}\right]$ $m_{dc}.\frac{d\Gamma}{dt} + m_a.(\omega_2 - \omega_1) = 0$ $\Gamma = \frac{m_L}{m_{dc}}$ $\omega_2 = \frac{0.622 \times \phi_2 \times P_{g2}}{P - \phi_2 \times P_{g2}}$
Heinrich et. al. [150] **(2.10)**	Studies of Steam Drying in a Fluidized bed	Looking at a fluidized bed drier, this model addresses the condensation phase along with the two separate drying phases	• Steam fluidized bed drying of aluminium particles • 3 separate phases: condensation, 1st drying period, 2nd drying period (falling rate) • Simultaneous differential equations • Assumes the entire drying process is based on mechanisms of heat transfer	Three separate equations are present depending on the condensation/drying phase modelled. Shown below is the equations for the first drying phase $\frac{\partial m_D}{\partial t} = -\frac{\partial m_D}{\partial z}dz - d\dot{m}_{UD}$ $\frac{d\xi}{d\tau_{II}} = \frac{m_p c_p\left(-NTU_{GP}(\overline{\Theta}_D - \Theta_P) + NTU_{pWGes}(\overline{\Theta}\right.}{m_{TS}c_p NTU_{GP}\left(X_{kr} - X_{hyg}\right)} \times \frac{1}{\left(\overline{\Theta}_D + (\vartheta_{Sat})/(\vartheta_{DEin} - \vartheta_{Sat}) + \left(\Delta h_{v,0}\right)/c_p\right.}$ $\Theta_{DAus} = \frac{NTU_{GP}\Theta_P + NTU_{GW}\Theta_W}{NTU_{GP} + NTU_{GW}} + \left(\Theta_{DEin} - \frac{NTU_{GP}\Theta_P + NTU_{GW}\Theta_W}{NTU_{GP} + NTU_{GW}}\right) \times exp[-(NTU_{GP} + NTU_{GW})]$ $\frac{d\Theta_P}{d\tau_{II}} = \frac{1}{NTU_{GP}}\left[NTU_{GP}(\Theta_D - \Theta_P) - NTU_{PWGes}\left(\Theta_p - \Theta_W\right)\right](1 - \Phi)$ $\frac{d\Theta_W}{d\tau} = \frac{m_P c_P}{NTU_{GP}m_W c_w}.NTU_{PWGes}\left(\Theta_p - \Theta_W\right) + NTU_{WG}(\overline{\Theta}_D - \Theta_W) - NTU_{WU}(\Theta_W - \Theta_U)$
(2.00)	equation reference for Appendix A1 nomenclature list			

Table 2.7 Summary of single particle drying models

Author	Model / Paper Name	Description	Major Characteristics	Equations
Woo et. al. [176] **(2.11)**	Master Curve Behaviour in Superheat	A lump drying model was developed for porous particles, which involves	• Single porous ceramic particle dried in steam • Lump drying • Master curve equation developed	$m_p C_p \frac{dT}{dt} = A_p h(T_a - \psi T_{sat}) - \frac{dm}{dt}\Delta H_{evap}$

	ed Steam Drying of Small Porous Particles	the development of a master curve		$\frac{dm}{dt}\Delta H_{evap} = \phi A_p h(T_a - \psi T_{sat})$
Komatina et. al. [134] **(2.12)**	A Model of Coal Particle Drying in Fluidized Bed Combustion Reactor	Using a shrinkage core mechanism the drying of a single coal particle was modelled and parametrically analysed	• Single particle air drying in a fluidized bed combustor • Shrinking core mechanism • Assumes complete drying at a temperature of 100°C	$\phi = 5.0572\exp(0.2747X_n^{0.3668}) - 5.0572\exp(0.1119X_n^{1.3002})$ $\rho.C_p\frac{\partial T}{\partial t} = \frac{1}{r^2}.\frac{\partial}{\partial r}\left(\lambda.r^2.\frac{\partial T}{\partial r}\right)$ $r = r_e \Rightarrow \lambda.\frac{\partial T}{\partial r} = \rho_w.q_d.\frac{dr_e}{dt}$ $r = R \Rightarrow \lambda.\frac{\partial T}{\partial r} = \alpha.A_c(T_b - T_s) - c_w.\rho_w.q_{sh}.\frac{r_e^2}{R^2}.\frac{dr_e}{dt}$ $q_d = \left[(1-c_w).C_{p,c} + c_w.C_{p,w}\right].(T_e - T_{in}) + c_w.q_e$
Olufemi and Udefiagbon [136] **(2.13)**	Modelling the Drying of Porous Coal Particles in Superheated Steam	Using a partial differential equation and solved through finite element analysis. The simulation considers transport and kinetics parameters as well as particle shrinkage.	• Steam drying of a porous coal particle • Transport/kinetic/shrinking parameters are considered • Uses partial differential equations • Receding core model • Finite element method was used in the calculation • +8%/-7% simulation variation	$\frac{\delta T}{\delta t} = -m\frac{\partial T}{\partial r} + \alpha\left\{\frac{1}{r}\frac{\partial T}{\partial r} + \frac{\partial^2 T}{\partial r^2}\right\}$ $\alpha = \frac{\kappa}{\rho c_p}$ $m = \frac{h}{\rho c_p}$ $\frac{\partial T}{\partial r} = 0\ for\ r = o$ $\kappa\frac{\partial T}{\partial r} = h(T_h - T)\ for\ r = r_p \neq r_f$ $q_w = \frac{hA_f(T_h - T_s)}{h_{lg}}\ r = r_f = r_p$ $q_w = \frac{\kappa A_f\left(\frac{\partial T}{\partial r}\right)}{h_{lg}}\ r = r_f \neq r_p$ $r_t = \sqrt[3]{\frac{3V_f}{4\pi}}$
Zhang and You [177] **(2.14)**	Experimental and numerical investigation of lignite particles in a fixed bed	Simultaneous modelling of macroscopic thin bed layer and microscopic thin particle layer drying, and verified through experiments	• Multiscale approach for coal particles dried in a fixed bed, with a acroscopic thin bed layer and a microscopic thin particle layer • Water split into free and bound water phases • Solved numerically • Can account for conditions such as stack height, temperature and velocity	$\frac{\partial(\rho_v^f)}{\partial t} = \frac{\partial}{\partial z}\left(D_{v.ef}\frac{\partial(\rho_v^f)}{\partial}\right) - \left(\frac{1}{\varepsilon_b}\right)\frac{\partial\left(V(\rho_v^f)\right)}{\partial z} + \left(\frac{6(1-\varepsilon_b)}{D_p}\right)\left(\frac{1}{\varepsilon_b}\right)h_m(\langle\rho_v\rangle_{sur}^g - \rho_v^f)$ $\frac{\partial(\rho_f C_{pf} T_f)}{\partial t} = \frac{\partial}{\partial z}\left(k_{a-eff}\frac{\partial(T_f)}{\partial z}\right) - \left(\frac{1}{\varepsilon_b}\right)\frac{\partial(\rho_f C_{pf} T_f V)}{\partial z} + \left(\frac{6(1-\varepsilon_b)}{D_p}\right)\left(\frac{1}{\varepsilon_b}\right)h_T(\langle T\rangle_{sur} - T_f)$ $T_f\big\vert_{h=0} = (T_f)_{in}$ $\rho_v^f\big\vert_{h=0} = (\rho_v^f)_{in}$
Kittiworrawatt and Devahastin [178] **(2.15)**	Improvement of a mathematical model for low – pressure superheated steam drying of a biomaterial	A liquid diffusion based model has been generated to simulate the transport of heat and mass during drying, creating a realistic mass transfer boundary conditions	• Predicts centre temperature and average moisture content of a steam dried carrot particle • 3 dimensional liquid diffusion model • Shrinkage is empirically modelled • Model implemented using COMSOL • Temperature rise is slower than experimental results	$\rho C_p\frac{\partial T}{dt} = \frac{\partial}{dx}\left(k\frac{\partial T}{dx}\right) + \frac{\partial}{dy}\left(k\frac{\partial T}{dy}\right) + \frac{\partial}{dz}\left(k\frac{\partial T}{dz}\right)$ $\frac{\partial X_f}{dt} = \frac{\partial}{dx}\left(D_{eff}\frac{\partial X_f}{dx}\right) + \frac{\partial}{dy}\left(D_{eff}\frac{\partial X_f}{dy}\right) + \frac{\partial}{dz}\left(D_{eff}\frac{\partial X_f}{dz}\right)$ With specific boundary conditions (only single example shown) $when\ T_s < T_{sat}, -k(\nabla T.n) = -L_v D_{eff}(\nabla X_f^1.n)$

				$D_{eff}(\nabla X_f^1.n) = E\left(\sqrt{\frac{M_{H_2O}}{2\pi R}}\left(\frac{P_{vap}}{\sqrt{T_s}} - \frac{P_{vap}}{\sqrt{T_{steam}}}\right)\right) - \dot{m}_{cond}$ $\dot{m}_{cond} = \frac{\bar{h}_{film}(T_{sat} - T_s)}{L_v}$
McIntosh, Malcolm J. [74, 75] **(2.16)**	Mathematical model of drying in a brown coal mill system	Developed for mill drying through single particle coal particle coal drying experiments. Later applied to a wide particle size distribution	• One dimensional air drying model for a single Yallourn brown coal particle • For mill drying systems • Scaled through applying a wide particle size distribution • Predicted moisture range is smaller than the experimental range	$MC = MC_o - \frac{M_g}{M_{wc}}\frac{(c_{pg1}T_{g1} - c_{pg}T_g)(1 + MC_o)}{(L_* + c_{pwv}T_g)}$ $MC_{i+1} = \sum_j MC_{i+1,j}\, W_j exp\left(-\left(\frac{1}{d_j^2}\right)\right)\int_{t_{i,j}}^{t_{i+1,j}} (Nu)E(- T_{wb})dt$
Hager et. al. [179] **(2.17)**	Modelling Steam Drying of a Single Porous Ceramic Sphere: Experiments and Simulations	A model developed on fundamental heat and mass equations. The method of lines was used to generate a set of ordinary differential equations for numerical analysis	• Models drying of 10mm ceramic spheres in steam • Using Darcy's law as a starting point • Does not consider initial condensation • Slightly under predicts drying temperature during transition from constant to falling drying rate regimes • Tortuosity is the only adjustable parameter • Mass transfer due to capillarity initial dominant eventually transitions into pressure driven gaseous flow due to internal pressures	$\frac{\partial X}{\partial t} = \frac{1}{r^2}\frac{\partial}{\partial r}\left[r^2\kappa\frac{\partial X}{\partial t}\right] + \frac{1}{r^2}\frac{\partial}{\partial r}\left[r^2\partial\kappa\frac{\partial T}{\partial t}\right] + \frac{1}{\rho_s r^2}\frac{\partial}{\partial r}\left[r^2\left[\frac{K_L}{\nu_L} + \frac{K_L}{\nu_G}\right]\frac{\partial P}{\partial t}\right]$ $\rho_s C_p\frac{\partial T}{\partial t} = \frac{1}{r^2}\frac{\partial}{\partial r}\left[r^2 k\frac{\partial T}{\partial r}\right] + \frac{1}{r^2}\frac{\partial}{\partial r}\left[r^2 L_V\frac{K_G}{\nu_G}\frac{\partial P}{\partial r}\right]$ $P = \varphi(X)P_{SAT}(T)$
Messai et. al. [29] **(2.18)**	Drying Kinetics of a Porous Spherical Particle and the Inversion Temperature	Using a macroscopic differential heat and mass equation, the model was tested in regards to permeability, diameter and operating variables	• Single particle drying in a steam and humid air atmosphere • Uses a macroscopic differential heat and mass equations • Solved numerically • Good accuracy, in some circumstances falling rate transition occurs later than observed in experimental results	$\langle\rho C_p\rangle = \frac{\partial\langle T\rangle}{\partial t} + \left(C_{pl}\langle\rho\rangle_l^l\langle U\rangle_l^l + C_{pl}\langle\rho\rangle_v^v\langle U\rangle_v^v\right)\nabla T = \nabla.\left(\lambda_{eff}\langle T\rangle\right) - \nabla H_v.\dot{m}_v$ $\rho_s\frac{\partial X}{\partial t}\left(\left(\left(\rho_l\frac{KK_{rv}}{\mu_1} + \rho_v\frac{KK_{rv}}{\mu_v}\right)\frac{\partial P_g}{\partial X} - \rho_l\frac{KK_{rl}}{\mu_1}\right) + \left(\left(\rho_v\frac{KK_{rv}}{\mu_v} + \rho_l\frac{KK_{rl}}{\mu_l}\right)\frac{\partial P_g}{\partial T} - \rho_l\frac{KK}{\mu_1}\right)\right.$
Looi et. al. [52] **(2.19)**	Drying kinetics of single porous particles in superheated steam under pressure	An assumption of a receding core is employed to numerically modelling previously found experimental data	• A single particle, receding core model is used for steam drying • Solved using the Crank–Nicholson method • For lignite particle, the model under predicts the drying rate, and has been attributed to particle cracking	$\frac{\partial T}{\partial t} = \alpha\left(\frac{2}{r}\frac{\partial T}{\partial r} + \frac{\partial^2 T}{\partial r^2}\right)\ \alpha = \frac{k}{\rho C_p}$ $\frac{\partial T}{\partial r} = 0\ at\ r = 0$ $k\frac{\partial T}{\partial r}\Big\|_{R_p^-} = h(T_a - T)\ at\ r = R_p \neq R_F$ $\frac{\dot{m_{evap}}}{A_F}h_{fg} = h(T_a - T_{sat})\ at\ r = R_F = R_p$ $\frac{\dot{m_{evap}}}{A_F}h_{fg} = k\left(\frac{\partial T}{\partial r}\Big\|_{R_F^+}\right)\ at\ r = R_F \neq R_p$

(2.00) equation reference for Appendix A1 nomenclature list

Table 2.8 Summary of thin layer drying models

Author	Model / Paper Name	Description	Major Characteristics	Equations
Midilli et. al. [132] **(2.20)**	A New Model for Single-Layer Drying	A new empirical model for single layer drying. Although there is no theoretical basis for the model it has been successfully applied for pollen and mushroom samples	• Single layer drying process in air • Verified for mushroom (not coal) • No theoretical basis • Author concludes more comparisons need to be carried out	$MR(a,b,k,n,t) = aexp(-kt^n) + bt$ Where the variables are in the form of: $(a,k,n,b) = x_1 + x_2\ln(T)$
Tahmasebi et. al. [143] **(2.21)**	Thermo-gravimetric study and modelling for the drying of a Chinese lignite	A range of thin layer models have been tested with the drying kinetics for Chinese lignite's have been described	• Applies many different thin layer equations to fixed bed drying of lignite • Found that Midilli-Kucuk equation to provides a best fit • Nitrogen atmosphere • Finds the correlation between specific tested variables i.e. particle size and drying temperature	$MR(a,b,k,n,t) = aexp\left(-k(t^n)\right) + bt$ Where the variables are in the form of: $(a,k,n,b) = x_1 + x_2(T) + x_2(T^2) + x_3(S) + x_4(S^2)$
Kim et. al. [54] **(2.22)**	Fluidized bed drying of Loy Yang brown coal with variation of temperature, relative humidity, fluidization velocity and formulation of its drying rate **(2.00)**	The development of drying rate formula initially derived from the Henderson model. The formula was modified depending on the relationship between humidity, velocity and temperature	• Air dried coal in a fluidized bed • The formulas developed are based on three variables • Derived from the Henderson model • Order of drying rate was found to be 0.25, and determined through trial and error	$\frac{dw}{dt} = -k(1-X)^n = -k\left(\frac{w-w_r}{w_i-w_r}\right)^n$ $k = [A_3(1).H + A_3(2)].[A_3(3).T + A_3(4)].V + [B_3(1).H + B_3(2)].[B_3(3).T + B_3(4)].$ Where A and B are experimentally derived constants With, T: temperature, H: relative humidity, V: velocity

equation reference for Appendix A1 nomenclature list

Chapter 3. Summary of Research Scope and Research Procedures

3.1. Research Objectives

The objectives of this thesis have been defined to address some of the gaps in knowledge identified and discussed in the literature review. These are aimed primarily in the characterization and comparison of steam fluidized bed drying of Victorian brown coal and include the drying, physical and chemical characterization of the dried coal.

These facets of characterization have been grouped into several different chapters, with each resolving an individual objective. The scope of this research is:

i. Investigation of the composition of water in Victorian brown coal

ii. Determination of the drying kinetics of Victorian brown coals in a fluidized bed – using steam and hot gas as a fluidization medium

iii. Analysis of the physical and chemical characteristics of fluidized bed and fixed bed dried Victorian brown coals

iv. Analysis of the combustion and gasification reactivity of dried coals

v. Development of a drying model to predict drying rate of a coal particle

The rationales for each objective are briefly discussed below.

i. Investigation of the composition of water in Victorian brown coal

While low rank coal has a large amount of water, the relationship and bond strength between water and coal varies between different ranks. While some information exists about the composition of water in Victorian brown coal, little information is available on how processing techniques affect this composition. Analysis of coals which undergo grinding as well as rewetting can allow greater understanding of coals properties. Additionally, comparisons between different types of coal, using Chinese lignite, will allow for further characterisation of coal, essentially determining how coal moisture varies depending on coal rank.

ii. Determination of the drying kinetics of Victorian brown coals in a fluidized bed – using steam and hot gas as a fluidization medium

Drying kinetics are essential for determining the optimum conditions for drying, as well as predicting coal drying in different scaled apparatus. While drying kinetics have already been investigated using different drying technologies, coals and conditions, relatively little information is publicly available on Victorian brown coal with steam as a fluidizing medium. Previous research [180] uses variable humidity but limited work using pure steam has been reported. The influence of system parameters on the drying of coals has also been established, but the relative change in drying ratios in different fluidization mediums has not been investigated.

To achieve these aims, two separate apparatus' have been constructed and operated. The first apparatus utilises a thermo-gravimetric system to determine the batch drying kinetics of Victorian brown coal. With a bed diameter of 0.06 m and a bed mass of 10 g the laboratory scale drying kinetics for drying temperature, fluidization velocity, particle size, fluidization medium and coal type is analysed. A second, larger fluidized bed with a diameter of 0.254 m and a bed mass of 3 kg is designed for both batch and continuous bed layouts and is used to compare the effect of temperature, fluidization medium and coal type.

An important aspect of the drying kinetics is the dried coal generated. The resultant coal is used in the analysis of the physical and chemical characteristics, in conjunction with this information the effect of a single variable can be linked to several different properties.

iii. Analysis of the physical and chemical characteristics of fluidized bed and fixed bed dried Victorian brown coals

The physical characteristics of coals can change as a result of drying, and may affect its usability. An aspect of brown coal drying which has not been thoroughly investigated is the change to the physical properties of coal. Surface area and porosity can change during the drying process and may affect properties such as moisture re-adsorption or reactivity towards combustion or gasification.

Particle attrition is also an issue during drying of brown coals. The vigorous nature of fluidization coupled with the comparatively weak structural strength of Victorian brown coals results in particle damage through attrition. The decrease in particle size increases elutriation and can change the fluidization characteristics of a fluidized bed. Understanding how the particle size changes as a function of moisture content, knowledge of the initial particle size and residence time is imperative to better control fluidized bed conditions.

A need exists for an accurate account of how the chemical composition, primarily oxygen functional groups, changes during the drying process. During the drying process, Victorian brown coals undergo a change in the chemical composition; the main changes in the coal structure is the formation or destruction of oxygen containing functional groups such as carboxyl, hydroxyl and carbonyl groups and can affect downstream processes such as combustion, gasification or liquefaction. Limited information is available on these changes in chemical composition necessitating further investigation.

As Victorian brown coals have a strong hydrophilic potential, fully dried coal (1 -2 % residual moisture) quickly re-adsorbs moisture if left exposed to atmosphere. The impact of the drying method on the re-adsorption potential requires examination as this has practical implications for the storage and combustion of coal, as increased moisture lowers the combustion efficiency. Understanding the impact of drying methods will allow better control of drying conditions.

iv. Analysis of the combustion and gasification reactivity for dried coals

Combustion and gasification processes are used for power generation and downstream processing such as chemical production. Understanding the applicability of specific drying techniques is essential for use of the dried coal in an industrial setting.

v. Development of a drying model to predict drying rate of a coal particle

Currently coal drying models present in literature still have a degree of uncertainty; with many models untested for coal a new drying model is required. However, developments in numerical approaches and the improvement of computing power has allowed Computational Fluid Dynamics (CFD) to be used in the design and scaling up of fluidized bed dryers. The objective is the formation of a model which remains simple enough to be easily implemented and applied in practice and simulation (CFD) software packages going into the future. In order to achieve this, a single particle model was developed using a master curve method for ceramic particles, to establish the initially suitability of the model. Once the model is found to correlate well with experimental data, the master curve method is expanded to coal particle drying.

3.2. Overview of the Study

This thesis is structured to provide a complete overview of the coal from as received condition, through to drying and drying kinetics, the physical and chemical properties of the dried coal and finally how the change in properties impact upon the use of coal in combustion and gasification processes. Throughout the thesis these properties are investigated for both air and steam fluidized bed drying to determine the impact of steam as a fluidization medium where compared to an established drying method.

The literature review provides an overview of the current state of coal drying in industry by providing a comparison and discussion of each drying technology. The broad nature of the literature has made it necessary for each experimental section to have its own literature review.

The initial literature review is followed by the Chapter 4 which investigates the composition of water in raw coal, analysing the effect of drying, re-wetting, particle size and coal type on the composition of water in coal. This enables a study of the initial moisture conditions within the coal which can also be linked to the drying time and particle size attrition in the subsequent chapters investigating the effect of drying on physical characteristics (Chapter 7).

Chapter 5 investigates the drying kinetics of Victorian brown coal in a variety of apparatus. The experiments will observe the drying time required to achieve equilibrium moisture content for Yallourn, Loy Yang and Morwell coals under varying conditions including the particle size, fluidization velocity and bed temperature, and comparing steam and air fluidized bed drying. A key for the investigation of scaling in a fluidized bed understands how the drying conditions affect the drying rate in two different scales.

The two proceeding chapters document the chemical and physical changes of the resultant coals as a function of drying methods and conditions. Due to the large number of samples, the physical and chemical characteristics are typically examined for one coal only. Usually Morwell brown coal, the effect of particle size, fluidization velocity, bed temperature and fluidization medium are taken to be consistent for all Victorian brown coals.

Chapter 6 investigates how the coal type, drying conditions and fluidization medium has the capacity to change the functional group composition, and can lower the coals effectiveness in combustion and gasification processes. To investigate this change, a combination of Fourier transform infrared spectroscopy, ultimate analysis and contact angle analysis has been

implemented to determine final chemical composition which is then linked to the differences in moisture re-adsorption in later chapters.

Chapter 7 examines the physical changes occurring in the fluidized bed during drying and will include several different aspects of coal structure. Analysis of the impact of drying method and conditions on the surface area and porosity of dried coal is tested on a representative Victorian brown coal. Further investigation of the change in physical properties shows the impact of fluidization on the particle size of the coal. The effects of residence time, moisture content and fluidization medium is sequentially analysed to create an accurate account of the particle size distribution change in both an air and steam fluidized bed.

Coal moisture re-adsorption (Chapter 8) is analysed for a range of coals and drying methods. Conclusions drawn from the differences in moisture re-adsorption will be validated from information gained in the physical and chemical changes observed in the preceding chapters.

In Chapter 9 a model has been developed for particles drying in a steam atmosphere. Using a lumped, master curve approach the model was initially developed for ceramic particles. Once validated the master curve method is transitioned into to Victorian brown coal particles. The master curve lump drying model has been developed to provide an easy method for predicting the moisture content in coal.

The final experimental chapter, (Chapter 10) characterises air and steam dried coals reactivity when tested in combustion or gasification conditions. This information correlates the kinetic parameters and change in physical and chemical properties to its impact on the resultant coals usability as fuel or chemical feedstock.

Conclusions from the study, along with its practical implications and recommendations for further work are presented in Chapter 11.

The relationship between individual chapters is shown in **Figure 3.1**. From the small scale apparatus and drying kinetics, the samples are used to analyse the physical, chemical, moisture re-adsorption and reactivity properties (1). The drying kinetics data is used to generate a basic drying model; however the findings from this model suggest the need for a more detailed single particle model (2). The composition of water in coal is found to have bearing on the physical breakage of coal during drying (3). Finally the chemical and physical

properties have been related to changes in the reactivity and the moisture re-adsorption of dried coal (4).

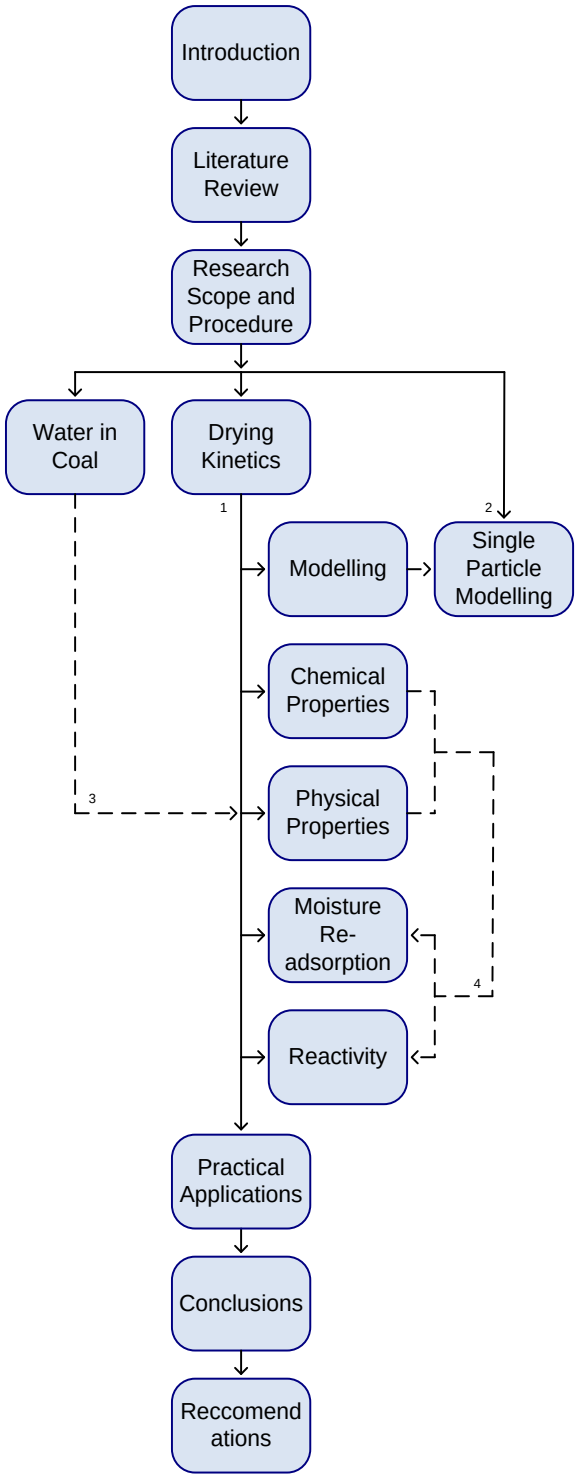

Figure 3.1 Thesis Structure

3.3. Research Procedure

A wide range of equipment and instruments were employed for the experimental part of the research presented in this thesis. The development of the drying kinetics required the design of specialised drying apparatus, while specific laboratory instruments were used for the determination physical and chemical characteristics.

This chapter overviews the operational methodology of the major apparatus' and brief justification of the design or operational choices made. This chapter will also discuss the choice of coals or drying conditions, as experimental runs using many of the analytical equipment require long analysis times or large quantities of samples, making full characterization unfeasible.

Only the major techniques for the coal characterization are fully discussed in this chapter due to the wide range of analysis used to characterise the coal. The operational and calculation methodology are discussed in the individual chapters, but details of the more detailed calculations are included in Appendix A2, A3 and A4.

This chapter briefly describes operational procedures for the following equipment and instruments used in this study:

- Continuous fluidized bed
- Batch thermo-gravimetric fluidized bed
- TA-Q100 differential scanning calorimeter
- PerkinElmer – Frontier FT-IR
- Netzsch STA449F3 Jupiter) thermo-gravimetric analyser (TGA)
- ASAP 2010 physisorption analyser
- Malvern Mastersizer 2000 particle size analyser
- Hyperion 2000 IR microscope and Bruker V80v FTIR spectrometer

Apparatus and techniques which were used, but not described in this chapter include:

- Ultimate analysis "PerkinElmer Series II CHNS/O Analyser 2400"
- Contact Angle "Powereach JC2000C"
- Moisture Analyser "Mettler Toledo HB43-S"

3.4. Choice of Coal and Apparatus

In this thesis, the choice of coal is based on the location, reserves and current use of the coal deposits. The majority of power generated in Victoria (90% [181]) uses coal from the Latrobe valley from three coal mines: Loy Yang, Yallourn and Morwell.

The proximate analysis showed in **Table 3.1** reveal similar overall moisture content, with low ash and low sulphur contents which typically characterises Victorian brown coal.

Throughout this thesis comparisons were carried out between Victorian brown coals and other coals, to compare the differences in properties such as moisture. In this case Chinese lignite has been chosen, as Chinese lignite have higher ash contents, lower volatile matter and lower moisture contents. Chinese lignite was also chosen for its potential in steam fluidized bed drying technology and because of increasing demand for coal drying in China.

Table 3.1 Proximate Analysis of low rank coals

Coal Type	Moisture $^{(wb)}$ (%)	Ash $^{(db)}$ (%)	(VM) $^{(db)}$ (%)	FC $^{(db)}$ (%)
Yallourn	64	5.0	45.7	49.3
Loy Yang	62	1.5	49.5	49.0
Morwell	60	4.6	41.0	54.4
Canadian	26	17.9	37.3	44.8
Shenhua No. 5	29	6.8	37.9	55.3
Shenhua No. 6	29	23.2	44.2	32.5

wb – wet basis; db – dry basis; VM – Volatile Matter; FC – Fixed Carbon

3.4.1. Thermo-gravimetric fluidized bed drying

An essential part of understanding drying mechanisms for individual materials is developing the drying kinetics. Use of a small scale apparatus will provide a fast and accurate indication of the drying kinetics. The smaller apparatus also allows easier analysis of resultant coal samples under variable conditions. The thermo-gravimetric apparatus is used for determination of fluidized bed drying kinetics and is distinctly different to many previous kinetic determination experiments which often relies on batch sampling systems [182]. The batch system requires the particles to be removed at specific time intervals for measurement of the moisture content, which results in low data resolution and creates added error due to product moisture loss during collection and analysis of the sample. A thermo-gravimetric method for sample analysis has recently been attempted in literature for a fluidized bed, but not for steam fluidized bed drying [54].

The recording method of the thermo-gravimetric apparatus is outlined in **Figure 3.2**. A suspended quartz vessel, with the coal sample, is placed in a three element split furnace. A hook, attached to the base of an electronic balance (Sartorius LA1200S) connects the vessel in the furnace to the electronic balance. The base of the vessel, which contains the gas line, is attached to the gas pre-heater by silicone tubing (as this allows for free movement of the reactor with no additional horizontal or vertical forces to act upon the reactor). This is an important consideration as the movement reduces apparatus error and offsets. For further details on the kinetics calculations through the buoyancy offset, please refer to Appendix A2.

Once attached the chosen fluidization gas (steam, hot air or hot flue gas) is passed through a preheater, allowing the gas to reach the desired temperature. The temperature of the fluidization gas determines the bed temperature, while the outer furnace is used to maintain the reactor wall temperature (at the same temperature), thus preventing condensation along the freeboard.

Drying occurs as the fluidization gas is passed through the sample bed. The loss of moisture is reflected by a drop of mass displayed on the electronic balance and is logged for determination of the kinetics. Once drying is complete the gas line is unhooked and the samples are removed from the vessel. When there is a significant amount of water in the fluidization gas (such as steam and flue gas) the sample is removed and stored quickly in a sealed container as exposure to the outside atmosphere may result in condensation (from the remaining steam in the reactor) and deviate from equilibrium moisture content.

3.4.2. Continuous feed fluidized bed drying

Information that can be used to make comparisons between smaller batch kinetics and the larger continuous kinetics is valuable to the scaling-up of fluidized bed drying. The apparatus used for the experiments are shown in **Figure 3.3**.

Apart from drying kinetics the larger scale apparatus is also used to observe how the effect of fluidization can change with the increase in size of the bed. A consequence of the increase in bed size could be the change in fluidization regime and bed properties, allowing parallel analysis with smaller scale experiments.

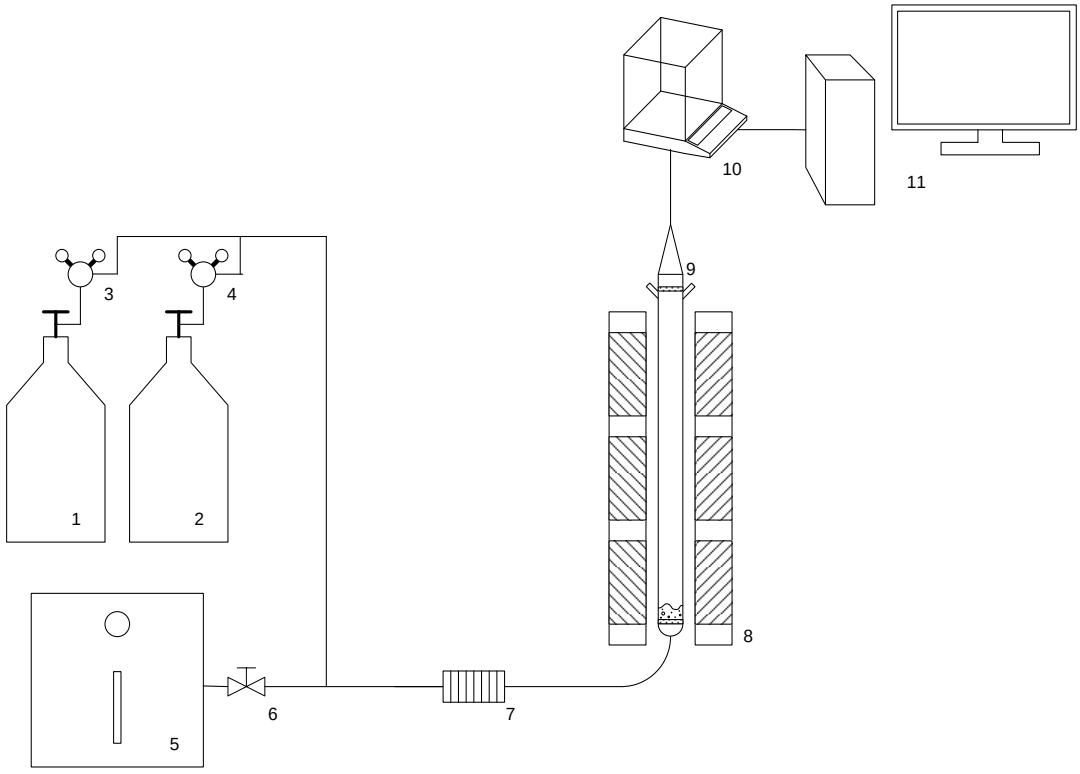

Figure 3.2 Thermo-gravimetric fluidized bed schematic

1. Nitrogen Cylinder; 2.Air Cylinder; 3.Nitrogen Regulator and Flow meter; 4.Air Regulator and Flow meter; 5. Steam Generator; 6. Steam Control Valve; 7. Gas Preheater; 8.Furnace; 9.Quartz vessel/reactor; 10. Electronic Balance; 11. Data Logging Computer

The apparatus was initially designed based on air fluidized bed driers using American lignite [139, 140]. The initial scale of the thermo-gravimetric bed of approximately 10 grams was extended to accommodate a bed mass of up to 5 kg. The fluidized bed has an internal diameter of 10 inches (0.254 m) with an outflow (and bed height) of 0.09 m above the distributor plate. The distributor consisted of a perforated plate with approximately 30% voidage. Below the distributor, steel wool was used to facilitate gas spreading and pressure differential from gas line to distributor plate. A 1 m viewing port is present to observe the fluidized bed, with a total of 2 m freeboard. The larger scale of the reactor and a different method of drying kinetic analysis necessitate a different operation of the apparatus to incorporate an initial dry bed.

The coal is dried by raising the fluidization medium (either air or steam) to the desired temperature and fed through the plenum chamber and distributor plate to fluidize the bed. The coal is fed through the bed using screw feeder system connected to a variable speed motor to control the flow of coal. As wet coal is added, the height of the bed increases

causing it to rise and overflow through the outlet and into the collection tray for analysis. Operating the fluidized bed at steady state over several hours allows steady state moisture content to be reached, with the equilibrium moisture content of the specific conditions determined. Residence time was calculated by the volumetric flow into the vessel and overall volume of the bed.

Figure 3.3 Continuous feed fluidized bed drier

3.4.3. Differential Scanning Calorimetry

Differential scanning calorimetry (DSC) provides a method to identify the different interactions between water and coal and is used in variety of different applications.

The interactions between water and coal vary depending on the coal type. The strength of the coal-water bonds can be quantified by the temperature water freezes at. This knowledge is important because strength of the coal-water bonds can help determine to most effective drying for different coal types based on moisture content and is further detailed in the literature review (Chapter 2).

Two major techniques were used in determining the water contents, known as – Differential scanning calorimetry (DSC) and hydrogen nuclear magnetic resonance (H-NMR). While

some authors suggest DSC typically overstates bulk water by up to 12% depending on assumptions [5], DSC remains a viable method for determining moisture composition.

A differential scanning calorimeter operates by uniformly increasing or decreasing the temperature of a sample while measuring the samples energy flow. A sudden increase or decrease in energy flow indicates a change in the particles properties, such as freezing point or glass transition.

The TA-Q100 DSC was used to control the temperature within the chamber by maintaining a balance between electric heating and liquid nitrogen, allowing for a steady decrease in temperature. The sample is placed on the chamber along with a blank cell (to generate a background heat flow for aluminium cell), with the receptacle sealed.

3.4.4. Fourier Transform Infrared Spectroscopy (Laboratory and at Australian Synchrotron)

Fourier Transform Infrared Spectroscopy (FT-IR) is used in the analysis of coal allowing the identification and change of the functional groups within a sample and therefore to understand the coal's chemical structure. Specific peaks at certain wavelengths along the FT-IR curve are collated and compared to obtain a semi-quantitative functional group value.

The laboratory FT-IR spectra were generated using the PerkinElmer Frontier FT-IR. Drying changes many of the functional groups within coal; in particular oxygen functional groups. The functional group composition has the capacity to affect properties such as the reactivity [183], moisture re-adsorption [184], combustion characteristics [185, 186] and hydrophobicity [187].

The disc is required to be transparent as the IR beam is required to pass through the disc within the wavelength region of interest. Literature and experimental trials show this is possible when coal is mixed in a ratio of 2:100 (or 0.04:0.2 g sample to KBr). The low ratio is due to the dark colouring of coal, and the dispersion required for the beam line to pass through. The coal particles are ground to distribute the coal evenly through the KBR. While grinding does not affect the chemical properties of the coal the surface functional groups (which are most prone to change) are diluted by the remainder of the coal. This may result in a reduced trend. The KBr/Coal discs are created by pressing the sample using an automatic (SPEX Sample Prep 3635) press, with a pressure of 10 bar for 10 seconds and then placed

within the FT-IR to analyse the sample. This method of FT-IR spectroscopy is presented in literature, where various coals and biomasses were used [188, 189].

Fourier Transform Infrared Spectroscopy (FT-IR) was also conducted at the Australian Synchrotron. The Synchrotron infrared analysis uses an in-situ method, allowing the IR spectra to be collected during drying. Compared to laboratory IR a benefit of the single particle analysis is the functional group content of the initial particle is always the same, reducing the variation and error from heterogeneous differences in the coal, and no longer requiring normalization required in literature [65, 188, 189].

Preparing the coal for analysis, the samples are pressed to ensure the particle is thin enough to provide adequate transition through the particle. The coal sample is placed between two diamond plates, which crush and flatten the coals as they are screwed together. The sample is transferred to the BaF2 slide and sealed in the sample stage, with the nitrogen used to purge any remaining air from the atmosphere. An optical microscope is used to select multiple particles for analysis, which is re-focused to provide sharp of the particles. With an aperture size of 10×10 μm, an analysis point is chosen at the edge of the particle (as this is the thinnest section of the particle). The temperature is increased and the spectrum is taken, similar to the method outlined in Kirtania et. al [190]. The accuracy of the microscope allows the same particle to be consistently analysed, making the spectra more accurate than laboratory FT-IR.

The analysis of the spectra uses OPUS 7.2 software, and undergoes several steps to allow the spectra to be directly comparable. At higher temperature drifting occurs and several steps are taken to reduced background signal from the Nitrogen flow, sample slide and aperture windows. Once the spectrum is collected a baseline is subtracted normalised to provide greater resolution of the peaks and reducing the noise. The heights of the peaks are then compared as the intensity of the peaks corresponds to the functional groups present in the sample.

3.4.5. Thermo-gravimetric Analysis

A thermo-gravimetric analyser (TGA) operates by increasing or decreasing the temperature of a sample, while continuously measuring the samples mass. Properties such as reactivity can be determined by correlating the mass change, temperature and operating atmosphere.

In this thesis, thermo-gravimetric analysis is used to study three properties: the combustion reactivity, ignition temperature and gasification reactivity of air and steam fluidized bed dried coal.

The combustion and gasification reactivity are measures of the dried coal's performance if used for traditional power generation or in gasification systems. The ignition temperature describes the coals suitability as a start-up fuel. As limited information of steam fluidized bed drying is publically available, analysis of the fluidization medium and bed temperature will help determinate the optimal conditions and is achieved by comparing the relative reactivity of the dry coal. The drying conditions may affect some of the coal properties (functional group composition and porosity) which in turn can influence the capacity for storage and transportation of the resultant coal.

To gain this data the dried coal were ground and sieved to a uniform particle size between 90 and 106 µm which is the particle size used in combustion boiler plants or entrained flow gasifiers.

3.4.6. Surface Area and Porosity

The surface area and porosity of the dried coal is an important part of the determination of the physical characteristics of the dried coal. It is important because these properties affect properties such as combustion or gasification reactivity and moisture re-adsorption potential.

Different drying techniques have the capacity to change [91, 93, 94] the surface area and porosity of the coals. The surface gas adsorption was measured using the ASAP 2010, which measures and calculates the surface area and pore volume of coals.

The Dubinin-Radushkevich method was found to characterise the surface area well [191-193]. While many different adsorption gases can be used for pore characterization, Carbon dioxide (CO_2) was used over Nitrogen (N_2) as the latter requires operation at lower temperatures causing pore destruction during analysis and resulting in less reliable data and smaller surface area.

3.4.7. Particle Size Distribution

The coal particle size in a fluidized bed will determine its fluidization properties and the extent of elutriation occurring from a bed. While it is generally considered that fluidized bed drying causes particle breakage during fluidized bed drying [20, 194], there is currently no available literature describing the breakage occurring in a fluidized bed for Victorian brown

coals. A Malvern Mastersizer 2000 was used to observe the particle size from this breakage. The instrument operates using a laser which is diffracted when striking particles flowing across it. The diffraction of the laser can be quantified with larger particles causing narrower angles of diffraction, while smaller particles have much wider angles. The Malvern Mastersizer 2000 has the capacity to accurately determine the particle size distribution with greater resolution for particle size fractions, a lower particle quantity requirements, higher weight measurement accuracy and smaller error than traditional sieving separation.

The physical operation of the Malvern Mastersizer 2000 is straight forward, with the calibration processes requiring greater attention. The Mastersizer can be operated in either an air dispersant or a liquid dispersant, however the Scirocco 2000 dry cell was determined to be the most applicable due to the particle size range (0.5-1.2 mm), density and hydrophobicity of the sample. The operating conditions required for accurate Mastersizer results and calibration method is found in Appendix A3.

Chapter 4. Water in Coal

This first chapter of experimental research analyses the composition and change in coal-water interactions focussing on the drying of coal, the composition of water within different coals and the effect of the coals state on the water composition.

Literature information on the composition of Victorian brown coal is not sufficient as variation within a coal seam means that properties such as moisture composition can be different. The determination of the moisture composition of the Victorian brown coal in this experiment will accurately characterise the coal, not only for water analysis but also in correlation with many other drying effects observed.

A study of coal-water interaction is carried out on three Victorian brown coals and Chinese lignite under a range of conditions. Firstly, water peak for each type of coal is separated, analysed and compared to literature values. The differences between coals will be discussed. The final two sections will study the effect of drying on the moisture composition when the coal is re-wetted or ground.

Differential scanning calorimetry has been used on a variety of coals, however little information is available on the types of water in Chinese lignite. Additionally, DSC analysis is not available on the effect of particle size, either through sieving or milling of the coal. While milling is a common process in the coal industry, its effect on the water content is not understood, and may impact downstream processes.

4.1. Water in Coal

4.1.1. Literature Review

Coals have water inherently present in them, with the amount depending on coal type. Victorian brown coals have approximately 60 – 65% water, resulting in problems for transportation, storage and usage. The water present in coal has a significant effect on the efficiency of coal combustion during power generation which means it needs to be dried before being efficiently utilized.

Water within coal does not conform to a single type. Typically such water is divided into three distinct groups [35, 195-197]: Bulk water, bound water and non-freezable water. These different forms of water vary depending on coal type, oxygen functional groups present and coal pore structure [198]. The bulk water (not shown in **Figure 4.1**) is weakly attracted to the coal structure, with properties similar to normal water (334 J/g) [199]. Bound water (**Figure**

4.1) occurs in smaller pore sizes, typically less than several hundred microns and exhibits different properties to the bulk phase [199, 200]. Bound water has a higher potential for secondary hydrogen bonding (formed between non-freezable water and a water molecule [199]) causing a lower freezing temperature [201]. Non-freezable water is characterized as water not otherwise observed in the freezing process, and interacts with the hydroxyl groups in the coal structure through hydrogen bonding [202]. Non-freezable water is the last form of water removed from the coal structure during drying, and is more difficult to completely remove due to the stronger bonding [197].

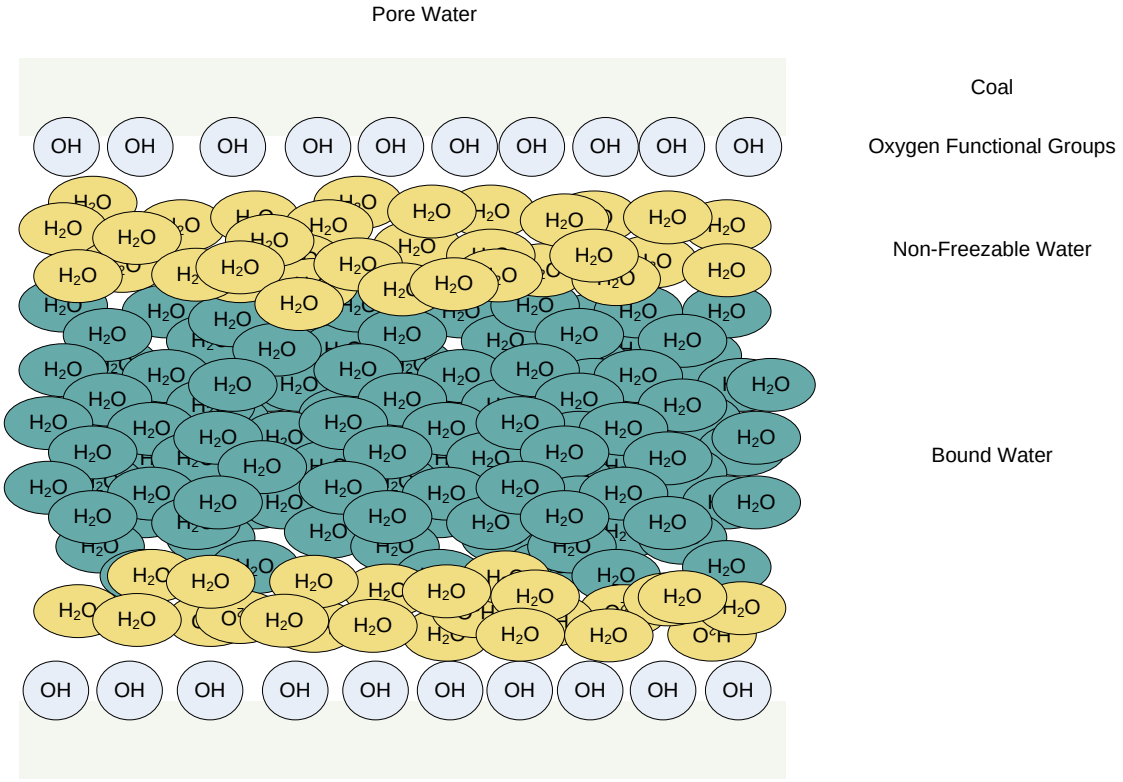

Figure 4.1 Composition of water present in coal pores [201]

There is a need to understand the water ratios in different coals and how they react to changing conditions. Since different water types correspond to different levels of bonding to the coal quantifying the different water ratios enables a more accurate prediction of the levels of required energy and time for moisture removal for each type of coal. Additionally, certain drying technologies such as vortex drying or mechanical dewatering cannot remove non-freezable water from coal, reducing their effectiveness for specific coals. A comparison between Victorian brown coals and Chinese lignite can be used to understand how water varies between coals.

Previous work analysing the water content has shown that bulk water freezes at approximately -15ºC (258K), while bound water freezes at -47ºC (226K) [203]. Standard DSC data shows the non-freezing water has no observable energy peaks occurring at temperatures as low as -150ºC (123K) and the assumption is made that beyond -150ºC (123K) no further freezing will be seen [204]. The standard method for determination of non-freezable water uses calculation by difference, based on the determination of bound water, bulk water and the overall moisture content of the coal.

Low temperature differential scanning calorimetry (DSC) has been used to investigate the breakdown of the water content by analysing the energy release corresponding to the phase change as the different types of water in coal freezes [195]. The enthalpy peaks measured are used to calculate the mass of water freezing and with moisture determination, the distribution of the three types of water can be found.

A complication in the attribution of bound water is the possibility of separate water/coal interactions between dissolved salts and H_2O creating apparent bound water peaks. Fei et al. [204] looked at the cause of the bound water peak occurring not through water-coal interactions but water interactions with NaCl and other dissolved salts in the coal's pore water [201]. However, the DSC bound peaks were still observed using acid washed coal, indicating bound water in coal is due to water coal interactions.

Recent work investigating water in coal using differential scanning calorimetry has found the composition of bulk (free) water and bound water for low rank coals, while also observing the non-freezing portion of water (previously undetected) using heating in DSC [205]. Using an Indonesian and a Chinese lignite Tahmasebi et. al. investigated the effect of moisture content and drying on water composition, and found that heat treatment effected both the pore structure and oxygen functional groups, results in a reduction of bound water re-adsorption.

4.1.2. Materials and Method

A range of Victorian and Chinese coals were chosen for DSC analysis with the experimental conditions shown in **Table 4.2**, with the coal properties in **Table 4.1**. Victorian coals are characterized by high moisture and low ash content, while Shenhua lignite has medium moisture and low to medium ash content. After preliminary analysis, Canadian lignite was used as a comparison with Chinese coals, as they contain similar overall moisture and ash content (**Table 4.1**).

Table 4.1 Proximate analysis of low rank coals

Coal Type	Moisture Content (wb) (%)	Ash Content (db) (%)	(VM) (db) (%)	FC (db) (%)
Yallourn	64	5.0	45.7	49.3
Loy Yang	62	1.5	49.5	49.0
Morwell	60	4.6	41.0	54.4
Canadian Lignite	26	17.9	37.3	44.8
Shenhua No. 5	29	6.8	37.9	55.3
Shenhua No. 6	29	23.2	44.2	32.5

wb – wet basis; db – dry basis; VM – volatile matter FC – fixed carbon

Differential scanning calorimetry (DSC) was conducted using the TA-Q100 at a scanning rate of 10ºC/min with 5ºC/min, 10ºC/min and 15ºC/min rates tested. The experimental data was conducted in duplicate to verify the results. Pure water was used to test the precision of the DSC technique for the enthalpy of fusion measuring the water mass and energy released to create a machine offset value. The operation of the apparatus is outlined in Chapter 3. The total moisture content was required as a part of the calculation for the non-freezable water and this was determined using a halogen moisture analyser. A drying temperature of 105ºC was used until a constant mass was obtained. To determine the effect of re-wetting the samples were equilibrated for 72 hours with a known water mass (30% wet basis) before DSC was run to simulate moisture re-adsorption through weathering and storage.

Table 4.2 Experimental parameters

Variables	Parameters
Coal Type	Yallourn, Loy Yang, Morwell, Shenhua No. 5, Shenhua No. 6, Canadian Lignite
Temperature Ramp Rate	-10 K/min
Minimum Temperature	-75°C
Particle Size	0 – 3.35 mm
Sample Mass	~4.2 mg
Re-wetting Moisture Content	30%
Equilibrium Time	72 hours

After obtaining the DSC data, the peak areas are integrated to find the overall energy change for freezing. This energy release is used with the enthalpy of freezing to find the mass of water frozen [201]. After accounting for both bulk and bound water, the remaining of water content is assumed to be non-freezable.

The method for calculating the water groups within the coal was based on experimental findings and the overall moisture content [206, 207].

$$MC.m_c = m_{bu} + m_{bo} + m_{NF} \quad (1)$$

Where: MC is the total moisture content, m_c is the mass of the coal, $m_{bu}m_{bo}$ and $m_{NF}$is the masses of the bulk, bound and non-freezable water respectively.

The calculations of m_{bu} and m_{bo} are found by:

$$m_{bu} = h_{bu}/h_{f,bu} \quad (2)$$

Where: h_{bu} is the experimentally determined enthalpy released during the bulk water freezing and $h_{f,bu}$ is the heat of fusion of the bulk water (334 J/g).

$$m_{bu} = h_{bo}/h_{f,bo} \quad (3)$$

Where: h_{bo} is the experimentally determined enthalpy released during the bound water freezing and $h_{f,bo}$ is the heat of fusion of the bound water (18 J/g) [203].

4.1.3. Analysis of the Water Peaks

Analysis of DSC trends between coal types show substantial differences between Victorian brown coals and Chinese lignite. In **Figure 4.2**, the difference between water types are highlighted. Morwell coal (top) is representative of Victorian brown coals and shows a significant trough at approximately -12ºC (255K) which corresponds to the loss of bulk water and is analogous to standard water freezing peaks. The loss in bound water mass is present at -47ºC (226K), but is not observable in **Figure 4.2** due to the scale of the curve and the relatively small masses present (compared to the large bulk water values). By contrast, all observable water in Shenhua lignite's are situated within the bound water region, taking place between -23ºC (250K) and -55ºC (218K).

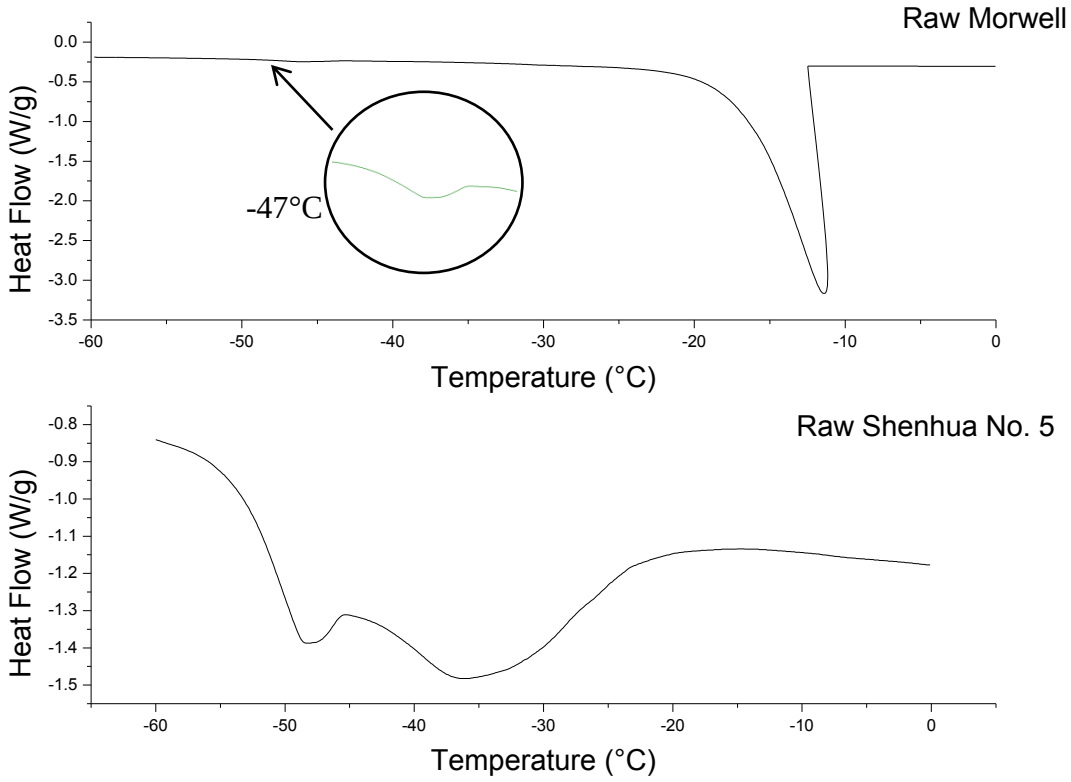

Figure 4.2 Comparison of Morwell and Shenhua coals DSC characteristics

Furthermore, the double troughs seen in the Shenhua curve (**Figure 4.2**) are not consistent with the small bound water trough found in the Victorian brown coals. To quantify the double troughs, curve fitting was employed using Origin Pro 8.0, with the double troughs broken into separate Gaussian curves (**Figure 4.3**). With little to no DSC data publically available for Chinese lignite's, parallels can be drawn between Shenhua lignite and American coals, which exhibit similar double bound water peaks [203]. In comparison, analysis of Canadian lignite shows that with similar ash and moisture contents, the bound water present is much smaller (**Table 4.3**). Although not shown graphically no secondary peak was observed.

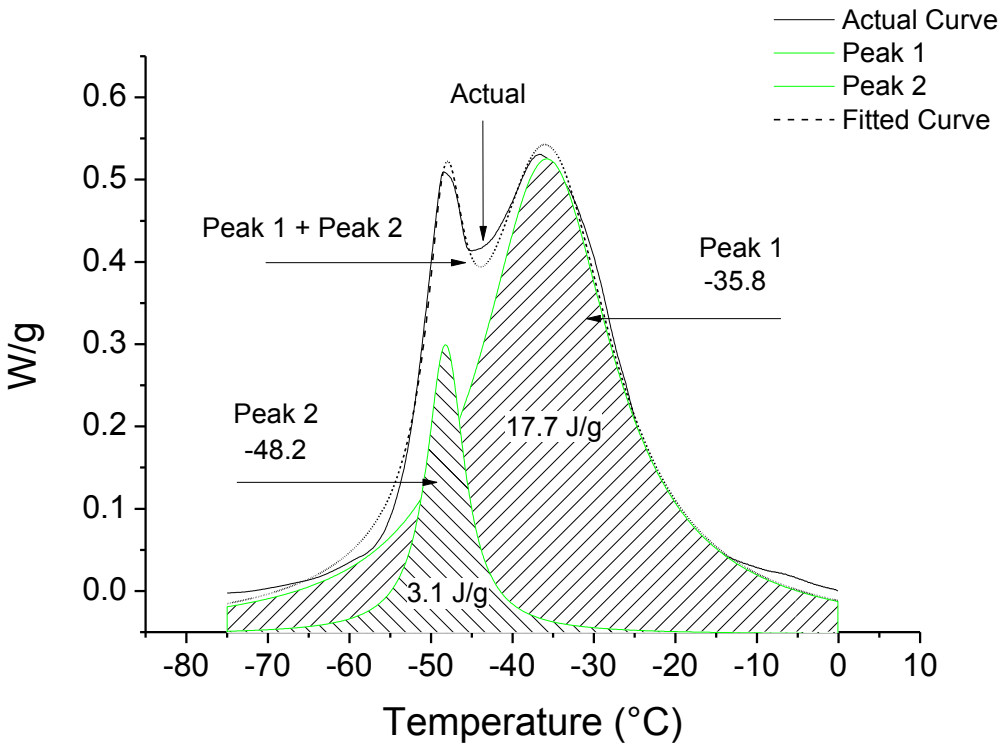

Figure 4.3 Mathematical curve fitting for individual bound water peaks in Shenhua Raw Coal

Curve fitting for the inverse heat flow, results for Shenhua coals show two separate peaks in the bound water region, with freezing temperatures and areas shown in **Figure 4.3**. The peaks were separated mathematically into their individual values; with the curve fitting software showing a correlation co-efficient (R^2) value of 0.9954, with a Chi-square value of 1.766×10^{-4}, indicating a close fit to original DSC curve. The resultant two distinct peaks occur at approximately -36ºC (237K) and -48ºC (225K), consistent with coals from South Bank, Beulah Zap and Wyodak [199, 203]. The cause of the two separate peaks was not identified in literature which attributes both as bound water and no further explanation. A reason for this trend may be a due to two different forms of bound water, strongly-bound and weakly-bound water, undergoing the same form of bonding, but to a stronger or lesser extent. Another possible reason is the different strength of bound water bonded to specific oxygen functional groups (typically hydroxyl, carboxyl, methoxyl and carbonyl groups [5]), with different groups causing different level of bonding.

The tables (**Table 4.3 – 4.6**) presenting differential scanning calorimetry presents data in two ways, the mass of water present shown in g/100g (coal), and the percentage based on total

water. This shows the mass of each component of water in wet coal, and the corresponding percentage of total water.

Table 4.3 Water composition of different low rank coals

Coal Type	Bulk Water		Bound Water		Non Freezable	
	$g(H_2O)^1$	$(\%)^2$	$g(H_2O)^1$	$(\%)^2$	$g(H_2O)^1$	$(\%)^2$
Yallourn	41.8±3.1	(70.5)	6.6±2.9	(11.1)	10.9±5.3	(18.4)
Morwell	33.1±4.1	(55.6)	6.4±2.6	(10.8)	20.1±4.9	(33.6)
Loy Yang	30.5±2.8	(55.4)	2.7±0.6	(4.9)	21.9±2.9	(39.7)
Shenhua No.6	0±0	(0.0)	7.4±7.1	(25.4)	21.8±4.6	(74.6)
Shenhua No. 5	0±0	(0.0)	8.7±3.9	(29.9)	20.3±3.9	(70.1)
Canadian	0.6±0.4	(2.5)	0±0	(0.0)	25.2±0.4	(97.6)

1 g(H2O)/100g(coal); 2 Percentage of water present

Table 4.3 shows the experimentally determined difference in water composition of various coals, primarily between Shenhua and Victorian brown coals. Victorian brown coals comprises mainly of bulk water with significant amount of non-freezable water. In multiple studies by Norinaga et. al. (1998) [203] Victorian brown coals have 7 to 26 % bound water (on a total water % basis) and is similar to that reported by Fei et. al. (2005) [204] who found 16% to 29% bound water. The differences may be attributed to the different batches of coal used in the studies. The values which we have obtained show a variation for Victorian brown coal of between 4.9 to 11.1 % of the overall moisture content. While these values are lower than given in literature the variation in coal composition (due to seam position and the heterogeneous nature of coal) may account for these differences.

Shenhua No.5 and Shenhua No.6 are similar coals, mined from the same region. While they maintain many similar properties, the major difference is their ash content. They are used to illustrate a consistent trend between the Shenhua lignite's, with similar double peaks and percentage of bound water

Victorian brown coal has a larger overall water content than Shenhua lignite; however the composition is also different. Victorian brown coal has a smaller quantity of bound water and much higher quantity of bulk water (which is not present the Shenhua lignite). Canadian lignite has a similar moisture and ash content to Shenhua lignite, but almost all of the water resides is in the non-freezable form. This indicates that the moisture composition is not related to the overall moisture content or ash content.

4.1.4. The Effect of Physical Changes on Water Composition

Variation in particle size and the effect of mechanical milling on particle size is investigated to understand the physical changes to coal and how that affects the moisture content. Morwell coal is used to represent Victorian brown coals shows no variation in water composition with decreasing particle size through sieving (**Table 4.4** and **Figure 4.4**). As the different size fractions maintain a similar level of elemental ratios and have undergone identical conditions up until the point of sieving, any change in moisture ratios at this stage would be as a direct result of the storage, milling and separating conditions encountered. Smaller size fractions show a decrease in the bulk water but are not indicative of a true composition change as there is correspondingly smaller moisture content in the particles which are reflected in the constant mass values of non-freezable and bound waters. This indicates during the sieving process to obtain this size range moisture is stripped, with the moisture removed classified as bulk water.

Table 4.4 Water composition in different particle sizes

Size Fraction	Bulk Water		Bound Water		Non Freezable		Total Moisture
(µm)	$g(H_2O)^1$	$(\%)^2$	$g(H_2O)^1$	$(\%)^2$	$g(H_2O)^1$	$(\%)^2$	(%)
0 - 106	16.7±3.2	(38.5)	8.3±2.4	(19.1)	18.5±5.6	(42.4)	43.5
106 - 250	27.5	(48.4)	5.4	(9.5)	23.9	(42.1)	43.5
250 - 1180	32.9±2.5	(54.9)	5.8±0.6	(9.7)	21.2±3.1	(35.4)	56.7
1180 - 2000	33.1±4.1	(55.6)	6.4±2.6	(10.8)	20.1±4.9	(33.6)	59.9
2000 - 3350	35.5±2.3	(59.2)	4.9±0.3	(8.1)	19.6±2	(32.7)	59.9

1.g(H2O)/100g(coal); 2 Percentage of water present

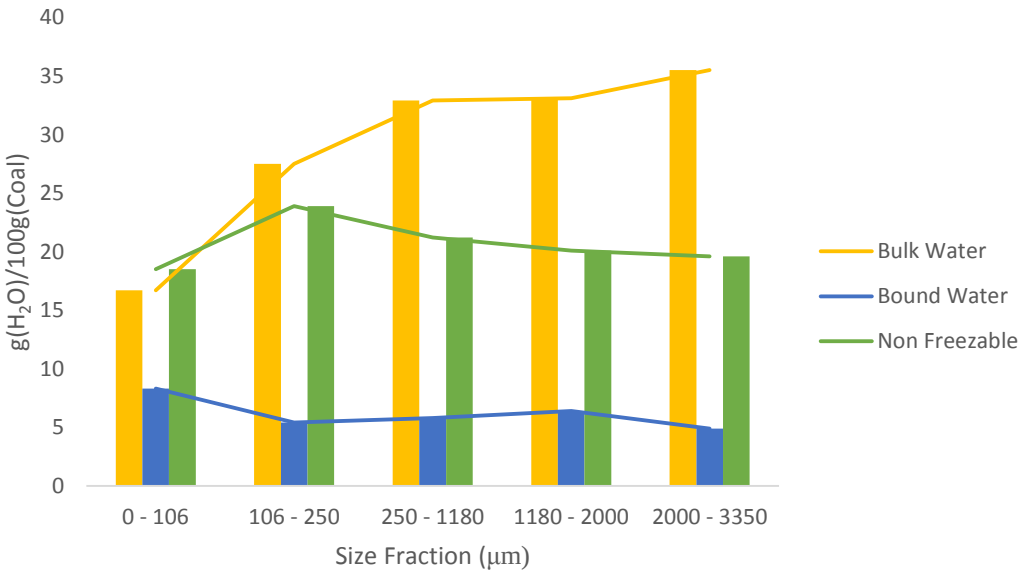

Figure 4.4 Water composition in different particle sizes

Morwell coal was again used to analyse the effect of milling on water content by comparing 1.18 -2.00 mm sized particles to that milled from the same batch (using a mortar and pestle). **Table 4.5** highlights the difference between the original and milled coal and indicates an increase in bound water. While there was also a reduction in overall moisture content of the coal, the percentage of bulk water within the sample remains consistent. However, a shift occurs with the reduction of non freezable water and the increase of bound water. While the change is approximately 8% of the total water composition, the change in mass shows the increase in bound water is within the variation limits of the coal.

Table 4.5 The effect of milling on raw Morwell coal

Milling	Bulk Water		Bound Water		Non Freezable		Total Moisture
	$g(H_2O)$[1]	(%)[2]	$g(H_2O)$[1]	(%)[2]	$g(H_2O)$[1]	(%)[2]	(%)
Morwell	33.1±4.1	(55.6)	6.4±2.6	(10.8)	20.1±4.9	(33.6)	59.9
Milled Morwell	25.2±2.1	(53.4)	9.0±1.3	(19.1)	13.0±1.0	(27.6)	47.2

1.g(H2O)/100g(coal); 2 Percentage of water present

In similar tests with Shenhua lignite, a larger change is observed (**Table 4.5**). Similar to Victorian brown coal, a decrease in total moisture is observed from approximately 29% to 25%. However, a large change in the bound water was present. The bound water composition reduces from 30% to 5% and, unlike the Victorian brown coal, has a large enough mass change well outside the variation of the samples. Continually, an increase in non freezable moisture mass is observed in the milled sample. The decrease in overall bound water may be due to, in part, the changes in the DSC peak structure.

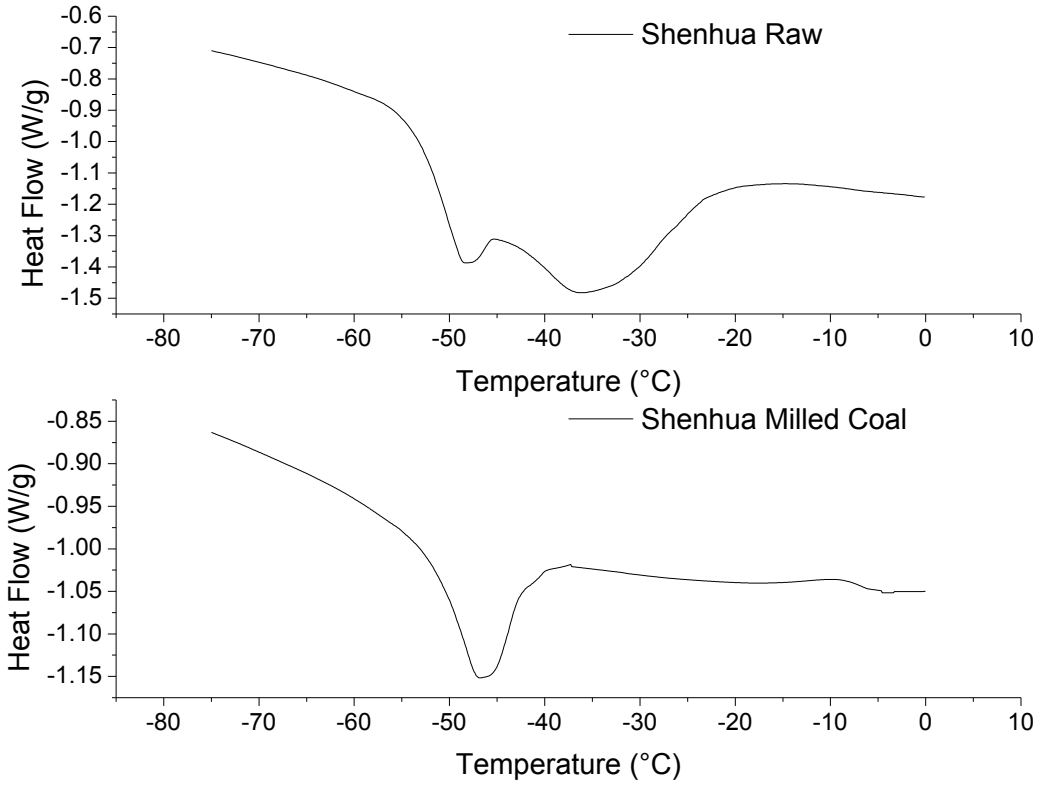

Figure 4.5 Comparison between DSC results of as-received and milled Shenhua lignite

The double peak shown in the initial Shenhua lignite sample was no longer observed (**Figure 4.5**). The removal of the peak may be due to the milling process, as the force of milling causing pore destruction resulting in the loss of this peak. Another reason may be the transition between one form of water bonding to another, resulting in the increase to one peak, while the other peak is no longer present. The transition to the latter peak would indicate a larger percentage of stronger bound water, requiring longer drying times and more energy to remove the same amount of water.

Table 4.6 The effect of milling on raw Shenhua lignite

Milling	Bulk Water		Bound Water		Non Freezable		Moisture
	$g(H_2O)^1$	$(\%)^2$	$g(H_2O)^1$	$(\%)^2$	$g(H_2O)^1$	$(\%)^2$	(%)
Shenhua No. 5	0.00	(0.00)	8.68±3.92	(29.94)	20.3±3.92	(70.06)	29.0
Milled Shenhua No 5.	0.00	(0.00)	1.11±0.18	(4.40)	24.06±0.18	(95.60)	25.2

1.g(H2O)/100g(coal); 2 Percentage of water present

The current hypothesis is that milling strips a portion of moisture away (resulting in the lower moisture values) while pushing water into the coal pore structure causing the pores to open and allowing greater opportunities for bound water to form. This result explains the decrease in bulk water in Victorian brown coals. In Shenhua lignite, the decrease in bound water and increase in non-freezable water would signify water is interacting more strongly with the oxygen functional groups, forming a greater quantity non-freezable water.

4.1.5. DSC of Dried Coals

At equilibrium water absorption of dried coal will be in the non-freezable form, regardless of the method used for drying or coal type. This is shown using Morwell coal as an example in **Figure 4.6**. No remaining water was found in either the bulk or bound water for coals samples dried by vacuum, oven or atmosphere. The residual moisture content varies from 2 to 7% depending on drying method and coal type. This result is expected because non-freezable water being the last water to be removed due to stronger hydrogen bonding, so any remaining water after drying would naturally not be seen through DSC's temperature range of -80^{o}C (193 K).

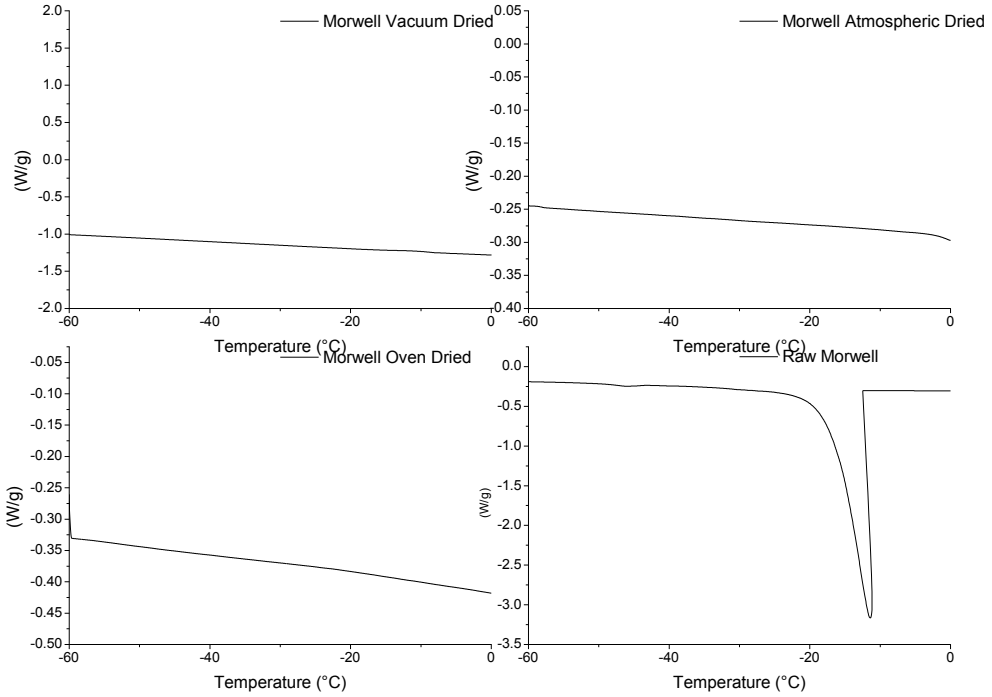

Figure 4.6 Typical DSC curves for Morwell Coal

4.1.6. DSC of Re-wetted Coal

Analysing the effect of re-wetting on coal, emphasis was placed on the change in bound water during the rewetting process. Chinese Shenhua Lignite was chosen over Victorian brown coals because of the larger, more quantifiable amounts of bound water. This allows for better, more accurate determination of the changing trends. The percentage of bound water found in the Victorian brown coals would not be enough for any trend to be determined.

Table 4.7 The effect of re-wetting of Shenhua coal

	Bulk Water		Bound Water		Non Freezable		Total Moisture
	$g(H_2O)^1$	$(\%)^2$	$g(H_2O)^1$	$(\%)^2$	$g(H_2O)^1$	$(\%)^2$	(%)
Raw Coal	0.00	(0.00)	8.68±3.92	(29.94)	20.3±3.92	(70.06)	29.0
Re-Wetted	8.6±2.27	(28.67)	0.47±0.52	(1.56)	20.93±1.76	(69.76)	30.0

1.g(H2O)/100g(coal); 2 Percentage of water present

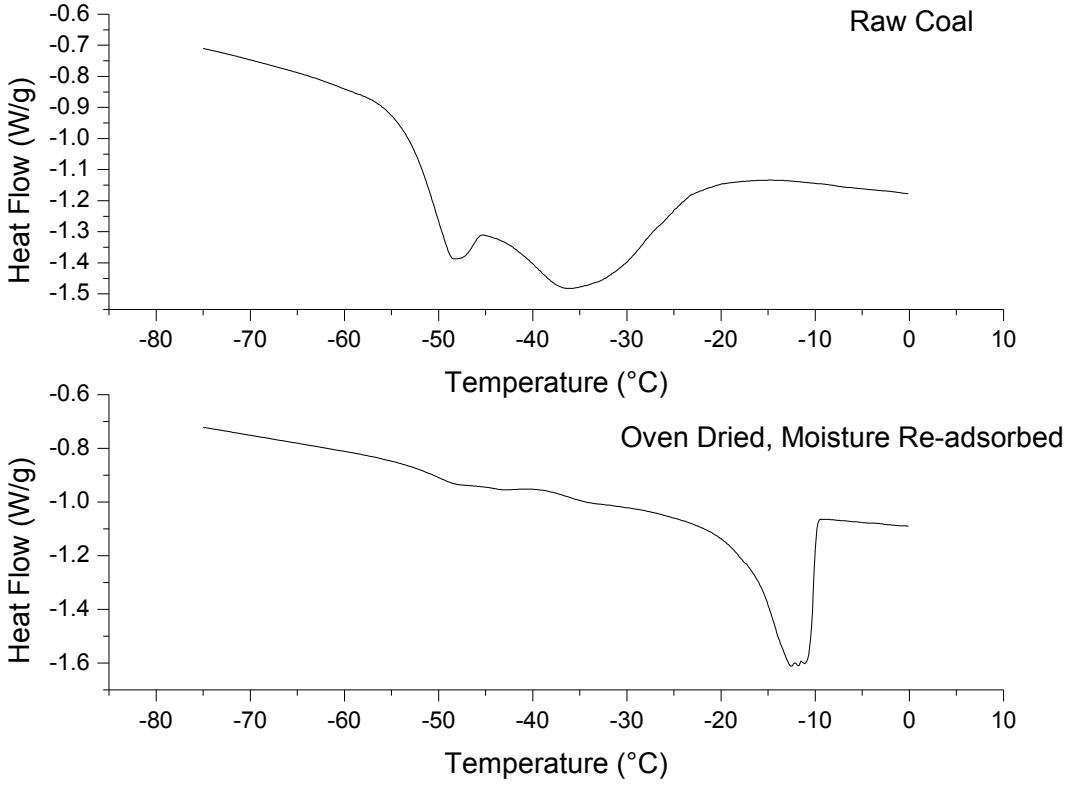

Figure 4.7 Comparison between re-wetted and as received Shenhua lignite

Water introduced to dried Shenhua lignite to recreate the same water content as the initial raw coal (30%, wet basis) show a shift in how the water is bonded to the coal. In **Figure 4.7**, the comparison between raw Shenhua lignite and re-adsorbed lignite highlight a change to

retained moisture from bound water to bulk water. While the bound water occurs in lesser amount (**Table 4.7**) in the re-wetted coals, the majority of water is in the form of non-freezable and bulk water. The non-freezable water mass remains the same in both forms of coal (**Table 4.7**) indicating that non-freezable water returns to its previous levels after drying. Bound water does not reform and is no longer present (in the same scale) it is attributed to damaging of the 100 μm pore sizes, which is alluded to in Mraw et al. [208]. Previous findings by Svabola et al. [198] show at low pressures 'primary site adsorption' (oxygen functional groups, non-freezable water) absorb majority of reintroduced water, and this is consistent with the moisture re-introduction into Shenhua lignite.

4.2. Conclusions

The important findings for this chapter are summarised:

- The water in Victorian brown coal has a different breakdown than Chinese lignite, with larger amounts of bulk, and smaller amounts of bound water present
- Chinese lignite has a double peak within the bound water region (-36 and -48°C), which has been attributed to different strength bound water. This double peak is not present on the Victorian or Canadian coal tested
- Sieved coal shows no difference in the water masses of bound and non-freezable water. Any loss in moisture is due to the stripping of the bulk water
- Milling Chinese lignite shows a drop in bound water and an increase in non-freezable water mass. This would suggest milling of Chinese lignite should be conducted after drying to prevent non-freezsable water transition and to reduce the required energy for water removal
- Milling Chinese lignite also shows one of the bound water peak disappears
- The rewetting of Chinese lignite shows the non-freezable water returns to previous levels, however the bound water does not return to previous levels. This indicates that rewetted Chinese lignite would require less energy to dry compared to the original lignite.

Chapter 5. Drying Kinetics

Chapter 4 explained that water composition of Loy Yang, Yallourn and Morwell brown coal is similar to each other. The next step for this thesis is analysing the rate at which drying occurs.

This chapter will primarily examine the characteristics of two specific drying processes, steam fluidized bed drying (SFBD) and air fluidized bed drying (AFBD) using a range of conditions that can affect drying time as a function of coal type, drying temperature, fluidization velocity, fluidization medium, initial particle size and bed size. This information on drying conditions can be optimised for energy efficiency and modelled to provide drying data. Furthermore the drying kinetics of coal samples will provide a basis for the analysis of their physical and chemical characteristics (Chapter 6 and Chapter 7).

This drying kinetics chapter presents information in separate sections: the drying kinetics in a batch thermo-gravimetric analysis (small apparatus), the drying kinetics in larger fluidized bed, both batch and continuous, along with a comparison between different scales of the apparatus, with the effect of drying conditions and fluidization on scaling. A scaling factor is also created to describe the effect of bed size on drying time. The relationship between these experiments is shown in **Figure 5.1**.

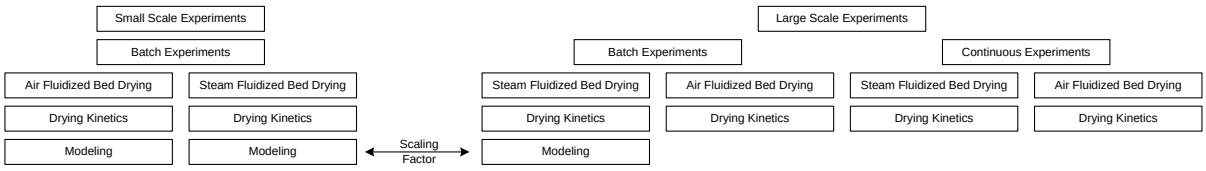

Figure 5.1 Chapter 5 experimental flowchart

Information from this chapter is present in the publication: D. Stokie, M.W. Woo, S. Bhattacharya, Comparison of Superheated Steam and Air Fluidized-Bed Drying Characteristics of Victorian Brown Coals, Energy & Fuels, 27 (2013) 6598-6606. [209]

5.1. Drying Kinetics

5.1.1. Literature Review

Steam fluidized bed drying (SFBD) was originally developed at Monash University by Professor Owen Potter and in the 1970's [26, 57]. Although initially envisioned as a single stage fluidized bed, many variations have resulted in trying to increase drying efficiency.

This includes the development of a multi-level cascade system [33] and implementation of internal waste heat utilization systems (WTA) at RWE facility in Germany [61]. Steam fluidized bed drying can also be integrated into a power station by using low grade steam, resulting in a cycle which has comparable or lower energy requirements for moisture removal on a wt.(H_2O)/wt.(Coal) basis [8, 33]. Compared to steam fluidized bed drying, air fluidized bed drying is more susceptible to spontaneous combustion, especially when drying highly reactive coals such as Victorian brown coals. However, it has been successfully applied at the Great River Energy site, with typical moisture reduction from 38% to 29% [4, 157, 158].

Currently neither superheated steam nor air fluidized bed drying technology are commercially utilized for Victorian brown coal. A small steam fluidized bed plant was opened in 1992 at the La Trobe Valley, Victoria to supply auxiliary fuel for the Loy Yang A Power Station. Designed by Rheinbraun and Lurgi, the 150,000 tonnes per year (dry coal) plant used steam supplied from Loy Yang A Power Station as a fluidization medium. Although the plant ran successfully, the facility was closed in 2003 because it was perceived to be expensive compared to the available alternatives such as coal briquettes or natural gas [20].

While some information is available on air fluidized bed drying kinetics [51, 54, 140, 210] there is little information about kinetics using steam as a fluidization medium for drying of Victorian brown coals. Work undertaken by Kim et. al. [54] observes the effect of humidified air (up to 40% relative humidity) on drying rate. As little experimental information is available, modelling equations have been used to approximate the drying of a particle or fluidized bed under a steam atmosphere [67, 142, 150, 176, 211, 212]. However these equations were primarily used for ceramic particles, fixed bed or single particle drying.

While the drying kinetics have been previously researched for a variety of different parameters, including the fluidization medium, coal type and bed pressure the specific details of the research has been outlined in detail in the literature review in Chapter 2. The literature review concludes that the application of steam fluidized bed drying for Victorian purposes is limited, as information on drying kinetics, chemical composition, physical and structural changes as well as resultant combustion properties are not available. Investigating these factors will provide a greater understanding of the practicality of fluidized bed drying of Victorian Brown coals [51] which will enable scaling up of fluidized bed drying process for Victorian brown coals and eventually aiding efforts to commercialize the technology.

This chapter addresses the issue of drying kinetics by investigating key differences between air fluidized bed drying and superheated steam fluidized bed drying. This is achieved by examining the effect of initial particle size, fluidization velocity and bed temperature on drying times. These values are then used to compare the differences in drying times of air and steam fluidization mediums to determine which model can best represent the drying of Victorian brown coals under both air and steam fluidization, that can be used for scaling up purposes in the larger apparatus. By combining information obtained in the smaller and larger apparatus, a scaling factor was created to describe the change in drying kinetics according to bed size.

A more in depth literature review describing the current status of both air and steam fluidized bed drying, and analysis of drying conditions and kinetics can be found in Chapter 2.

5.2. Small Scale Apparatus

5.2.1. Materials and Methods

The drying conditions for the smaller batch apparatus is summarised in **Table 5.1**, with the equipment discussed in detail in 3.3. These conditions have been chosen according to the parameters most commonly used in industry and within limitations of the apparatus [20, 60, 61, 71].

Table 5.1 Experimental parameters

Variables	Parameters
Coal Type	Loy Yang, Yallourn, Morwell
Fluidizing Medium	Air, Steam
Temperature	130 – 200 °C
Velocity	0.32 – 0.67 m/s
Particle Size	0.5 – 1.7 mm
Bed Mass	10 g

The smaller batch thermo-gravimetric system is used for the drying analysis and the method is outlined in Appendix A2.

5.2.2. Minimum Fluidization Velocity Calculation

An important requirement for the fluidization of particles is the minimum fluidization velocity. This velocity determines the minimum velocity required for fluidization within a

bed, and is the lowest theoretical velocity than the bed can be operated at. The minimum fluidization velocity was calculated using the Wen and Yu correlation [51, 213, 214]:

$$\mathrm{Ar} = {d_p}^3 \rho_g (\rho_s - \rho_g) g/\mu^2 \quad (5.1)$$

$$\mathrm{Re} = \left[33.7^2 + 0.0408\mathrm{Ar} \right]^{1/2} - 33.7 \quad (5.2)$$

$$\mathrm{Re} = u_{mf} d_p \rho_g / \mu \quad (5.3)$$

A minimum fluidization velocity of 0.23 m/s was calculated using an average particle size of 1.5 mm. The velocities used for the drying experiments vary between approximately 1.4 to 2.7 times the U_{mf}. With the variation in particle size, an absolute velocity was used and remains unchanged for the different minimum fluidization velocities, similar to previous literature [51]. This was chosen to present conditions typical of industrial drying conditions [20] where particle size range is <3 mm [20] and a single velocity is chosen for the complete size range.

Using a bed with particle size between 1.2 and 1.7 mm sized dry coal shows that fluidization occurs at approximately 0.25 m/s. Bed height (**Figure 5.2**), which is an indicator of fluidization, increases starting at 0.25 m/s and stopping at approximately 0.65 m/s. To calculate the bed expansion, multiple photographs were taken with a scale, with the bed height based on the difference between the solid bed and gas phase. This helps in the measurement of minimum experimental fluidization velocity and determines the bed rise and overflow characteristics of the continuous fluidized bed apparatus.

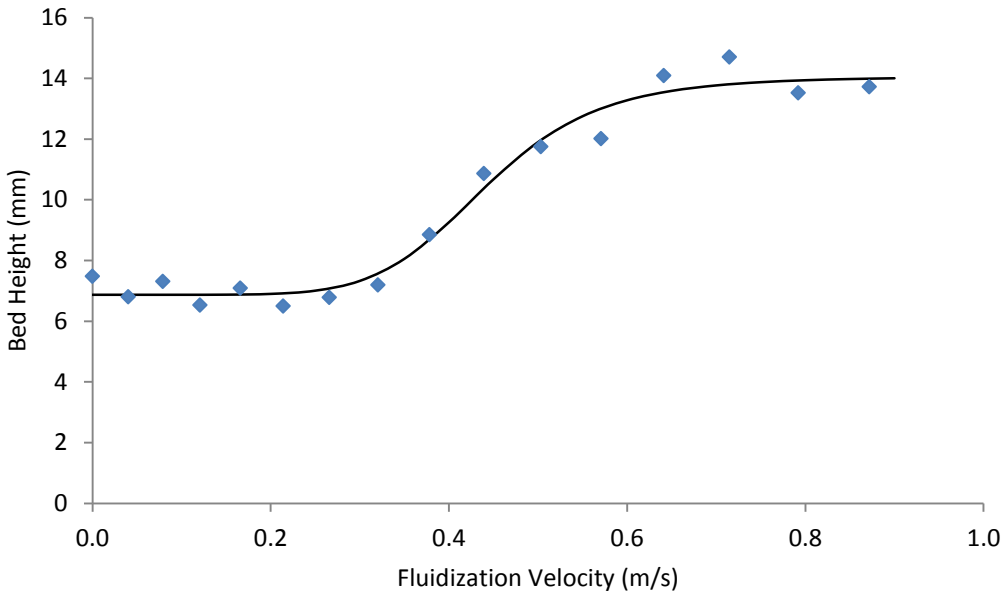

Figure 5.2 Bed height as a function of fluidization velocity

5.2.3. Batch Drying Kinetics

Three different Victorian brown coals – Loy Yang, Yallourn and Morwell – were dried with a sample size of 10g used in each experiment. Drying time was measured with regard to the variation in particle size, fluidization velocity, fluidizing gas temperature and medium. System parameters in **Table 5.1** show similar conditions used for both air and steam fluidization mediums to enable a comparison between drying times.

Figure 5.3 – Figure 5.5 show the variation in particle size, gas velocity and gas temperature under both air and steam fluidization medium, with each figure representing a single type of coal. There is no significant change in trend using either air or steam as fluidization medium.

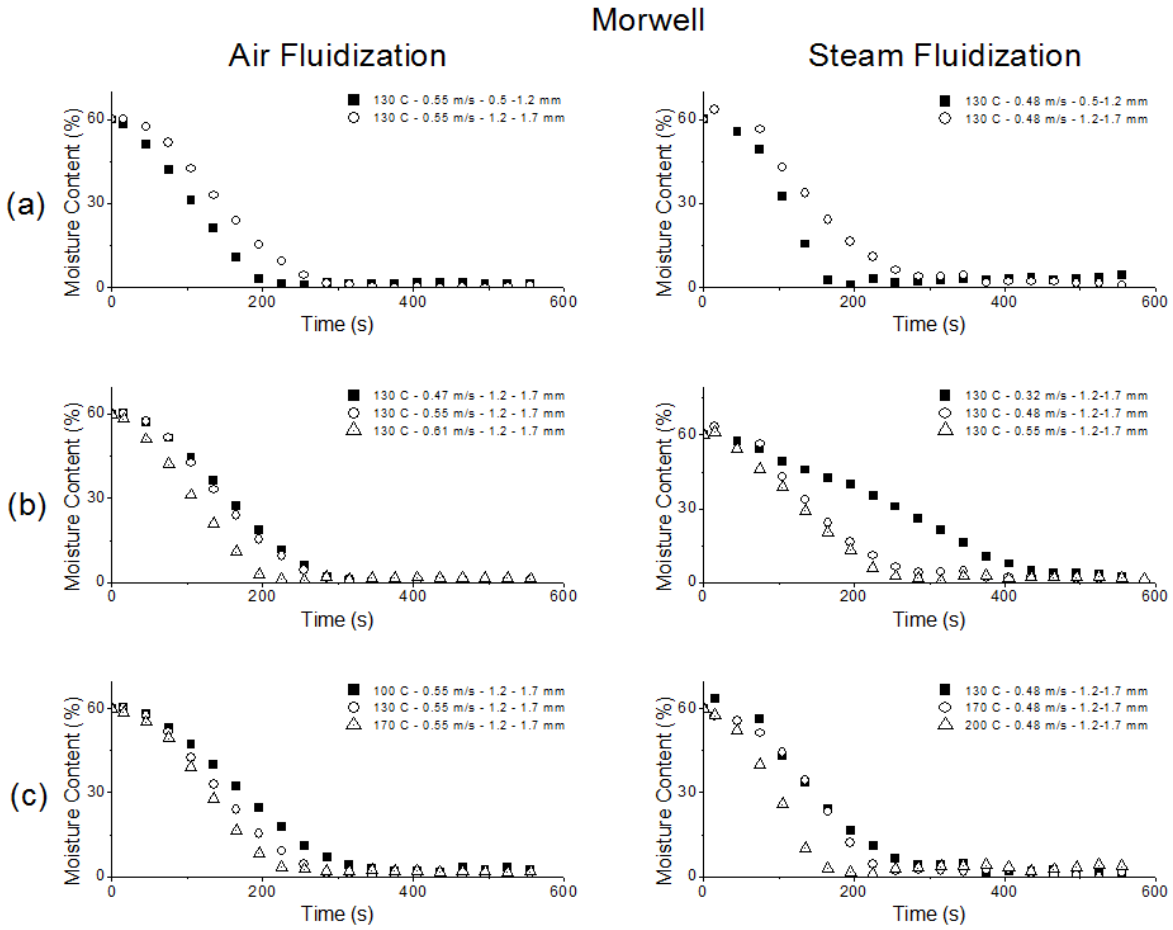

Figure 5.3 Morwell Coal Drying Kinetics - air and steam fluidized bed drying: (a) The effect of initial particle size (b) The effect of fluidization velocity (c) The effect of bed temperature

Figure 5.3 – Figure 5.5 shows a difference in drying profile between air fluidized bed drying (AFBD) and steam fluidized bed drying (SFBD). AFBD operated with an initial heating period where little or no drying occurs, followed by a steady rate drying period and a falling rate period which ends when the moisture content reaches equilibrium. SFBD followed a similar profile differing only in the initial heating period. Moisture condenses across the particles surface during the heating period resulting in an observable weight gain (as highlighted by the arrows). This is shown as an initial increase in bed mass before decreasing as drying progresses and is typical of lower temperature steam kinetics.

Using feed particle sizes (1.2 – 1.7) mm and temperature of 130°C the fluidization velocity was varied: three air fluidization velocities (0.47 m/s, 0.55 m/s and 0.67 m/s) and three steam fluidization velocities (0.32 m/s, 0.48 m/s and 0.55 m/s).

Figure 5.3 – Figure 5.5 (b) showed that increasing the velocity resulted in decreased drying time in both air and steam. Previous work with Loy Yang brown coal [54] using hot air corroborates this observation, with other work by Jeon et. al [51] using Indonesian brown coal shows similar trends. Using two similar velocities (0.47 and 0.55 m/s) in a single fluidization medium, a ratio of the two times was taken. This ratio indicated the proportional drying time decreases with increasing velocity. The drying time ratio of air $(t_{0.55}:t_{0.47})_{air}$ at 0.88 and steam $(t_{0.55}:t_{0.48})_{steam}$ at 0.84 show the closeness of the two ratios indicating that a change in fluidization medium does not provoke any observable difference in the drying ratio of the tested velocities. This suggests a proportional increase in air fluidized bed drying can be used to predict drying time changes in a steam fluidized bed drier. Ratios are used to allow the investigation of the effect on a single variable within the fluidized bed drier. Because the required drying time in air and steam differ, the effect of temperature can be compared between the two mediums but not quantified; creating a drying time ratio allows a numerical value to be obtained which expresses the variation in drying time without as a dimensionless variable, which can then be compared.

An increase in fluidization gas temperature caused a decrease in drying time as shown in **Figure 5.3 – Figure 5.5** (c). Air fluidized drying was conducted at 100°C, 130°C and 170°C, while steam fluidized bed drying was conducted at 130°C, 170°C and 200°C. Jeon et. al. [51], Levy et. al. [140] and Kim et. al. [54] reported that various coals dried in an air fluidized bed behave similarly at temperatures ranging from 40°C to 150°C. This trend is also observed using steam fluidized bed drying of other materials such as rice [182] and ceramics [52]. Using a similar method to the analysis of fluidization velocity the directly comparable ratios at temperatures 130°C and 170°C show for air the ratio $(t_{170}:t_{130})_{air}$ is 0.87, while for steam the ratio $(t_{170}:t_{130})_{steam}$ is 0.89, indicating that increasing the gas temperature across the particle bed increases drying time. This suggests that drying time for steam fluidized bed drying can be extrapolated from air fluidized bed drying. Messai et. al. [29] examined the inversion temperature for porous spherical particles and found it to occur at 152°C. Inversion temperature is a mathematically determined temperature where steam drying becomes more effective than air drying. The inversion temperature varies depending on properties such as fluid flow regime and defined by Messai [29]. As the value calculated by Messai et. al. is almost exactly between the two temperatures used experimentally no major difference between steam and air fluidized bed drying ratios were expected. While the heat transfer rate are similar at this temperature steam fluidization still retains the added benefits of smaller

equipment, reduced emissions, reduced fire and explosion hazards, and improvements in product quality [29].

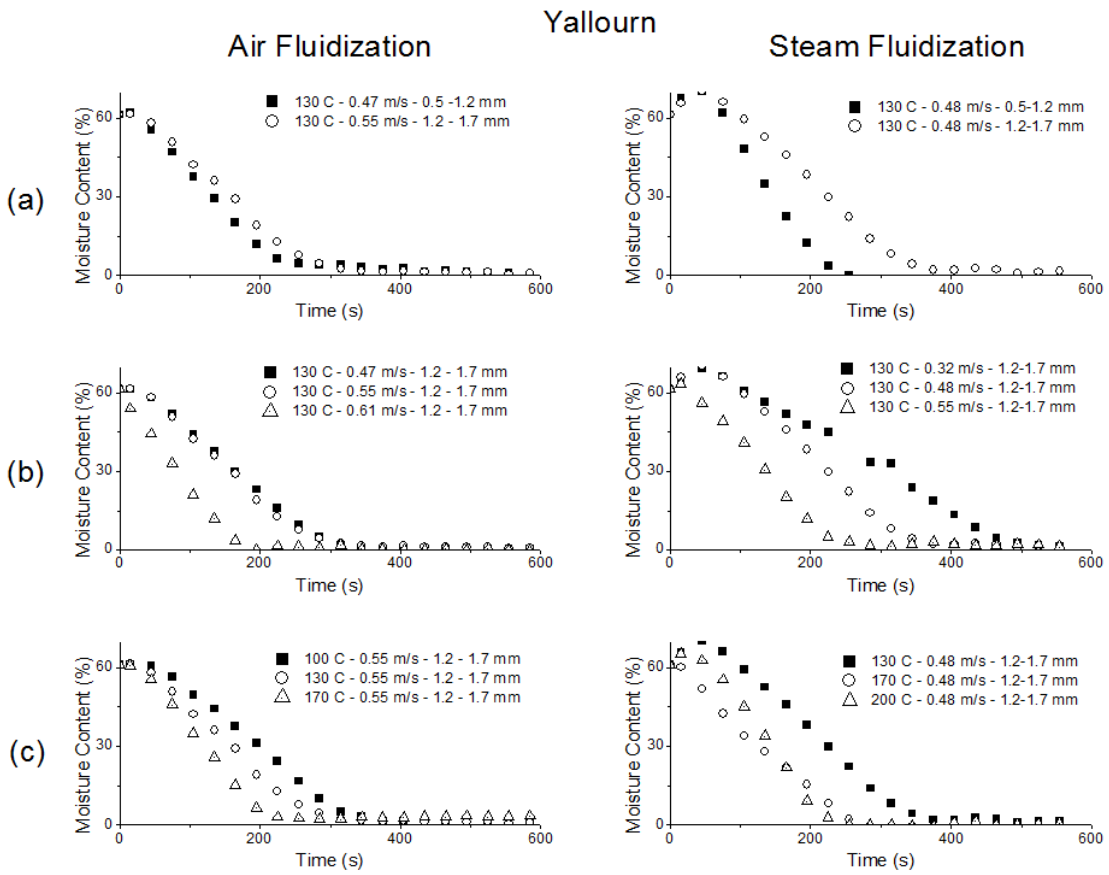

Figure 5.4 Yallourn Coal Drying Kinetics - air and steam fluidized bed drying: (a) The effect of initial particle size (b) The effect of fluidization velocity (c) The effect of bed temperature

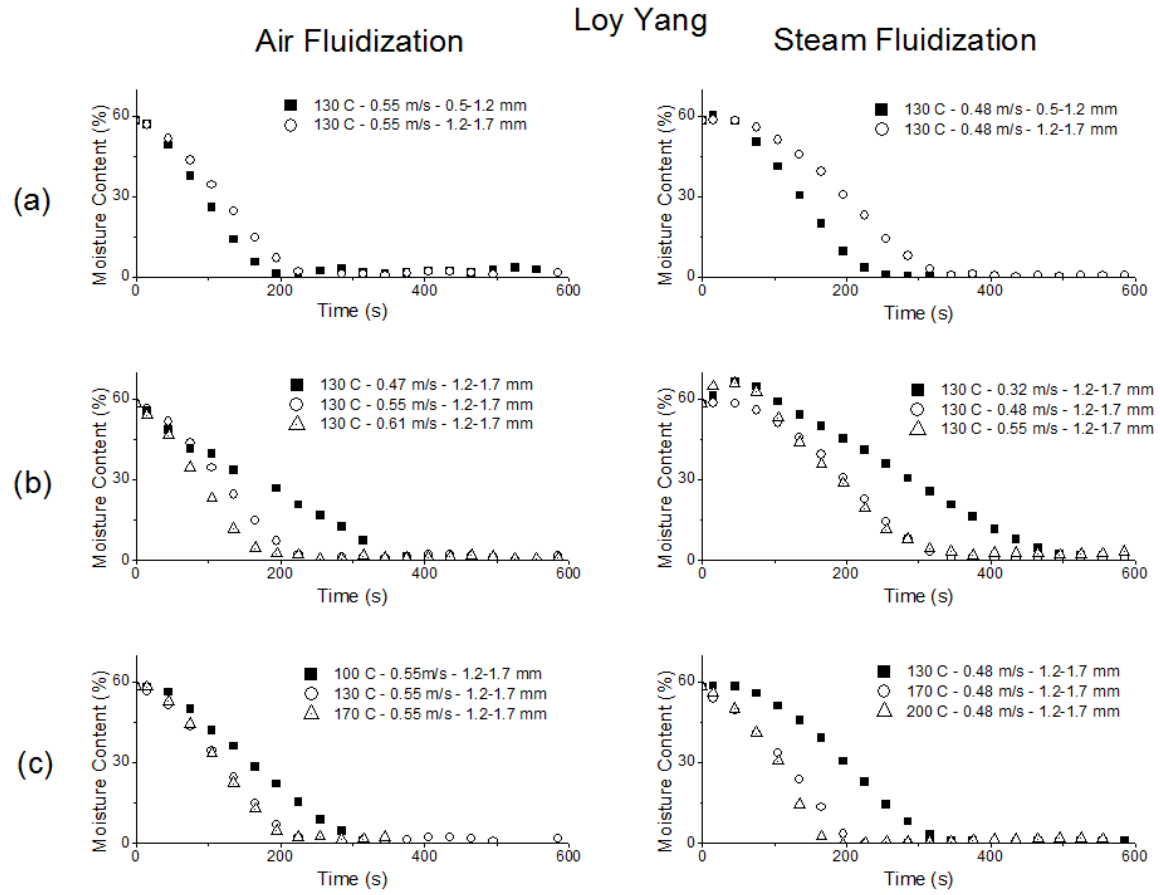

Figure 5.5 Loy Yang Coal Drying Kinetics - air and steam fluidized bed drying: (a) The effect of initial particle size (b) The effect of fluidization velocity (c) The effect of bed temperature

The effect of varying particle sizes on drying times is shown **Figure 5.3 – Figure 5.5** (a) with an observation that coal with a decreased particle size also has a decreased drying time. Investigation by Jeon et. al. [51] using Indonesian brown coal reveals drying occurs more rapidly at larger particle sizes; however the drying rates were based on a fluidization velocity 1.5 times higher than minimum fluidization velocity, not a single absolute velocity. The average ratio for air drying is 0.84 $(t_{0.5\text{-}1.2}: t_{1.2\text{-}1.7})_{air}$, when compared to steam drying at 0.73 $(t_{0.5\text{-}1.2} : t_{1.2\text{-}1.7})_{steam}$. This suggests that reducing the particle size in a steam atmosphere increases the drying rate more compared to an air atmosphere. The reason can be interpreted from the kinetics, with a smaller amount of condensation observed across the smaller particles, reducing the amount of additional moisture that needs to be removed compared to that in the 1.2-1.7 mm particles. The added moisture content would accentuate the difference in drying times.

The final moisture content in the steam dried coals is shown to be consistently higher than for air fluidized bed dried coals. The equilibrium moisture content occurs due to the humidity of the atmosphere in which they are dried as well as the temperature. Observed in Kim et. al. [54] the higher relative humidity's result in higher equilibrium moisture contents. For the three coals tested, the steam equilibrium value is between 2.8 to 5.1%, while the air moisture values are 0.6 to 1.3%. The higher moisture content in steam fluidized bed dried coal means, if dried to completion, steam fluidized bed dried coals will have lower combustion efficiencies during power generation. However, in practice industry drying typically targets a 15% moisture content therefore the lower equilibrium moisture content is less relevant. A potential impact of the moisture content may be more applicable for gasification processes, where H_2O in the gasification stream results in different gasification reactions, and changing the gasified products obtained.

5.2.4. Modelling

Mathematical modelling is required for the design and scaling-up of an appropriate drying technology. While numerous models are available in literature selecting the best model for the drying kinetics is an essential requirement. The drying data was expressed into a moisture ratio:

$$M_R = (M - M_e)/(M_0 - M_e) \quad (5.4)$$

Where, M_R is the moisture ratio, M is the moisture content at any instance during the drying process M_e is the equilibrium moisture content and M_0 is the initial moisture content.

A range of existing models were compared and tested for both air and steam fluidized bed drying of Morwell brown coal. Previously collated in Tahmasebi et.al [143] these mathematical models were applied to fixed bed drying of Chinese Lignite. **Table 5.2** shows a range of equations used in the determination of empirical models.

Table 5.2 Empirical models given by Tahmasebi et.al. (2013) [143]

Model Name	Model Equation
Newton	$X = \exp(-kt)$
Henderson and Pabis	$X = a.\exp(-kt)$
Logarithmic	$X = a.\exp(-kt) + c$
Wang and Singh	$X = 1 + at + bt^2$
Diffusion Approach	$X = a.\exp(-kt) + (1-a).\exp(-kbt)$
Verma	$X = a.\exp(-kt) + (1-a).\exp(-gt)$
Simplified Fick Diffusion	$X = a.\exp(-\mathrm{c}.(\mathrm{t}/L^2))$

Midilli-Kucuk	$X = a.\exp(-k(t^n)) + bt$
Page	$X = \exp(-kt^n)$
Modified Page	$X = \exp(-(kt)^n)$

To determine the best fit for each of these models, regressions were undertaken using commercially available data processing software (Origin Pro 8.0). R^2 maximization and χ^2 minimization was used as a criterion to judge the fit of the models. R^2 is known as the co-efficient of determination (or correlation co-efficient) and is widely used to determine the fitting of curves for data. R^2 values closer to the value of one show a better fit to the experimental data. Another way to judge curve fitting is by using chi-square. Origin Pro 8.0 uses chi-square minimization algorithms to fit the experimental data, with a chi-square (χ^2) value closer to zero indicating a better fit. Analysing the change in temperature, the models associated with **Figure 5.6** Midilli-Kucuk model with experimentally obtained data for air fluidized bed dried coal at varied temperatures were examined under air fluidized bed drying. Shown in **Table 5.3** for temperatures of 100°C, 130°C and 170°C each model is iteratively converged and the R^2 and χ^2 recorded. Comparing fitting values, the Midilli-Kucuk equation [132] has the greatest R^2 values (on average 0.9993) and lowest χ^2 values (0.0001).

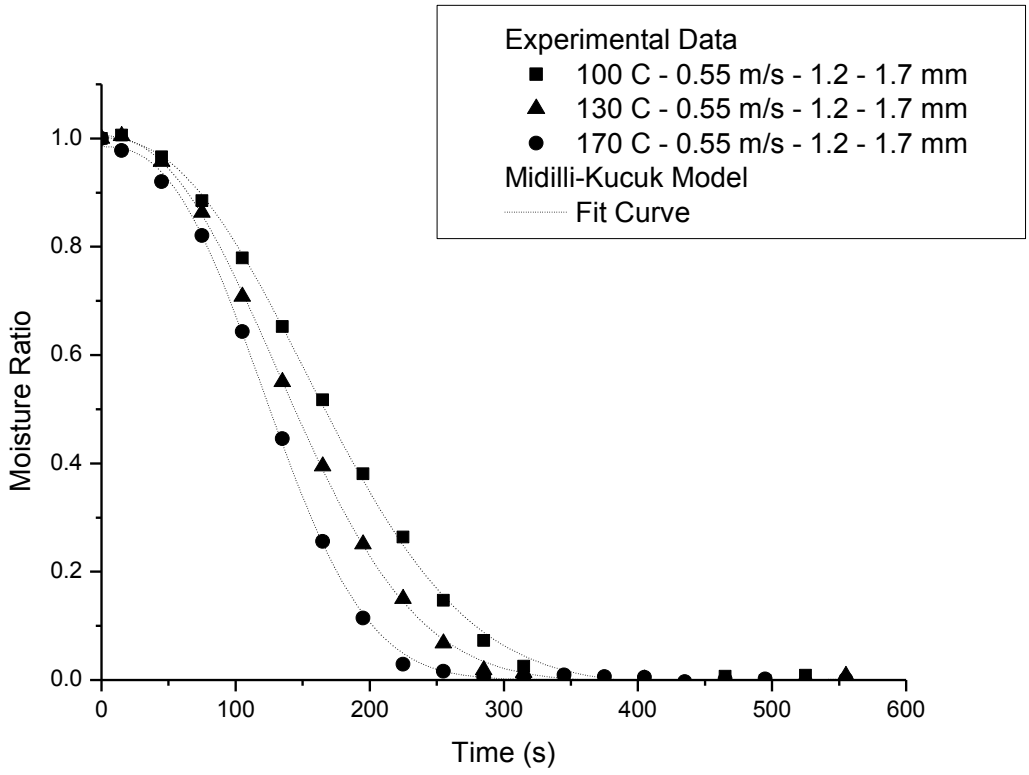

Figure 5.6 Midilli-Kucuk model with experimentally obtained data for air fluidized bed dried coal at varied temperatures

This method is repeated for steam fluidized bed drying, showing similar results. Highlighted in **Table 5.3** and **Figure 5.7** the Midilli-Kucuk equation allows for the best fit of the experimental data, observed in both R^2 and χ^2 values. When comparing experimental data to the model a close fit is seen. Only the condensation (appearing only at 130°C) cannot be accurately accounted for, with the model predicting a higher moisture ratio (approximately 1.05) at the initial time (t = 0) instead of the typical ratio of 1, this is due to the model not capable of accounting for the rapid increase in mass, and instead assumes an instantaneous increase. Taking the initial higher moisture ratio as condensation the predicted moisture content is less than the experimentally observed condensation mass, suggesting the Midilli-Kucuk equations will under predict the condensation mass. While the Midilli-Kucuk does not take into account initial condensation, the model predicts the moisture loss curve accurately, with average R^2 and χ^2 values at 0.9966 and 0.0005 respectively.

As the Midilli-Kucuk model is shown to be the best fit for both air and steam fluidized bed drying over the complete range of conditions, the method is further used on the drying data, with varying fluidization velocities and particle size. The model was found to adequately represent the fluidized bed drying data over the range of conditions from the experiments (**Table 5.3**).

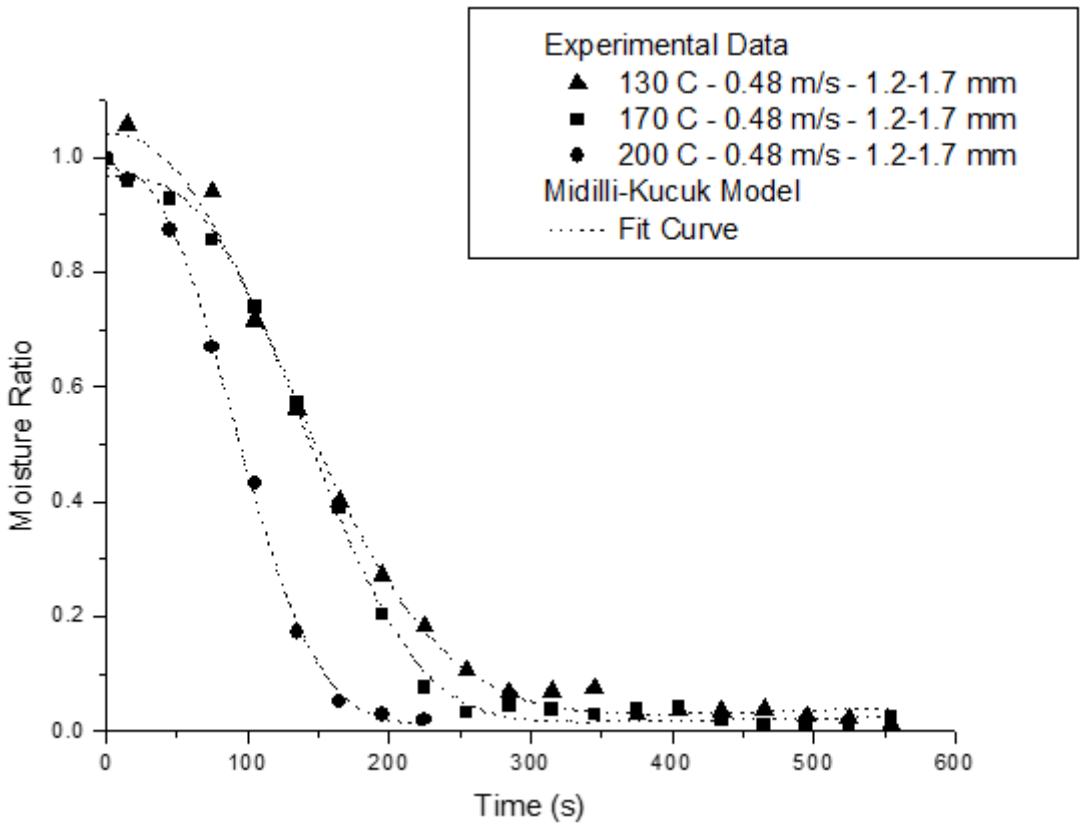

Figure 5.7 Midilli-Kucuk model with experimentally obtained data for steam fluidized bed dried coal at varied temperatures

However, as already discussed in the literature review empirical models have distinct advantages and limitations. While it is beneficial to determine the most applicable empirical model for Victorian brown coal (the Midilli-Kucuk equation) Kucuk et. al. [128] cautions that empirical equations are dependent on experimental data. For this reason a theoretically based single particle model has the capacity for greater level of implementation and usability in industry, and can provide information on local drying characteristics which is not obtainable through empirical modelling. This type of model would result in greater characterisation of coal behaviour in a fluidized bed and give greater clarity to the design of driers.

For this reason, further work to develop a semi-empirical model has been conducted and outlined in the following chapters (Chapter 9).

Table 5.3 Midilli-Kucuk co-efficients for air and steam fluidized bed drying kinetics

Sample Name	Model Co-efficients	R^2	χ^2
	Steam Fluidized Bed Drying		
130 C - 0.48 m/s - 1.2-1.7 mm	a = 1.041 k = 0.0000128947 n = 2.19608 b = 0.0000730379	0.99518	0.000655

170 C - 0.48 m/s - 1.2-1.7 mm	a = 0.9681 k = 0.000000683973 n = 2.77669 b = 0.0000461255	0.99732	0.000392
200 C - 0.48 m/s - 1.2-1.7 mm	a = 0.9807 k = 0.00000701119 n = 2.53362 b = 0.000129402	0.99715	0.000333
130 C - 0.48 m/s - 0.5 - 1.2 mm	a = 0.99736 k = 0.00000022091 n = 3.21472 b = -0.0000227978	0.99475	0.000655
130 C - 0.32 m/s - 1.2-1.7 mm	a = 1.01962 k = -0.00267 n = 0.00000000787505 b = -0.00211	0.96754	0.00426
130 C - 0.55 m/s - 1.2-1.7 mm	a = 1.00514 k = 0.0000326201 n = 2.0611 b = -0.0000154478	0.99651	0.00051
Air Fluidized Bed Drying			
100 C - 0.55 m/s - 1.2 - 1.7 mm	a = 1.00171 k = 0.00000553964 n = 2.29308 b = -0.0000228283	0.99887	0.000182
130 C - 0.55 m/s - 1.2 - 1.7 mm	a = 1.00508 k = 0.0000081126 n = 2.28537 b = -0.00000907837	0.99967	5.12E-05
170 C - 0.55 m/s - 1.2 - 1.7 mm	a = 0.98494 k = 0.00000304566 n = 2.54834 b = 0.00000170738	0.99945	8.15E-05
130 C - 0.55 m/s - 0.5 - 1..2 mm	a = 0.98303 k = 0.000034477 n = 2.12764 b = -0.00000848007	0.99694	0.000405
130 C - 0.61 m/s - 1.2 - 1.7 mm	a = 0.98303 k = 0.0000345756 n = 2.1269 b = -0.0000069531	0.99901	0.000403
130 C - 0.47 m/s - 1.2 - 1.7 mm	a = 1.00113 k = 0.0000068241 n = 2.29186 b = -0.0000135026	0.99695	0.000156

5.3. Large Scale Apparatus

5.3.1. Batch Materials and Methods

Designed as both a batch and a continuous fluidized bed drier, experiments undertaken with the larger rig were used to compare the effect of scaling on the fluidized bed drying kinetics. The batch experiments utilized 1 kg wet (as received) coal and the moisture content of the bed was measured as a function of drying time. The coal was collected by opening a collection port and extracting a sample of the bed. Based on experience the sample was then left in the open atmosphere for approximately 10 seconds to allow the steam adjacent and amongst the coal sample to dissipate, prior to storing and analysis. The samples were placed in a sealed vial and stored in a drying, cool environment to prevent moisture readsorption before analysis. The continuous feeding experiments utilize a larger bed mass (3kg), feeding wet coal with an overflow method of sample collection, with its detailed operation outlined in Chapter 3. The conditions for sample collection remained consistent for each kinetic variable.

The purpose of the larger apparatus was to provide a comparison to the smaller apparatus previously tested, therefore a similar fluidization velocity and temperature was used. However, a larger initial particle size range was required (1.2 to 2.3 mm) due to the increase in bed mass. This size range was typically used at RWE steam fluidized bed facilities in Germany [20, 60, 61, 71]. The full range of conditions can be found in **Table 5.4**.

Table 5.4 Experimental parameters

Variables	Parameters
Coals	Loy Yang, Yallourn, Morwell, Shenhua
Temperature	130 to 200 °C
Fluidization medium	Steam, Air
Velocity	~0.45 m/s

Particle size (diameter)	1.2 to 2.3 mm
Bed diameter	0.254 m
Bed mass (batch)	1 kg
Bed mass (continuous)	3 kg
Residence time (continuous)	140 to 50 minutes

5.3.2. Batch Drying Kinetics

Using Yallourn brown coal, drying kinetics at two temperatures, 130°C and 170°C, were produced with the large batch experiments. Complete drying occurs when the coal reaches its equilibrium moisture content. For the large scale experiments this was determined to be when the change in moisture content was less than 5%. In **Figure 5.8**, increasing the drying temperature from 130 to 170°C resulted in a reduction in drying time from 40 to 25 minutes. Both 130 and 170°C showed a period when little drying occurred, followed by a steady decrease in mass (corresponding to a constant rate period), with a falling rate period occurring until drying ceases. The larger batch system gives an accurate account of the equilibrium moisture content, with moisture equilibrating at 6.5% and 1.5% suggesting that the increase in temperature reduces the equilibrium moisture content. Using a similar calculation method to the smaller apparatus, the drying ratio between 130 and 170°C in the larger apparatus $(t_{130}: t_{170})_{steam}$ was calculated to be 0.63.

The results in **Figure 5.8** highlighted described an inherent feature with the batch system in the larger fluidized bed. During the early drying times, full fluidization does not occur. The bed partially fluidizes, with some sections initially drying faster than others. This is reflected in the drying kinetics through artificially high or low moisture values. While the kinetics 'corrects' itself once full fluidization occurs, the moisture readings within these periods show greater amounts of variation.

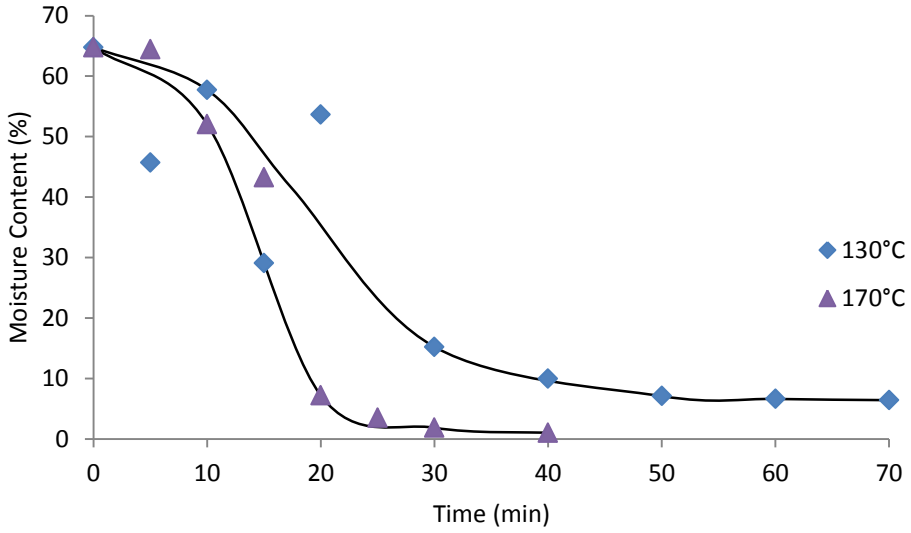

Figure 5.8 Batch fluidized bed drying, 1kg Yallourn brown coal

Under the same conditions, as illustrated in **Figure 5.9**, Loy Yang brown coal was examined. Unlike Yallourn brown coal, Loy Yang brown coal has a shorter drying time for both 130 and 170°C; 30 minutes and 20 minutes, respectively. At 130°C, both Loy Yang and Yallourn coal had a similar drying structure, with a small amount of time required for drying to begin. However, at 170°C the heating up time was not observed. This was attributed to the lower moisture content in the Loy Yang coal. This resulted in a faster heating up period, therefore a quicker start to drying. The equilibrium moisture content was also different in Loy Yang coal. While 130°C still has a greater amount of moisture at equilibrium, the difference between the 130 and 170°C is smaller, with a moisture content of 3.6% and 1.1% respectively. Calculating the difference between the drying times, a drying ratio of $(t_{130}: t_{170})_{steam} = 0.67$ was found. Due to time and feedstock constraints only a single kinetic experiment was conducted for each variable. As a result variation in the data points are more prevalent. This has been attributed to stickiness between coal particles through initial condensation mass. In order to smooth the kinetic graphs, further work could be conducted to duplicate and triplicate the results. The stickiness observed in these experiments have been discussed in more detail in Chapter 5.3.5.

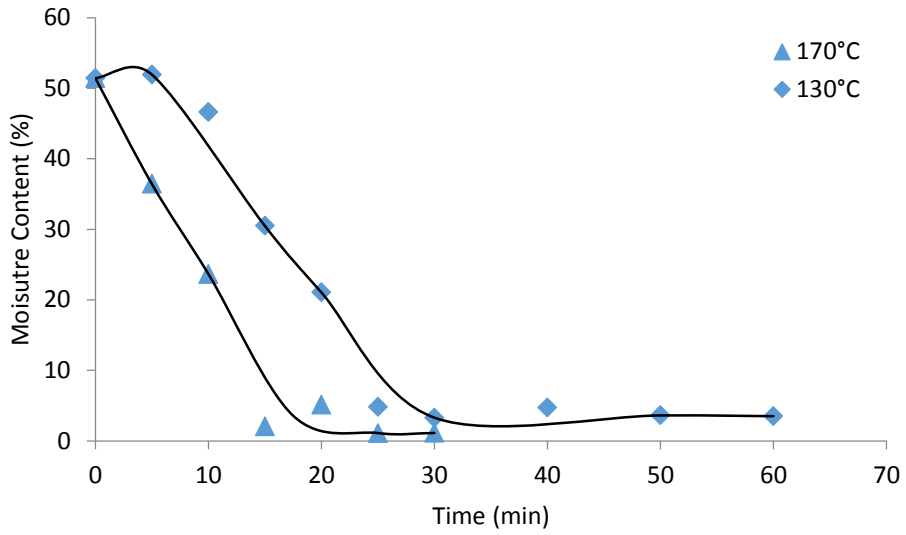

Figure 5.9 Batch fluidized bed drying, 1kg Loy Yang brown coal

5.3.3. Comparing Scale

Comparing between the small scale and the large scale apparatus, a difference in drying time was observed. Ten grams of Loy Yang coal took approximately 6 minutes and 4 minutes to dry for 130 and 170 °C respectively, in the small rig. Compared to the larger bed, a drying time of 30 and 20 minutes was required. Similarly, 10g of Yallourn coal took 6.5 minutes and 5 minutes (130 and 170°C) to reach equilibrium moisture in the small rig while it for the large rig, 40 and 25 minutes was required, respectively (highlighted in **Figure 5.10**). In both cases the increase in scale required up to 600% additional drying time. Comparing the drying times for the smaller apparatus to the larger apparatus, the drying characteristics of the coal should theoretically be the same, regardless of the mass of the bed, as similar fluidization conditions were used. Therefore, the longer drying time could have been due to the effect of a larger bed height. As the steam passes a larger bed, the temperature of the steam decreases, reducing the heat transfer at the top of the bed compared to the heat transfer above the distributor. If this is true, in view that similar bed heights were used throughout the large rig experiments, there should be a unified approach to translate the kinetics obtained from the small rig to describe the drying behaviour of the coal using the big rig.

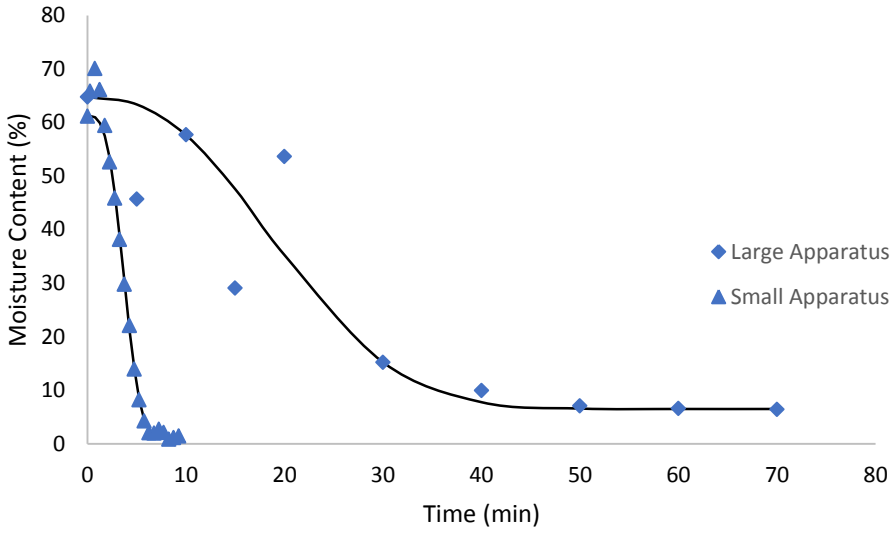

Figure 5.10 Difference between small and large scale drying kinetics (Yallourn, Steam, 130°C)

To compare the effect of bed scale, the curve fitting model previously developed was adapted to generate a correlation which can allow the model to be applied to both small and big sets of kinetic data. From earlier kinetic studies, the Midilli-Kucuk equation (Equation 5.5) was found to fit well with the kinetic data, however, when analysing the Midilli-Kucuk equation over longer periods of time, the *b* term resulted in an increase in moisture content which was a discrepancy in extrapolating the kinetics.

$$X = a.\exp(-k(t^n)) + bt \qquad (5.5)$$

The Midilli-Kucuk equation was then modified by removing the *b* term as shown in Equation 5.6 and is similar to the Page model. While the Page model has different co-efficients to the Midilli-Kucuk model, the Page has a very similar fit to the Midilli-Kucuk model and is shown in **Figure 5.11**.

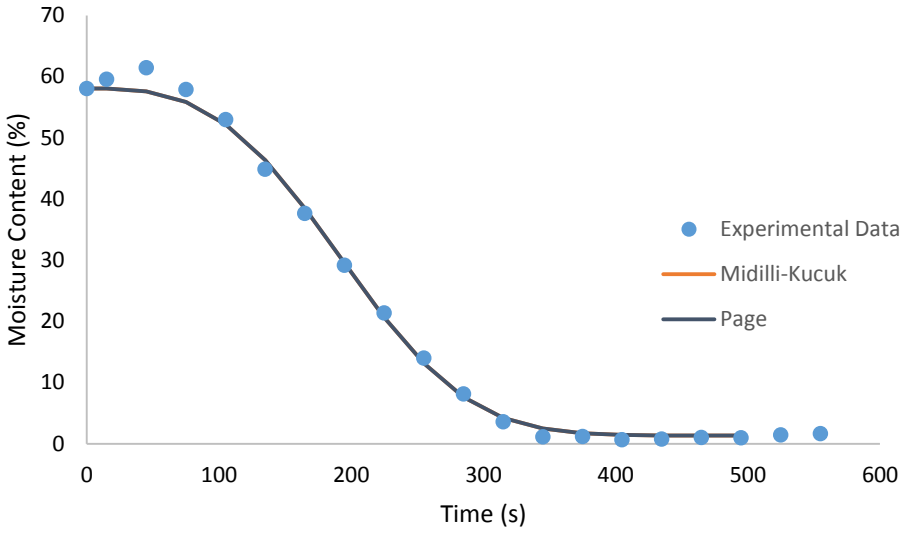

Figure 5.11. Comparison between Midilli-Kucuk and Page equations (Yallourn, steam fluidized bed drying, 130°C)

$$X = a.\exp(-kt^n) \quad (5.6)$$

The co-efficients for Loy Yang and Yallourn coal at 130 and 170°C were generated from the small scale kinetic data are shown in **Table 5.5** and fitted well with the experimental data, with a correlation co-efficient above 0.99. The parameter *a* represents the initial moisture ratio of the coal before drying, and has been set to 1, otherwise the unbounded curve fitting has a small amount of variation in *a* which is not representative of the actual initial moisture content.

Table 5.5. Small scale curve fitting parameters

Temperature (°C)	Coal Type	*a*	*k*	*n*	R^2
130	Loy Yang	1.000	8.83×10^{-8}	3.013	0.9984
170	Loy Yang	1.000	9.20×10^{-4}	1.445	0.9975
130	Yallourn	1.000	2.21×10^{-8}	3.197	0.9988
170	Yallourn	1.000	4.99×10^{-4}	1.524	0.9906

The co-efficients determined were used as a basis for the modelling of the larger bed drying kinetics, fitting the larger kinetics using the parameters determined in the smaller apparatus. In order to translate the smaller scale fitting parameters to the larger kinetics, a scaling coefficient was introduced, d_1. The position of d_1 (the scaling co-efficient) within the small rig kinetics equations were investigated for the different combinations of temperatures and coal, and was collated in **Table 5.6** and **Table 5.7**

Table 5.6. Loy Yang scaling parameters

Equation		130°C		170°C	
		d_1	R^2	d_1	R^2
$X = a.exp\left(-k.d_1.(t^n)\right)$	(5.7)	0.0082	*0.9913*	0.1013	*0.9726*
$X = a.exp\left(-k.(t^{n.d_1})\right)$	(5.8)	0.7658	*0.9849*	0.7730	*0.9510*
$X = a.exp\left(-k.\left(t^{n^{d_1}}\right)\right)$	(5.9)	0.7581	*0.9849*	0.3007	*0.9510*
$X = a.exp\left(-k^{d_1}.(t^n)\right)$	(5.10)	1.2955	*0.9913*	1.3275	*0.9726*

Table 5.7. Yallourn scaling parameters

Equation		130°C		170°C	
		d_1	R^2	d_1	R^2
$X = a.exp\left(-k.d_1.(t^n)\right)$	(5.7)	0.0034	*0.8374*	0.0573	*0.9042*
$X = a.exp\left(-k.(t^{n.d_1})\right)$	(5.8)	0.7624	*0.8313*	0.7421	*0.8229*
$X = a.exp\left(-k.\left(t^{n^{d_1}}\right)\right)$	(5.9)	0.7666	*0.8314*	0.2922	*0.8229*
$X = a.exp\left(-k^{d_1}.(t^n)\right)$	(5.10)	1.3230	*0.8374*	1.3762	*0.9042*

Observing the fit for the d_1 parameter, the four forms of the scaling equations showed reasonable fit, with a correlation co-efficient lower in Yallourn brown coal than in Loy Yang. The lower correlation co-efficient for Yallourn brown coal can be attributed to noise in the kinetic data, which reduces the correlation co-efficient values. Nevertheless, it was still an acceptable fit.

From the four equations tested, Equations 5.8 and 5.10 showed an almost constant scaling factor (0.76 and 1.31 for Loy Yang and Yallourn respectively) could be used across the different experimental data. Comparing the two equations, the difference between Equations 6.8 and 6.10 is shown in **Figure 5.12** and shows Equation 5.10 has greater accuracy in during the earlier drying periods. Equation 6.10 showed a slightly lower correlation co-efficient and slightly higher variation in d_1, however it described the early stages of the kinetics, especially the heating period, more accurately. From **Table 5.6** and **Table 5.7**, the scaling parameter in Equation 5.10 varied from 1.30 to 1.38, which is consistent enough to conclude that a single scaling factor can be used.

This confirms the hypothesis put forward earlier in the chapter. In view that the scaling parameter is consistent regardless of coal type and temperature used, as discussed earlier, this scaling factor is a parameter accounting for the effect of bed height on the drying behaviour.

Future work investigating the detailed relationship between bed height and the scaling parameter will be required and the results from this work can form the basis for this future work.

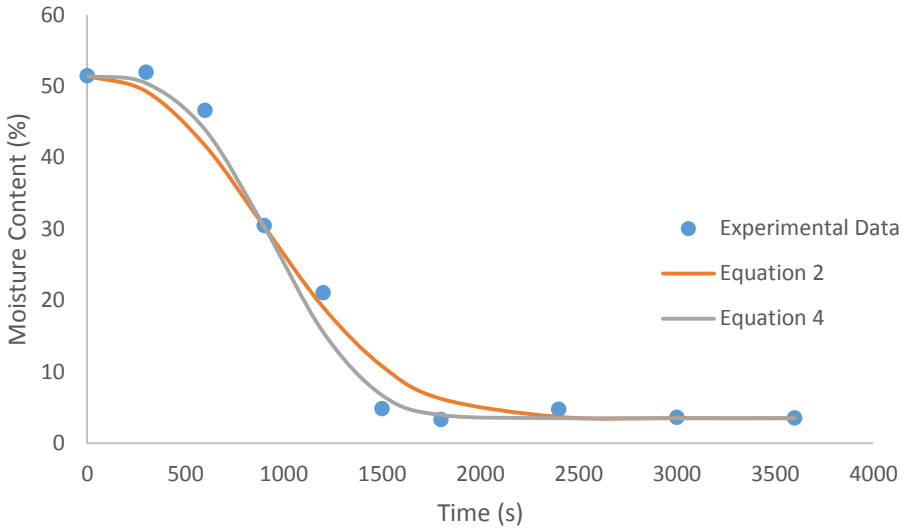

Figure 5.12. A comparison between Equation (2) 5.8 and (4) 5.10 (Loy Yang 130°C)

Comparing the model to the Loy Yang brown coal experimental data, **Figure 5.13** showed that the model fits both the 130 and 170°C drying kinetics accurately. In both cases the model fitted well with the experimental data, and was corroborated by a correlation co-efficient of approximately 0.97. For Yallourn brown coal, the model produced a relatively larger deviation form experiments for both 130 and 170°C. At 130°C the drying kinetics showed a reasonable fit, with an initial heating up period before the constant drying rate period. For this set of data, the constant rate period was not a smooth curve, however it still accurately predicted the final drying time required. At 170°C the model was less accurate, initially under predicting the moisture content, and then over predicting the final moisture content. While on average the moisture content was represented reasonably well, the model over predicted the final moisture content by approximately 4%. The discrepancy is attributed to the initial heating period observed in both the small and large apparatus. In the small apparatus a heating period was observed at 130 but not at 170°C, and has been factored into the Page equations. At 170°C, Yallourn coal in the larger apparatus showed a heating period which is not present in the smaller experiments and therefore the corresponding Page equation. The difference between the smaller and larger apparatus kinetics reduces the accuracy of the model.

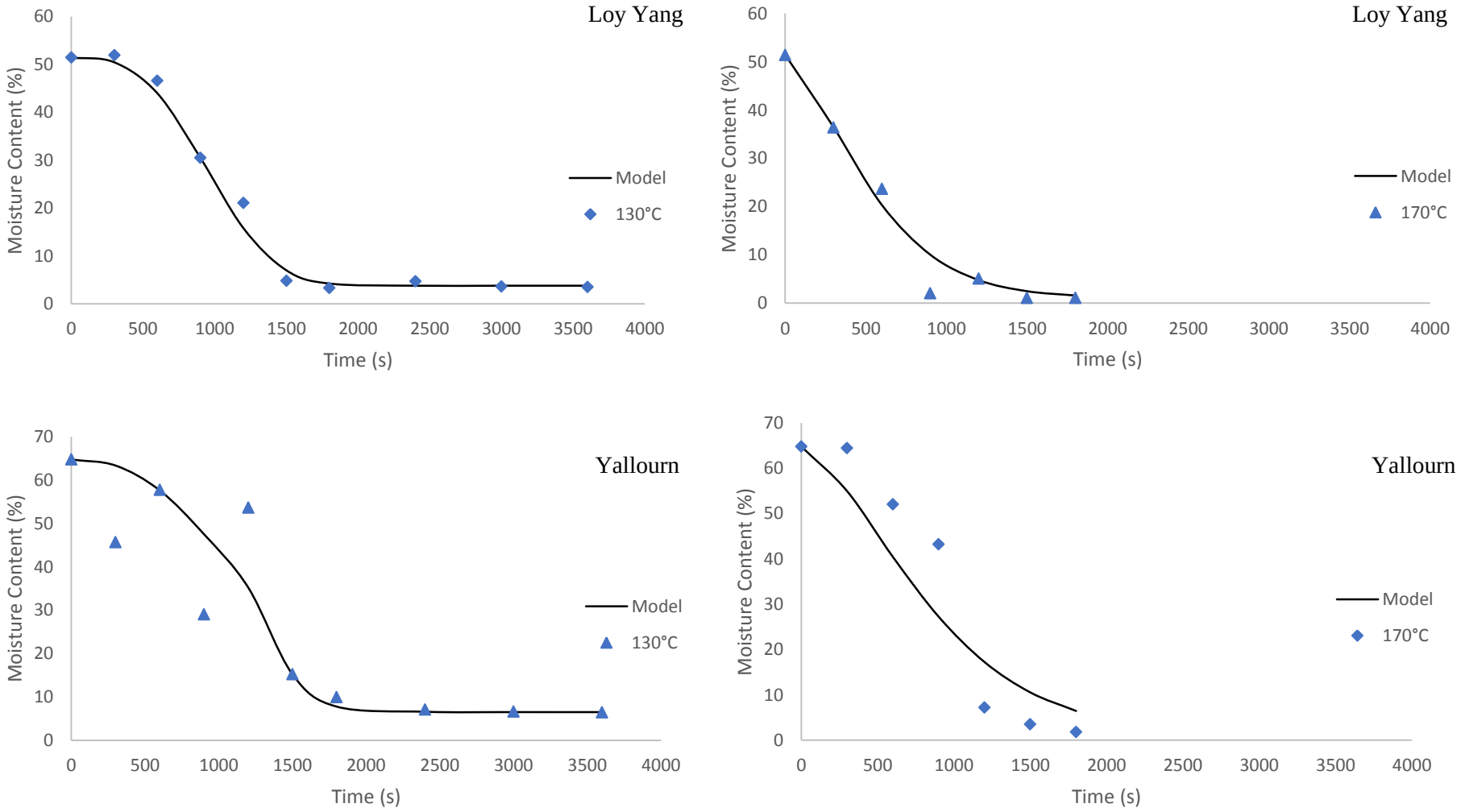

Figure 5.13. Model scaling for Loy Yang and Yallourn coal

This was highlighted in **Figure 5.14**, which showed the fitting of the model without the initial heating period, the model followed the experimental data closer, and had a closer equilibrium moisture value.

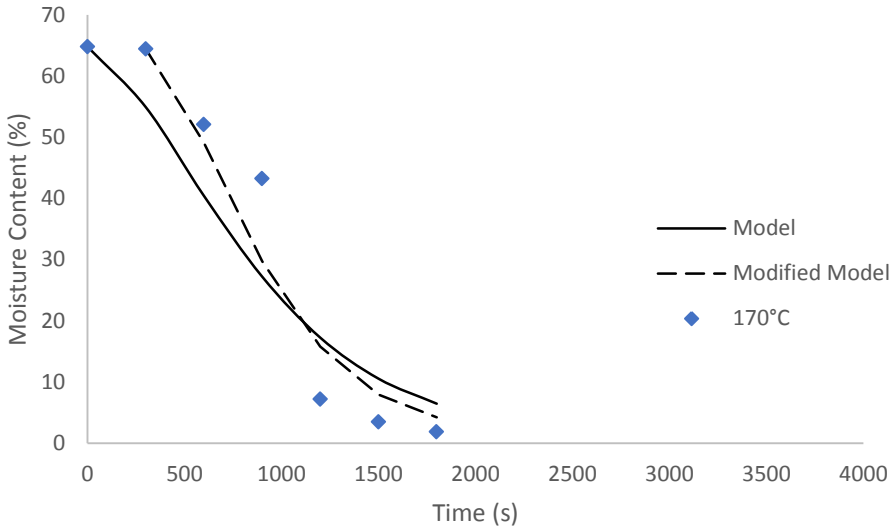

Figure 5.14. Modified Page model for 170°C Yallourn coal

As discussed earlier in the chapter, the drying ratio's between 130 and 170°C were calculated for the two coal types. In the smaller apparatus the drying ratios analysis showed that the different drying conditions provoked the same magnitude of response, regardless of the coal type. Using the larger apparatus this was verified and a comparison with the smaller apparatus was also made. For Loy Yang and Yallourn brown coal the drying ratios $(t_{130}: t_{170})_{steam}$ were 0.67 and 0.63 respectively. With an average drying ratio of 0.65, the results in the large apparatus verified the results in the smaller apparatus, showing an increase in temperature provokes a similar magnitude of response, regardless of coal type or bed size. Comparing the drying ratios from the small scale to the large scale apparatus, the increase in drying temperature showed different drying ratios. In the smaller bed an average drying ratio $(t_{130}: t_{170})_{steam}$ of 0.88 was observed. This ratio was higher than the larger bed ratio of 0.65 and indicated that the increase of the drying temperature made a larger difference in the bigger bed when compared to the smaller bed. Making reference to the constant scaling factor observed earlier, delineating the effect of the bed height in affecting the drying time, it appears that the bed height minimizes the effect of variation in temperature on the drying behaviour. As the height of the bed increases the steam temperature decreases (due to the heat transfer from the particles at the base of the bed). The 1 kg bed has a higher bed and would

result in the particles at the top of the bed interacting with lower temperature steam, resulting in slower heat transfer.

5.3.4. Kinetics During Continuous Drying

The experimental conditions used in the larger apparatus were similar to the batch experiments, with the primary aim to investigate the effect of scale and continuous operation on the drying behaviour. Using the larger apparatus continuously requires the initial bed to be dry rather than wet. In the batch systems the raw coal almost immediately fluidises, however this does not occur in the larger 3kg bed. To avoid de-fluidisation an initial bed of dried coal was used to promote fluidization before the wet coal was continuously added. When the wet coal was fed into the bed, the increase in bed height caused the bed to overflow via the outlet, where it was collected and analysed. Once the outlet moisture content became consistent, this value was determined to be the steady state outlet moisture content. The impact of specific variables was determined by comparing the output moisture contents of the coal at various drying conditions.

In the larger apparatus the trends observed in the continuous drying process was similar to that from the smaller apparatus. The temperature was varied under similar conditions: 1.2 – 2.3 mm, ~0.45 m/s, 2.3 kg/h coal feed (50 minutes residence time) and Yallourn as well Loy Yang coal were used. The increasing the drying temperature (**Figure 5.15**) resulted in a reduced outlet moisture content. From 130°C to 200°C the stabilised outlet moisture ranges from 4% to 1.5%. A higher drying temperature increases in drying rate and reduces the equilibrium moisture content.

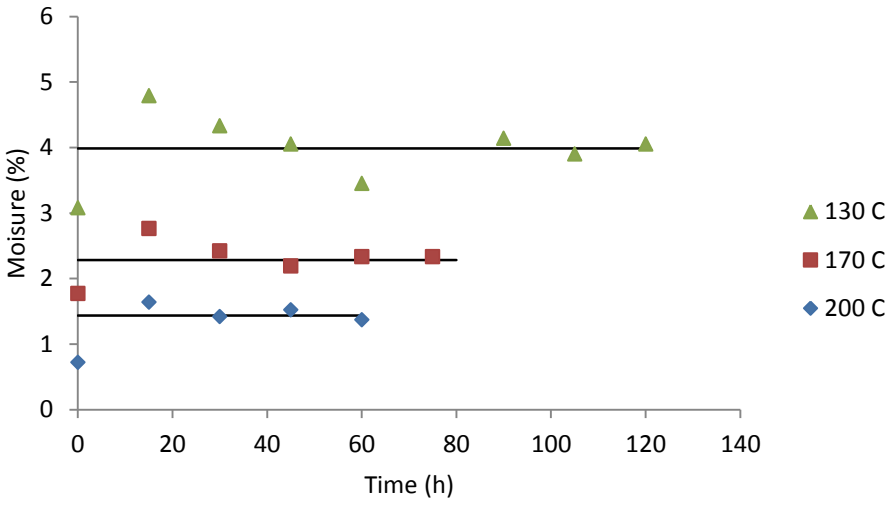

Figure 5.15 The effect of drying temperature on the outlet moisture content

Comparison was then made between the usage of air and steam as the fluidization mediums at a temperature of 135 °C using particle size of 1.2 to 2.3 mm and a velocity of 0.45 m/s for both Loy Yang and Yallourn brown coal. The results in **Figure 5.16** showed that air fluidized bed drying produced coal with a lower moisture content. A residence time of 50 minutes dries the coal to its equilibrium moisture content, and is shown in **Figure 5.17**. Examining the start-up time for the coal to reach its equilibrium moisture content, Loy Yang coal (a particle size range of 1.2 – 2.3 mm and a steam temperature of 135°C) required approximately 40 to 60 minutes before equilibrium moisture is reached. Compared to the batch dried conditions, the coal required 30 minutes to reach equilibrium moisture.

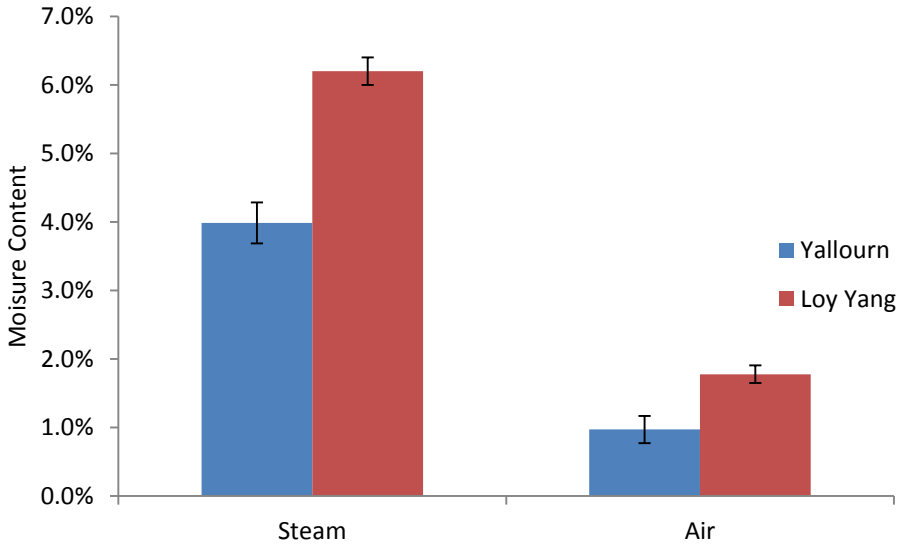

Figure 5.16 The impact of drying medium on output moisture content

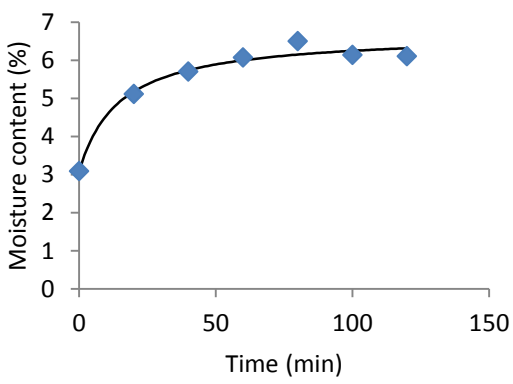

Continuous coal feed fluidized bed

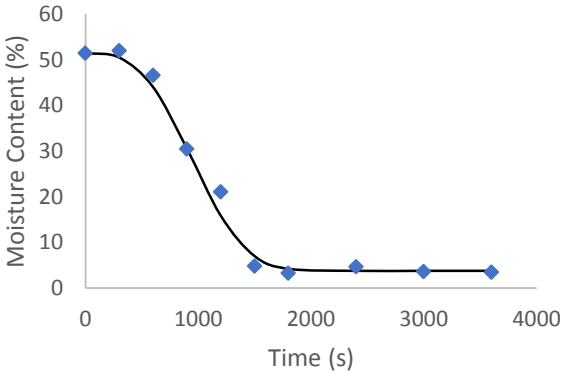

Batch fluidized bed

Figure 5.17 The start-up time required in a continuous fluidized bed vs. the drying time required in the smaller apparatus

Table 5.8 shows there was little difference in the final moisture contents between the continuous large rig operation and the small rig batch operation for Yallourn and Morwell coal. Comparing the large scale apparatus to the earlier batch experiments in the smaller apparatus (which represents ideal drying conditions) difference in the resultant moisture content is within 0.5%wt. For Loy Yang coals, however, the differences were slightly larger with the continuous operation producing slightly higher moisture content of approximately 1-3%wt show some difference. This can be attributed to the heterogeneous nature of coal than to incomplete drying. As previously stated, a separate batch of Loy Yang coal was used in the larger experiments, this is characterised with a lower initial moisture content and a higher equilibrium moisture content and accounts for differences in equilibrium moisture content shown in **Table 5.8**.

At the beginning of the continuous operation experiments, it was hypothesized that due to the increased bed height (13 mm vs. 80 mm) a larger temperature drop across the bed would be observed and this could have increased the equilibrium moisture content of the coal. However, **Table 5.8** shows that the equilibrium moisture content is consistent regardless of apparatus size. This suggested that within the range of the bed height evaluated in this work, the initial fluidization medium temperature can be taken as the basis for determining the equilibrium moisture content.

Table 5.8 Comparison of equilibrium moisture contents

Coal Type	Fluidization Medium	Temperature (B)	Temperature (C)	Moisture Content (B)	Moisture Content (C)	Residence Time (C)	Temperature drop (B)
Yallourn	Steam	200	~195	Not Available	0.44%	Low (50 min)	~-12°C
Yallourn	Steam	170	~170	Not Available	2.28%	Low (50 min)	~-30°C
Yallourn	Air	130	~135	0.62%	0.80%	Low (50 min)	Not Available
Yallourn	Steam	130	~135	4.14%	4.01%	Low (50 min)	~-12°C
Loy Yang	Air	130	~135	0.75%	1.7%	Low (50 min)	Not Available
Loy Yang	Steam	130	~135	2.86%	6.2%	Low (50 min)	Not Available
Morwell	Steam	130	~135	5.06%	5.14%	High (70 min)	Not Available
Morwell	Steam	170	~175	Not Available	2.74%	High (70 min)	Not Available
Loy Yang	Steam	130	~135	2.86%	3.96%	High (70 min)	Not Available
Shenhua	Steam	130	~135	Not Available	4.31%	High (70 min)	~-8°C

(C) Continuous Apparatus (B) Smaller Batch Apparatus

5.3.5. Observations

A qualitative assessment on the limitations of the large fluidized bed is the fluidization characteristics. Analysis on the effect of the residence time in the drying behaviour (using Loy Yang coal at 0.45 m/s, 1.2 – 2.3 mm and 130°C) was achieved by increasing the wet coal feed rate (full set of preliminary results not shown here). Because complete drying was observed, increasing the coal feed rate and reducing the residence time is beneficial as it will increase the process efficiency. However, this method of reducing residence time is limited by the changing bed characteristics. As residence time decreases partial de-fluidization within the bed is observed, slowing or even stopping fluidization. Through trial and error the lowest stable residence time was 50 minutes.

The de-fluidization occurred due to clumping of the raw coal in the bed. At lower temperatures the wet coal does not disperse within the fluidized bed. This phenomenon was only observed during steam fluidized bed drying, with similar conditions under air fluidized drying not provoking the same behaviour. At lower drying temperatures the inlet coal generates greater amounts of condensation, this was in conjunction with a static feed point into the bed and the density differences between wet and dry coal cause the wet coal to immediately stick together. At faster feed rates the wet coal cannot adequately disperse into the bed. The increased density in the bed caused the steam to circumnavigate the larger clump in opposed to breaking the clumps, slowing the drying rate and reducing the fluidization within the bed.

This effect was also seen in the smaller apparatus, where the gas flows around the coal mass. While the steam initially causes the cake formation, as the coal particles quickly increase in temperature, the lump will eventually undergo sufficient drying to allow the particle to disperse and full fluidization to quickly resume. Under extreme conditions the coal mass preferentially lifts off the sintered plate rather than break, and is shown in **Figure 5.18**. The caking was seen in both 1.2 – 1.7 mm and 0.5 – 1.2 mm particle sizes; however the full caking observed in **Figure 5.17** was more prevalent in smaller particle sizes.

Figure 5.18 Loose caking of Victorian brown coal in vessel freeboard

This effect limits the flow rate of the coal in the larger apparatus, and based on the analysis of the fluidization velocity in the smaller and larger apparatus (to a maximum of 0.6 m/s), it was concluded that increasing the fluidization velocity was not an appropriate method to prevent caking. Combining this conclusion with the results in **Table 5.8**, which showed that drying is essentially complete, the results suggest that the limiting factor in the current experimental set up was the fluidization effects discussed. Based on the previous observations, some recommendations are given below to increase the coal throughput while preventing the caking effect:

- Pre-heat the inlet coal to prevent initial condensation of steam and to reduce the coal density difference

  Rationale: As the de-fluidization has been partially attributed to the condensation across the particle, preheating through energy integration will increase the inlet coal temperature, preventing condensation and promoting bed mixing.
- Increase the drying temperature to prevent condensation occurring

  Rationale: Another method of reducing condensation is to increase the inlet temperature of the fluidization medium. The caking effects were not observed at 170°C.
- Vary the coal inlet position

  Rationale: If the wet coal is spread evenly across the bed, the wet coal would not have the available mass to cause clumping and this will allow for a greater feed rate to be used.

For power generation, operating at lower temperatures can be more energy efficient, therefore initial heating has the greatest viability for increasing the throughput within the bed. In conjunction with excess waste heat (though integrated heat utilization) the energy efficiency could be maintained while allowing for a large coal throughput without resorting to inefficient increases in temperature.

5.4. Conclusions

Key findings from the analysis of the small apparatus experiments are listed below:

- Drying kinetics show in air and steam fluidized bed drying have the same trend, with smaller particle sizes, higher velocities and higher temperatures decreasing drying time
- A similar change in temperature and fluidization velocity results in a similar drying ratio however for a similar particle size change the steam fluidized bed dried coal has a greater proportional decrease in drying time, and has been attributed to a reduced condensation mass
- Modelling of the drying kinetics shows that the Midilli-Kucuk equation is viable for the analysis of fluidized bed kinetics, but a more detailed model has been identified for further work, and is investigated in Chapter 9.

Key findings in the analysis of the large rig experiments are listed below:

- The larger batch drying experiments show the 130 and 170 °C drying ratios are consistent regardless of coal type
- Using the Page equation, the small scale batch kinetics can be translated into larger scale batch kinetics through a common scaling co-efficient (d_1) which was deduced to be related to the bed height
- Larger continuous fluidized bed drying showed similar trends based on outlet moisture content, with higher temperatures resulting in lower moisture contents. This was due to higher temperatures resulting in lower moisture contents
- Even with the continuous larger rig operation, similar equilibrium moisture content was achieved when compared to equilibrium moisture content of the coal determined from the small rig. This showed that for the range of bed height and drying times evaluated in these experiments, the equilibrium moisture data can be directly translatable to the big scale operation

Chapter 6. Chemical Characteristics

This chapter investigates how drying conditions affect the chemical characteristics of coal. Understanding the change in chemical composition of coal will determine the practicality and usability of Victorian brown coal in processes such as combustion, gasification, pyrolysis and liquefaction [65]. Chemical characteristic affect properties such as: water in coal [5, 198], moisture re-adsorption [37, 38, 42, 215, 216] and reactivity [217]. These properties are investigated in Chapter 4, Chapter 8 and Chapter 10.

Two factors identified as the most likely cause of chemical change are, the drying medium (air and steam) and temperature (130°C to 200°C) which will affect the functional group composition and hydrophobicity of the resultant coal.

The initial aim of the chemical characteristics was to use FT-IR analysis to characterise functional groups present in Victorian brown coals. However in 2013 Tahmasebi et. al. [65] published a body of work which overlaps with this thesis. The FT-IR results presented in this chapter will characterise the difference between air and steam fluidized bed drying using Morwell coal, confirming results presented by Tahmasebi et. al. [65] which used Loy Yang and Yallourn coals.

Information from this chapter is present in the submitted publication: David Stokie, Srikanth Srivatsa, Sankar Bhattacharya "The Effect of Drying and Pyrolysis on Surface Function Group Evolution in Brown Coal and Chinese Lignite using Synchrotron In-situ Infrared Analysis"

6.1. Laboratory Infrared Analysis

6.1.1. Literature Review

Victorian brown coals have (on a dry, ash free basis) 25% oxygen content, comprising 50% acidic compounds such as phenolic hydroxyl, free carboxylic acid and carboxylate, and 50% with carbonyl groups, ether linkages and heterocyclic ring structures [218]. Perry found coal varied by approximately 2-3% in carbon and volatile matter (on a dry basis) depending on seam depth, as volatile matter decreases with seam depth [218].

There have been few investigations on laboratory Fourier transform infrared (FT-IR) spectroscopy [219]. Analysis of the organics released from peat and lignite in a steam fluidized bed shows organic release comprised of aliphatic mono- and di- carboxylic acids methanol, aliphatic aldehydes, anhydroglucoses and furanoic compounds. At short residence

times the release of hydrophilic and lipophilic organic groups increases tenfold as temperature increases from 190°C to 350°C [220]. Estimation of the carbon-oxygen ratio through curve fitting carbon spectra through X-ray photoelectron spectroscopy (XPS) is conducted and shows the concentration of unidentified carbon and oxygen functional groups on the surface increases as temperature approaches 50°C. The functional groups are determined to be predominantly oxygen atoms singly bonded to one or two carbon atoms, however these cannot be differentiated using the C spectrum [221].

Tahmasebi et. al. (2011) investigated the chemical characteristics during drying of a range of coals, drying methods and conditions using ex-situ Fourier transform infrared (FT-IR) spectroscopy to assess the effect of microwave, steam and air drying on Chinese lignite [188]. They reported that increase in drying temperature using superheated steam results in a minor decrease in aliphatic hydrogen, but carboxyl and carbonyl content decreases sharply. Microwave drying shows a similar trend, with small amounts of aliphatic hydrogen removed and significant decreases in oxygen functional groups. Air drying of Chinese lignite initially increases aliphatic hydrogen content up to 200°C followed by a sharp decrease at 250°C. In the three drying methods the aromatic carbon was observed to not change [188]. Tahmasebi et. al. (2012) also analyses the effect of temperature in a steam, air and nitrogen fluidized bed on Victorian brown coals, using Loy Yang and Yallourn coals obtained similar results to previous Chinese samples. Air fluidization causes a decrease in aliphatic structures, carbonyl and carboxyl groups. Drying in steam causes a decrease in hydroxyl, carboxyl and carbonyl groups, and minor changes to aromatic carbon. Nitrogen drying shows similar decreases in oxygen functional groups but with an increase in aromaticity [65, 189].

Yurun et. al. (1998) investigated drying temperature using (Turkish) Beypazari lignite. At temperatures ranging between 50°C to 150°C alkyl groups converts to aldehydes 50°C and to carboxylic acids at 150°C. Methylenic to ketone transition occurs between 50°C and 150°C, with the methylenic groups converting to ketones at 50°C and is at a maximum at 100°C [222]

When drying in an inert atmosphere, pyrolysis can also occur depending on temperature. Pyrolysis is the release of volatile matter with the resultant coal eventually turning into a char, which can then be used for processes such as gasification. For Victorian brown coal, drying and pyrolysis is known to happen in three stages: below 150°C is predominantly moisture loss, 150 to 310°C is when some of the alkyl aromatics are evolved, with

carbonization occurring above 310°C [223]. The change in coals functional groups during pyrolysis has the capacity to change the usability of the dried coal, impacting upon its potential for gasification, carbonization, liquefaction or combustion processes and can lead to the reduction of the coals calorific value [224].

6.1.2. Materials and Methods

Various apparatus' are used to analyse the chemical characteristics of the dried coal, including a PerkinElmer Series II CHNS/O Analyser 2400 and a PerkinElmer Frontier Fourier transform infrared (FT-IR) spectrometer. The apparatus and experimental parameters used are shown in **Table 6.1**.

Table 6.1 Experimental parameters

Variables	Parameters
Coal type	Loy Yang, Yallourn, Morwell
Pellet buffer	Potassium Bromide (KBr)
FT-IR sample mass	2 mg
FT-IR pellet mass	200 mg
CHNS mass	0.9 to 2.2 mg
Drying medium	Air, Steam
Fluidization velocity	0.48 m/s
Drying temperature	100 to 200 °C
Particle size	1.2 to 1.7 mm
CHNS sample runs	3 to 5 runs
FT-IR sample runs	2 runs

The oxygen functional groups are analysed from selected coal samples used in measuring drying kinetics (Chapter 6). Using FT-IR data, it is observed that oxygen functional groups show the greatest level of change which will significantly affect properties such as moisture re-adsorption, hydrophobicity and reactivity.

Due to the small mass of coal used in KBr pellets during FTIR analysis, small variations in coal mass results in different adsorption values. To compare the functional groups, aromatic carbon (C_{ar}) is used to normalise inherent errors from sample analysis, as literature shows the aromatic carbon does not change at low temperatures [65].

6.1.3. The Impact of Drying Temperature on Morwell Coal Functional Group Composition

The analysis of the impact of drying temperature on the functional group composition was conducted using Morwell coal and compared to the results found in Tahmasebi et. al. [65]. The results in **Table 6.2** show that an increase in steam temperature results in methyl: methylene ratio increasing, followed by a decrease at 170°C. This is attributed to the loss of methylene aliphatic groups in the formation of aromatic rings and is supported by the increase in aromatic carbon: aliphatic hydrogen ratio. The decrease in carbonyl groups are observed in **Table 6.2** along with the Oxygen/Carbon (O/C) ratio. A consistent decrease of the O/C ratio indicates a decrease in oxygen content with increasing temperature, and is consistent with results in Tahmasebi's [65]. The decrease in oxygen can affect properties including moisture re-adsorption potential, hydrophobicity and ignition temperature (discussed in Chapter 6, Chapter 8, Chapter 10)

Table 6.2 The impact of steam temperature the functional group composition of Morwell coal

	$C_{ar}/(COOH+C_{ar})$	$(C=O)/C_{ar}$	$COOH/C_{ar}$	CH_3/CH_2	C_{ar}/H_{al}	O/C
Raw	0.59	3.27	0.68	0.16	1.98	0.62
130°C	0.64	2.54	0.57	0.37	3.71	0.58
170°C	0.62	3.00	0.64	0.38	2.44	0.55
200°C	0.69	2.71	0.46	0.30	2.49	0.54

During air fluidized bed drying aliphatic hydrogen (H_{al}) decreases at higher drying temperatures, while the carbonyl groups show an initial decrease before steadily increasing. The methyl/methylene (CH_3/CH_2) ratio increases, indicating the decrease of methyl groups due to oxidation. This mechanism is also consistent with an increase in oxygen functional groups previously outlined in Tahmasebi [65]. Carbonyl and carboxyl content initially decreased when dried to 130°C before increasing. The results in **Table 6.3** show a similar profile with $COOH/C_{ar}$ dropping 25% before increasing with drying temperature. The increase in C_{ar}/H_{al} indicating a decrease in H_{al}, and increase in oxygen aliphatic sites at high temperatures.

Both steam and air experiments show the oxygen/carbon ratio decreasing. For steam fluidized bed drying in **Table 6.2** the oxygen content decreases consistently, while for air fluidized bed drying (**Table 6.3**) the oxygen content initially increases before sharply decreasing, and

behaving similarly to that observed in the FT-IR analysis. Both trends displayed oxygen/carbon ratios similar to Tahmasebi [65, 188, 189].

Table 6.3 The impact of air temperature the functional group composition of Morwell coal

	$C_{ar}/(COOH+C_{ar})$	$(C=O)/C_{ar}$	$COOH/C_{ar}$	CH_3/CH_2	C_{ar}/H_{al}	O/C
Raw	0.59	3.27	0.68	0.16	1.98	0.62
100°C	0.66	2.92	0.51	0.29	2.15	0.54
130°C	0.64	2.34	0.57	0.26	3.26	0.57
170°C	0.60	1.79	0.66	0.39	4.10	0.52

6.2. Synchrotron Infrared Analysis

Laboratory infrared spectroscopy uses an ex-situ method, requiring a mass of pre dried coal to be crushed and dispersed in a Potassium Bromide (KBr) pellet. Due to the dispersion the infrared beam is not focused on a single particle but a range of particles, meaning the bulk surface functional groups are measured. The Synchrotron infrared analysis uses an in-situ method, allowing the IR spectra to be collected during drying and pyrolysis. Compared to laboratory IR, a benefit of the single particle analysis is that the same particles are examined at all temperatures, reducing the variation and error from heterogeneous differences in the coal, and no longer requiring normalization required in ex-situ analysis [65, 188, 189].

The purpose of this section is to investigate, in-situ, the effect of temperature and residence time on the functional group evolution of low rank coals. Because the chemical characteristics of dried coal can make an impact on usage of coal, it is important to establish the optimal drying conditions. The in-situ process allows examination of functional groups in single particles, providing more accurate data than bulk sample analysis. Analysing the increase in particle temperature allows for an accurate determination of when the loss in functional groups initially occurs, while the investigation into the effect of residence time provides important information on the drying time required as a function of particle size.

6.2.1. Materials and Methods

Morwell brown coal and No. 5 Shenhua lignite are used to determine the effect of increasing temperature on the functional group evolution. Morwell brown coal, Yallourn brown coal and No. 5 Shenhua lignite are also used to determine the effect of residence time on functional group evolution.

The experiments were carried out using the Infrared Microspectroscopy (IRM) beam line at the Australian Synchrotron. The sample slide and sample stage windows use a 0.5 mm

Barium Fluoride (BaF_2) disc to provide transparency at higher temperatures. The coals are dried under a 6 L/min nitrogen flow, which is used to purge any air remaining in the sample chamber as well as any gas evolved through the drying process. The full range of system parameters and samples tested is shown in **Table 6.4**.

The analysis of the spectra uses OPUS 7.2 software and follows a procedure for experiments, data collection and analysis detailed in Kirtania et. al [190] as well as Chapter 3. All the spectra are normalised between 0 and 1.

Table 6.4 Experimental parameters

Variable	Parameters
Particle Size	90-106 µm
Sheath Gas	Nitrogen
Sheath Flow	6 L/min
Coal Types	Morwell, Yallourn, Shenhua No.5
Temperature	30 – 550 °C
Residence Time	0 – 60 minutes
Ramp Temperature Rate	10 K/min
Slide Diameter	16 mm BaF_2
Slide Thickness	0.5 mm
Window Diameter	22 mm BaF_2
Window Thickness	0.5 mm
Sample Stage	Linkam FTIR600
Central Aperture	16 mm
Microscope	Hyperion 2000 IR microscope
Spectrometer	Bruker V80v FTIR spectrometer

The Infrared Microspectroscopy beam line at the Australian Synchrotron is capable of producing a range of wavenumbers up to 7800 cm^{-1}, however for coal the majority of the functional group wavenumbers occur between 1200 and 3700 cm^{-1} **Figure 6.1** shows the intensity peaks for Morwell coal and identifies the wavenumbers where peaks are clearly defined. The peaks are correlated with functional groups defined in **Table 6.5**.

Table 6.5 Functional groups and associated wavelengths

Band (cm^{-1})	Functional Group	References
3530	OH-π hydrogen bonds	[225, 226]
3425	Hydrogen bonded water	[65, 188, 189]
3150	Tightly bound cyclic OH tetramers	[225]
3280	OH-ether O hydrogen bonds	[225]
3230	Phenolic and carboxylic structures	[65, 188, 189]

2487 – 3156	Ketones (broad peak)	[227]
2993, 2930	Aliphatic hydrogen	[225]
2958	Methyl (–CH3)	[65, 188, 189]
2940	Aliphatic C-H stretching	[227]
2922	Methylene (–CH2–)	[65, 188, 189]
2896	Methane (C–H)	[65, 188, 189]
2870	Symmetric methyl (–CH3)	[65, 188, 189]
2850	Methylene (–CH2–)	[65, 188, 189]
2640	COOH dimers	[225]
2509 – 3010	COOH dimers	[228]
2370	Atmospheric CO_2 interference	[227]
2100-2260	Alkyne	
1850 – 2000	Alkene	[228]
1772	Esters, aliphatic COOH	[65, 188, 189]
1738	Esters, aliphatic COOH	[65, 188, 189]
1705	Aromatic COOH	[65, 188, 189]
1700	C= O stretching	[227]
1580 – 1865	C= O	[228]
1652	Highly conjugated C=O	[65, 188, 189]
1561	COO- aromatic ring	[65, 188, 189]
1488	COO- aromatic ring	[65, 188, 189]

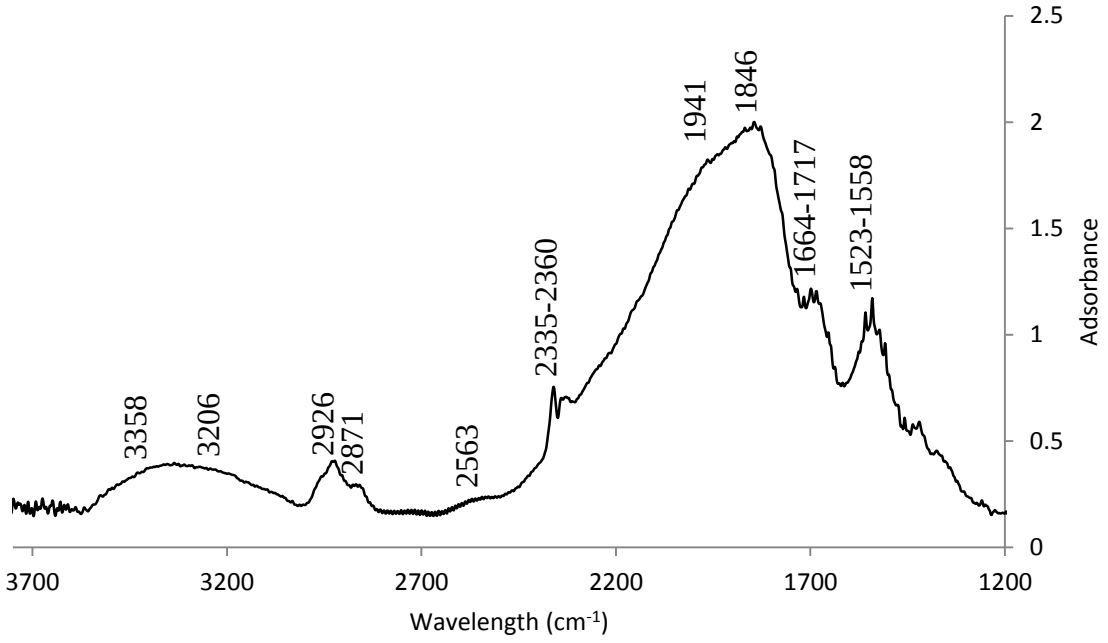

Figure 6.1 Morwell brown coal infrared spectrum at 80°C

6.2.2. The Effect of Temperature

With the increase in temperature, the functional groups present in Morwell brown coal undergoes significant changes (**Figure 6.2**). At 140°C, a major decrease peak intensity for hydrogen bonded water (3360 cm^{-1}) is observed, decreasing rapidly as the temperature increases. From literature, hydrogen bonded water is more closely associated with a wavenumber of 3425 cm^{-1} [65], however hydrogen bonded water is generally observed as a broad peak between 3200 – 3500 [229], and may obscure the non-bonded phenolic and carboxylic wavenumbers typically observed in a similar region (3230 cm^{-1}). This suggests the hydrogen bonding between the water molecules and oxygen containing groups begin to break at 140°C, therefore at temperature approximately 140°C, intrinsic water present in the coal structure should be readily removable. This is in line with results from laboratory based infrared spectroscopy, which finds a similar decrease in Loy Yang and Yallourn brown coals at 130°C [65].

At approximately 140°C an initial reduction in functional groups with wavenumbers between 1800 and 2200 cm^{-1} is also seen, with a faster drop in intensity observed at 200°C. These wavenumbers are correlated with the carbonyl (1850 cm^{-1}), alkene (1940 cm^{-1}) and alkyne (2173 cm^{-1}) surface functional groups. Also occurring at 200°C, a wider range of functional groups decrease. Methylene, symmetric methyl, methane (2850 – 3000 cm^{-1}), esters, aliphatic COOH, highly conjugated C=O (1650 – 1750 cm^{-1}) and COO^- aromatic rings (1500 – 1600) also significantly decrease in intensity. From Tahmasebi et. al. [65], these changes are observed to occur at 130°C, not 200°C. The difference has been attributed to the instantaneous nature of the spectra measurements. It is hypothesised that the functional group loss does occur at 130°C, however not noticeably until either a higher temperature or a longer residence time. An overview the observed functional groups in Morwell coal is summarised in **Table 6.6**. In **Figure 6.2** peaks functional groups are observed at 2300 – 2400 cm^{-1} at all temperatures. These indicate the presence of carbon dioxide (CO_2) in the sample, and are taken as interface from atmospheric CO_2.

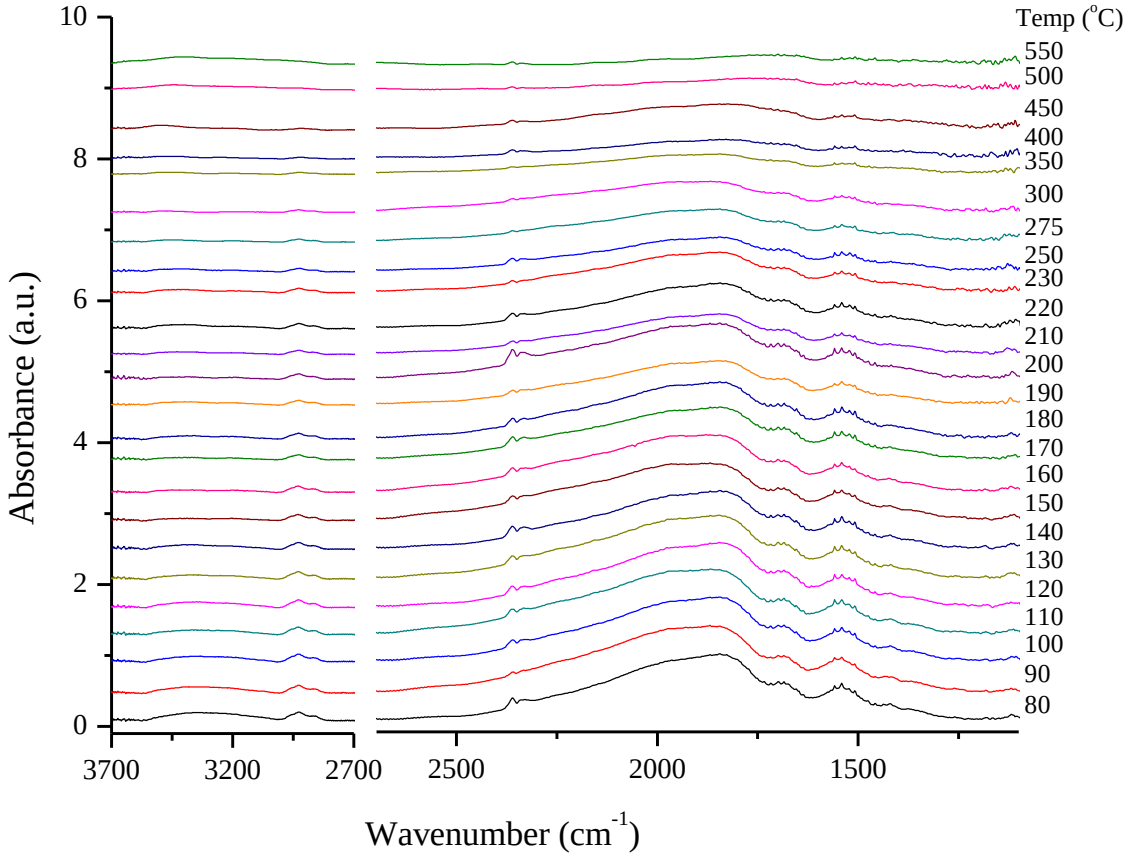

Figure 6.2 The effect of temperature on Morwell brown coal infrared spectrum

Table 6.6 Functional group change in Morwell brown coal with temperature

Observed Wavenumbers (cm^{-1})	Functional Groups	Transition Temperature	Description
1500 – 1600	COO^- aromatic ring	Minor: 80 to 200°C Major: 200 to 250 °C onwards	Minor intensity decreases from 80 to 200°C Intensity drop is observed between 200 to 250°C A constant intensity decrease at afterwards
1650 – 1750	esters, aliphatic COOH, highly conjugated C=O	Minor: 80 to 200°C Major: 250°C onwards	Minor intensity decreases from 80 to 200°C Intensity drop is observed between 200 to 250°C A constant intensity decrease at afterwards
1850	C=O	Major:140 to 160°C Major: 200 to	An initial drop is observed between 120 to 140°C, A secondary, larger, drop is seen

		250°C onwards	from 200 to 250°C A constant intensity decrease at afterwards
1940	alkene	Major:140 to 160°C Major: 200 to 250°C onwards	An initial drop is observed between 120 to 140°C, A secondary, larger, drop is seen from 200 to 250°C A constant intensity decrease at afterwards
2173	alkyne	Major:140 to 160°C Major: 200 to 250 °C onwards	An initial drop is observed between 120 to 140°C, A secondary, larger, drop is seen from 200 to 250°C A constant intensity decrease at afterwards
2850 – 3000	methyl, methylene, symmetric methyl, and methane	Major: 200 to 250 °C onwards	A continual decrease is observed until 200°C, From 200 to 250 °C a large drop is observed After 250°C the decrease continues. At higher temperatures the signal increases, however no defining peaks are observed
3230	Phenolic and carboxylic structures	Consistent decrease	No major jumps are observed for this peak, with a steady decreases observed. It can be described as negligible after 180°C
3360	hydrogen bonded water	Major:140 to 160°C onwards	A drop in peaks is observed from the 140 to 160°C temperatures, After 160°C a consistent decrease is seen

Shenhua (Chinese) lignite functional group composition was also observed with the increase in temperature (**Figure 6.3**) Similar to Morwell brown coal, Shenhua lignite shows initial drops in alkene (1970 – 2040 cm^{-1}), and alkyne (2160 cm^{-1}), functional group intensity at 140°C. However, Shenhua lignite also shows drops in esters, aliphatic COOH, aromatic COOH, C= O and COO- aromatic rings (1415 – 1775 cm^{-1}), as well as CH_3, aromatic and aliphatic hydrogen (2874 – 3954 cm^{-1}). Comparatively, these reductions occur earlier than what has been observed in Morwell brown coal. When compared to Tahmasebi et. al. [189], where the aliphatic hydrogen remained unchanged up until 200°C and major decreases observed after 250°C, aliphatic hydrogen loss occurs earlier in the synchrotron, with the majority of the functional groups lost by 200°C. This is attributed to the synchrotrons increased ability to analyse the surface functional groups of a single particle. An overview of the functional group progression for Shenhua coal is shown in **Table 6.7**.

Table 6.7 Functional group change in Shenhua lignite

Observed Wavenumbers cm^{-1}	Functional Groups	Transition Temperature	Description
1415 – 1775	esters, aliphatic COOH, aromatic COOH, C= O and COO- aromatic ring	Major: 140 – 160 °C	All functional groups generally decrease until 140°C. A rapid loss occurs after 140°C until 200°C. After 200°C minor decreases occur, with a smaller jump from 400°C to 450°C. This shows the majority of the functional groups are been lost after 200°C
1970 – 2040	alkene		
2160	alkynes		
2600 – 2850	ketone		
2874 – 2954	CH_3, aromatic and aliphatic hydrogen		
3366	hydrogen bonded water		

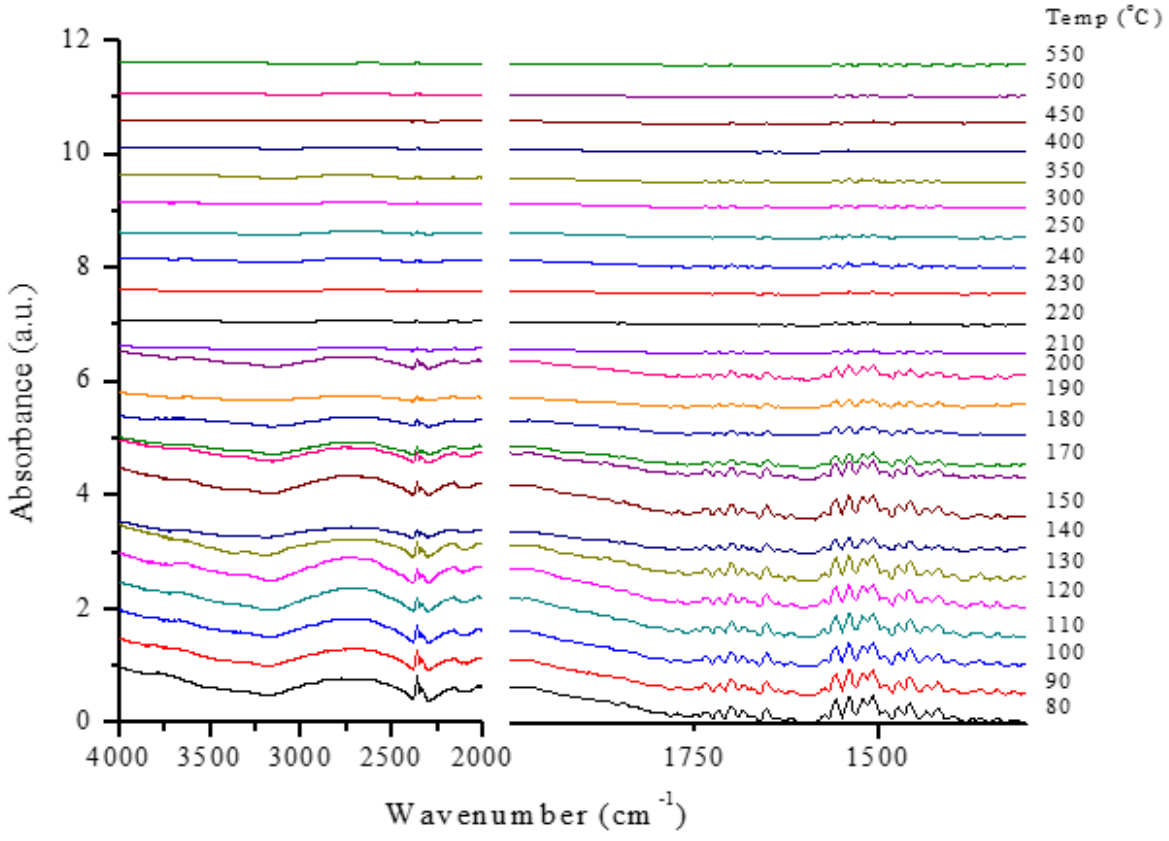

Figure 6.3 The effect of temperature on Shenhua lignite infrared spectrum

Comparing Morwell brown coal to Shenhua lignite, Morwell brown coal shows functional group loss occurring at a higher temperature (400 to 550°C) while Shenhua lignite functional

group loss occurs primarily before 200°C. This indicates the Shenhua lignite appears to be more sensitive to drying temperature than Morwell coal.

6.2.3. The Effect of Residence Time

While laboratory based coal drying experiments typically require 5 to 10 minutes [209] for the moisture content to reach drying equilibrium, residence times between 30 and 60 minutes are often used in industry [20]. The longer residence times result in additional changes to the functional group composition.

Investigating the effect of residence time on Morwell brown coal, an ambient temperature of 130°C was used, with spectra obtained in 10 minute intervals. Comparing the initial spectra to residence times up to 30 minutes (**Figure 6.4**) shows an initial change occurring from 0 to 10 minutes, and a relatively stable spectra onwards. After 10 minutes the intensity of alkene (1940 cm^{-1}), alkyne (2173 cm^{-1}), hydrogen bonded water (3430 cm^{-1}), methylene, symmetric methyl and methane (2850 – 3000 cm^{-1}) functional groups decrease. At 20 and 30 minutes the spectra exhibits little change, with a minor reduction in intensity at 2750 cm^{-1} and 2950 cm^{-1}, indicating a minor decreases in the methyl functional groups.

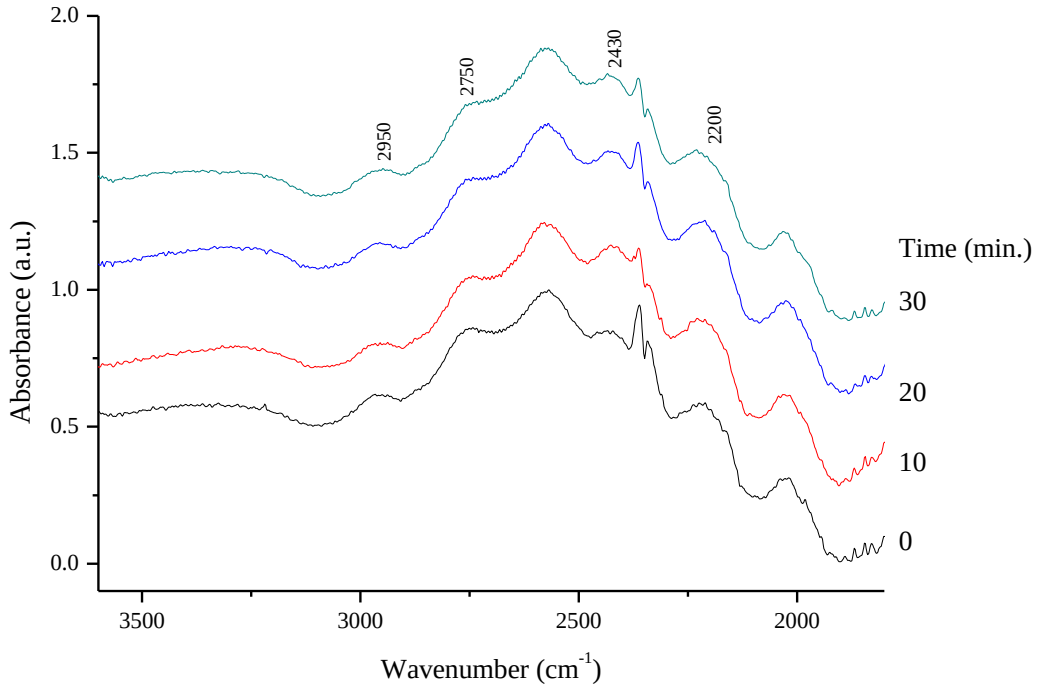

Figure 6.4 Morwell coal functional group change as a function of residence time (130°C)

Comparing Morwell brown coal to Yallourn brown coal (**Figure 6.4**), a similar trend emerges. After 15 minutes, decreases are observed between methylene, symmetric methyl and methane (2800-3000 cm^{-1}), alkyne (2165 cm^{-1}), hydrogen bonded water (3430 cm^{-1}) and COOH dimers (2700 cm^{-1}). Beyond 15 minutes, hydrogen bonded water (3430 cm^{-1}), methylene, symmetric methyl, methane (2850 – 3000 cm^{-1}) and alkynes (2165 cm^{-1}) show minor decreases.

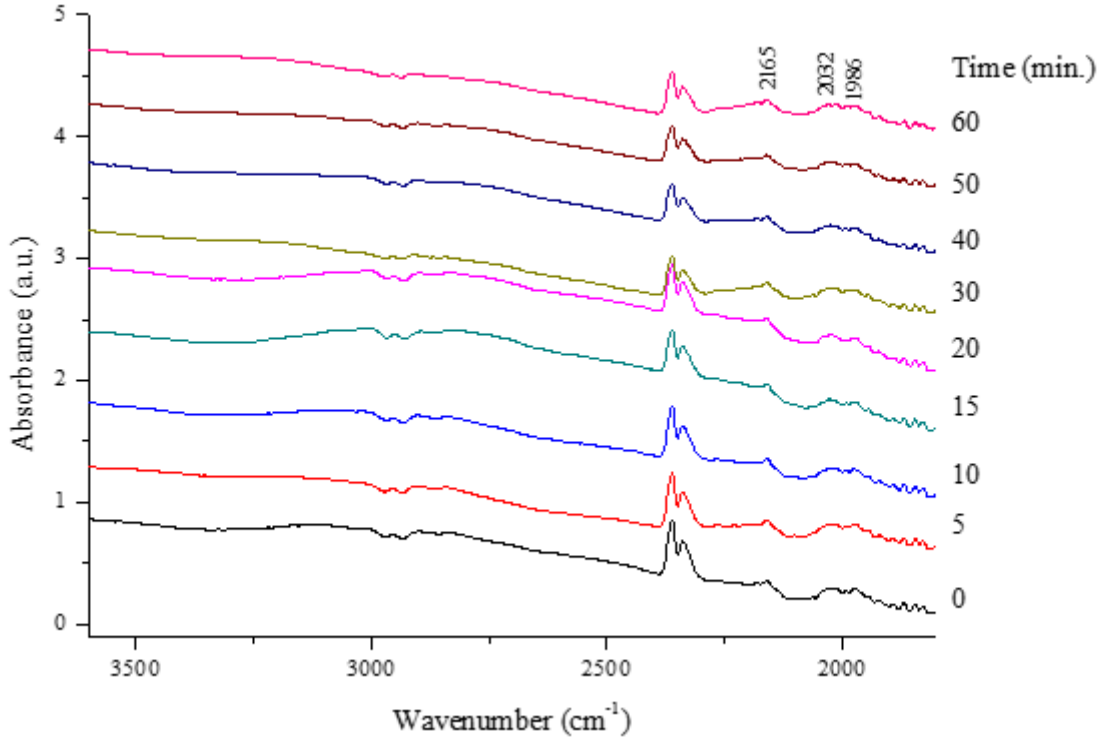

Figure 6.5 Yallourn coal functional group change as a function of residence time (130°C)

After 10 minutes Shenhua lignite (**Figure 6.6**) displays a reduced intensity for hydrogen bonded water (3430 cm^{-1}), methylene, symmetric methyl, methane (2850 – 3000 cm^{-1}), alkyne (2100 cm^{-1}) and aliphatic COOH (1738 – 1772 cm^{-1}). At 20 and 30 minutes the surface functional groups show additional loss, with methylene, symmetric methyl, methane (2850 – 3000 cm^{-1}) and alkynes (2165 cm^{-1}) consistently decreasing.

Comparing the effect of residence time on the three different coals, a similar trend is seen. At 130°C, the majority of the functional group changes occur within the initial residence time of 10 minutes. For both Victorian brown coal and Shenhua lignite, methylene, symmetric methyl, methane (2850 – 3000 cm^{-1}) and alkyne (2165 cm^{-1}) functional groups continue to be

removed as the residence time is increased, however in Shenhua lignite the reduction appears more readily.

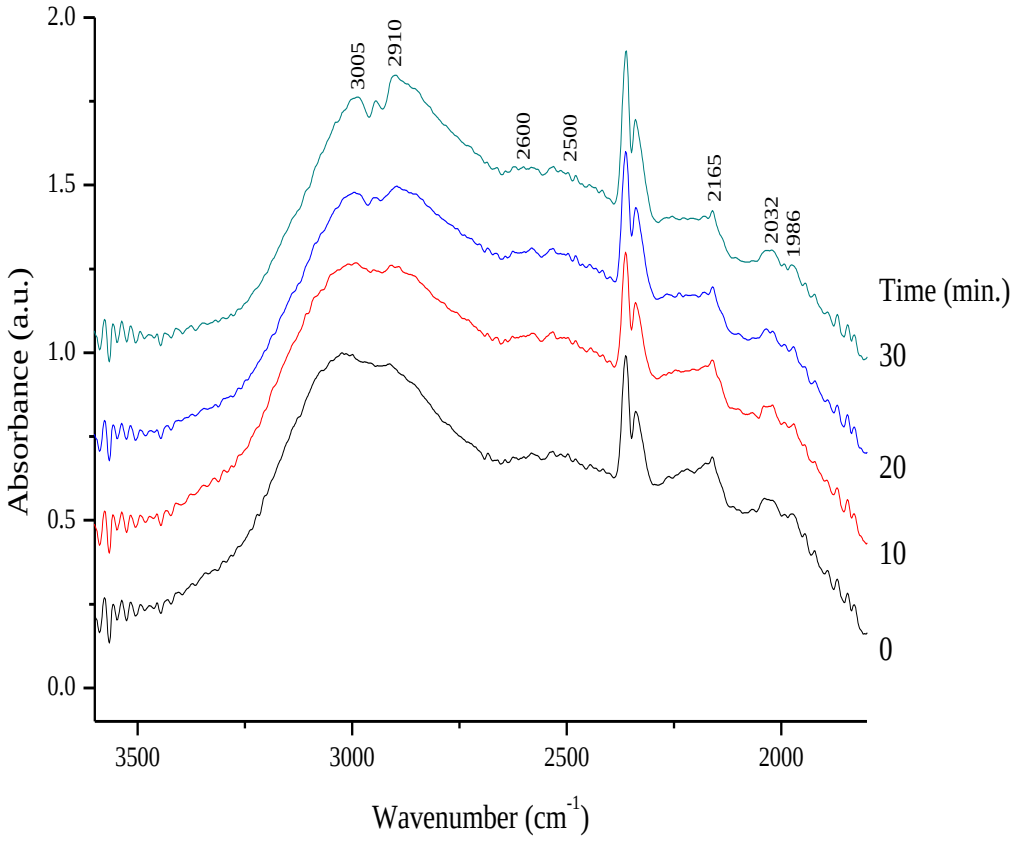

Figure 6.6 Shenhua coal functional group change as a function of residence time (130°C)

Comparing the effect of a higher temperature (170°C) in **Figure 6.6** , Morwell brown coal shows a consistent drop in intensity for alkyne functional groups (2165 cm^{-1}), with drops in 2470 cm^{-1} and 2635 cm^{-1} (COOH dimers) observed after 15 minutes residence time. At 2800 – 3000 cm^{-1} (methyl, methylene and methane), 3300 cm^{-1} (phenolic and carboxylic) a decrease in intensity is also initially seen at 20 minutes, with a large drop in intensity at 25 and 30 minutes.

Assessing the effect of residence time at 130°C and 170°C for Morwell coal, at 130°C there is little effect of a longer residence time on functional group evolution, however at 170°C many functional groups show consistent degradation, observable 15 to 25 minutes after the temperature is reached. In previous studies [209] we established that the required drying times of Morwell coal is around 5 to 6 minutes. This synchrotron FTIR results show that

major functional group loss may not occur within the drying time required for Morwell coal particles.

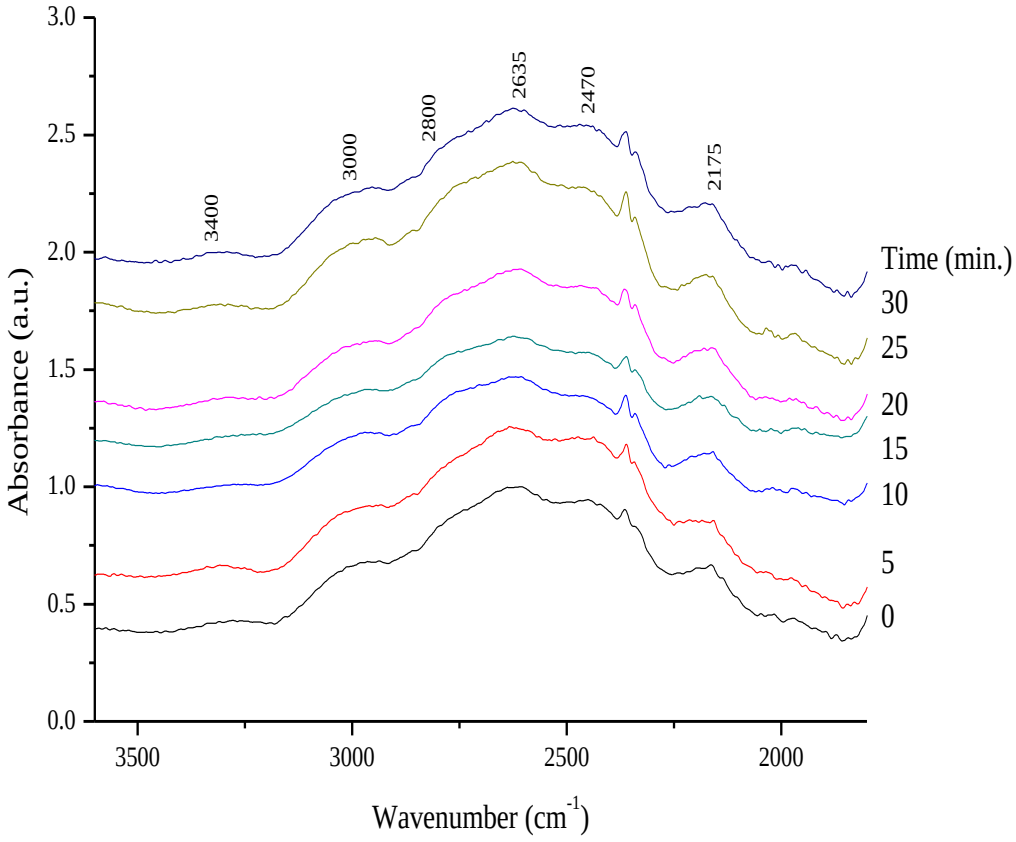

Figure 6.7 Morwell coal functional group change as a function of residence time (170°C)

6.2.4. Implications

Comparing the effect of temperature on Morwell brown coal and Shenhua No.5 lignite suggests that Shenhua lignite is more susceptible to temperature. While they initial decrease are observed at similar temperatures, Shenhua lignite rapidly loses the majority of its functional groups by 200°C. This indicates that Shenhua lignite is more temperature sensitive and should be dried at temperatures below 200°C, even for short drying times.

For Morwell coal, minor change occurs at 130°C, while a much larger change is present at 170°C. At 130°C a residence time of up to 30 minutes has little impact on functional group composition apart from a minor reduction in methyl groups , while at 170°C a drying time over 15 minutes results in functional group loss. This provides a guideline for maximum drying time available before functional group loss occurs.

Yallourn and Shenhua coals show degradation at 130°C. For Yallourn the degradation is limited to the alkyne functional groups, while Shenhua lignite loses Alkyne's, COOH and aliphatic hydrogen. This indicates that coal rank is also a factor when observing functional group loss, and functional group loss is more prevalent in Shenhua lignite during drying.

6.3. Contact Angle Analysis

6.3.1. Literature Review

Another chemical characteristic which may change with drying is hydrophobicity. Hydrophobicity can be determined through a comparison of contact angles. The contact angle corresponds to liquid molecules attraction to solid molecules, with a stronger attraction (hydrophilic) resulting in lower contact angles (lowest possible angle approaching 0°). If a contact angle is greater than 90° the substance is considered hydrophobic while contact angles above 120° are considered highly hydrophobic while 150° is super hydrophobic [230, 231].

Previous work investigating the influence of coal rank on the contact angle has found that hydrophobicity is dependent the oxygen/carbon ratio and the surface hydrophobicity increases with removal of mineral matter. Tests using a range of coals, including Victorian brown coals, has shown that the contact angle hysteresis increases with coal rank [187].

Keller [232] investigated the effect of porosity and extent of oxidization on coal/water contact angle producing set of equations to describe the contact angle of water on coal which is found to be in good agreement with experimental values [232].

Mineral matter also impacts upon the wetting of the coal surface. Gosiewska et. al. finds increases in surface mineral matter reduces the advancing and receding contact angle. Gosiewska et. al. also found that larger mineral matter grains causes larger contact angles, with the shape of the grain making no difference to the contact angle [233].

Drying has the capacity to change the hydrophilic – hydrophobic characteristics of coal, which potentially affect downstream process such as froth flotation. Currently, there are multiple methods for determination the contact angle. Two current methods in use are the compressed pellet method and the rate of penetration method. Both have been discussed in further detail in He, Ying [234].

6.3.2. Materials and Methods

The investigation on contact angles was carried out collaboratively with the University of Science and Technology Liaoning (USTL), China. A range of Victorian brown coals were analysed, with the contact angles for different fluidization mediums (steam and air) and temperatures (130 to 200°C) determined. Experimental conditions are shown in **Table 6.8**.

Table 6.8 Experimental parameters

Variables	Parameters
Coal Tested	Morwell, Loy Yang, Yallourn
Fluidization Medium	Air, Steam
Drying Temperature	130 to 200°C
Fluidization Velocity	0.48 m/s
Particle Size	1.2-1.7 mm
Pellet Mass	200 mg
Pelletization Pressure	30 MPa
Pelletization Time	3 minutes

The method of contact angle analysis was:

1. Approximately 300 mg sample was weighed and hand ground for 1 minute to reduce particle size, with 200 mg used in the creation of a briquette
2. The sample was placed under 30 MPa pressure for 3 minutes to form the briquette
3. Using ultrapure water, a single drop was placed on the pellet and the contact angle measured using a POWEREACH JC2000C contact angle meter
4. A minimum of 10 readings for the contact angle was taken, using at least 3 different pellets

6.3.3. The Impact of Coal Type on Coal/water Contact Angle

Three different drying methods were used to analyse the effect of coal type on the contact angle; steam fluidized bed drying (SFBD), air fluidized bed drying (AFBD) and fixed bed drying (**Table 6.9**). Air fluidized bed dried coals show a difference in contact angles, Yallourn coal having highest contact angle, followed by Morwell and Loy Yang brown coals. The difference in contact angles appears to be approximately 7°, with an average standard deviation of 2.2°. This is similarly observed in both steam fluidized bed dried and fixed bed dried coals, indicating that the contact angle for each type of coal remains the same regardless of drying method. Loy Yang coal's low contact angle corresponds to its lower moisture re-adsorption equilibrium values as discussed in Chapter 8. Larger contact angles suggest a

greater level of hydrophobicity, indicating a link between re-adsorption potential and contact angle.

Table 6.9 The impact of coal type on the water/coal contact angle

Coal Type	Contact Angle (°)	Standard Deviation (°)	Contact Angle (°)	Standard Deviation (°)	Contact Angle (°)	Standard Deviation (°)
	Air Fluidized Bed		Steam Fluidized Bed		Fixed Bed	
Yallourn	87.53	1.82	85.97	1.45	84.41	1.71
Morwell	80.55	3.29	78.26	1.45	80.55	1.46
Loy Yang	72.82	1.57	71.29	1.83	69.43	1.76

However, regardless of coal type the contact angle of dried coal remains less than 90°, which allows the conclusion that Victorian brown coals are not hydrophobic when dried. With a similar contact angle the three Victorian brown coals do not require distinction based on hydrophobicity. It also means that hydrophobicity based process such as froth flotation, agglomeration and granulation can be assumed for all Victorian brown coals if a single coal i.e. Morwell is investigated.

6.3.4. The Effect of Drying Method on Coal/water Contact Angle

The data in **Table 6.9** is re-arranged to show the effect of drying method is observed in **Table 6.10** for Loy Yang, Yallourn and Morwell brown coals. An average difference in drying methods of 1.8° is seen but with an average standard deviation of 1.8° this change is insignificant and thus no conclusion deduced.

Table 6.10 The impact of drying method on the water/coal contact angle

Drying Method	Contact Angle (°)	Standard Deviation (°)	Contact Angle (°)	Standard Deviation (°)	Contact Angle (°)	Standard Deviation (°)
	Yallourn		Loy Yang		Morwell	
Air fluidized bed	87.53	1.82	80.55	3.29	72.82	1.57
Steam fluidized bed	85.97	1.45	78.26	1.45	71.29	1.83
Fixed bed	84.41	1.71	80.55	1.46	69.43	1.76

As discussed in the literature review, the factors governing change in contact angle are mineral matter and oxygen/carbon ratio [187]. While steam fluidized bed drying does display a different oxygen/carbon ratio (shown in **Table 6.2**), this is too small to cause observable change in the contact angle. The similar contact angles, regardless of drying method and

fluidization medium suggest that fluidization, using either air or steam as a fluidization medium does not affect downstream processes such as agglomeration or briquetting.

6.3.5. The Impact of Drying Temperature on Coal/water Contact Angle

Due to the limited amount of sample available for analysis, the investigation into the impact of drying temperature was limited to steam fluidized bed dried coal. The same range of temperatures as the drying kinetics (Chapter 5) was used and results are shown in **Table 6.11** and **Table 6.12**.

Table 6.11. The effect of drying temperature on water/coal contact angle using Loy Yang coal in a steam fluidized bed drier

Temperature (°C)	Contact Angle (°)	Standard Deviation (°)
130	71.29	1.83
170	72.89	0.65
200	74.08	2.09

Table 6.12. The effect of drying temperature on water/coal contact angle using Morwell coal in a steam fluidized bed drier

Temperature (°C)	Contact Angle (°)	Standard Deviation (°)
130	78.26	1.45
170	79.72	3.52
200	80.16	1.51

Table 6.11 and **Table 6.12** show increasing drying temperature have no observable effect on the contact angle. While a correlation is seen between the increasing bed temperature and contact angle, the trend is minimal. A 1.2° increase within a 1.8° standard deviation obscures the increase in contact angle.

A reason for the minor variation in contact angle may be due to systematic error in the procedure. As surface functional groups are subjected to the greatest rate of change, it is preferential to analyse surface functional groups only. Unfortunately the large size of dried particles necessitates grinding before briquetting. While this is essential for analysis, the impact of mixing will mean the surface functional groups are dispersed throughout the briquette causing dilution by additional coal mass, and resulting in smaller changes to contact angle.

Current information indicates that only coal type appears to make a difference on contact angle, with drying medium and temperature not having any impact on contact angle or

hydrophobicity. While it is expected that hydrophobicity may change at higher temperatures, any further increases in drying temperature is not practically considered for industrial fluidized bed drying.

6.4. Conclusions

The chemical characteristics for Victorian brown coal can be summarised as follows:

- Air and steam fluidized bed drying changes oxygen functional groups.
- As temperature increases during air fluidized bed drying there is an initial increase in oxygen functional groups, followed by a steady decrease. During steam fluidized bed drying there is only a steady decrease. These values confirm results obtained by Tahmasebi et. al. [65]
- Through Synchrotron infrared analysis the O-H and C=O functional groups in Victorian brown coal begin to break down at 120 to 140°C, while the methyl, methylene and methane groups reduce at 200 to 250°C. Shenhua lignite's functional groups show a large decrease transitioning between 140°C and 160°C, with almost no functional groups remaining by 200°C
- At 130°C Yallourn coal shows reductions in intensity at 2165 cm^{-1} regardless of residence time, while Shenhua lignite shows a more consistent functional group decrease after 20 minutes
- At 170°C drops at 2470 cm^{-1} and 2635 cm^{-1} (COOH dimers) are seen after 15 minutes, and drops at 2800 – 3000 cm^{-1} (methyl, methylene and methane), 3300 cm^{-1} (Most likely phenolic and carboxylic) and 3621 cm^{-1} (intermolecular bonded alcohol and phenol) occurring at 25 minutes
- The water/coal contact angle, which is a measure of hydrophobicity, does not change with drying temperature or medium
- The contact angle varies depending on coal type, but the change is relatively small
- Regardless of drying method or coal type, dried coals always remain in the hydrophilic contact angle region

Chapter 7. Physical Characteristics

Drying coal can change its physical characteristics, and has the capacity to affect downstream processes. This chapter provides the physical characterisation of the dried coal, as little information is available on the effect of steam fluidized bed drying on Victorian brown coals. This information will explain how the variable drying conditions affect key physical conditions, allowing for a greater level of control of the conditions during drying. The combination of physical and chemical properties can be used to explain information discussed in Chapter 10 and corroborates results discussed in Chapter 8.

A range of individual properties are analysed and compared, observing the effect of drying medium (air or steam), temperature (100°C to 200°C), fluidization velocity (0.32 to 0.61 m/s) and initial particle diameter (0.5 to 1.7 mm) on the surface area and porosity of the dried coal. The next section analyses the effect of moisture content, drying method (fixed bed, air fluidized bed and steam fluidized bed) and residence time on the particle size distribution. The last section investigates the effect of moisture content on structural strength of coal.

Information from this chapter is present in the accepted publication: David Stokie, Meng Wai Woo, Sankar Bhattacharya "Attrition of Victorian Brown Coal in a Fluidized Bed Drier" Drying Technology

7.1. Surface Area and Porosity

7.1.1. Literature Review

An important physical characteristic of Victorian brown coal is its surface area and porosity. Victorian brown coal is porous and by reducing its pore volume and surface area the gas/solid reaction interface is reduced and may result in slower or reduced reactivity. While it is known that the drying process is capable of changing and destroying the pore structure [235], the change resulting from air and steam fluidized bed drying has not been detailed.

There are numerous methods of determining porosity and surface area, using techniques such as mercury/helium pycnometry [21] methanol adsorption, water probes [236], particle sizing and photo-extinction [237]. However, the method using gas adsorption of CO_2 and N_2 has been suggested [21] as surface area of coal is typically determined through CO_2 gas adsorption. Typically, CO_2 is chosen over N_2 to prevent low temperature coal contraction. The Dubinin-Polanyi analysis is the accepted method for analysis of Victorian brown coals with surface areas over 200 m^2/g [21].

Marsh (1987) showed the principal equations to determine the surface area and porosity for coals are the Langmuir, BET, Dubinin-Radushkevich (DR) and Dubinin-Astakhov (DA) equations. Problems with the surface area and porosity characterisation of coal typically arise from an unacceptably high or low predicted adsorbate monolayer, depending on the adsorbate used, with some methods predicting a surface area greater than the theoretical maximum (2600 m^2/g) [238]. The study also concluded that the DR and DA equations have the potential to provide important information, but the use of the definition 'equivalent surface area' is recommended – defined by Marsh as "the value of surface area which the adsorbent is exhibiting under the experimental or operating conditions of its use. The equivalent surface area is thus a variable parameter and not an absolute parameter" [238].

While DR and DA equations can be applied for numerous materials [239], they have been used for a range of coals and carbons to provide good results and can also be modified to gain greater accuracy for specific conditions [191-193]

7.1.2. Materials and Methods

The surface area and porosity for a variety of Victorian brown coals and drying conditions has been analysed using a surface area a analyser ASAP 2010. Due to the wide range of coals available, comparison of drying conditions has been undertaken using a single brown coal, Morwell, to represent all Victorian brown coals. The analysis conditions are shown in **Table 7.1**, with the operational methodology provided in Chapter 3. All analysis were performed in duplicate.

Table 7.1 Experimental Parameters

Variable	Parameters
Degas temperature	50°C
Degas shutoff conditions	<002 milliBar
Adsorption gas	CO_2
Analysis bath temperature	273.15°C
Sample Mass	0.4 – 0.8 g

An issue in the surface area and porosity analysis is the degassing period required before gas adsorption can be conducted. Degassing is required to remove any excess moisture from the sample before analysis, and is essential for the preservation of the apparatus. Degassing must be approached carefully as under the wrong conditions this has the capacity to overshadow the effect of drying. At 50°C under the degasification vacuum, there is minimal damage to the chemical characteristics (which is seen at 60°C) and allows for moisture re-adsorption

reversibility, which is a function of pore structure [37, 38, 215, 216]. These correlations would allow the coal to stay as close to the dried state as possible.

7.1.3. The Impact of Drying Conditions in a Steam Fluidized Bed

Using different temperatures (130°C – 200°C), velocities (0.32 – 0.55 m/s) and particle sizes (0.5 – 1.7 mm), the variation in surface area and porosity can be observed.

Table 7.2 shows the effect of drying temperature on surface area and pore volume with temperatures corresponding to the drying kinetics. There is minimal change in surface areas (between 164 m^2/g and 180 m^2/g) making it difficult to observe any specific correlation between surface area and temperature. Similarly, the micropore volume shows no specific trend with temperature, either increasing or decreasing.

There is no significant change between the surface area and pore volume and the drying temperatures to suggest the surface area or the porosity are affected by low temperature drying (in a steam fluidized bed drier). The variation can be account by a sample variation of ±8.5 m^2/g.

Table 7.2 The effect of drying temperature on surface area and pore volume in a steam fluidized bed drier

Drying Temperature (°C)	Equivalent Surface Area (m^2/g)	Limiting Micropore Volume (cm^3/g)
130	180	0.0723
170	164	0.0656
200	171	0.0682

This result is reflected in the effect of fluidization velocity discussed in **Table 7.3** whereby the variation in fluidization velocity (at 130°C) has no effect on the equivalent surface area or limiting micropore volume. This shows that increasing fluidization velocity does not generate any additional pore damage or surface damage during fluidization or drying.

It is important to note that an increased temperature will eventually affect the surface area and porosity; however the temperature requirements are much greater than the range used during drying, and are not focus of these experiments.

Table 7.3 The effect of fluidization velocity on surface area and pore volume in a steam fluidized bed drier

Fluidization Velocity (m/s)	Equivalent Surface Area (m^2/g)	Limiting Micropore Volume (cm^3/g)
0.32	183	0.0735
0.48	180	0.0723
0.55	182	0.0729

Table 7.4 shows the effect of particle size on the surface area and pore volume, indicating that a decrease in particle size results in a decrease in surface area and pore volume. At a higher temperature there is a much smaller variation with no defined trend, and can be shown in **Table 7.5**. The variations in surface area and volume in **Table 7.4** can be attributed to the heterogeneous nature of coal.

Table 7.4 The effect of initial particle size on surface area and pore volume (130°C) in a steam fluidized bed drier

Initial Particle Size (mm)	Equivalent Surface Area (m^2/g)	Limiting Micropore Volume (cm^3/g)
0.5-1.2	144	0.0577
1.2-1.7	180	0.0723

Table 7.5 The effect of initial particle size on surface area and pore volume (200°C) in a steam fluidized bed drier

Initial Particle Size (mm)	Equivalent Surface Area (m^2/g)	Limiting Micropore Volume (cm^3/g)
0.5-1.2	165	0.0661
1.2-1.7	171	0.0682

7.1.4. The Impact of Drying Conditions in an Air Fluidized Bed

Analysis of the change to surface area was also conducted in an air fluidized bed dried coal. **Table 7.6** shows with increasing temperatures there is a decrease in surface area and porosity. The consistency of results with variation in sample composition supports this observation. There is a sampling error of ±15 m^2/g which does not make it possible to establish a definite trend. As with steam fluidized bed drying, air fluidized bed drying temperature does not significantly change the surface area and porosity.

Table 7.6 The effect of drying temperature on surface area and pore volume in an AFB drier

Drying Temperature (°C)	Equivalent Surface Area (m^2/g)	Limiting Micropore Volume (cm^3/g)

100	175	0.0702
130	169	0.0676
170	160	0.0640

7.1.5. The Impact of Drying Method

The direct comparison of drying methods is shown in **Table 7.7**. Using Morwell coal at 130°C temperature, 0.48 m/s fluidization velocity and a 1.2-1.7 mm initial particle size, there is a maximum difference of ±11 m^2/g equivalent surface area.

Table 7.7 The effect of drying method on surface area and pore volume

Fluidization Medium	Equivalent Surface Area (m^2/g)	Limiting Micropore Volume (cm^3/g)
Steam	180	0.0723
Air	169	0.0676
Flue Gas	178	0.0715

There is no major variation in either the surface area or micropore volume comparing steam and flue gas fluidization mediums, with air fluidized bed drying exhibiting a minor decrease. This may be due to the equilibrium moisture content of the dried coal. Since steam fluidized bed drying and flue gas drying has moisture in their fluidization medium (100% and 25% respectively) the equilibrium moisture content of the resultant coal is higher. The removal of the remaining moisture within the coal (occurring in an air atmosphere) means the pore structure could collapse further [20, 21]. However, with such a small variation this conclusion cannot be confirmed. A different analysis method and more uniform samples are required to prove this trend.

7.1.6. The Impact of Coal Type

The surface area and porosity of different coals were analysed with Loy Yang, Yallourn and Morwell coals. They were dried in both an air and a steam fluidized bed drier. **Table 7.8** and **Table 7.9** show both Morwell and Yallourn coals have higher surface area and porosity than Loy Yang brown coal.

Table 7.8 The effect of coal type on surface area and pore volume in a steam fluidized bed drier

Coal Type	Equivalent Surface Area (m^2/g)	Limiting Micropore Volume (cm^3/g)	Micropore Error (cm^3/g)
MW	180	0.0723	0.000299
LY	160	0.0643	0.000338

YL	191	0.0766	0.000571

MW – Morwell; LY – Loy Yang; YL - Yallourn

Table 7.9 The effect of coal type on surface area and pore volume in an air fluidized bed drier

Coal Type	Equivalent Surface Area (m^2/g)	Limiting Micropore Volume (cm^3/g)	Micropore Error (cm^3/g)
MW	169	0.0676	0.000354
LY	156	0.0621	0.000339
YL	168	0.0675	0.000342

MW – Morwell; LY – Loy Yang; YL - Yallourn

While the differences appear to be marginal (25 and 15 m^2/g in steam and air respectively) the trend across drying methods is consistent. The differences are most likely due to the position in the seam where the coal was mined, and as such should be considered an artefact of the coal batch and not a trend based on drying method, or a definitive statement true across any Victorian brown coal used.

7.2. Attrition

7.2.1. Literature Review

Attrition is an important factor during fluidized bed processing of particles as it changes particle size, and is defined as the particle wearing away through abrasion. Attrition typically occurs when mechanical force act upon particles [194], and is expected to occur during coal drying processes such as entrained flow drying, rotary drying and fluidized bed drying [20, 73].

Victorian brown coal is a soft coal and is susceptible to breakage [59]. During drying fluidization can damage coal particles due to the vigorous nature of a fluidized bed where the continuous force acting upon the coal particles over long residence times can result in particle attrition [240]. However, attrition has not been investigated for Victorian brown coal especially during fluidized bed drying. In previous studies changes in particle size range was recorded in the form of initial particle size (0 to 6 mm) and an outlet particle size (0 to 4 mm) [20] but the change in particle size was not been attributed to the fluidization of the particles or through natural attrition/breakage during most drying processes.

Coal attrition results in the creation of coal fines, which can affect the operation of a drier and downstream equipment where the dried coal is used. Fine particles can be harmful to the

environment if released into the atmosphere, as coal fines are classified as pollutants. The Environmental Protection act (1970) in Victoria limits particulate matter emission to between 0.25 to 0.5 g/m^3. Thus coal drying facilities are required to use filters or cyclones to remove the coal fines generated, increasing the capital and operational costs associated with drying [241, 242]. Smaller, dry particles in a hot atmosphere will increase the potential for auto-ignition [243], significantly increasing the danger during drier operation. Therefore an important part of analysing the physical changes during drying is the impact on particle size of the coal being dried.

While particle attrition during drying has not been investigated, previous work has been conducted using coal and char in more extreme conditions, such as combustion, pyrolysis or gasification where particle fragmentation through rapid temperature rise and gas expansion [240, 244-249]. Attrition experiments have been conducted in a fluidized bed using quartzite particles, with a model produced to predict the effects of initial particle diameter, attrition number and fluidization number [250]. However this is not applicable to coal and does not investigate the impact of drying. An earlier study testing a mixture of limestone and coal establishes the applicability of a 'surface-reaction' model to investigate the component attrition rates [194]. While the attrition rate was found to be proportional to surface area, the elutriation loss of smaller particles is more severe. The model suggested larger coal and smaller limestone particles being desirable for the reduction of attrition during coal combustion. This information is dependent on the multicomponent mixture and cannot be transferred into drying processes.

This section examines the effect of initial moisture content and residence time on the particle size distribution of dried coal during fluidized bed drying. The change in particle size distribution has been investigated in both steam and air fluidization mediums to investigate the role fluidization and fluidization medium plays on the attrition of particles. During coal drying a natural amount of physical shrinkage and thermal attrition occurs. In order to differentiate between physical attrition (which occurs during fluidization) and thermal attrition, fixed bed drying was also employed to provide a comparison to fluidized bed drying and help investigate the impact of fluidization on the particle size distribution. This will provide an accurate account of the attrition as a factor of fluidization and what will occur naturally during drying.

7.2.2. Materials and Methods

In the small scale experiments (using the small scale apparatus, Chapter 3.4.1 and Chapter 5.2) Morwell brown coal was used to represent Victorian brown coals, and displays typical Victorian brown coal properties with high moisture (60%) and low ash (4.6%) content. The coal sample was sieved to an initial size range of 0.5 to 2.5 mm. As a comparison, the Niederaußem WTA-2 fine grain steam fluidized bed drier in operation in Germany which a particle size range of 0 to 2 mm [61]. A detailed apparatus methodology is described in Chapter 3, and a complete calculation and calibration methodology outlined in Appendix A3, The operating conditions and sample characteristics are outlined in Table 7.10.

Table 7.10 Experimental Parameters

Condition	Variable
Coal type	Morwell
Initial particle size	0.5-1.2 mm
Drying method	Air fluidized, steam fluidized, fixed bed
Drying temperature	130°C
Fluidization velocity (when applicable)	0.55 m/s
Residence time	0 – 60 minutes
Vibrational rate	50%
Air pressure	1.5 bar
Obscurity range	0.5 – 3 %
Drying mass	10g (raw)
Analysis mass	20g (raw)
Average number of analysis	10

Two fluidized beds, one small and one large, and a fixed bed drier was used in this study. The details of these apparatus are in Chapter 3. For both the smaller fluidized and fixed bed samples, a 10 gram sample mass along with a fluidization velocity of 0.55 m/s and a drying temperature of 130°C was used. Using the Wen and Yu correlation [51, 213, 214], a minimum fluidization velocity (U_{mf}) of 0.11 m/s was calculated for a 0.5 mm particle. To create the fixed bed samples a gas velocity of 0.06 m/s was used to remove the moisture from the bed without fluidization occurring.

The larger fluidized bed samples are taken under similar conditions to the smaller apparatus, with fluidization velocity of approximately 0.5 m/s, temperature of 130°C, a 3000 g bed mass and a 50 minute residence time. A difference between the smaller and larger apparatus is the particle sizes used. Due to the larger amount of coal required, a particle size range of 1.2 to 2.5 mm was used.

To analyse the impact of moisture content, samples were obtained at 1 minute intervals through separate experiments, within the operating time range from 0 minutes (raw coal) to 10 minutes (completely dried coal) Further samples were taken at 30 minutes and 60 minutes to measure the impact of residence time on particle size following drying. Similarly, from the larger bed the samples were collected after a residence of 50 minutes. The moisture content was immediately analysed using a moisture analyser and preserved in a desiccator.

The particle size distribution was determined using a Malvern Mastersizer 2000, which has a 2000 μm detection limit. A suction pressure of 1.5 bar, vibratory feed rate of 50%, with an average obscuration of 1% was used during the measurements, with the calibration described in Appendix A3.

7.2.3. The Impact of Moisture Content

The impact of moisture content on the attrition rate is most clearly seen in the initial 10 minute period where the drying occurs. With samples analysed once a minute, the results show the impact of drying on the particle size distribution in a fluidized bed. In **Figure 7.1** which shows the change in particle size distribution during steam fluidized bed drying, the distribution can be observed to shift after 4 minutes of drying. The raw coal remains unchanged for the first 3 minutes, then the particle distribution rapidly shifts between 3 to 4 minutes, with much larger percentage of smaller particles resulting during drying. After 4 minutes the particle size distribution is unaffected by further increase in residence time. **Figure 7.2** indicates that when air replaces steam as a fluidizing medium a similar trend is observed, where the particle size distribution does not reveal particle size changes after the first 4 minutes of drying suggesting that the particle size change occurs mostly within the first 3 to 4 minutes.

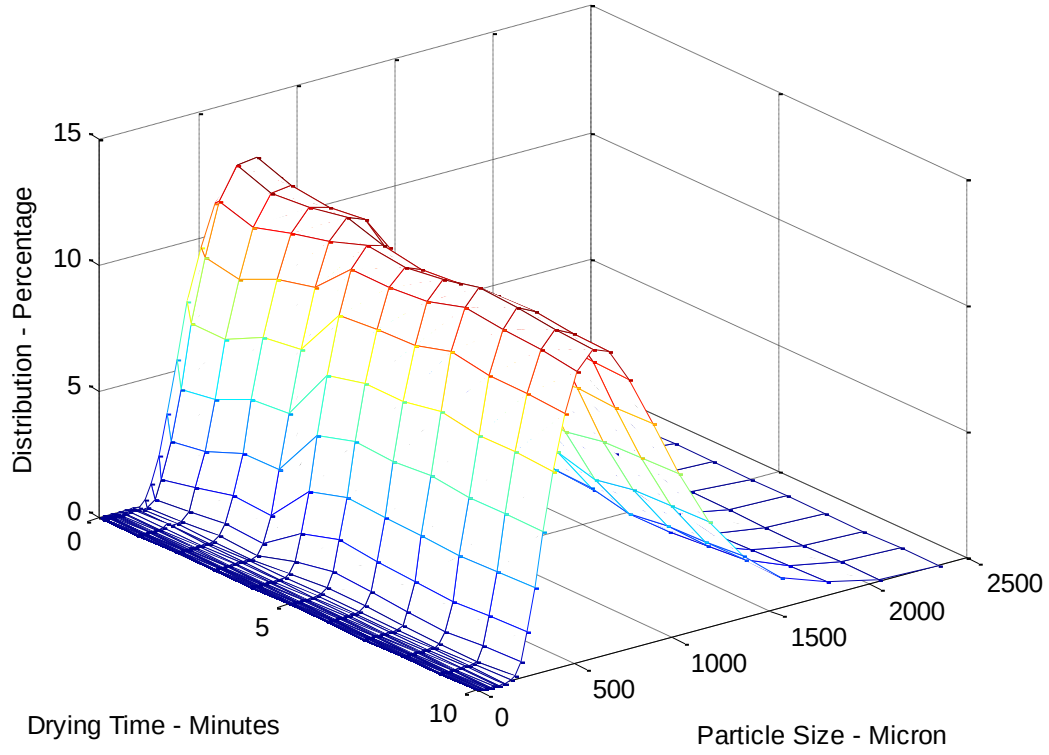

Figure 7.1 The change in particle size distribution in a steam fluidized bed as a function of drying time

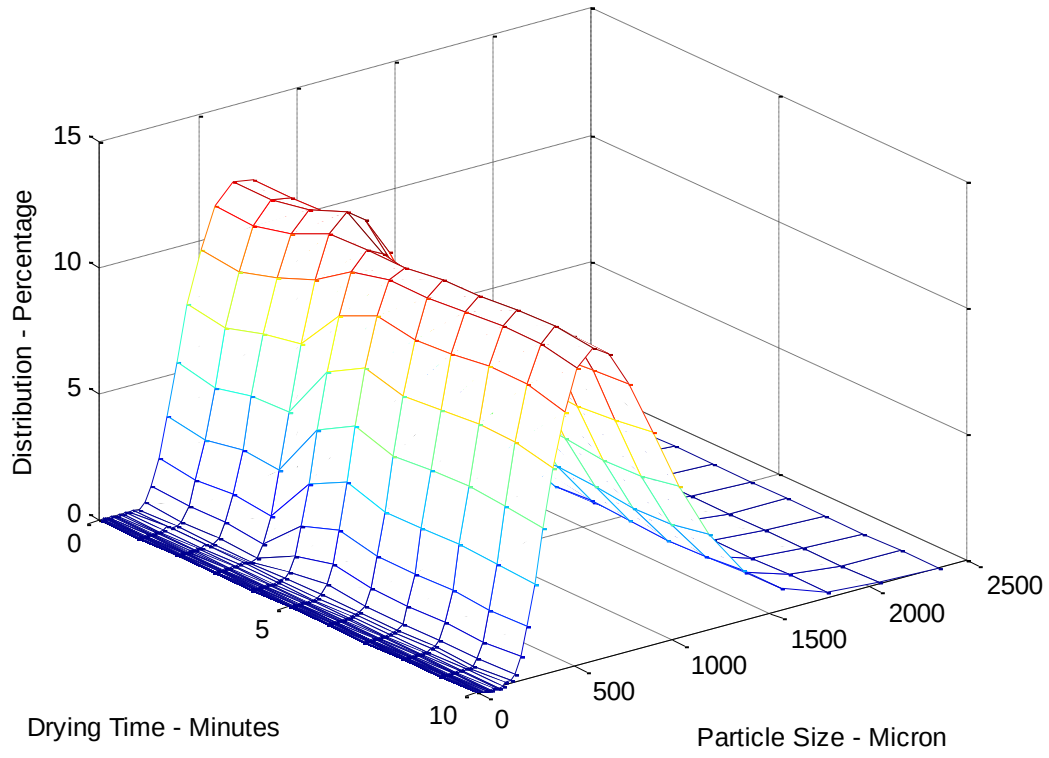

Figure 7.2 The change in particle size distribution in an air fluidized bed as a function of drying time

The results in **Figure 7.1** and **Figure 7.2** were replotted as a function of the coal particles' moisture corresponding to the drying times. During steam fluidized bed drying (**Figure 7.3**) the particle size distribution change occurs from 34% to 16% moisture wt(H_2O)/wt(Coal). Similarly in **Figure 7.4** it can be observed that during air fluidized bed drying particle size distribution change from 35% to 21% wt(H_2O)/wt(Coal).

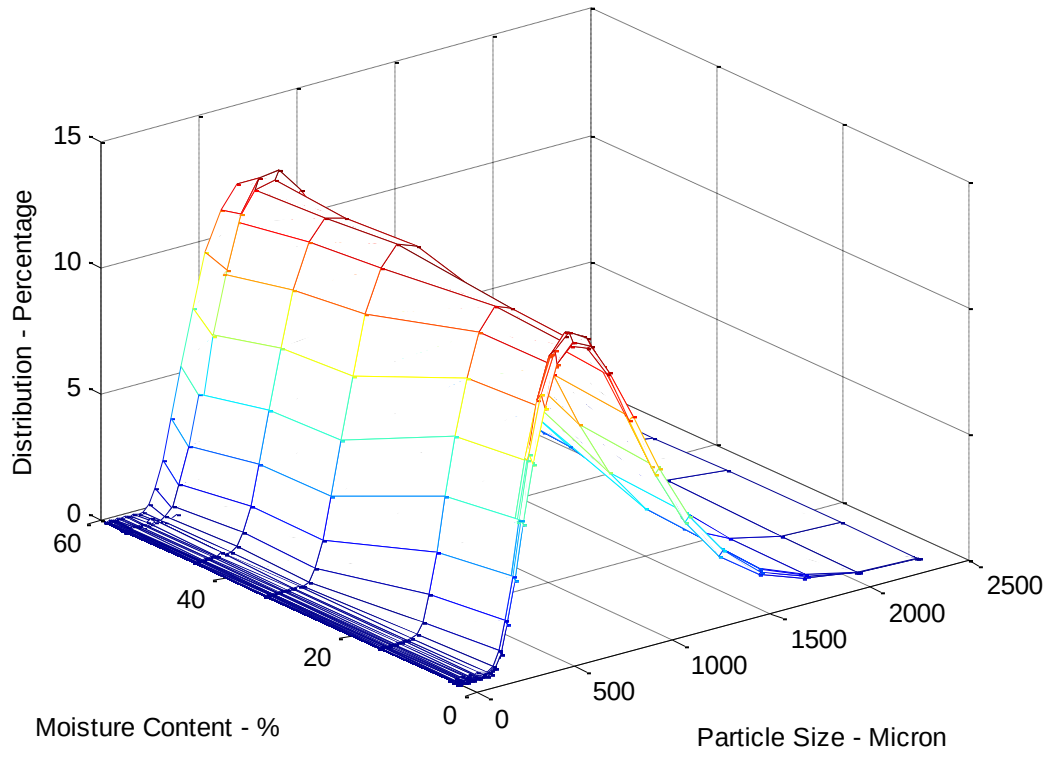

Figure 7.3 The particle size distribution in a steam fluidized bed as a function of moisture content

As significant attrition was observed with a similar moisture threshold, the possible correlation between water composition and particle size reduction is investigated. As discussed previously in Chapter 2, water exists in different states in coal: non-freezable, bound and bulk water [5, 198]. Bulk water consists of adhesion water and inter-particle water, and is often binds many small coal particles together [8, 33]. Using differential scanning calorimetry (DSC) to quantify the different states of water within the sample, the water states of Morwell coal has been determined. **Table 7.11** (taken from Chapter 4) shows the water state of Morwell brown coal, with large quantities of bulk and non-freezable water, with small amounts of bound water. During the drying process, bulk water is removed first, followed by bound water and finally non-freezable water. According to this order of removal the data in **Table 7.11** shows that the removal of non-freezable water occurs at approximately

20% wt(H_2O)/coal. At the moisture range 35% to 16% particle disintegration was found to occur, encompassing the complete removal of bulk water (20% wt(H_2O)/coal taken from **Table 7.11,** transitioning into the removal of non-freezable water. Further complete removal of non-freezable water results in no additional change to the particle size distribution suggesting that the absence of bulk water is the main cause of breakage.

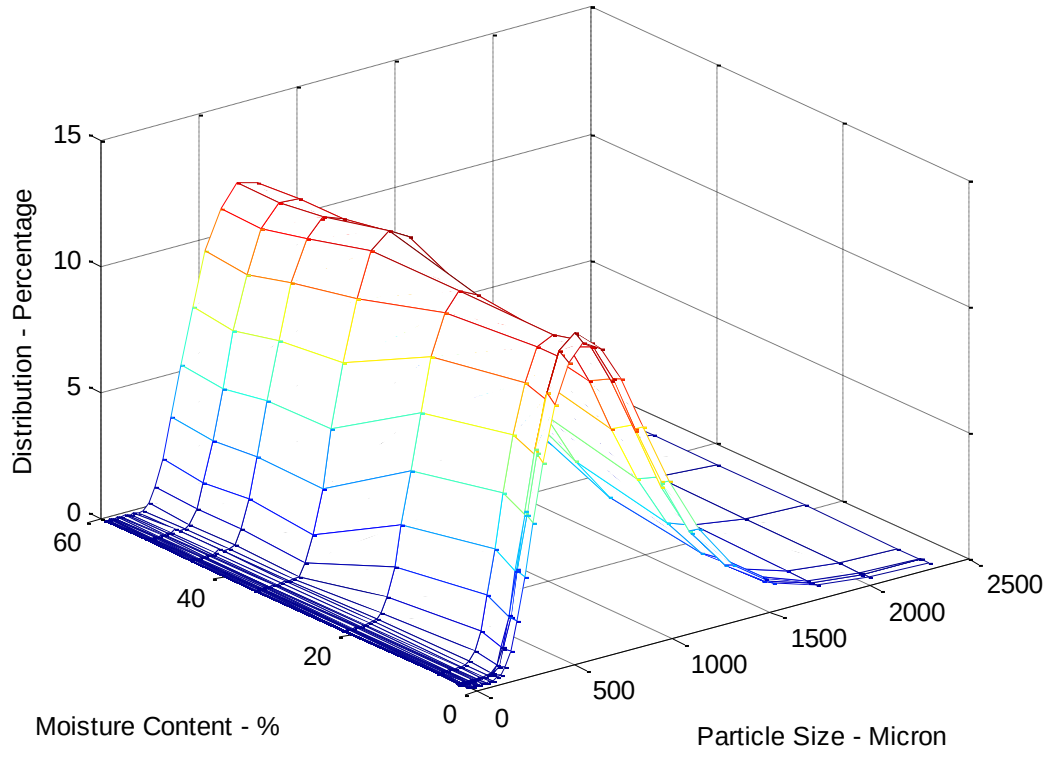

Figure 7.4 The particle size distribution in an air fluidized bed as a function of moisture content

Table 7.11 Water content per 100g of Morwell Victorian Brown Coal

Coal Type	Bulk Water		Bound Water		Non-Freezable		Total Moisture
	g(H_2O)		g(H_2O)		g(H_2O)		(%)
Morwell	33.1±4.1	(55.6)	6.4±2.6	(10.8)	20.1±4.9	(33.6)	59.9

Knowing that particle breakage happens in the absence of bulk water, it is important to establish if breakage is caused by thermal effects or mechanical forces during drying. For this study breakage has been defined as the reduction in particle size which occurs as a part of drying, regardless of the process used. Attrition is defined as reduction in particle size which occurs due to the specific drying process, in this case, fluidized bed drying.

Fixed bed drying was used to differentiate breakage (which occurs as a part of most thermal drying) from attrition in a fluidized bed. As there is no external force acting on the fixed bed, any change to particle size distribution is considered as breakage. Further analysis compared numerically the size distributions between air and steam fluidized bed coals, with values chosen for comparison: d(0.1), d(0.5) and d(0.9). This represents the particle size at 10%, 50% and 90% of the total volume distribution. By comparing the change in the values, the variation in the particle size distribution can be quantified. Fixed bed drying provides a baseline to air and steam fluidized bed drying, and indicates the extent of attrition as a function of fluidization as well as fluidization medium. **Table 7.12** shows that after 10 minutes of fluidization the amount of thermal attrition are similar in air and steam fluidized bed drying. This indicates that no additional attrition occurs in a fluidized bed (air or steam), and particle breakage occurs naturally in the course of drying. The results in **Table 7.12** indicate that the extent of particle breakage is also similar for air and steam fluidized bed drying, with a d(0.5) of 556.7 μm and 569.7 μm respectively. This means that the variation in fluidization medium makes no difference to the particle size distribution.

Table 7.12 Particle diameter at 10%, 50% and 90% sample volume, for raw, fixed bed, air and steam fluidized bed dried coals

	d(0.1) (μm)	d(0.5) (μm)	d(0.9) (μm)
Raw	371.4	664.5	1159.3
Air Fluidized	311.8	556.7	943.8
Steam Fluidized	322.7	569.7	983.3
Fixed Bed	336.0	581.6	976.2

Another cause of change in particle size is due to shrinkage following drying. Evans [215] found, at 25°C, when using raw Yallourn coal containing 200g of water per 100g of dried coal, shrinkage begins to significantly occur at 80g and is at a maximum at 16g of moisture per 100g of dried coal [215] due to the destruction of 30 nm micro capillaries. This corresponds to a moisture content of 44% to 14% respectively. While shrinkage through pore destruction has been observed at a similar moisture content to the thermal breakage documented at 130°C in these experiments (35% to 16/21%), shrinkage during drying is regarded to be less likely or only partially responsible for the change in particle size distribution. This is because no additional particle size change occurs at lower moisture contents where shrinkage is still observed (14% to 7%) and is less likely to cause the creation of fines observed during the drying process. It can be concluded that within this drying period

and fluidization conditions, fluidization and fluidization medium does not impact the attrition of Morwell brown coal.

7.2.4. The Impact of Residence Time

With no attrition observed as a result of fluidization within 10 minutes, a longer residence time was used to analyse the effect of fluidization on the particle size of dried coal. The impact of residence time on samples taken at 30 minutes and 60 minutes is showed in **Figure 7.5**. Steam fluidized bed drying does not exhibit any particle size change with the increase in residence time, with the particle size distribution showing no difference at 30 minutes and 60 minutes.

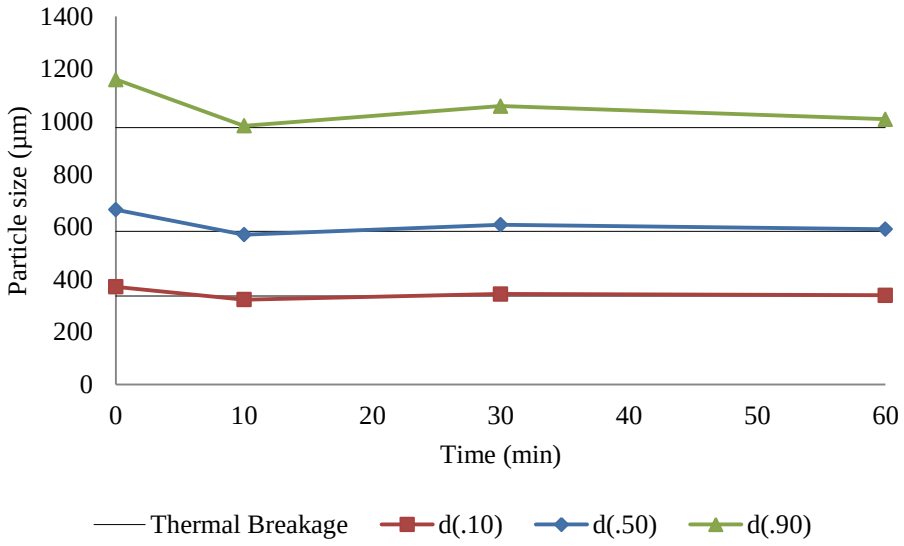

Figure 7.5 The impact of residence time on particle size in a steam fluidized bed

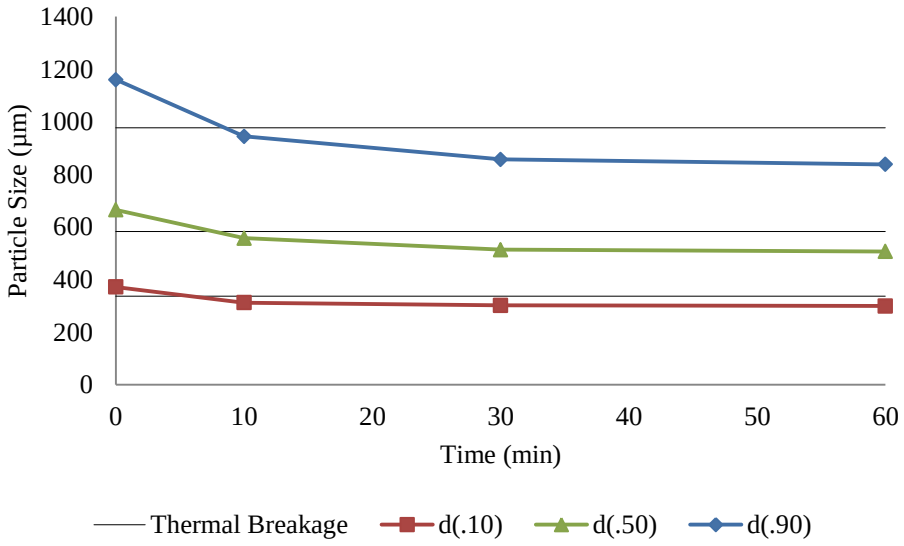

Figure 7.6 The impact of residence time on particle size in an air fluidized bed

Compared to **Figure 7.6**, the particle size of air fluidized bed dried coal decreases between 10 to 30 minutes and the size distribution is unchanged for the remainder of the experiment. At longer residence times, any attrition is considered to be a result of the different methods of drying. Investigation of wood particles [69, 251] show that when drying in a pressurised steam drier, the particles form a product with better bending, tensile strength, with reduced water re-adsorption rates. Furthermore, oil palm empty fruit branch fibres have exhibited increased strength as a result of steam drying [252]. Literature mentions that particles dried by steam fluidized bed drying have greater briquette strength [69]. It is reasonable to conclude that coal dried in a steam fluidized bed is affected in the same manner. The increased strength may allow the steam dried particles to withstand the force of fluidization better than air fluidized bed drying. In the analysis of air fluidized bed drying against thermal breakage data, a 140 micron difference exists in the d(0.9) values, while a 75 micron and a 35 micron difference is seen in the d(0.5) and d(0.1) values respectively.

In **Figure 7.7** the particle population of the fixed bed dried coal is subtracted from the air fluidized bed dried coal (at 60 minutes) and is used to highlight how attrition changes the particle population within the sample. It shows a much higher percentage of larger particle sizes centred at 450 µm, with the proportion of particles greater than 680 µm reduced.

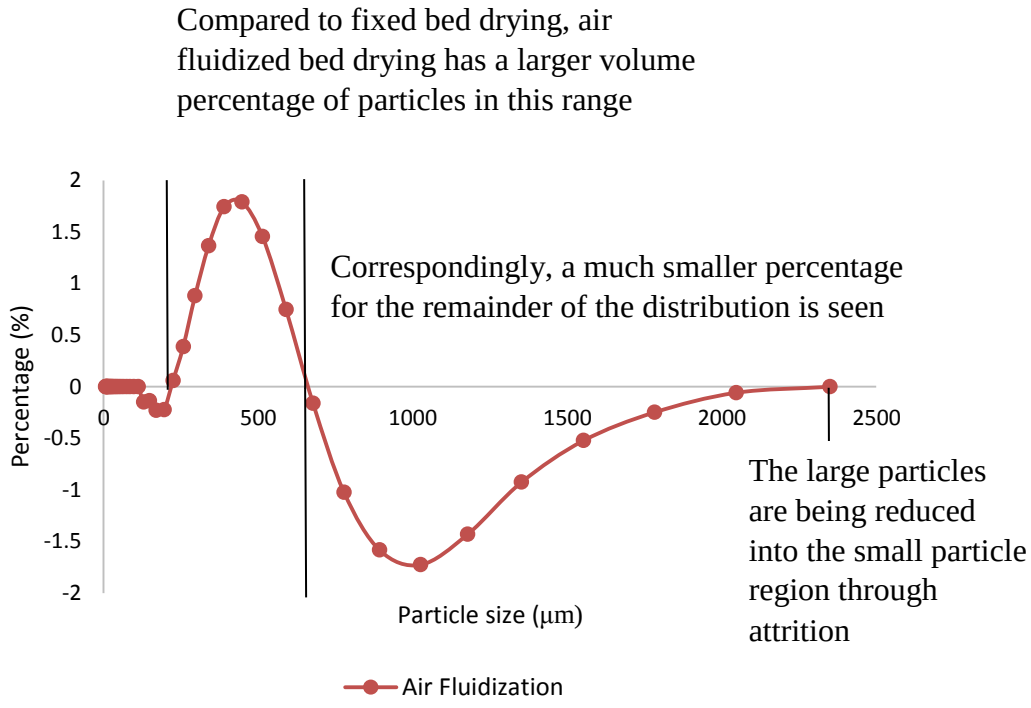

Figure 7.7 Particle size distribution in an air fluidized bed after 60 minutes without thermal breakage

It is possible that there is more attrition in larger particle sizes due to the increased momentum of the particle in the fluidized bed. But a large variation is not seen in **Figure 7.7** is due to the small percentage of larger particle sizes within the sample.

Looking at the comparative percentage between 10 minutes air dried and 60 minutes air dried, discussed in **Figure 7.7**, an interesting phenomena can be seen. With the only cause of variation during this time period determined to be attrition, the rate of attrition in the samples (as a function of particle size) can be discussed.

The complete data, shown in **Figure 7.7**, and the fitted data shown in **Figure 7.8** compare the percentage of particles after 60 minutes of fluidization correlated with the percentage of particles in a fixed bed. The results show a greater percentage of larger particles are removed compared to the smaller particles. Below a particle size of approximately 650 µm there is a greater percentage of particles present. This shows that at increased fluidization times, the particle size population between 650 µm to 2000 µm decrease, but increases between 650 µm and 0 µm. Most notably however, the change in percentages due to fluidization appears to be linear. While the lower particle size fractions (not shown) are subject to greater variational differences due to elutriation, product loss and relative small analysis mass – which results in the upswing at the small particle sizes, they can be considered noise. The linearity is shown in detail with a R^2 fit of 0.9925 shows the accuracy of the line fit. This would suggest that particle attrition of a specific particle is a linear function of the initial particle size. While this is an interesting development, and may have a practical use in the development of a particle population model in a fluidized bed, further analysis on the effect of residence time, velocity, temperature, humidity, initial particle size range and coal type before a complete discussion on the phenomena can be achieved.

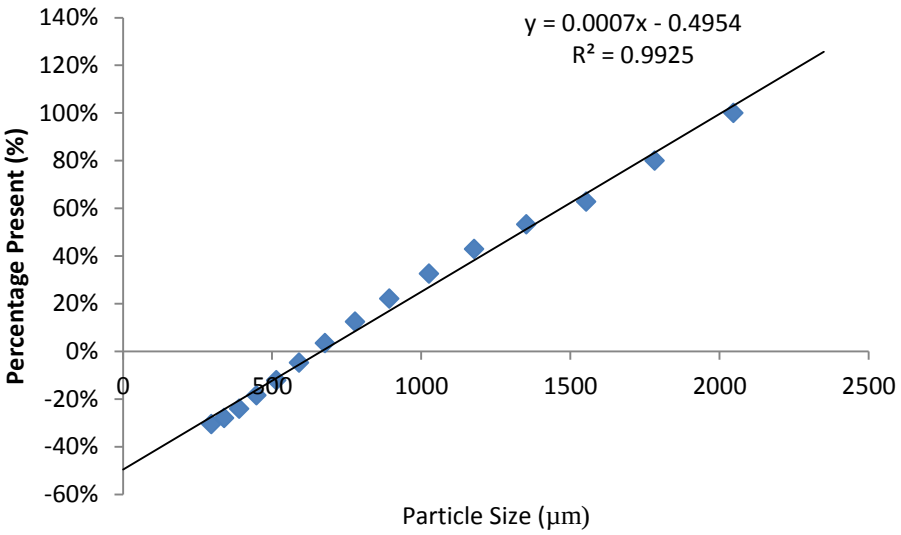

Figure 7.8 The linear change in particle population in an air fluidized bed

7.2.5. Modelling

As the initial reduction in particle size is strongly dependent on the moisture content, an experimentally derived model has been developed to predict the particle size as a function of moisture content during drying. The equation found to best fit the cumulative particle size distribution is:

$$P_d = A_2 + (A_1 - A_2)/(1 + (d/x_o)^p) \quad (7.1)$$

With P_d being the cumulative percentage of the sample at a diameter d, and A_2, A_1, x_o and p the experimentally derived equations. The cumulative particle size distribution at 0 to 10 minutes were fit, with the constants A_2, A_1, x_o and p correlated as a function of moisture content (x). Once fitted, the equations for the constants are placed into the cumulative particle distribution equation and the accuracy of the resultant model is analysed.

Air fluidized bed drying and steam fluidized bed drying are found to have similar curve fitting parameters, with A_1, x_o and p exhibiting linearity. A_2 is significantly different, showing a decreasing trend and is best fit with a polynomial equation. The equations generated for both air and steam fluidized bed dried coal are summarised in **Table 7.13**.

Table 7.13 Curve fitting equations for A_2, A_1, x_o and p in an air and steam fluidized bed

Constant	Air Fluidized Bed Equations	Steam Fluidized Bed Equations
A_1	0.00023x - 0.079	-0.0000090x - 0.093
A_2	$0.00028x^2$- 0.0060 x + 101.10	$0.00017x^2$ + 0.0034x + 100.95
x_o	2.44x + 542.19	2.29x + 561.09

p	-0.0027x + 3.87	-0.0019x +3.89

Table 7.14 and **Table 7.15** compares the model against the experimental data, showing in for the particle distribution analysed the R^2 fitting parameters for air and steam fluidized bed drying are accurate, with R^2 values over 0.999. It can be concluded that the chosen equations allow for a good fit of the experimental data, as shown in **Figure 7.9**.

Table 7.14 Model accuracy in an air fluidized bed drier

Moisture Content (%)	Drying Time (min)	R^2
59.24	0	0.999138884
52.72	1	0.999562874
45.61	2	0.999583747
35.27	3	0.998525189
21.23	4	0.998567175
6.45	5	0.999103681
3.04	6	0.999723299
2.71	7	0.999751305
2.9	8	0.999795325
2.91	9	0.999752153
1.53	10	0.99956866

Table 7.15 Model accuracy in a steam fluidized bed drier

Moisture Content (%)	Time (min)	R^2
59.24	0	0.998502133
55.89	0.1	0.999241864
56.56	1	0.999446699
45.33	2	0.999642045
33.78	3	0.99850662
15.67	4	0.999365232
3.57	5	0.999713032
3.18	6	0.999739585
3.77	7	0.999631198
4.29	8	0.99972101
4.46	9	0.999722196
3.53	10	0.999745494

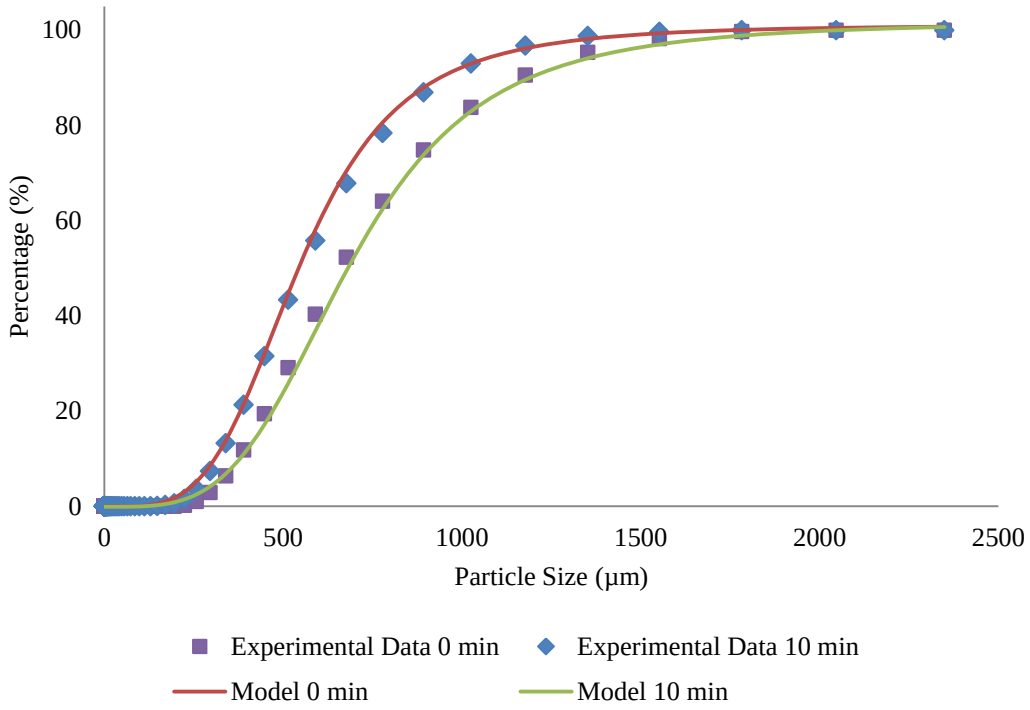

Figure 7.9 Model vs. Experimental data for selected particle size distributions in an air fluidized bed

7.2.6. Attrition in a Larger Fluidized Bed

Similar to the attrition experiments already discussed, attrition has also been analysed in the larger fluidized bed. The larger experiments use Loy Yang instead of Morwell brown coal, however the variation in coal properties is minor. Additionally the initial particle size (1.2 – 2.3 mm) is larger in the larger fluidized bed. To analyse the large particle size, the particles are sieved into three categories, <1.7, 1.7-2.0 and 2.0-2.3 mm. The <1.7mm particles are analysed through the Mastersizer while the larger mass fractions are measured using the sieve masses. To correlate the data from both processes the particle density is assumed to be consistent, allowing the sieved mass fraction and the Mastersizer volume fraction to be used together.

The structure of the curves is different to the smaller apparatus, with two peaks observed, and may be a function of the two separate methods used for analysis, sieving and the Mastersizer. **Figure 7.12**, a decrease in larger particle sizes is observed after drying, with a drop in particle population volume over 1500 µm size. Initially 30% of raw coal is larger than 1700 µm, after air or steam fluidized bed drying the percentage volume drops to approximately 10%. This

shows that the larger particle sizes appear to undergo more attrition than the smaller particle sizes.

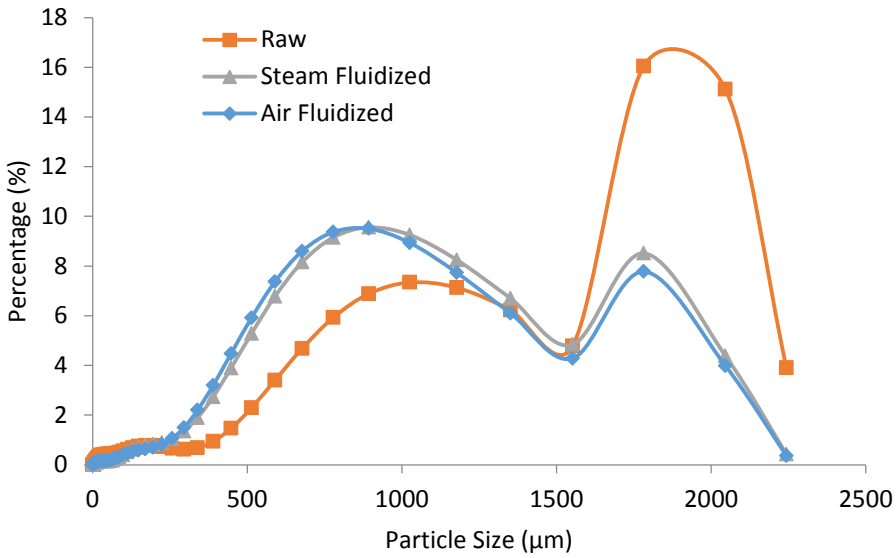

Figure 7.10 The particle size distribution in the larger fluidized bed

As seen in **Figure 7.12**, steam fluidized bed drying has a higher percentage of particles between 1000 µm to 2300 µm, which is similar to the smaller scale experiments which shows steam fluidized bed drying has slightly higher particle sizes than air fluidized bed drying.

The particle distribution values in **Table 7.16** show a difference of 300 µm in d(0.5) and d(0.9) values after drying. The d(0.1) particle size increases, indicating the smallest size fraction increases in volume percentage, and is consistent with fine elutriation during drying. Unlike the smaller scale apparatus there is not a large enough difference in values to corroborate the trends shown in **Figure 7.10**.

Table 7.16 Particle distribution after drying in a fluidized bed

	d(0.1) (µm)	d(0.5) (µm)	d(0.9) (µm)
Raw	180.79	1110.4	1951.8
Steam Fluidized	288.16	812.1	1673.7
Air Fluidized	283.25	779.97	1659

Figure 7.11 shows the change particle size distribution in the small scale apparatus after drying occurs. As already discussed a particle size of 650 µm has no loss or gain in volume percentage, while the largest increase in particle size is 250 µm. This trends is not observed in the larger apparatus, as the largest increase in particle population occurs at approximately 250 µm in the small apparatus but 390 µm in the large apparatus. Because the temperature

and velocity of the larger apparatus is the same, it is unlikely that the change in particle sizes is due to the size of the bed. This suggests the stable particle size is a function of either the coal type or initial particle size.

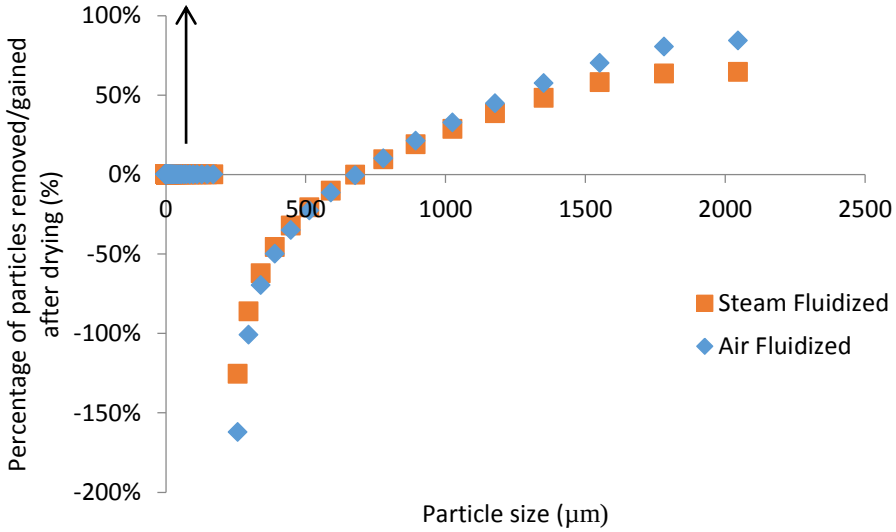

Figure 7.11 The change in particle size distribution in the small fluidized bed

7.3. Conclusions

The physical characteristics for Victorian brown coal after drying can be summarised as follows:

- The surface area and porosity show no changes when the drying temperature, fluidization velocity, particle size and drying medium are varied under typical industry conditions
- Particle breakage is shown to occur during the transition between bulk/bound water to non-freezable water. This occurs regardless of fluidization medium and occurs to the same extent as fixed bed drying. From the experiments it can be concluded that breakage as a function of drying is not drying method dependent.
- Further attrition due to fluidization does not occur in a steam fluidized bed, but does occur in an air fluidized bed
- The percentage change in the particle population during the attrition (in an air fluidized bed) is found to be linear, with the largest proportional change occurring to the larger particle sizes

- The breakage as a function of moisture content can be accurately modelled in the form of: $P_d = A_2 + (A_1 - A_2)/(1 + (d/x_o)^p)$ for both air and steam fluidized bed drying of Morwell brown coal

Chapter 8. Moisture Re-adsorption

Moisture re-adsorption is an important consideration in the practical use of low rank coals. As coal is dried using different methods, including steam fluidized bed drying; it is necessary to determine the extent of moisture re-adsorption in dried coal. Previous chapters have examined the effect of drying on the physical (Chapter 7) and chemical (Chapter 6) characteristics which can impact the potential for moisture re-adsorption.

The hydrophilic nature of dried coal can result in significant amount of moisture re-adsorption from the atmosphere if there is a delay between drying and use. This chapter studies the effect of drying method on the extent of moisture re-adsorption, with the aim to determine the impact of drying medium plays on moisture re-adsorption and find the moist suitable drying method for product storage or non-immediate use.

This chapter will provide an overview of different drying methods and the extent of moisture re-adsorption. Steam or air as a fluidization medium was used for drying, with the resultant coal exposed to the atmosphere. These experiments were conducted with oven dried samples so comparisons can be made to traditional forms of drying.

Information from this chapter is present in the publication: D. Stokie, M.W. Woo, S. Bhattacharya, Comparison of Superheated Steam and Air Fluidized-Bed Drying Characteristics of Victorian Brown Coals, Energy & Fuels, 27 (2013) 6598-6606. [209]

8.1. Moisture Re-adsorption

8.1.1. Literature Review

The primary aim of drying coal is to increase the efficiency of coal combustion for power generation through the removal of water, thus the final moisture content is crucial. The moisture content can also affect other properties, and generates additional issues in transportation, storage and milling; as well as producing additional considerations such as low temperature oxidation and spontaneous combustion, as dried coals having an increased tendency to self-heat.

Monazam used American lignite to develop a moisture adsorption model relating equilibrium moisture of both coal and char to relative humidity and time [253]. The hydration rate is dependent on particle size and atmospheric temperature, while the equilibrium moisture content is dependent on temperature and relative humidity. Using Czech coals, Švabova [42]

found that in coals with high concentrations of carboxylic contents the adsorption isotherms correspond to the Dent model. This is attributed to the water adsorption on primary sites was dominant at low pressures; and an increased adsorption at secondary sites at higher pressures.

Previous investigation into drying and moisture re-adsorption behaviour has been conducted using Indonesian low rank coal. Li et. al. [254] found the re-adsorption rate was dependent on drying temperature, coal particle size and relative humidity. The increase in drying temperature reduces moisture re-adsorption causing coal to shrink due to the collapse in pore structure, with higher temperatures resulting in greater pore collapse.

Minimisation of moisture reabsorption has been outlined by Karthikeyan [184], who suggested varying operating conditions can reduce the susceptibility of re-adsorption. 50% of the carboxylic acid was removed using a temperature between 100 to 250°C while aliphatic compounds were removed at higher temperatures of 200 to 400°C. Karthikeyan shows higher temperature dried coals have reduced moisture content; with moisture reabsorption of coal dried at 350 to 450°C at 11% moisture after re-adsorption, which is 3% lower than coal dried at 150°C. This lower moisture content was attributed to the formation of tar around the particle surface. Correspondingly, investigation by Allardice and Evens, found the water sorption isotherms depends on the hydrophilic functional groups [37, 38, 215, 216]. Allardice found the water content for the monolayer varies between 7.2-8.3g/100g of dry Yallourn coal. Moisture re-adsorption was found to be similar for four Victorian brown coals, despite variation in carboxylic group content and surface area. However the authors noted that the variation between these coals were small [20].

It is important to determine the effect of different drying methods on the re-adsorption potential of coal, focusing on Victorian brown coal (Yallourn, Loy Yang and Morwell) this work investigates the cause for moisture re-adsorption by linking the data with previously obtained physical and chemical changes.

8.1.2. Materials and Methods

To determine the moisture re-adsorption of Victorian brown coal, two separate methods were used. Initially, a Mettler Toledo HB43-S halogen moisture analyser was used to determine to absolute moisture content at set intervals. While the data showed a distinct trend, the inaccuracy of the instrument and the small masses used necessitated the use of more precise moisture determination.

The alternative method chosen used a more sensitive AND GR-200 electronic balance, to determine the moisture content at set intervals using differential mass increase. The residual moisture in the sample is determined, while a second sample is weighed and exposed to the atmosphere. By observing the change in mass of the samples over time the extent of moisture re-adsorption was determined. The various samples and operating conditions are shown in **Table 8.1**. Due to the amount of coal required, a single sample was used, with the consistency of the trends and the final equilibrium moisture content determined by the longer experimental time.

Table 8.1 Experimental parameters

Variables	Parameters
Coal Used	Loy Yang, Yallourn, Morwell
Drying Method	Fixed and fluidized bed dried
Fluidization Medium (When applicable)	Air and steam
Bed Temperature (Drying)	130°C
Fluidization Velocity (When applicable)	0.48 m/s
Particle Size	1.2 – 1.7 mm
Exposure Time	0 – 72 hours
Sample Mass	1.5 – 3 g
Temperature	22 – 25°C
Relative Humidity	55 – 70%

8.1.3. The Impact of Coal Type on Moisture Re-adsorption

Three typical brown coals, Loy Yang, Yallourn and Morwell were used to determine the re-adsorption properties under similar drying and re-adsorption conditions (shown in **Table 8.1**) affect.

To determine if there are any trends between coal type several different drying conditions (air fluidized bed, steam fluidized bed and fixed bed) were used in conjunction. The three figures, **Figure 8.1 – 8.3** show the impact of coal type in different drying mediums.

Figure 8.1 shows Loy Yang coal has the least moisture re-adsorption at equilibrium in an air fluidized bed, followed by Yallourn and Morwell, with a difference of approximately 0.40% moisture content. In a steam fluidized bed (**Figure 8.2**) Loy Yang coal still has noticeably lower moisture re-adsorption follow by Morwell and Yallourn, as shown in **Table 8.2**. This trend is repeated in a fixed bed in **Figure 8.3**.

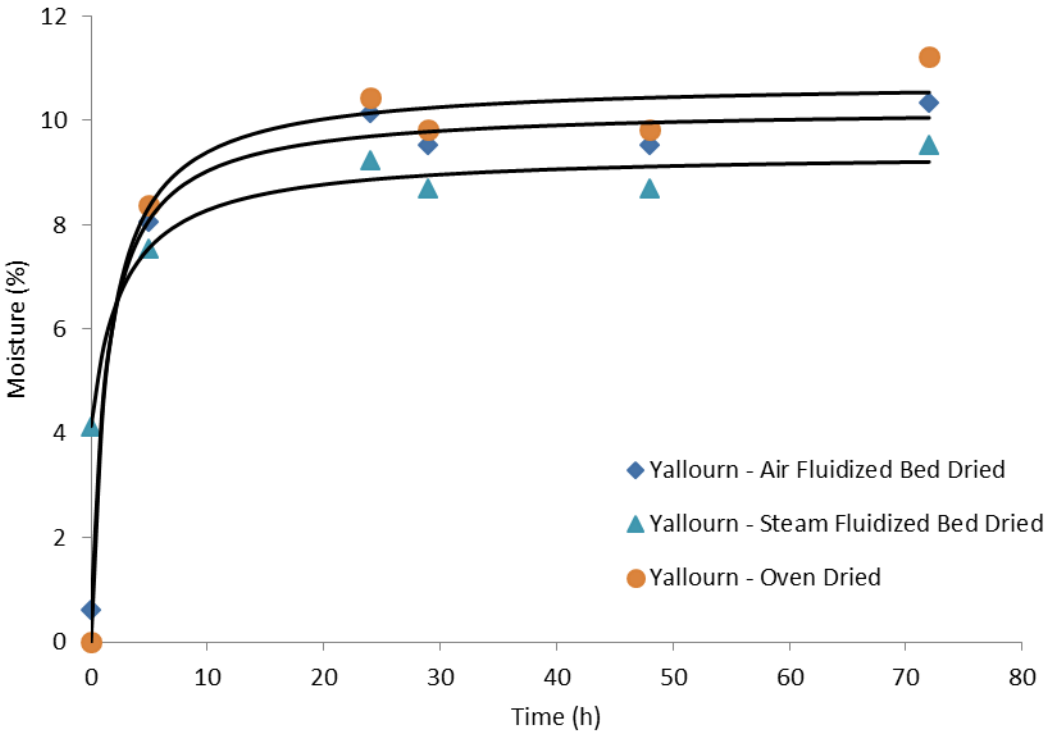

Figure 8.1 The percentage moisture re-adsorption on different coals dried in an air fluidized bed

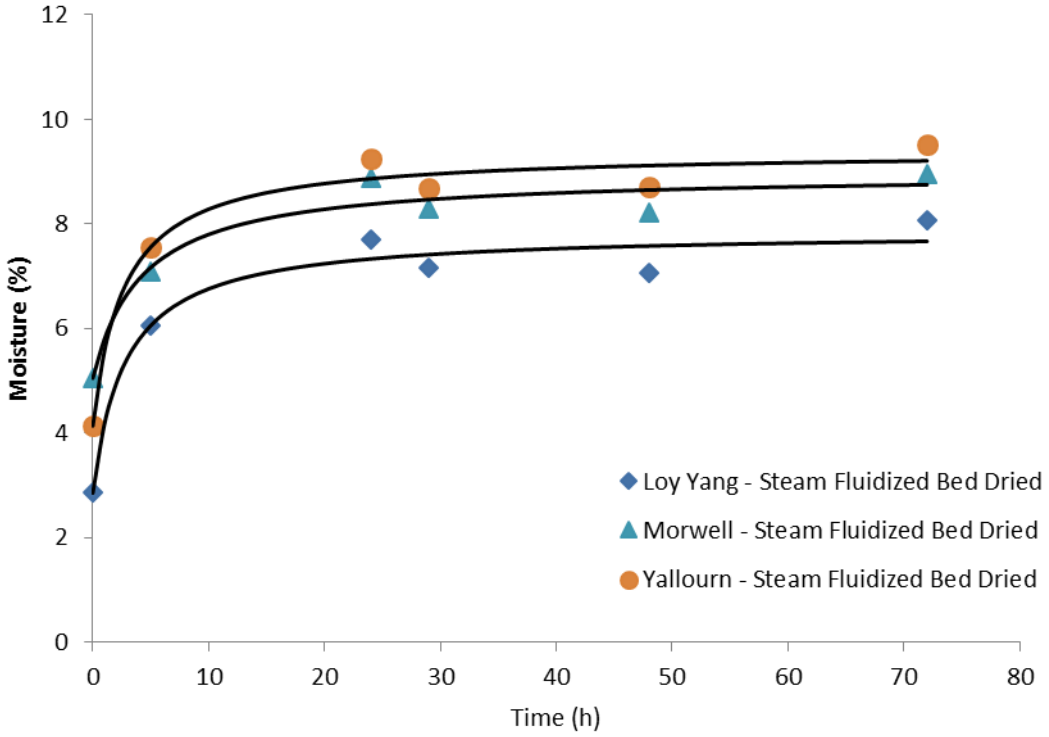

Figure 8.2 The percentage moisture re-adsorption on different coals dried in a steam fluidized bed

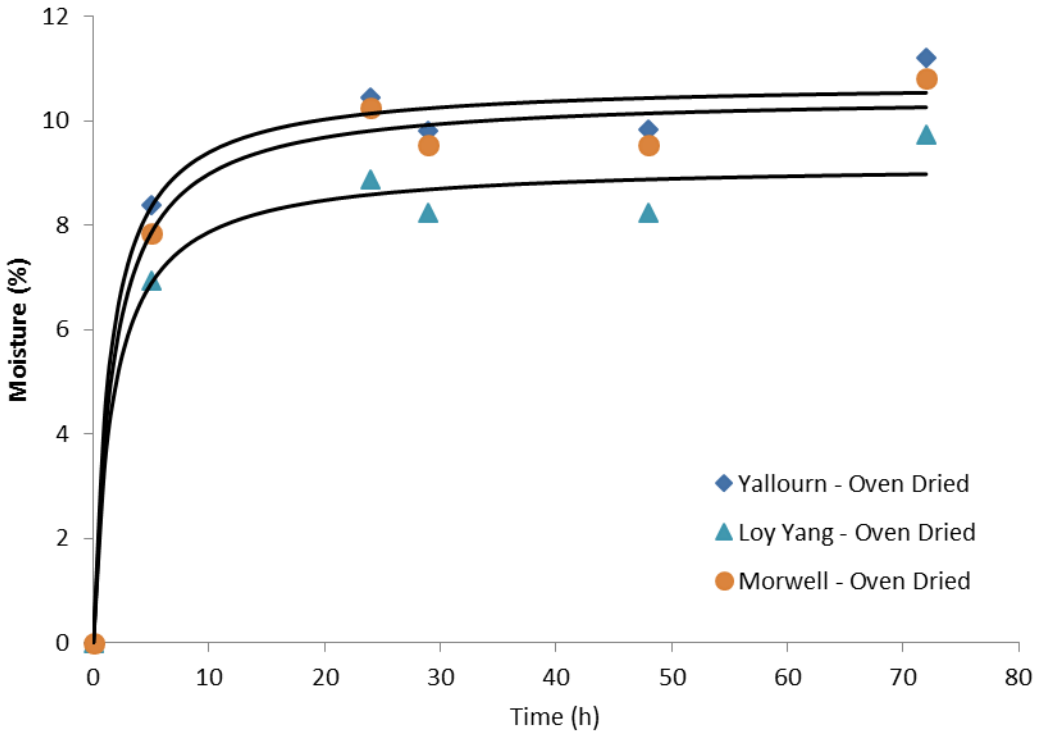

Figure 8.3 The percentage moisture re-adsorption on different coals dried in a fixed bed

The equilibrium moisture values summarised in **Table 8.2** show a clear trend. In air fluidized bed drying, Loy Yang coal showed 0.38% and 0.75% (wt(H_2O)/wt(coal)) less moisture than Yallourn and Morwell coal respectively. However, in steam fluidized bed drying and fixed bed drying the moisture content is noticeably larger by 1.30% and 2.00% respectively.

Table 8.2 The equilibrium moisture re-adsorption percentage

	Coal Type		
Drying Method	Yallourn	Loy Yang	Morwell
Air Fluidized Bed	10.01%	9.63%	10.38%
Steam Fluidized Bed	9.17%	7.63%	8.71%
Fixed Bed	10.49%	8.93%	10.21%

While the extent of re-adsorption does vary, the trends between coals are constant. Morwell and Yallourn coal are similar, retaining 0.55 – 1.41 % more moisture than Loy Yang coal (with a margin of error of 0.37%) depending on the drying method. Loy Yang coal re-adsorbs up to 20% less moisture from the atmosphere.

In conclusion, Loy Yang coal will re-adsorb less moisture than Yallourn or Morwell coals, regardless of drying conditions and is optimal for long term storage for power generation.

The lower equilibrium moisture results in higher combustion efficiency due to the smaller amount of energy required for water vaporization.

8.1.4. The Impact of Drying Method on Moisture re-adsorption

Data from the previous section can be rearranged to focus on the effect of different drying methods for each type of coal (steam fluidized bed drying, air fluidized bed drying and fixed bed drying).

The initial moisture content (which is the moisture content at drying equilibrium) varies depending on the fluidization conditions; with steam dried coal having larger amounts of initial moisture than air fluidized bed or fixed bed drying. Within the first six hours air fluidized and fixed bed dried samples adsorb a greater amount of moisture than steam fluidized samples. Re-adsorption almost flattens onwards, equilibrating at approximately 18 hours.

Steam fluidized coal equilibrating at a lower moisture content than air fluidized coal, regardless of coal type. The difference in coal re-adsorption for steam and air fluidized bed drying remain constant, averaging 1.6% moisture mass difference between the drying methods. The natural variation of humidity and temperature through the day/night cycle causes minor fluctuation in the equilibrating moisture content.

The impact of the drying method on moisture re-adsorption is observed as **Figure 8.4** and **Figure 8.5**. Both Yallourn and Loy Yang coals show a lower moisture re-adsorption in a steam fluidized bed compared to air fluidized bed or fixed bed. While variation occurs in single values in the oven dried coals after 72 hours the trends distinctly show both air fluidized and fixed bed dried coals re-adsorbing larger quantities of moisture than steam fluidized bed dried coals. Previously seen in **Table 8.2**, the results show that, on average, Yallourn coal has 0.85% less moisture when dried with steam. Similarly Loy Yang coals which have 2.02% less moisture present when dried in steam. With standard deviations of 0.05% and 0.15% moisture respectively, these results indicate that moisture difference is statistically significant.

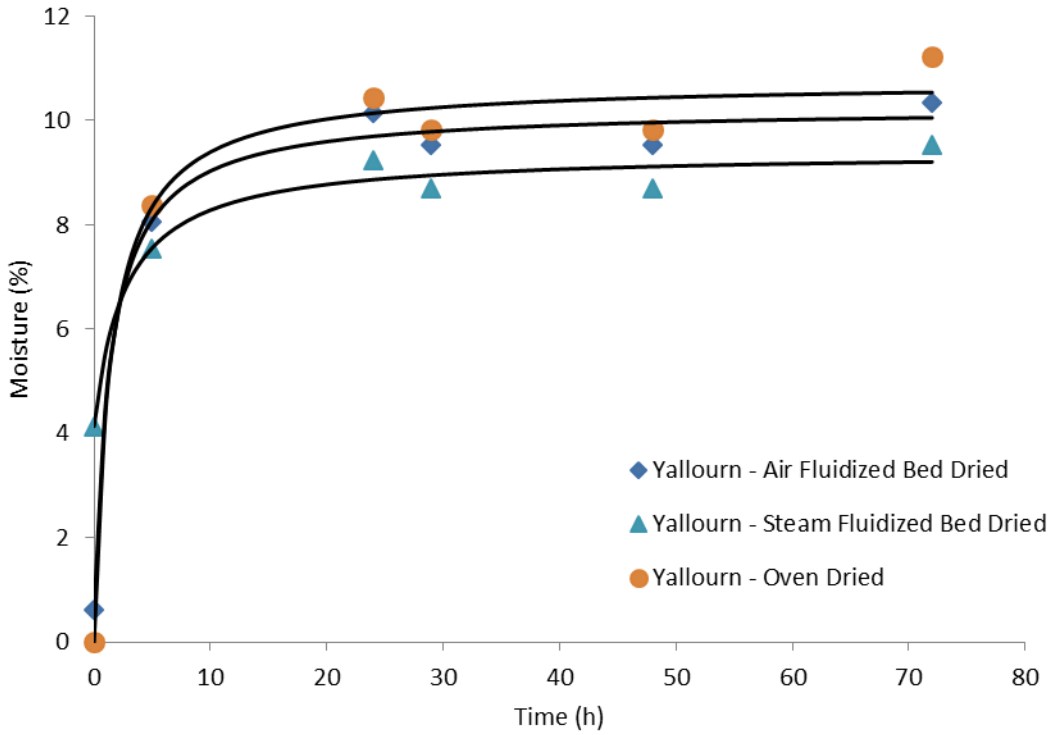

Figure 8.4 Moisture re-adsorption of Yallourn coal in various drying conditions

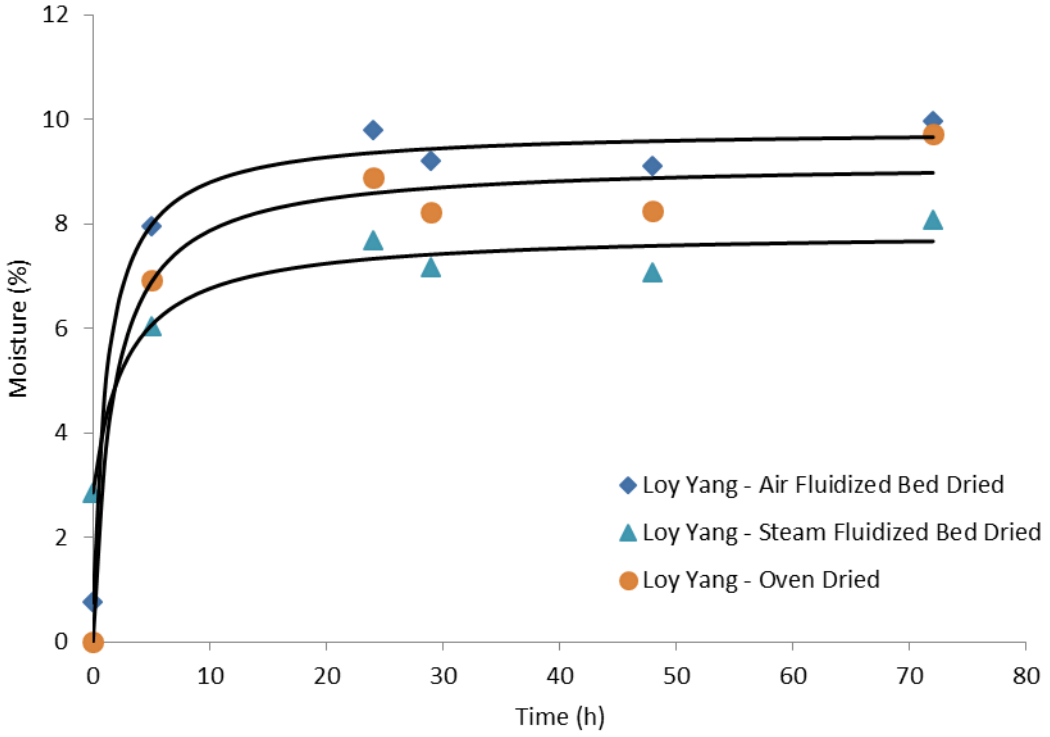

Figure 8.5 Moisture re-adsorption of Loy Yang coal in various drying conditions

Figure 8.6 shows the effect of drying on Morwell coal is very similar to that of Yallourn and Loy Yang, steam fluidized bed drying resulting in a 1.67% drop in equilibrium moisture content as compared to air fluidized bed drying.

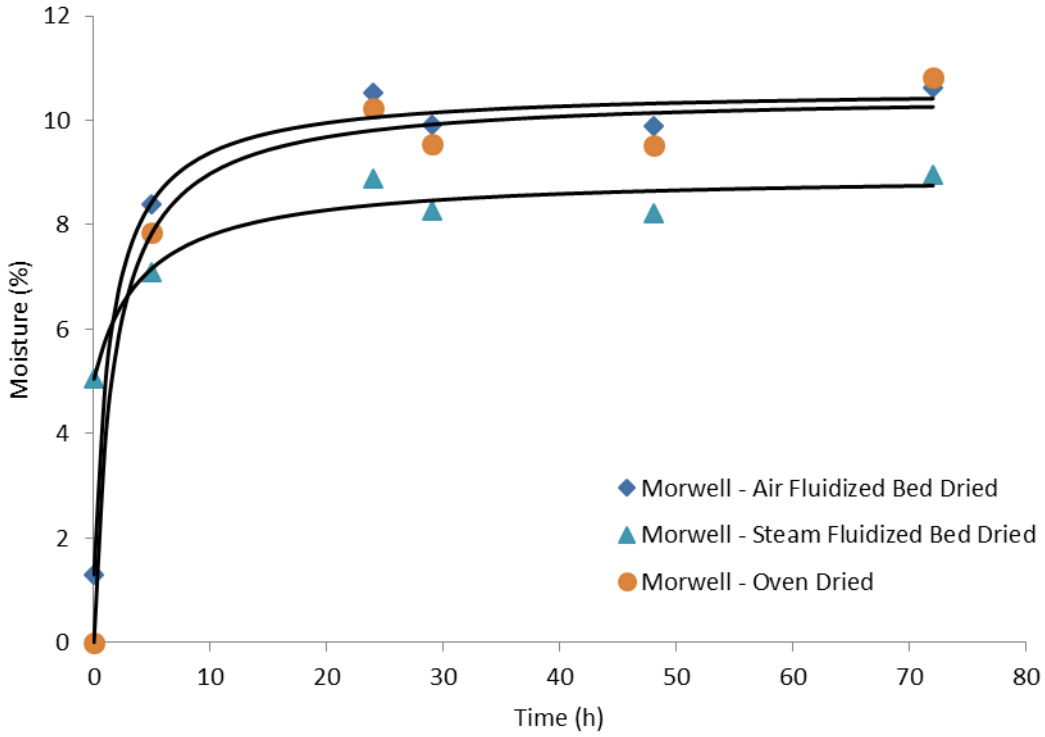

Figure 8.6 Moisture re-adsorption of Morwell coal in various drying conditions

In the Figure 8.4 – 8.6, a drop in re-adsorbed moisture is observed. This corresponded to a decrease in the relative humidity of the atmosphere, opposed to the characteristics of the coal. Once the relative humidity was stabilised, the moisture re-adsorption returned to previous levels.

Results from these experiments support the use of steam fluidized bed drying of coal because of the lower moisture re-adsorption which allows safer storage and transport of Victorian brown coal, and eventually more efficient combustion.

8.1.5. Moisture Re-adsorption Characteristics and Causes

The cause of different amounts of moisture re-adsorption using various drying methods and coal types need to be investigated. Earlier literature review investigated and emphasised changes in physical characteristics and chemical characteristics. In Chapter 7 the physical characteristics were investigated, while in Chapter 6 the chemical compositional changes have been determined.

The suggested physical changes to the coals pore structure during moisture re-adsorption is influenced by the drying methods. If the pore structure is more significantly damaged, reduced or blocked through steam fluidized bed drying, moisture re-adsorption will be impeded, thus reducing available area for water bonding to occur.

The surface area and porosity analysis was outlined in Chapter 7 and with no observable variation in the surface area or porosity.

Table 8.3, using Morwell brown coal to represent the three coals analysed reveals no significant difference between air and steam fluidized bed dried coal, enabling a conclusion in Chapter 7 that any variation is due to specific sample characteristics and not drying conditions. The physical changes causing the variation in moisture re-adsorption does not appear to be valid with no observable variation in the surface area or porosity.

Table 8.3. Surface area and porosity comparison between air and steam fluidized bed dried Morwell coal.

Fluidization Medium	Equivalent Surface area (m^2/g)	Limiting Micro-pore Volume (cm^3/g)
Steam	180	0.0723
Air	169	0.0676

The other possible cause of moisture re-adsorption is change to the chemical composition.
The functional group change due to drying medium has been determined in Chapter 6 using Morwell coal to represent Victorian brown coal and Fourier transform infrared spectroscopy (FTIR), with the method outlined in Chapter 6 and Appendix A4. The analysis shows that steam fluidized bed dried coal has approximately four times more hydrogen bonded water than air fluidized bed dried coal which is an acceptable observation because of higher equilibrium moisture content of steam dried coal (1.3% versus 5.1% $m(H_2O)/m(Coal)$) and water below 26% is known to strongly bind to the coal (Chapter 4). Another important observation is the oxygen functional groups, especially carboxylic groups which are the primary participants of hydrogen bonding in the coal structure [5, 42]. **Figure 8.7** shows steam fluidized bed dried coal have less oxygen functional groups than the air fluidized bed dried coal, resulting in a reduction in moisture re-adsorption potential [5, 42].

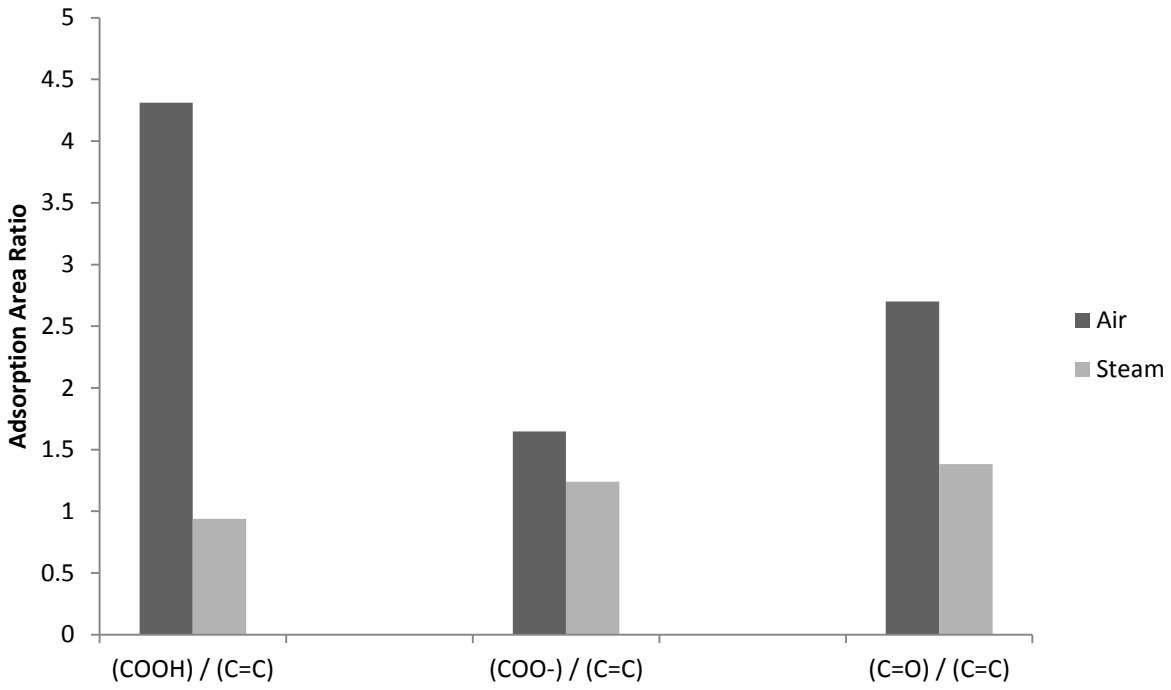

Figure 8.7 Oxygen functional group comparison between air and steam fluidized bed dried coals for Morwell brown coal

8.2. Conclusions

Key findings from the analysis of the moisture re-adsorption are listed below:

- Moisture re-adsorption of Victorian brown coals depending on the coal type and method dried
- Loy Yang coal shows significantly less moisture re-adsorption than Yallourn and Morwell coals (regardless of drying method)
- Steam fluidized bed dried coal re-adsorbs less moisture than air fluidized or fixed bed dried coals (regardless of coal type)
- The difference in moisture re-adsorption has been attributed to the difference in oxygen functional group composition within the coal, which changes depending on the drying method

Chapter 9. Single Particle Superheated Steam Drying Modelling

The empirical models derived from the small scale laboratory data in Chapter 5 can also be used as a quick guide in designing new drying systems, as well as in selecting suitable operating drying conditions. This is mainly because the model is directly correlated with the dryer operating conditions and can be easily used by the industry. Recent development in numerical approaches and the improvement of computing capacity has allowed the Computational Fluid Dynamics (CFD) technique to be used as a complementary approach for the design and scaling up of fluidized bed dryers. The standard correlations and empirical models (such as those developed in Chapter 5 can be used to provide a scope of size of the fluidized bed. The CFD technique can then be used to evaluate the finer mechanical details of the designed equipment. This is attributed to the CFD modelling approaches which numerically discretizes the fluidized bed and predicts the hydrodynamics and drying behaviour at the local spatial positions within the dryer. Such capabilities, however, also points an additional requirement which is the need to describe the drying behaviour of the coal corresponding to the local hydrodynamic conditions. In the preceding chapter, the empirical model developed was only correlated to the global drying conditions with the aim of being a quick engineering tool. Therefore, for further development in the area of superheated steam fluidized bed modelling, there is a need to develop a drying model which is capable predicting the drying behaviour of the coal particles corresponding to the local steam conditions within the domain of the simulation. Development of such a model is the aim of this chapter.

This chapter consists of three sections. The first section discusses the theoretical development of the drying model arriving at the concept of the superheated steam drying master curve approach. The second section analyses the accuracy of this model on drying of ceramics as a model of porous particles analogous to coal particles. The last section discusses its validity on coal particles and suggestions to further improve the model. It is noteworthy that the literature review on existing superheated steam drying model can be found in Chapter 2 in this thesis document and had not been included in this chapter to avoid repetition.

Information from this chapter is present in the publication: M.W. Woo, D. Stokie, W.L. Choo, S. Bhattacharya, Master curve behaviour in superheated steam drying of small porous particles, Applied Thermal Engineering, 52 (2013) 460-467. [176]

9.1. Modelling

9.1.1. Model Development

Drying of porous particles such as ceramics and coals are often modelled through a diffusion method, where the moisture diffusion equation is solved by numerically discretizing the particles into concentric shells or solution domains [52]. While this method enables detailed analysis of the transport of moisture within the particle during the superheated steam dehydration process, the approach has high numerical requirements which do not lend itself for implementation in larger scale simulations like the CFD technique. For incorporation into larger simulation frameworks, therefore, a lump model approach [6,7] is desirable and this was the basis taken in the model development in this thesis.

Assuming that evaporation occurring during heating is negligible, heat transfer during the initial period, where the drying rate is constant, can be modelled as:

$$m_p C_p \frac{dT}{dt} = A_p h\left(T_a - T_p\right) \tag{9.1}$$

To calculate the heat capacity of the particle during drying, a mass weighted heat capacity between the particle solid and the moisture can be used:

$$C_p = xC_{p,c} + (1-x)C_{p,l,w} \tag{9.2}$$

Where:

$$x = \frac{1}{1+X} \tag{9.3}$$

And X is the dry basis moisture content. When particle temperature reaches the saturation temperature, the heat transfer can then be described as follows accounting for the evaporation of moisture:

$$m_p C_p \frac{dT}{dt} = A_p h(T_a - \psi T_{sat}) - \frac{dm}{dt}\Delta H_{evap} \tag{9.4}$$

The driving force for heat transfer is the temperature difference between the superheated steam and the particle surface. However typically only the average particle moisture is known in a drying process or numerically captured in such lump system modelling approach. Assuming a receding evaporation front, the average particle temperature will be in between the saturation temperature of the receding core and the surface temperature. Taking the saturation temperature of the receding front as a basis a surface multiplier term (ψ) is used

and describes the correlation between surface and saturated temperatures as the drying front recedes. Effectively ψT_{sat} then describes surface temperature of the particle (Equation 9.5). Rearranging Equation (9.4),

$$\psi = \frac{T_a}{T_{sat}} - \frac{m_p C_p \frac{dT}{dt} + \frac{dm}{dt}\Delta H_{evap}}{A_p h(T_a - T_{sat})} \quad (9.5)$$

If experiments were undertaken measuring how the temperature and moisture content of a coal particles changes throughout the drying history in superheated steam, this expression can then be used to compute the surface temperature multiplier term at each period of drying.

Analysing the physical considerations in Equation 9.5, the surface temperature multiplier is limited at the lower bound of unity when the initial surface temperature at saturated conditions is equal to the saturation temperature. The upper bound occurs at when drying has completed and the change in mass and temperature is zero. At such conditions, the particle surface temperature should also equate the superheated steam temperature. Mathematically, for achieving this upper bound condition, the maximum value of the surface multiplier term then conveniently takes the form of the ratio of the superheated steam temperature and the saturation temperature:

$$\psi_{max} = \frac{T_a}{T_{sat}} \quad (9.6)$$

$$\psi_{min} = 1 \quad (9.7)$$

The change in mass due to drying can be described as:

$$\frac{dm}{dt}\Delta H_{evap} = \phi A_p h(T_a - \psi T_{sat}) \quad (9.8)$$

This form assumes that the mass transfer is driven by the rate of convective energy transfer into the particle. The falling rate term (ϕ) delinerates the fraction of energy transferred into the particle through convection and actually reaches the evaporative drying front. Similar to the surface multiplier term, this parameter has to be experimentally determined. Rearranging Equation (9.8):

$$\phi = \frac{\frac{dm}{dt}\Delta H_{evap}}{A_p h(T_a - \psi T_{sat})} \quad (9.9)$$

With similar measurements on the particle temperature and mass throughout the drying process, the falling rate term can then be evaluated at different stage of the drying process. As the falling rate term (ϕ) is already a 'normalized' dimensionless term, denoting the fraction of the total convective heat transferred energy, it is bounded by the following form (Equation 9.10 and 9.11). In the beginning of the dehydration process, when the drying front is at the proximity of the particle surface, the energy transferred into the particle directly translates to the energy reaching the drying front, As drying proceeds to completion the drying front recedes and part of the energy transferred into the particles is 'stored' or heats up the dry crust section of the particle.

$\phi_{min} = 0$ (When approaching equilibrium moisture) (9.10)

$\phi_{max} = 1$ (At the initial instance of dehydration) (9.11)

The theoretical concept developed so far was aimed at theoretically obtaining semi-empirical parameters which will describe the drying behaviour of a porous particle dehydrating under superheated steam conditions. This approach was partly inspired by the characteristic behaviour and versatility of such semi-empirical parameters determined in reports of the Reaction Engineering Approach in modelling droplet drying in hot air conditions.

This concept was firstly evaluated using single particle superheated steam drying data of single ceramic particles. The validated concept was then extended to and compared with experimental data of single Loy Yang brown coal particle.

9.1.2. Ceramic Particle Master Curve Behaviour

Experimental data was taken from Hagar et. al. [179] to validate the model with variations in drying temperature determined and shown in **Table 9.1**.

Table 9.1 Ceramic drying model conditions

Case	Temperature *(℃)*	Volumetric flux rate *($kg/m^2 s$)*	Velocity *(m/s)*
A	125	0.1	0.18
B	150	0.25	0.48
C	175	0.35	0.72

At each of these conditions, Hagar et al. [179] reported data on the mass and temperature of the particles throughout the entire drying process. The extracted data from these mass and temperature change data is included in Appendix A5. Other properties are required to define

the ceramic drying system, including the properties of ceramic particle and steam. Many of these change dynamically as a function of temperature as shown in **Table 9.2**.

Table 9.2 Ceramic drying model, particle properties

Properties	Values or Equations
Liquid water specific heat $(C_{p.l,w})$	4217 *(j/kg K)*
Ceramic specific heat $(C_{p.c})$	880 *(j/kg K)* [52]
Steam specific heat $(C_{p.s})$	$1824.1 - 0.21976T + (2.3487 \times 10^{-4})T^{2\ k}$ *(j/kg K)*
Steam density(ρ_s)	$0.7882 - 0.0023T + 0.000003T^{2\ k}$ *(kg/m^3)*
Steam viscosity (μ_s)	$(1.7096 \times 10^{-8})T^{1.1146\ k}$ *(kg/m K)*[255]
Latent heat of vaporization (ΔH_{evap})	2256500 *(J/kg)*
Radius *(m)*	0.010 *(m)* [179]
Steam thermal conductivity (k_s)	$0.0184 - (5.17 \times 10^{-5})T + (-1.16 \times 10^{-7})T^2$ *(w/m.K)* [256]

k - Kelvin

The Ranz-Marshal equation is generally used calculate the heat transfer co-efficient, however, Hager et. al. [179] found that the experimental heat transfer co-efficient describing their experiments deviated from the Ranz-Marshal correlation. Hager's experimental data redefined the Ranz-Marshal correlation (Equation 9.12) which is used in calculation of the heat transfer co-efficient:

$$h = \left(2 + 0.616Re^{0.52}Pr^{1/3}\right)\left(\frac{k_s}{2R_p}\right) \tag{9.12}$$

This heat transfer correlation was used in the computation of the surface multiplier and the falling rate term from the experimental data. From the experimental data by Hager et. al. [179], the surface multiplier term for each drying condition was computed and is illustrated in Figure 9.1. It was found that the experimentally determined (ψ) can be reduced into a single curve by normalising the surface temperature multiplier and the particles temperature in the following manner:

$$\psi_n = \frac{\psi - \psi_{min}}{\psi_{max} - \psi_{min}} \tag{9.13}$$

$$T_n = \frac{T - T_{sat}}{T_a - T_{sat}} \tag{9.14}$$

The collapsed surface multiplier data is shown in **Figure 9.2** with only minor variations at low temperatures. This collapsed data can be taken as the master surface temperature

multiplier curve. The advantage of having a collapsed 'master curve' is that the curve is now independent of the steam drying conditions and is a semi-empirical characteristic property of the material; making it translatable to other ambient conditions. The fitted equation for the normalised surface temperature multiplier was found to be:

$$\psi_n = 1.7325T_n + 2.2931T_n^2 + 1.6129T_n^3 \quad (9.15)$$

For superheated steam drying, the heat transfer rate is the dominant effect controlling mass transfer, driven by the temperature difference between ambient and particle temperature. Therefore the normalised temperature can be used to delineate the extent of drying; showing how the surface multiplier term changes with the extent of drying.

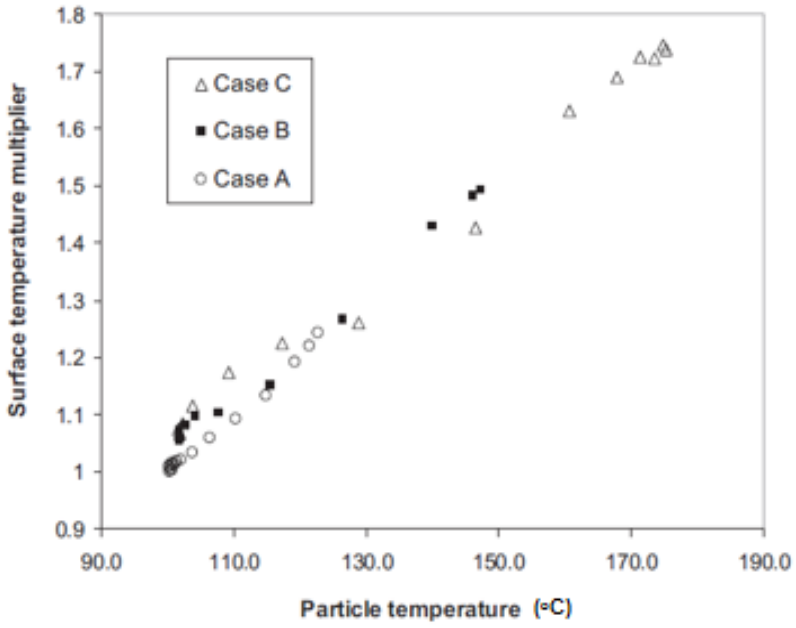

Figure 9.1 The surface temperature multiplier at different drying conditions (ceramic)

Similarly, the falling rate term was generated from a master curve correlating drying time and predicted surface temperature. As drying progresses the resistance to heat transfer increases and can be graphed as shown in **Figure 9.3**. Differing from the surface temperature curves, the particle moisture was used to denote the extent of during. Usage of particle moisture to denote the falling rate behaviour of drying is commonly employed in the literature.

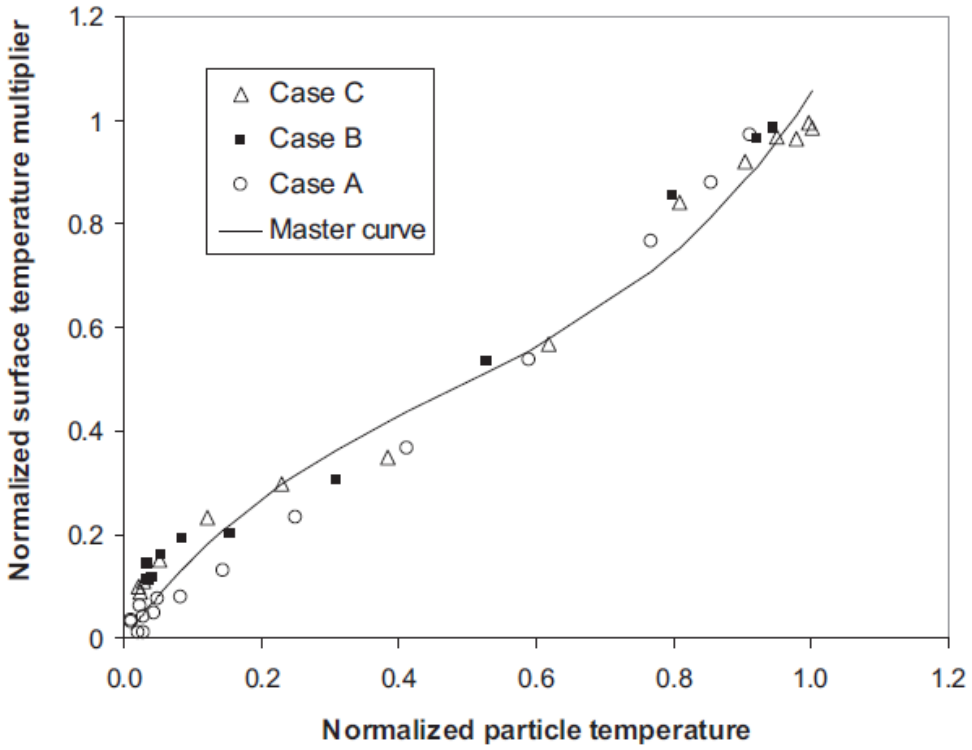

Figure 9.2 The normalised surface temperature master curve (ceramic)

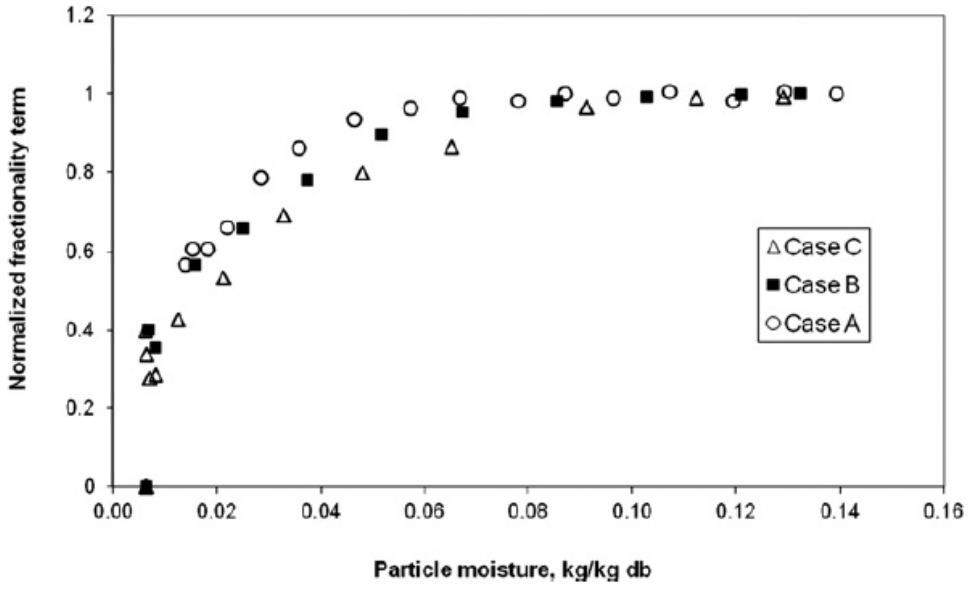

Figure 9.3 The falling rate multiplier at different drying conditions (ceramic)

The individual falling rate curves were then collapsed using the following form for the moisture content

$$X_n = \frac{X - X_{eq}}{X_{ini} - X_{eq}} \tag{9.16}$$

The collapsed moisture curve in **Figure 9.4** then takes the following fitted mathematical form:

$$\phi = 5.0572\exp(0.2747X_n^{0.3668}) - 5.0572\exp(0.1119X_n^{1.3002}) \quad (9.17)$$

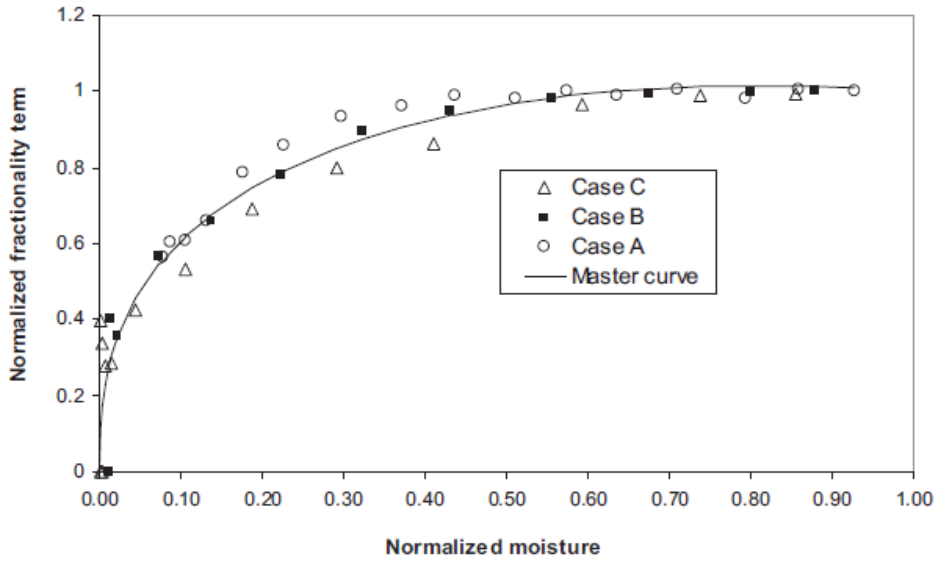

Figure 9.4 The normalised falling rate master curve (ceramic)

This 'master curve' is then evaluated on its capability to be extrapolated to different superheated steam drying conditions. It is noteworthy that this is the main rationale in developing the master curve concept as it is intended for future implementation in larger CFD simulation frameworks in which the drying conditions change throughout the simulation domain of the fluidized bed. The three different drying conditions in **Table 9.1** were used for the evaluation.

In using the master curve concept, the drying process was then simulated using Equation 9.1 and Equation 9.8; these equations were solved using the first order Euler method. At each instance in the drying process, the surface temperature multiplier term in Equation 9.1 and the falling rate term in Equation 9.8 are then obtained from the master curves Equation 9.15 and Equation 9.17, respectively.

The result of the model prediction is shown in **Figure 9.5 – 9.7** and fits well with the experimental data. Some discrepancy in the beginning of the drying process was observed as the model predicted a slight cooling effect which was not observed in the experiments. Nevertheless, this discrepancy is negligible. At 500 seconds in **Figure 9.5**, 180 seconds in **Figure 9.6** or 100 seconds in **Figure 9.7** a particle cooling of less than 0.1°C is seen.

At the lower superheated steam drying temperature, the model predicted a faster increase in particles temperature and slightly higher final moisture. On the other hand relative good match with experimental data was achieved for the higher temperatures. These discrepancies may be attributed to the scatter in the data when the master curves were empirically fitted. Nevertheless, making comparison with other established superheated steam drying model for porous particles [67, 142], the current model showed good agreement with experimental data.

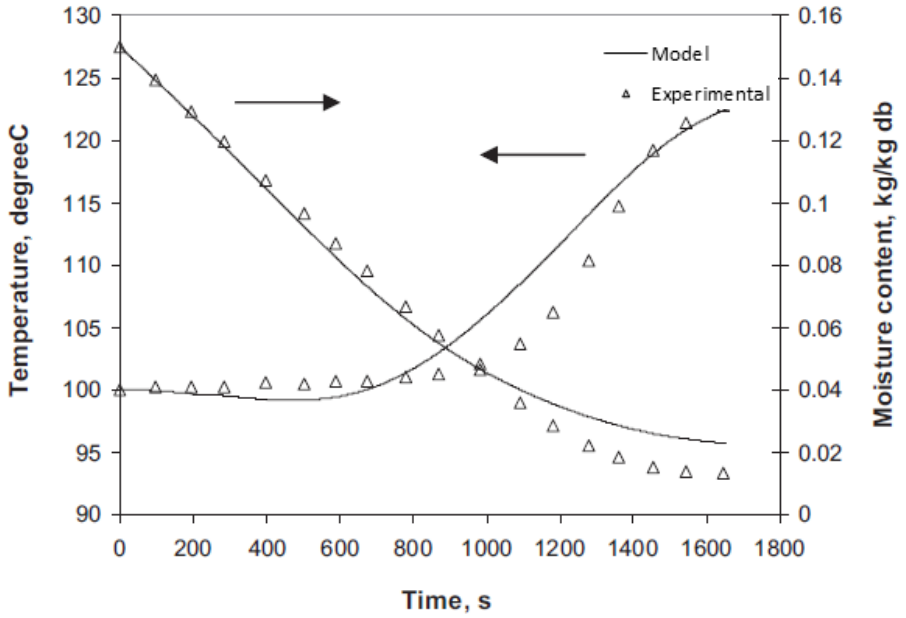

Figure 9.5 Experimental vs. Model comparison for case A (ceramic)

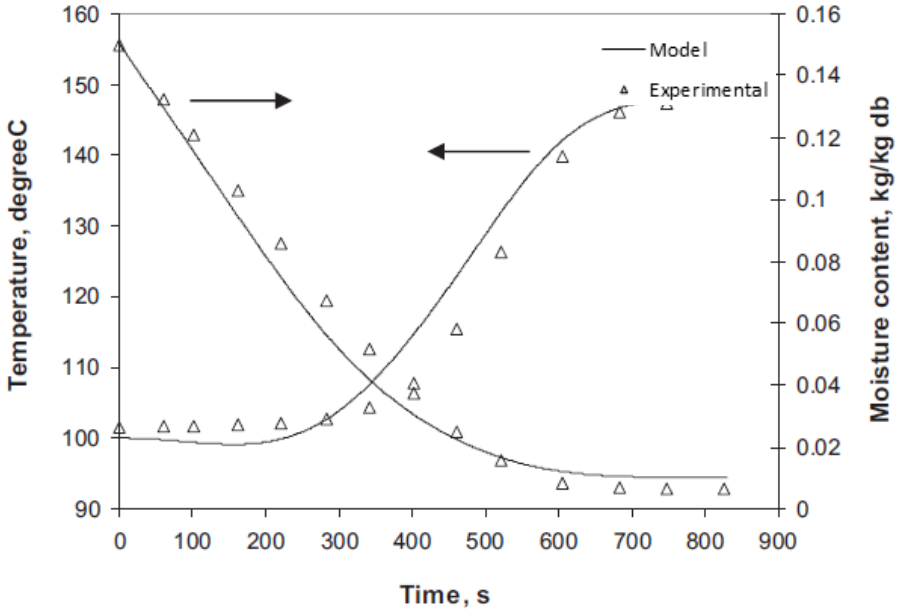

Figure 9.6 Experimental vs. Model comparison for case B (ceramic)

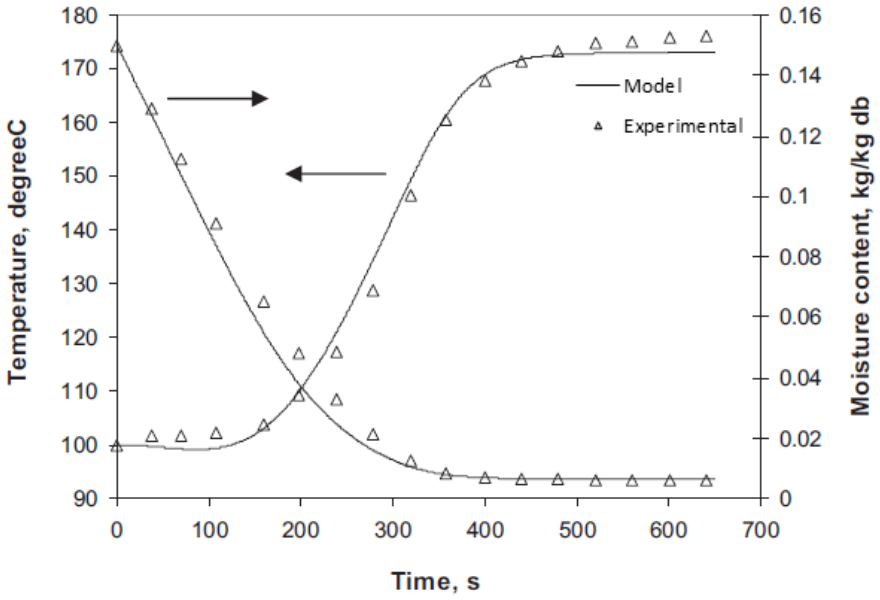

Figure 9.7 Experimental vs. Model comparison for case C (ceramic)

9.1.3. Coal Master Curve Behaviour

From the validation of this approach with porous ceramic particles, the next objective was to apply this model to the superheated steam drying of Victorian brown coals. Single particle superheated steam drying experimental data with Loy Yang coal was obtained from a paper by Kiriyama et. al. [256], and is shown in **Figure 9.8**. The drying conditions form the experiments by Kiriyama et. al. is tabulated in **Table 9.3**. The velocity of the superheated steam was 0.02 m/s and, depending on particle size, the initial moisture content of the coal particles ranged from 60 – 63.1 %.

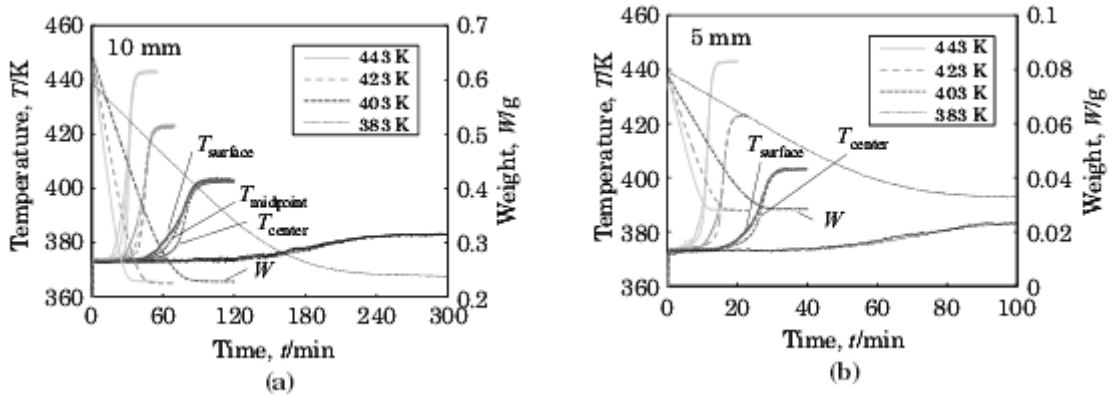

Figure 9.8 Drying kinetics of Loy Yang coal particles, taken from Kiriyama et. al. [256]

Table 9.3 Coal drying model conditions

Case	Temperature *(℃)*	Particle Size *(D - m)*
A	170	0.01
B	170	0.005
C	150	0.01
D	150	0.005
E	130	0.01
F	130	0.005
G	110	0.01
H	110	0.005

Similar steam and water properties as shown in **Table 9.2** were used for this part of the simulation; the specific heat capacity of brown of 1280 *(j/kg K)* [256] was, however, used to reflect on the drying behaviour of brown coal and not that of ceramic particles.

Similar to Hager et. al. [179], Kiriyama showed that heat transfer characteristics of their experimental followed a modified heat transfer co-efficient differing from the Ranz-Marshal equation for particle/droplet evaporation. Comparison between the unmodified Ranz-Marshal equation and the experimentally obtained heat transfer co-efficients show variation, Kiriyama et. al. [256] experimentally determined the heat transfer co-efficient to take the following form:

$$h = 0.0401/r + 18.7 \quad (9.18)$$

Equation 9.18, however, does not account for the effect of the ambient convective conditions and is a simplified expression based on the experimental conditions. Heat transfer correlations are typically correlated to also account for change in the ambient temperature (affecting the properties of the steam) and the hydrodynamics of the steam contacting the particles. This aspect is even more critical if the correlation is to be used in larger CFD frameworks in which the local steam condition changes within the simulation domain of the fluidized bed dryer. Therefore, even with the limited experimental data available, it will be of interest to express the heat transfer correlation in a more generalised form, typically including the Nusselt, Reynolds and Prandlt numbers.

Therefore, using the particles temperature and mass change data under different drying conditions from the experiments by Kiriyama et. al. [256], the heat transfer co-efficient was recalculated for each instance in the drying process by rearranging Equation (9.1) into the following form:

$$h = \frac{m_p C_p \frac{dT}{dt}}{A_p(T_a - T_p)} \tag{9.19}$$

The calculated values were then recalculated via the Nusselt number and are plotted against the $Re^{1/2}Pr^{1/3}$ form (**Figure 9.9**). The fitted mathematical expression of the heat transfer correlation then takes the form,

$$Nu = 3.748\left(Re^{1/2}Pr^{1/3}\right) \tag{9.20}$$

As this recalculation of the heat transfer co-efficient using the temperature gradient is an ill-posed inverse mathematical procedure, any negative heat transfer co-efficient values (discrepancies) particularly determined towards the end of the dying process when the temperature gradient approaches zero, was omitted in the fitting process.

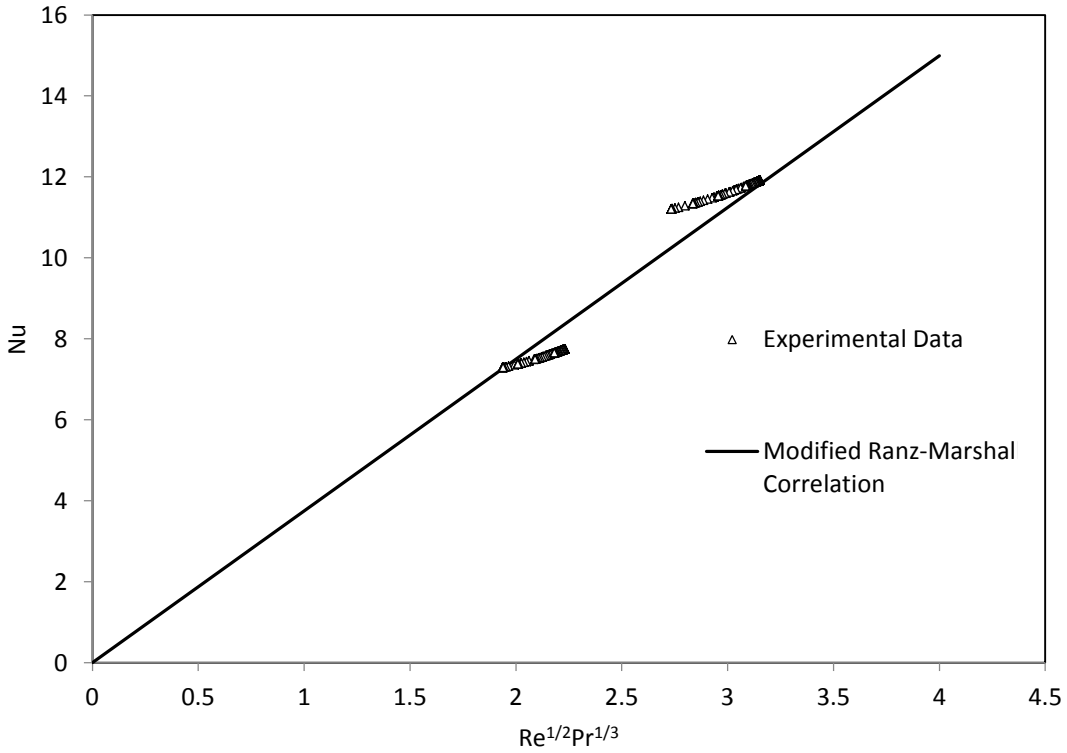

Figure 9.9 Modified Nusslt, Reynolds and Prandlt number correlation

The same procedure outlined in the preceding section was then used to determine master curves for the surface temperature multiplier and falling rate parameter data for the Loy Yang coal particles. Computed values for the surface multiplier term is shown in **Figure 9.10**. Some scatter of the calculated values below the theoretical limits were observed. This was regarded to be the effect of the ill-posed mathematical procedure in using the experimental

temperature and mass change gradients in the computation; at regions approaching zero mass change or temperature change, large discrepancies might be mathematically induced. Therefore, calculated surface temperature multiplier less than 1 (the theoretical lower limit) were omitted in future processing of the data.

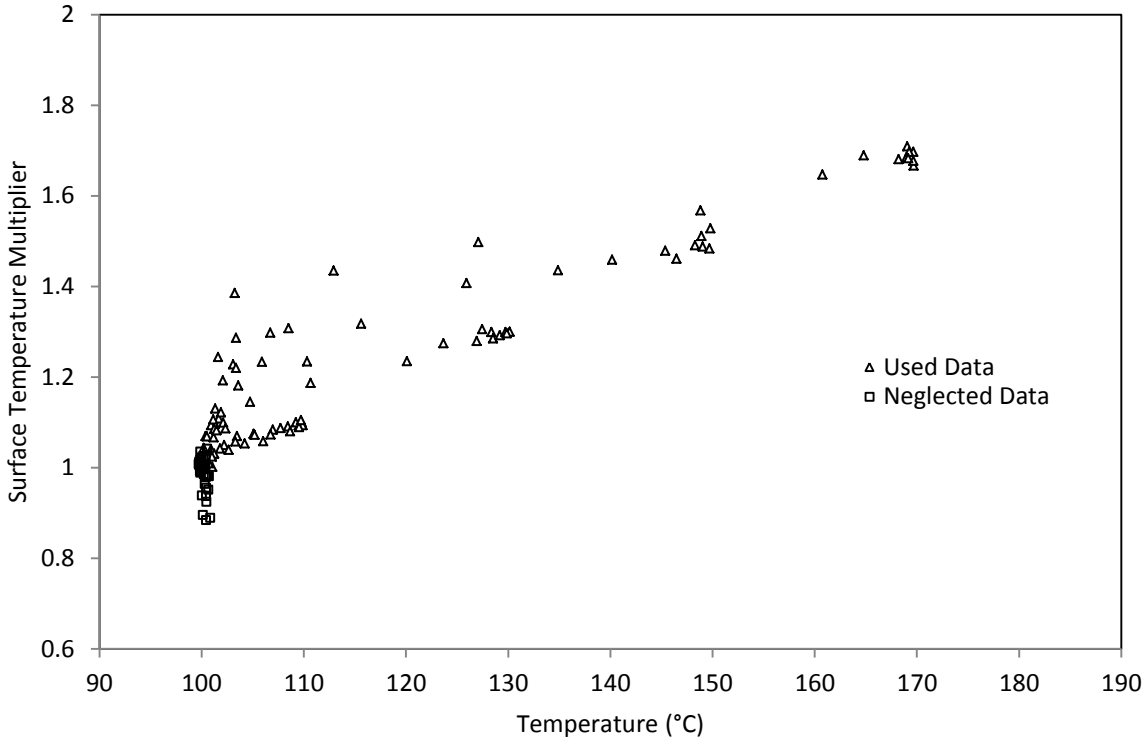

Figure 9.10 The surface temperature multiplier at different drying conditions (coal)

Using the same normalization approach outlined earlier, the surface multiplier curves were then collapsed into a master curve shown in **Figure 9.11**, mathematically taking the form,

$$\psi_n = 8.169T_n - 51.55T_n^2 + 166.3T_n^3 - 271.5T_n^4 + 216.2T_n^5 - 66.64T_n^6 \qquad (9.21)$$

The trends observed are similar to that of the ceramic master curve with a sudden drop closer to the saturation region. Larger data scatter was also observed with the computation using the coal dying data. On the other hand, a notable difference is that the surface temperature of the coal particles might have a higher tendency to exhibit a sudden increase in surface temperature when compared to ceramic particles. This is delineated by the sudden increase in the surface multiplier term followed by an approximately linear increase in the surface multiplier term as progressive higher normalized temperature.

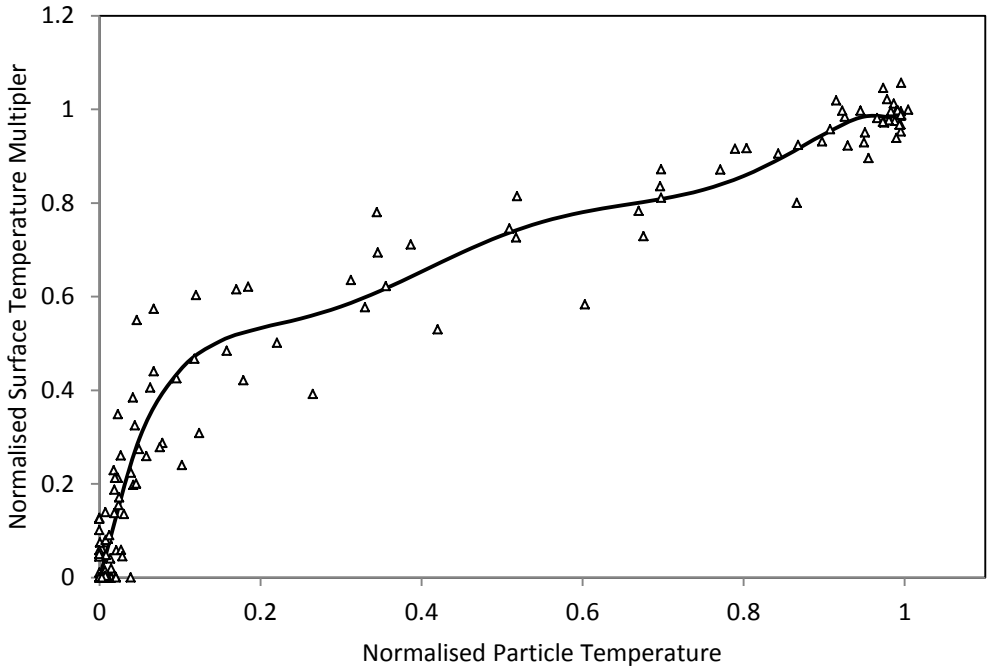

Figure 9.11 The normalised surface temperature master curve (coal)

The normalized falling rate master curve was also computed as function of the reduced particle surface temperature and is shown in **Figure 9.12**. The fitted mathematical expression of the master falling rate term curve takes the following form:

$$\phi_n = 1.013\exp(-0.00588X_n^{1.013}) - 0.4884\exp(-52.14X_n^{-0.222}) \quad (9.22)$$

The difference between the falling rate master curve for coal and ceramic is shown in **Figure 9.12**. Ceramic particles show an earlier decrease in the falling rate master curve, with a decrease occurring at 0.6 normalised moisture content (X_n). Coal particles however have this drop occurring much later, at approximately 0.2 X_n. This is attributed to the initial moisture content in the particle as well as the difference in water-substrate interactions occurring within the particle.

Using the two characteristic master curves determined, the model was then used to predict the drying process corresponding to the experimental conditions listed in **Table 9.3**. Eight separate conditions are compared between experimental data and the model. As with the application to ceramic particle drying, this model shows good agreement with experimental data.

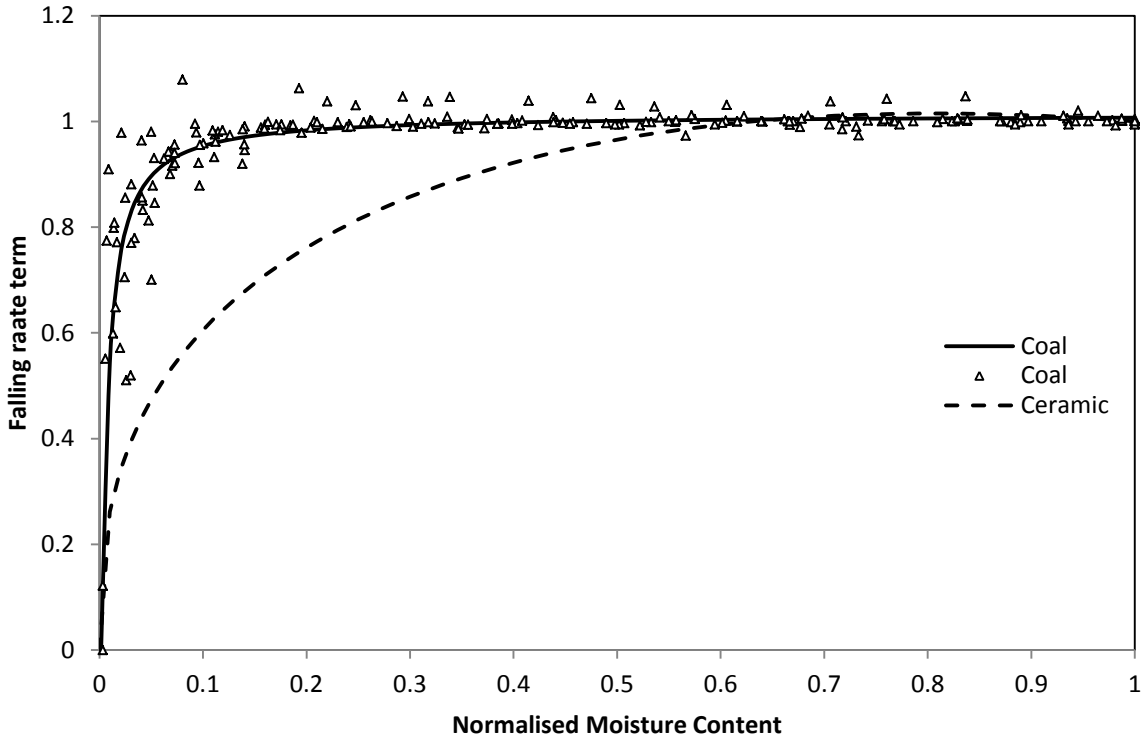

Figure 9.12 The normalised falling rate master curve (coal)

An overall trend observed is that the model tends to predict a faster initiation of the temperature rise period during the drying process. This is similar to that observed for the ceramic particles. In general, the model has a tendency to predict slightly higher final particle moisture. The advantage of the available coal particle drying data over the preceding ceramic particle drying data is the availability in the variation of the coal particles size. Evaluation of the model prediction for different coal particles size revealed no significant differences in the trend in which the prediction match the experimental data (best highlighted in Case A and B in **Figure 9.13**). Surprisingly, the discrepancy between the prediction and the experimental data was found to be more significant at lower temperatures (Cases E to H in **Figure 9.14**).

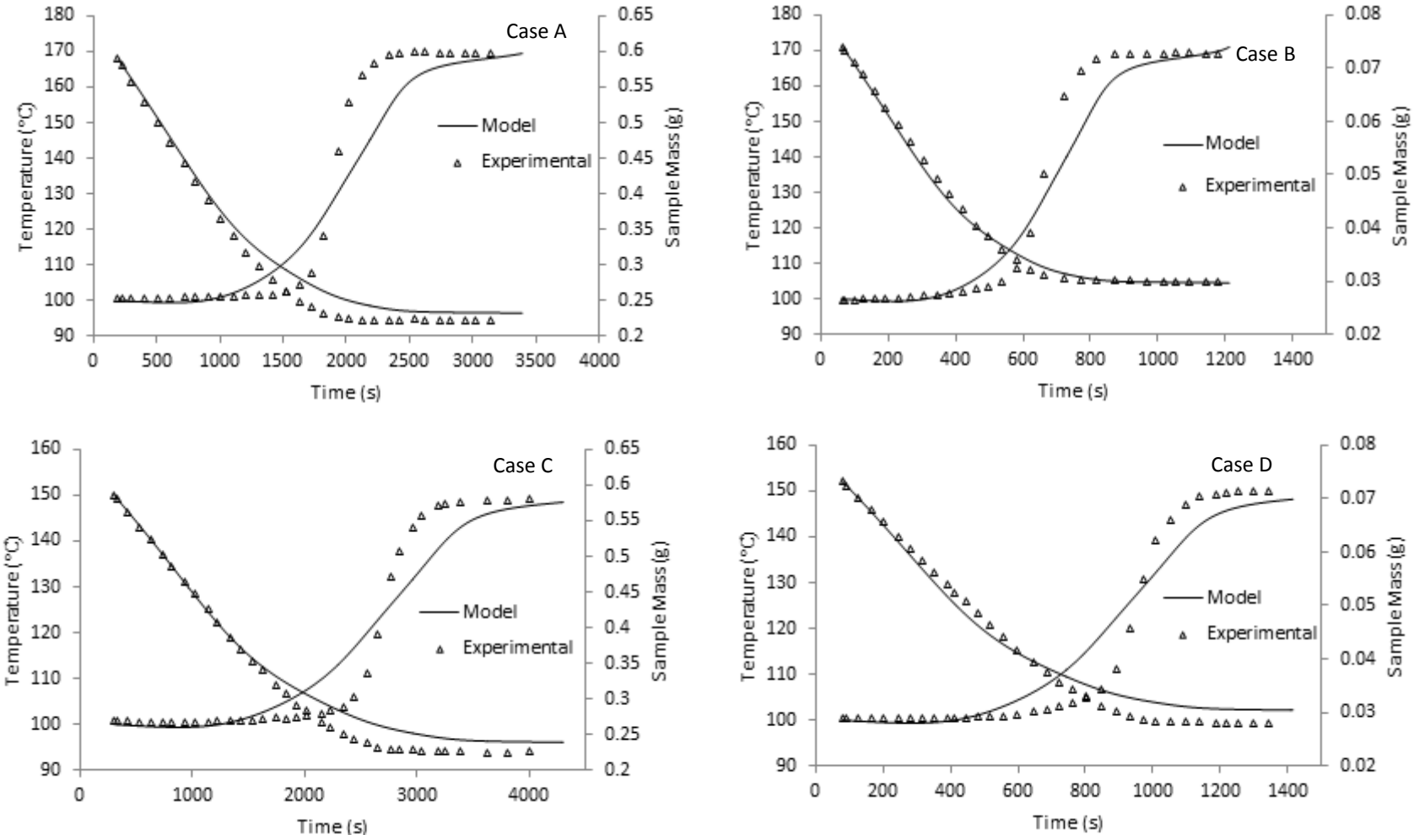

Figure 9.13 Experimental vs. Model comparison for case A – D (coal)

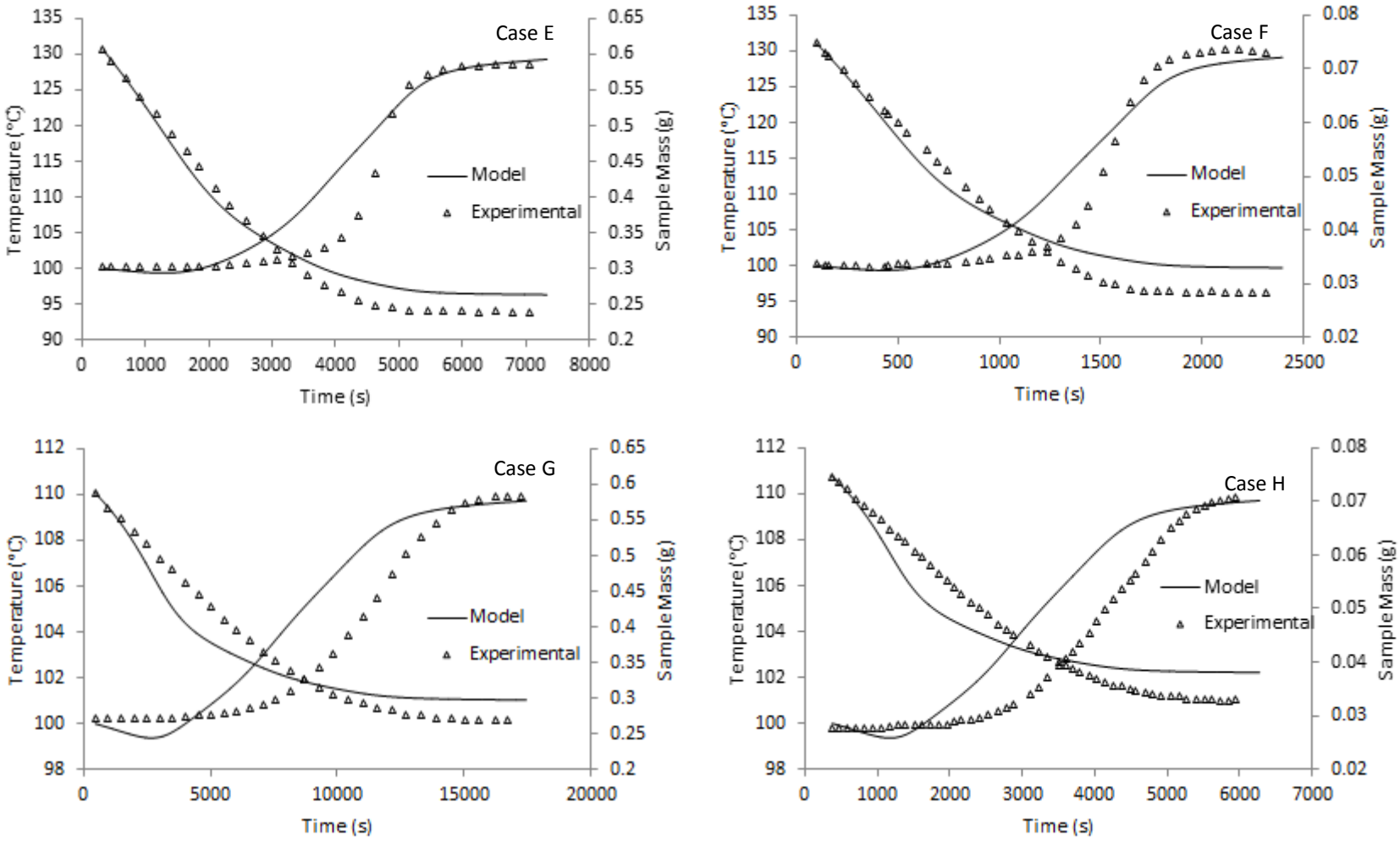

Figure 9.14 Experimental vs. Model comparison for case E – H (coal)

Sensitivity analysis by arbitrarily varying the different parameters in the model revealed that the shape of the moisture change and temperature change profile was significantly affected by the heat transfer co-efficient (not shown here for brevity). In the current simulation approach, this dependency on the heat transfer co-efficient could have been further magnified as mass transfer is also driven by heat transfer (Equation 9.8) and hence the strong dependency on the heat transfer co-efficient. It is noteworthy that the heat transfer correlation used in this modelling work was determined using limited experimental data from Kiriyama et. al. [256]; limited in a way that there was not a wide range in the possible computed $Re^{1/2}Pr^{1/3}$ values. With the available experimental data available, the deviation from the best fitted heat transfer correlation can be observed in **Figure 9.15**. Nevertheless, even with the discrepancies observed, the model prediction showed reasonable agreement with the experimental data comparable to the accuracies reported for some of the models reported in the literature, such has Chen et. al. [67, 142]. We speculate that the accuracy of the model may be further improved if a more accurate heat transfer correlation can be developed from single particle superheated steam experiments, this can be conducted through specific correlation experiments or by applying the same approach to similar drying experiments such as Komatsu et. al.[257]. In view of the significant differences in the heat transfer correlation for superheated steam particles drying when compared to the conventional Ranz-Marshal correlations, as observed by Hager et al. and in this current analysis, this will certainly be an important factor as well as for future work.

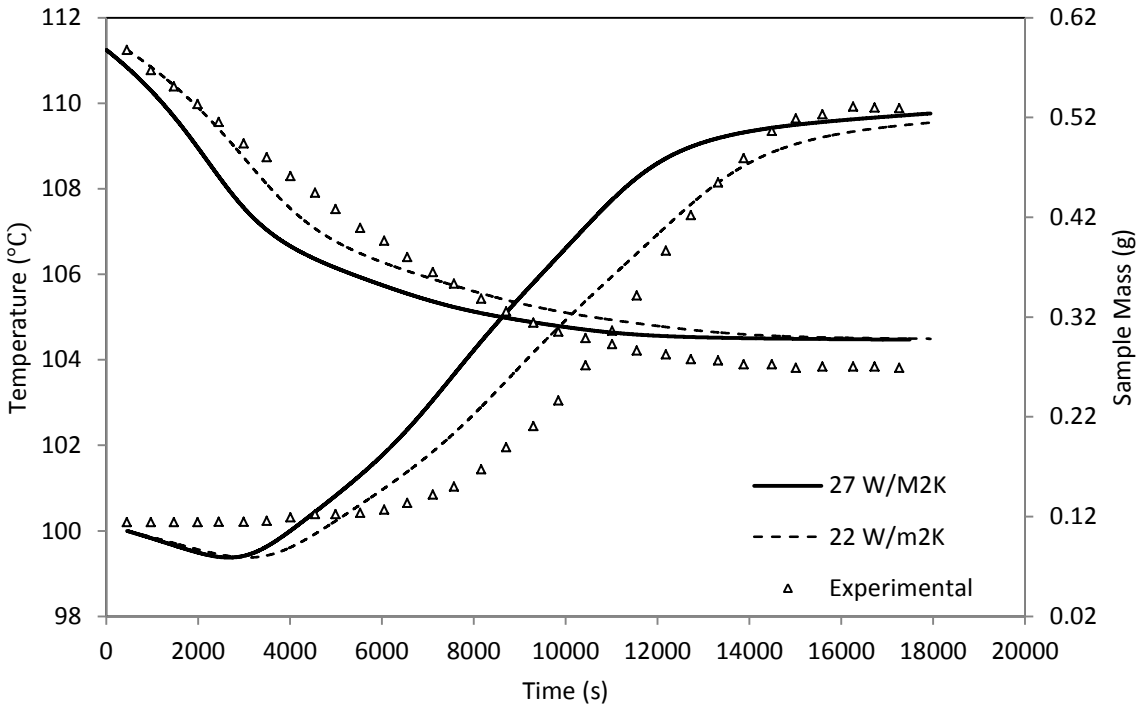

Figure 9.15 Sensitivity analysis of the heat transfer co-efficient for Case G

9.2. Conclusions

Key findings in the analysis of the ceramic and coal drying models are listed below:

- A complete range of drying conditions can be described by generation of two dimensionless terms: the falling rate delineator and surface temperature multiplier
- The new model developed in this chapter is now validated for porous particles dried under superheated steam conditions: ceramic and Loy Yang coal particles
- A set of characteristic master equations was developed for Loy Yang coal (and Victorian brown coal in general) which describes the drying behaviour of the coal particles
- The flexibility of the model to translate to different drying conditions and low numerical requirements will allow the model to be easily implemented in larger numerical frameworks such as in CFD simulations of the superheated fluidized bed dryers.

Chapter 10. Combustion, Gasification and Ignition Point Analysis

The physical and chemical characteristics of dried Victorian brown coal have the capacity to affect the combustion and gasification reactivity. The variation encountered in Chapter 6 and Chapter 7 show many of the coal characteristics are altered by the change in drying methods and conditions.

To examine the effect of drying conditions on combustion and gasification reactivity was analysed over a range of temperatures (130°C to 200°C), drying methods (air/steam fluidized bed drying, oven drying, apparatus scaling) and moisture contents (raw, dried and moisture re-adsorbed) being analysed. Then, using the same drying conditions the second section provides a comparison of the ignition temperatures between the same drying conditions. The ignition temperature, used in determining the point where a particle is ignited, was determined for both air and steam fluidized bed dried coal.

10.1. Combustion and Gasification Properties

10.1.1. Literature Review

Two methods of generating power from coal are currently viable, the combustion and gasification processes. While combustion is mainly used in power generation, gasification has a potential in future power generation technologies as well as the chemical industry. It is important to establish the reactivity of the dried coal to determine the feed rate and gasifier/combustor sizes [258]. One area which has not been explored is how different drying technologies affect the resultant coal's combustion or gasification potential. This potential can be quantified by the analysis and comparison of the reactivity of the coal. Reactivity is affected by porosity and pore distribution size, surface area, coal rank and inorganic constituents of coal [259, 260]. While the drying method can affect many of these properties, it is unclear how the steam and air fluidized bed drying affect the reactivity of dried Victorian brown coals.

Combustion reactivity of coal and char has been previously investigated, with a wide range of coals tested. Higher temperature heat treatment of coal decreases reactivity, while lower rank coals exhibit higher reactivity in general when compared to high rank coals. Additionally, high concentrations of magnesium and calcium also improve reactivity [261]. Coal composition shows inertinite rich low rank coal is more reactive than vitrinite rich high rank coal, controlling both reactivity and the atomic hydrogen to carbon ratio [183]. The volatile

matter in Turkish lignite has shown to affect its reactivity, with the removal of volatiles resulting in lower reactivity's [259].

High heating rates and pressures results in a reactivity increase plateauing at 1000 K/s. Reactivity was found to be at a minimum at a pressure of 40 bar during hydropyrolysis with Cai et. al. concluding that upper limit of char reactivity is related to tar release [262]. This is consistent with results in Messsenbock et al. [263], who observed the end values are independent of the pressure and composition of the reactive gas and the reactivity of both pyrolysis and gasification decrease with increasing pressure. Conversely, Chan et. al. demonstrated a positive effect of pressure upon combustion reactivity using Collie coal [264].

Gasification is an alternative for power generation which is currently used for a range of downstream processes due to its potential use as a chemical feedstock. Generating a combination of CO, H_2, CO_2 and CH_4 the gasification process produces specific ratios of product gases by heating the particles under a specific atmosphere (typically a mix of CO_2, O_2 or steam). These product gases are then used in a wide range of applications, such as the production of chemicals such as Dimethyl Ether (DME) [10] or in advanced power systems which can allow for integrated carbon capture systems, with potential technologies including chemical looping [265].

Using Bowmans coal, Ye et al. found that gasification rate is independent of particle size. Similar to combustion reactivity, high inorganic content contributes to increasing gasification reactivity, with acid washed coal showing much lower reactivity [266]. They also found the combination of different cations present within the coal provokes a greater effect than the sum of the effect of its individual cations [266].

Using North Dakota lignite, Radovic et al. also assessed the effect of inorganic constituents on the gasification reactivity [267], finding the deactivation of active carbon sites is reduced in the absence of calcium and the demineralised calcium impregnated char has reactivity 3 magnitudes higher than demineralised char, the reactivity decreasing with the increasing severity of pyrolysis.

Drying by hydrothermal dewatering was found to lower coal reactivity and oxygen content when drying at low temperatures [217]. Dewatering at higher pressures damages pore structures, decomposes oxygen functional groups removes ionic species. The removal of sodium chloride during the drying process, had little effect on the pyrolysis yield. The

removal of water, freezable or non-freezable, had no effect on char or tar yields. Experiments show drying at temperatures lower than 250°C had small effect on pyrolysis and gasification behaviour. The authors conclude that further study is required to fully understand the behaviour of dried coals [260].

Mechanical thermal dewatering shows that pore structure changed as a result of the dewatering process but has no effect on pyrolysis yields. Dewatering at temperatures above 250°C reduced organic and inorganic yield, decreasing tar formation and reducing reactivity. The variation of drying conditions by Zheng et. al. during the MTE process was shown not to affect the resultant chars reactivity. Any drop in char reactivity was attributed to the loss of water soluble inorganics, such as NaCl [268].

10.1.2. Materials and Methods

A single brown coal, Morwell, was chosen to represent all Victorian brown coals. The properties of Morwell brown coal is displayed in **Table 10.1**.

Table 10.1 Morwell brown coal properties

Coal	Moisture Content $^{(wb)}$ (%)	Ash Content $^{(db)}$ (%)	(VM) $^{(db)}$ (%)	FC $^{(db)}$ (%)
Morwell	59.9	4.6	41.0	54.4

Ash Constituent	Percentage (%)
SiO_2	3.9
Al_2O_3	2.1
Fe_2O_3	15.0
TiO_2	0.1
K_2O	0.5
Mg	18.5
Na_2O	3.8
CaO	34.0
SO_3	22.2
P_2O_5	<0.1

wb – wet basis; db – dry basis; VM – Volatile matter; FC – Fixed carbon

To investigate the combustion and gasification reactivity, a Netzsch STA449 F3 Jupiter thermo-gravimetric analyser (TGA) was used. The methodology was presented in Chapter 3, operational conditions are summarized in **Table 10.2**.

Table 10.2 Thermo-gravimetric analyser (TGA) operating and sample conditions

Operating Condition	Combustion Reactivity	Gasification Reactivity

Sample Mass	5 mg	5 mg
Particle Size	90-106 µm	90-106 µm
Gas Atmosphere	79% N_2	75% CO_2
	21% O_2	25% N_2
Gas Flow-rate	100 ml/min	100 ml/min
Ramp Rate	5 K/min (<75°C)	5 K/min (<75°C)
	10 K/min (>75°C)	10 K/min (>75°C)
Maximum Temperature	800°C	1000°C

The combustion and gasification reactivity is calculated using the following equation:

$$R_T = -\frac{1}{w}\left(\frac{dw}{dt}\right) \quad (10.1)$$

Where reactivity is R_T, w is the initial mass of the coal and dw/dt is the rate of mass loss. For comparison of the data, the reactivity is defined as the instantaneous reactivity and is calculated at any point in time, as shown in **Figure 10.1**. Reactivity can be difficult to compare across different literature or resources due to its dependence on many of the TGA conditions. Operational variables such as temperature control (isothermal or non-isothermal temperatures), particle size, gas flow, temperature ramp rate, sample mass and gas composition will all affect the resultant reactivity data. Currently there is no universal standard for reactivity with the two methods used, isothermal or non-isothermal. As the purpose of this chapter is to provide an internal comparison between drying methods and conditions, non-isothermal reactivity was chosen, with an average peak reactivity compared ($R_{T,\,inst,\,max}$).

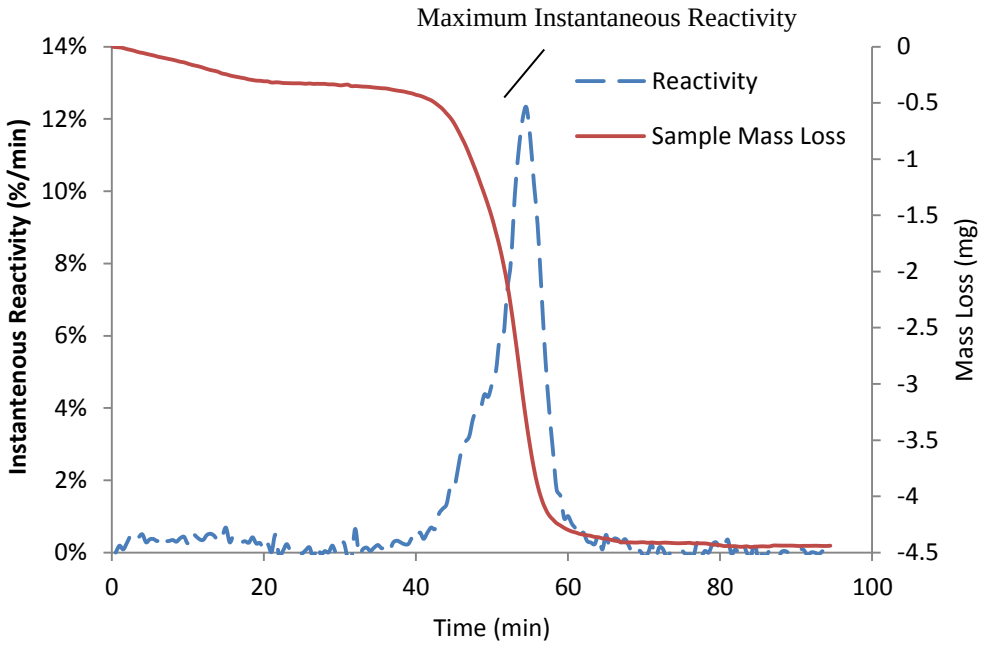

Figure 10.1 The calculation of instantaneous combustion reactivity (air fluidized bed dried sample, 130°C)

10.1.3. The Effect of Drying Temperature

Samples taken from the drying kinetics in Chapter 5 were analysed using the thermo-gravimetric analyser (TGA) to determine the reactivity. The samples chosen were taken to highlight the effect of the greatest deviation between the typical industry conditions (130°C) and the highest drying temperature, which were judged to have the highest possibility of affecting the reactivity. **Table 10.3** shows the variation in drying temperature having no noticeable effect on the combustion reactivity of the air fluidized bed dried coal, while a decrease is observed in the steam fluidized bed dried coal.

Table 10.3 Combustion reactivity depending on drying method and temperature

	$R_{T,\ inst,\ max}$ (%/min)	
Drying Temperature (°C)	Air fluidized bed dried	Steam fluidized bed dried
130	12.2	13.0
170	12.0	~~
200	~~	11.7

The reduction in oxygen functional group (with an increase in drying temperature) is the cause of reactivity reduction as discussed in detail in Chapter 6 [217].

However, variations of reactivity within the sample are expected to occur due to the heterogeneous nature of Victorian brown coal. Multiple sampling, the apparatus buoyancy

and peak averaging estimate a variation of up to ±0.75%. With this in consideration it can be concluded that the change in drying temperature does not provoke a statistically significant reactivity change in dried coals from either an air or steam fluidized bed drier.

In a similar experiment, **Table 10.4** shows the effect of drying temperature on gasification reactivity. As with combustion reactivity, there was little change to the gasification reactivity with changing drying temperature. While a small decrease in reactivity occurred in both air and steam fluidized bed drying, the decrease was insignificant to allow a trend to be established (based off standard deviation analysis of the results). A variation of 0.63% for air and 0.84% for steam is observed based on the average maximum reactivity and it can be concluded that the drying temperature makes no impact of reactivity in either an air or steam fluidized bed drier.

Table 10.4 Gasification reactivity depending on drying method and temperature

	$R_{T, inst, max}$ (%/min)	
Drying Temperature (°C)	Air fluidized bed dried	Steam fluidized bed dried
130	5.7	6.0
170	5.4	~~
200	~~	5.4

10.1.4. The Effect of Moisture Re-adsorption

An important part of drying brown coal is the effect of moisture re-adsorption on the physical property of the coals. As mentioned in Chapter 8, the dried coal can re-adsorb up to 10% moisture, thereby changing the physical characteristics (Chapter 7). While this is certain to impact upon the overall energy required for combustion, the impact on the reactivity is not clearly known. After 72 hours of exposure to the atmosphere the samples previously used in the moisture re-adsorption experiments were compared to the freshly dried samples. In **Table 10.5**, the re-adsorption of moisture shows an increase in combustion reactivity for air fluidized bed dried coal, while there was no change in combustion reactivity to steam fluidized bed dried coal. The re-adsorption of moisture caused a consistent decrease of approximately 1% in gasification reactivity regardless of the drying medium. A combustion reactivity variation up to ±0.75% and an average gasification standard deviation of 0.89% is an acceptable error in the calculation. The variation within the analysis and composition coupled no underlying fundamental cause indicate that the results obtained are not statistically significant.

Table 10.5 Moisture re-adsorbed coal combustion and gasification reactivity

	$R_{T, inst, max}$ (%/min)	
Coal State	Combustion Reactivity	Gasification Reactivity
Air fluidized bed dried	12.2	5.7
Air re-adsorbed coal	13.4	4.9
Steam fluidized bed dried	13.0	6.0
Steam re-adsorbed coal	13.0	4.8

10.1.5. The Effect of Drying Method

An important aspect of quantifying the effect of steam fluidized bed drying is its effect on reactivity using different drying methods. As previously stated, the drying method has the capacity to change the combustion or gasification reactivity. Due to the incompatibility between literature and the experimental findings, a comparison between drying methods has been conducted. **Table 10.6** shows that differences in reactivity does exist between air and steam fluidized bed dried coal (0.8%) the variation in samples and experimental errors will account for such discrepancy. It can be concluded that the drying methods do not cause any significant changes to either the combustion or gasification reactivity, when dried at 130°C.

Table 10.6 The impact of drying method on reactivity

	$R_{T, inst, max}$ (%/min)	
Coal State	Combustion Reactivity	Gasification Reactivity
Air fluidized bed dried	12.2	5.7
Steam fluidized bed dried	13.0	6.0

The impact of drying scale upon the reactivity is shown in **Table 10.7**. Samples used were collected from the larger apparatus discussed in Chapter 5. The variation in reactivity between the smaller vessel samples and the larger scale apparatus coal is observed. Bed size and residence time is dependent on the drying apparatus, with the fluidization time varied from 10 to 50 minutes. Using similar drying conditions (130°C, steam fluidization) the results show variation well within acceptable limits indicating that reactivity does not change with the scale of the drying.

Table 10.7 The impact of drying apparatus on steam fluidized bed dried coal reactivity

	$R_{T, inst, max}$ (%/min)	
Coal Drier	Combustion Reactivity	Gasification Reactivity
Thermo-Gravimetric Drier	13.5	6.0
Continuous Feed Drier	12.6	5.3

10.2. Ignition Temperature

10.2.1. Literature Review

The coal ignition temperature is defined as the lowest temperature required for initiating combustion and is used in the design of a coal burner and control in the start-up procedure [186]. During start up, if the furnace temperature is below the ignition point the coal will not burn. Inserting the coal at temperatures higher than the ignition temperature is safer but takes longer and requires more starting fuel [186].

Currently there is no standard on the determination of ignition temperature of coal, with most literature suggesting either a differential approach [186] of determining ignition point using a fixed percentage mass loss as an indicator, or determining the ignition point by analysing the divergence between air and inert atmosphere weigh loss [269, 270]. Both these methods are conducted using a thermo-gravimetric analyser (TGA). Other non-thermo-gravimetric methods also suggest applying the ignition point analysis methodology from plastic analysis [271] or the use of a photomultiplier to detect ignition through a visual flash [185].

Previous work using a range of coals and chars has shown a decrease in ignition point is dependent on an increasing particle size and oxygen concentration, while an overall trend shows increasing ignition temperature is seen with decreasing volatile matter [185, 186].

10.2.2. Materials and Methods

The determination of the ignition temperature (T_i) has been conducted using the Netzsch STA449 F3 Jupiter thermos-gravimetric analyser (TGA). The divergence method as outlined by Tognotti et al. and Mortari et al. [269, 270] was used to determine the ignition temperature.

In **Figure 10.2**, the ignition point through to divergence can been seen where the temperature where the pyrolysis curve deviates from the combustion curve.

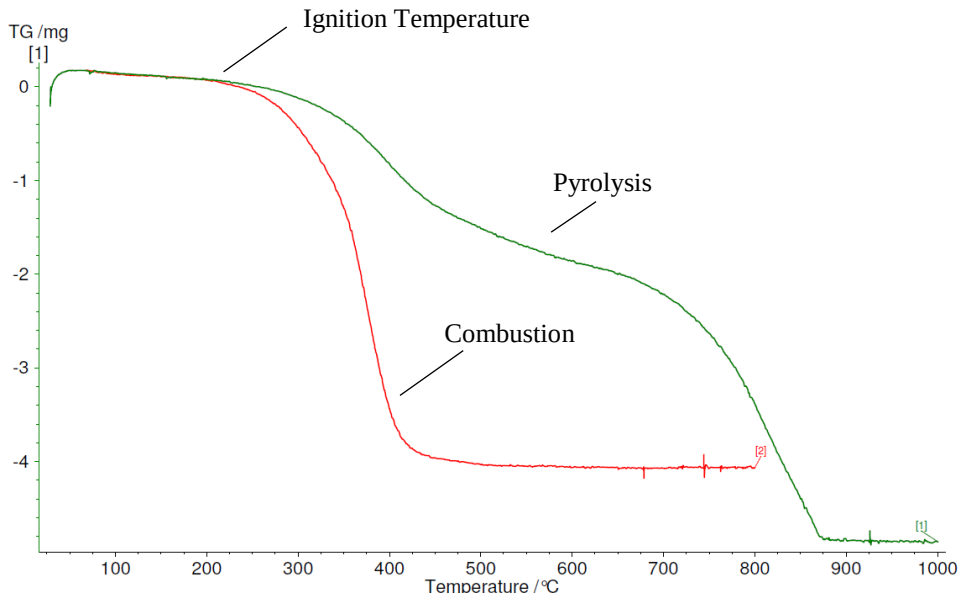

Figure 10.2 Ignition temperature divergence

10.2.3. The Effect of Drying Temperature

Using the conditions and variables discussed earlier in this chapter, the ignition characteristics of the previous variables can be observed. The effect of drying temperature on the ignition temperature is seen in **Table 10.8**, with no trend observed. With steam fluidized bed drying (T_i) there was only a 2°C ignition temperature variation, whereas there was a much greater variation with air fluidized bed drying (23°C). However, experimental data showed an average variation of ±20°C suggesting that no trends can be observed as the impact of drying temperature on the ignition temperature.

Table 10.8 The effect of drying temperature on ignition temperature

	T_i (°C)	
Drying Temperature (°C)	Air Fluidized Bed Dried	Steam Fluidized Bed Dried
130	257	232
170	234	~~
200	~~	230

10.2.4. The Effect of Moisture Re-adsorption

Moisture re-adsorption is a concern for the storage or transport of Victorian brown coal. As discussed previously in Chapter 8, understanding how this affects the ignition temperature can make a large impact on the usability and stability of the dried product.

In **Table 10.8** the impact of moisture re-adsorption is shown for both air and steam fluidized bed dried coal, with no trend in the ignition temperature observed. Steam fluidized bed drying

shows a minor increase after moisture re-adsorption, while air fluidized bed shows a decrease. While air fluidized bed dried and its corresponding moisture re-adsorption has a difference of 45°C, outside the sample variation of ±20°C, the cause for this difference has been attributed to the heterogeneous nature of coal.

Table 10.9 The effect of moisture re-adsorption on ignition temperature

	T_i (°C)	
Coal State	Air Fluidized Bed Dried	Steam Fluidized Bed Dried
Dried Coal	257	233
Moisture Re-Adsorbed Coal	212	240

10.2.5. The Effect of Drying Method

The incompatibility between our experimental data and literature makes it necessary to compare drying technologies. **Table 10.10** compares different drying conditions, with oven drying showing the lowest ignition temperature, followed by steam and then air fluidized bed drying. With approximately 20°C difference between samples, the variation makes it hard to attribute the changes in ignition temperature to any drying method.

Table 10.10 The effect of drying method on ignition temperature

Drying Method	T_i (°C)
Fixed Bed Dried Coal	214
Steam Fluidized Bed Dried	233
Air Fluidized Bed Dried	257

The results do not show a trend with the different drying methods used. The difference in drying conditions between fixed bed dried coal and air fluidized bed dried coal is minimal, so no major trend was expected. When retaining the same temperature and particle size, the fluidization velocity the only change to drying conditions. There was no major difference in the chemical composition or physical characteristics to cause any discrepancy.

The effect of scale of apparatus (previously discussed in Chapter 5) on the ignition temperature was investigated. Similar the reactivity experiments, the difference in scale predominantly changes the residence time and drying particle size, but not fluidization medium, temperature and velocity. **Table 10.11** shows increasing the scale of drying has no impact on the ignition temperature.

Table 10.11 The effect of vessel size ignition temperature

Drying Method	T_i (°C)
Continuous Feed Drier	228
Thermo-Gravimetric Drier	233

10.3. Conclusions

The results on combustion and gasification characteristics along with the ignition temperature for dried Victorian brown coal under typical air and stream fluidized bed drying conditions can be summarised as follows:

- Drying temperature has no effect on the combustion reactivity, gasification reactivity or ignition temperature
- Drying method (air fluidized, steam fluidized or fixed bed) has no effect on the combustion reactivity or gasification reactivity
- While the ignition temperature does vary with drying method this has been attributed to the variation in the coal sample and not to the differences between fixed bed and air fluidized bed drying
- The scale of the apparatus has no effect on the combustion reactivity, gasification reactivity or ignition temperature

Chapter 11. Conclusions, Practical Implications and Recommendations for Future Work

This thesis provides an overview of Victorian coal from as received condition through drying under different conditions and scales. The resultant drying kinetics and resultant coal characteristics are used to determine how steam and air fluidized bed drying affect Victorian brown coals and Chinese lignites, and how it differs from other forms of drying.

11.1. Conclusions and Implications

11.1.1. Water in Coal

The water composition in Victorian coal differs when compared to Chinese lignite, showing it is comprised predominantly of bulk water (55% bulk, 10% bound and 35% non-freezable water), while Chinese lignite has no bulk water but a significant proportion of bound water (30% bound and 70% non-freezable water). The structure of bound water in Chinese lignite also differs from Victorian brown coals, displaying two separate freezing temperatures (-36°C and -48°C) compared to Victorian brown coal's one (-47°C).

In Victorian brown coal, milling has little impact on water composition or content except for a minor decrease in bulk water. Milling of Shenhua lignite results in a decrease in bound water and an increase in non-freezable mass. Moisture re-adsorption of Chinese lignite makes no change to mass of non-freezable water, however the bound water is reduced.

Milling reduced bound water and increases the non-freezable moisture in coal. This may have a negative effect on certain drying technologies. Technologies which find it difficult to remove chemically bound water (such as press dewatering or densified brown coal) would result in higher equilibrium moisture content.

11.1.2. Drying Kinetics

Coal drying in air or steam fluidized beds behave similarly. Smaller initial particle sizes, higher fluidization velocities and higher drying temperatures (within the range investigated) decreasing the drying time required. In the smaller apparatus a drying ratio (the ratio of drying times required to reach equilibrium, at 130°C, 0.48 m/s, 1.2-1.7 mm particle size used as a reference drying time) between 130 and 170°C is 0.88, but in the larger apparatus the drying ratio is 0.65. This showed that the drying temperature has the potential to have a greater impact in larger bed and has been attributed to a change in fluidization characteristics.

The drying time also increases between the small and large drier, in some cases from 6 to 30 minutes. The small scale kinetics are determined to be the ideal drying conditions while the larger kinetics are closer to the ones in large scale driers. Using the Page model and a specially defined scaling factor of 1.33, the small kinetics model has been transitioned to the larger drier and allows the effect of scaling to be predicted for a larger fluidized bed drier. The format of the modified Page expression is $X = a.exp\left(-k^{d_1}.(t^n)\right)$ where d_1 is the scaling factor.

The drying kinetics showed that the residence time and thus output moisture content for steam fluidized bed drying is governed by fluidization effects and not drying rate. The development of a scaling factor equation between the smaller and larger fluidized beds allows a better prediction of the moisture content and drying times required when transitioning between bed sizes. This allows for scaling to commercial sized fluidized beds.

11.1.3. Chemical Characteristics of Dried Coal

Through Synchrotron Infrared analysis, inert particle drying (Nitrogen opposed to steam) showed that functional groups in Victorian brown coals begin to break down at 140°C while significant drops occur at 200°C. Shenhua lignite showed a large decrease for all groups beginning at 160°C, with almost no functional groups remaining by 200°C. This indicates that Shenhua lignite is more temperature sensitive and should be dried at temperatures below 200°C to preserve the maximum calorific content and coal reactivity.

Also through Synchrotron Infrared analysis, at a steady temperature of 130°C Yallourn coal shows an Alkyne reduction regardless of residence time, while Shenhua lignite shows a reduced intensity for hydrogen bonded water, methylene, symmetric methyl, methane, alkyne and aliphatic COOH. At 20 and 30 minutes the surface functional groups show additional loss, with methylene, symmetric methyl, methane and alkynes consistently decreasing after 20 minutes. At 170°C a drop in COOH dimers is seen after 15 minutes, with loss of additional functional groups occurring at 25 minutes. Understanding the different timing for functional group loss allows for greater control over the functional group composition of the resultant coal through the manipulation of drying time, allowing the retention of components contributing to the calorific value of the coal.

11.1.4. Physical Characteristics of Dried Coal

Investigating drying in an air fluidized bed, steam fluidized bed and fixed bed (until equilibrium moisture is reached) the average particle size decreased by approximately 100 μm, from 665 to 569 μm, regardless of the drying method used. With the same particle size distribution for all types of drying, the results indicate that fluidized bed drying does not cause additional particle damage during drying. The decrease in particle size has been linked to the transition between bulk and non-freezable water, allowing the time and extent of particle distribution change to be predicted using the equation: $P_d = A_2 + (A_1 - A_2)/(1 + (d/x_o)^p)$.

At residence time between 30 and 60 minutes the particle size distribution of dried coal from a steam fluidized bed is unchanged relative to the distribution after 10 minutes, however a decrease in particle size is observed in an air fluidized bed. As the attrition occurs between 10 and 30 minutes, this indicates that air fluidized beds cause a greater amount of particle attrition than a steam fluidized bed over longer periods of time. Practically this may require the gas outlet stream for air fluidized bed drying to have a greater amount of treatment through filtering or separation.

11.1.5. Moisture Re-adsorption of Dried Coal

The moisture re-adsorption potential of Victorian brown coal has been determined over a 72 hour period. With the equilibrium moisture content reached after approximately 24 hours the extent of moisture re-adsorption depends on both coal type and drying methods. Loy Yang coal adsorbs slightly less moisture than Yallourn or Morwell coals, 7.6% vs. 9.2% for steam fluidized bed drying and 9.6% vs. 10% for air fluidized bed drying.

Steam fluidized bed dried coal has an equilibrium moisture content of 7.5% to 9% wt (H_2O)/wt (coal), which is a reduction of up to 2% re-adsorbed moisture when compared to air fluidized bed dried coal (9.5% to 10.3%). The physical and chemical properties using Morwell coal as a representative of the Victorian brown coals has been analysed, showing no change in the surface area or porosity, suggesting the changed equilibrium moisture content is not due to a physical affect. Using FTIR a reduction in the oxygen functional groups, especially carboxylic acid content is observed, proving that the reduction in moisture re-adsorption content is due to the change in functional groups. Understanding of moisture re-adsorption behaviour is important to the storage and transportability of Victorian brown coal.

11.1.6. Modelling

A lump drying model has been developed for drying in a steam atmosphere and is based off single particle drying data. Using the master-curve approach which creates two dimensionless variables – the surface temperature multiplier and the falling rate delineator – the temperature and moisture content of the particle at a given time is determined.

The results are first validated using literature data for ceramic particle drying with only minor variations in both the temperature and moisture prediction. At the lower steam temperatures, the model predicts a faster increase in particles temperature and slightly higher final moisture, with higher accuracy with experimental data achieved at higher temperatures. These discrepancies may be attributed to the scatter in the data when the master curves were empirically fitted.

Using the experimental data, a correlation using the Nusselt, Reynolds and Prandlt number for coal drying was used to calculate the heat transfer co-efficient for the particles. The master curve approach was again applied, with the drying curve predictions remaining in good agreement with the data provided in Kiriyama et. al. [256]; however greater deviation from temperature predictions occur. The model is less accurate when accounting for the rapid temperature increase. While this reduces the accuracy when compared to ceramic particles, the difference in temperature predictions are often seen in literature.

The development of an accurate and simple single particle drying model allows easier implementation into computational fluid dynamics (CFD) models. Future CFD models can use this model to predict bed drying kinetics as well as local conditions (such as temperature and heat transfer) within a drier. This information can then be used to influence driers design.

11.1.7. Reactivity of Dried Coal

This study compared the reactivity of coal generated after different types of drying, scale of apparatus and coal moisture content. The overall trend concluded is that steam fluidized bed drying under typical industry conditions has no observable impact to the usability of the resultant coal in either combustion or gasification processes, with no observable change to the ignition temperature. The results observed are consistent with previous understanding with the reactivity primarily determined by porosity and surface area showing little or no change [266]. Surface area and porosity remain unaltered and although the inorganic constituents

were not analysed, literature suggest that inorganic substance removed at temperatures less than 250°C does not strongly affect the reactivity [217].

This finding is important for the drying industry as it shows steam fluidized bed drying does not affect the combustion or gasification characteristics of Victorian brown coal.

11.2. Recommendations for Future Work

A number of interesting questions and different pathways have been found during this research. Some suggestions for future experiments include:

1. Investigation into how structural strength of dried Victorian brown coals changes with drying method (flue gas, steam fluidized bed) and temperature
    - While some tests were carried out in this research, further exploration will enable understanding of the strength of dried products as a function of drying medium and moisture content. These have practical implications for all drying methods, for coal transportability and applications
2. Investigation into the best state of coal (completely dried, partially dried and moisture re-adsorbed) for storage and transportation of the dried coal
    - The effect of drying medium and moisture content can affect the prospects of dried coal as a tradable commodity
3. The investigation of possible correlations between oxygen functional groups, water composition and the onset of the falling rate period of drying
    - By correlating these three phenomena it becomes possible to generate the single particle modelling term (falling rate multiplier) based off IR measurements and not kinetic data.
4. The analysis of drying conditions of adsorption and desorption isotherms
    - While the adsorption/desorption isotherms have been conducted on Victorian brown coal, the effect of drying conditions were not examined. Isotherms over a range of drying mediums, temperatures and humidity's would allow a complete characterisation of the moisture re-adsorption of coal.
5. A techno-economic study into the use and operation of steam fluidized bed drying
    - As the drying kinetics, physical and chemical properties have been investigated in this thesis; an opportunity exists to determine optimal operating parameter from an economic standpoint.

Appendices

Appendix A1. Drying Model Nomenclature

Table A1.1 Drying model nomenclature

(2.1) T – temperature (K) λ – latent heat of vaporization λ' – latent plus sensible heat Bi – Biot number r – radial portion r_e – receding core radius position R – radius ϕ – r-r_e/(r-r_e) ϕ_m – r_e/R (transient model) ϕ_{ms} – r_e/R (pseudo steady-state model) C_p – specific heat of coal C_{pw} – specific heat of water **Subscript/Superscript** θ – dimensionless time 0 – initial e – wet dry interface a – bed s – surface	**(2.2)** c – Specific heat t – time T – temperature ρ – density q – specific heat of vaporization α_* - co-efficient of interphase heat exchange β – effective drying rate **Subscript/Superscript** s – solid liq – liquid d – diameter cr – critical f – superheated steam 0 – at entry	**(2.3)** C – moisture content Bi – biot number D_{eff} – effective diffusion coefficient R_s – radius **Subscript/Superscript** i – initial e – equilibrium	**(2.4)** x – moisture content z – elevation d – diameter A – cross section u – velocity ρ – density K – volumetric co-efficient of gas interchange ψ – v – volume ε – void fraction in the emulsion h – heat transfer co-efficient d – diameter k – thermal conductivity D – molecular diffusion co-efficient T – temperature H – Volumetric heat transfer co-efficient γ – latent heat of evaporation S – surface area **Subscript/Superscript** b – bubble phase c – critical g – drying gas in – inlet mf – minimum fluidization bed – bed of dryer bt – total gas bubble p – solid particle be – bubble-emulsion phase br – bubble rise e – emulsion wv – water vapour t – total
(2.5) X – solids moisture content Y – gas moisture content m – mass transfer between gas and particles Cp – heat capacity φ – relative humidity t – time **Subscript/Superscript** in – inlet out – outlet	**(2.6)** Bi – Biot Number ϕ – r/R_o r – radial position R_o – radius k_p – thermal conductivity of coal W – moisture content λ – latent heat of vaporization v – kinetic viscosity of steam P – pressure T – temperature t – time K – coal permeability ρ – density **Subscript/Superscript** atm – atmosphere g – gas bed – bed p – particle c – receding core interface eq – equilibrium w – liquid water in – inlet sat – saturation	**(2.7) (2.8) (2.9)** Q_{heater} – heat loss Q_{loss} – power loss m_{dc} – mass of dried coal u_{sx} – dry coal internal energy m_L – mass of water u_L – waters internal energy m_a – air flow rate ω – humidity C_c – specific heat of coal C_L – specific heat of water C_{pa} – air specific heat h_g – enthalpy of saturated vapour **Subscript/Superscript** 1 – inlet 2 – outlet	**(2.10)** m – mass z – level coordinate t – time Θ – dimensionless temperature ϑ – temperature h – enthalpy of phase transition NTU – number of transfer units **Subscript/Superscript** D – steam UD – steam in transition p – particle G – gas TS – dry substance hyg – equilibrium moisture content Ges – total W – wall kr – critical
(2.11) m – mass C_p – specific heat capacity T – temperature t – time A – surface area of the particle	**(2.12)** T – Temperature t – Time ρ – Density C_p – Specific heat capacity r – distance from the centre	**(2.13)** T – temperature t – time m – mass of the dry particle r – radius κ – thermal conductivity	**(2.14)** ρ – density t – time D – diffusivity V – velocity ε – porosity

h – heat transfer co-efficient ΔH_{evap} – latent heat $X_{n,}$ ϕ, ψ – generated normalised terms **Subscript/Superscript** *a* – steam *sat* – saturated	of the coal particle q – specific heat R – radius λ – heat conductivity of coal α – heat transfer co-efficient **Subscript/Superscript** *e* – evaporation *w* – water *d* – drying *in* – initial *b* – bed *sh* – superheating *c* – coal	ρ – density c_p – heat capacity h – heat transfer co-efficient A – Area h_{lg} – latent heat of evaporation V_f – final particle volume **Subscript/Superscript** *p* – at particle radius *f* – drying front *h* – surrounding air *t* – transient	D_p – particle diameter h_m – mass transfer co-efficient h_T – heat transfer co-efficient k – thermal conductivity **Subscript/Superscript** *f* – drying gas *v* – water vapour *p* – constant pressure *surf* – surface *eff* – effective *b* – bound water
(2.15) ρ – density C_p – heat capacity k – thermal conductivity T – temperature t – time x,y,z – Cartesian coordinates D_{eff} – effective diffusivity $X_f = X - X_{eq}$ X – moisture concentration X_{eq}– moisture equilibrium L_v– latent heat of vaporization M_{H_2O}– molecular weight of water P_{vap} – vapour pressure in vapour phase T_{steam} – temperature of the drier R – universal gas constant T_s – temperature at particle surface P_s – vapour pressure at particle surface $\bar{h}_{film}$ –condensation heat transfer co-efficient $\dot{m}_{cond}$ – condensation flux	**(2.16)** *MC* – moisture content (coal) C_p – specific heat T – temperature L – latent heat of vaporization W – fraction of weight of coal t – drying time **Subscript/Superscript** *wc* – raw coal *g* – gas *wp* – water vapour *o* – at time = 0 *i* – at time i *j* – at diameter j	**(2.17)** X – moisture ratio t – time r – radius κ – moisture conductivity K – permeability ρ – density C_p – specific heat capacity P – pressure **Subscript/Superscript** *G* – gaseous *L* – liquid *S* – solid *SAT* – saturated	**(2.18)** ρ – density C_p – constant pressure specific heat T – temperature t – time U – velocity λ – thermal conductivity H – latent heat of vaporization m – vaporization rate X – moisture content K – permeability μ – dynamic viscosity **Subscript/Superscript** *l* – liquid phase *v* – vapour *s* – solid phase *g* – gas phase
(2.19) T – temperature t – time r – radial position k – thermal conductivity C_p – specific heat capacity ρ – density R – radial position h – heat transfer co-efficient m_{evap} – evaporation rate h_{fg} – latent heat of vaporization A – area **Subscript/Superscript** *F* – drying front *a* – atmosphere *sat* – saturation	**(2.20)(2.21)** T – temperature t – time *MR* – Moisture ratio	**(2.22)** X – drying fraction w – weight of water **Subscript/Superscript** *i* – initial weight of water *r* – remaining water weight *n* – drying rate order	**(0.1)** Nq – dimensionless number $\Re_{Nq}$ – dimensionless function m_{max} – drying rate K – factor v – linear velocity C_p – heat capacity φ – heat transfer co-efficient factor T – temperature H – enthalpy P – pressure **Subscript/Superscript** *i* – inlet *SS* – superheated steam *op* – optimum value *eq* – equilibrium value

Appendix A2. Small Scale Buoyancy Calibration

The physical operation of the smaller apparatus (outlined in Chapter 3) provides the raw data required for drying kinetics to be established. However, the thermo-gravimetric nature of the measurements results in a persistent noise which is attributed to the buoyancy effect. The buoyancy effect occurs in the majority of thermo-gravimetric processes and occurs when the force of the sheath gas (in this case fluidization medium) interacts with the vessel. The buoyancy is reflected as and change in the mass readings on the balance and needs to be removed before the kinetics are analysed.

Figure A2.1 presents the buoyancy without any coal or moisture present within the vessel and is used as a blank. It shows an initial, linear decrease when first connected to the gas line, with the inlet gas reducing the mass, and eventually levelling out after 100 seconds.

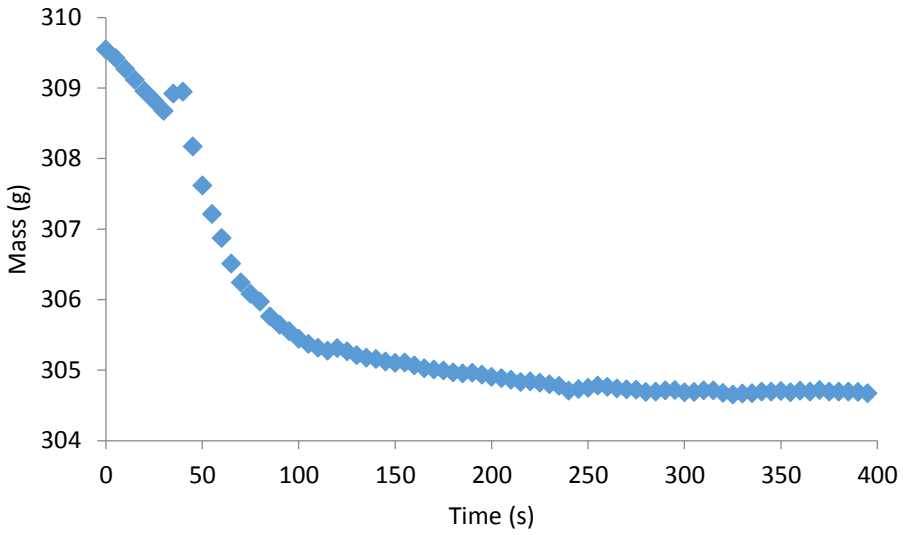

Figure A2.1 Reactor offset curve

Figure A2.2 shows the raw data, with the offset drying curves and the buoyancy effects present. The initial time is dominated by the offset, with an even larger mass jump at the steam inlet time, which can be explained as an increased condensation mass occurring across the particle bed. The values past 100 seconds have no major offsetting required and is regarded as the first stable point.

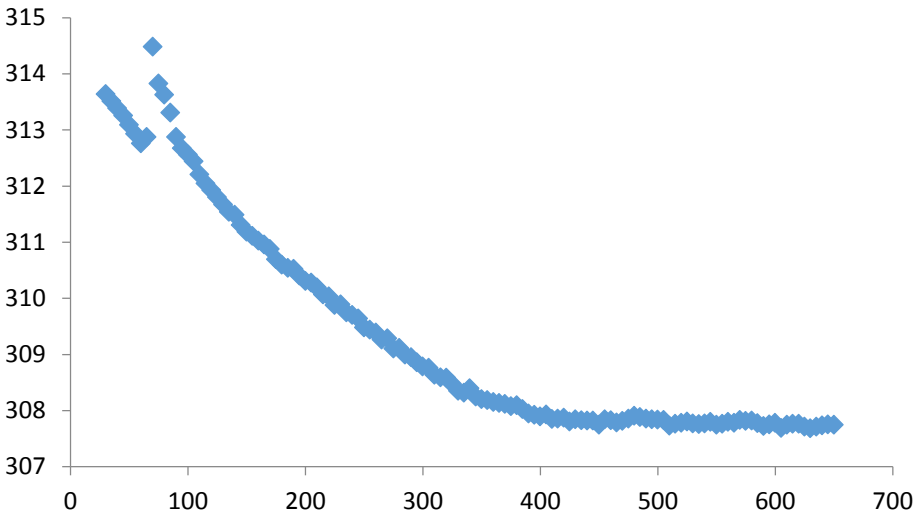

Figure A2.2 Raw kinetics data

Figure A2.3 shows a subtraction of the two, resulting in the final data curve, with the buoyancy section has been removed because of the inconsistency.

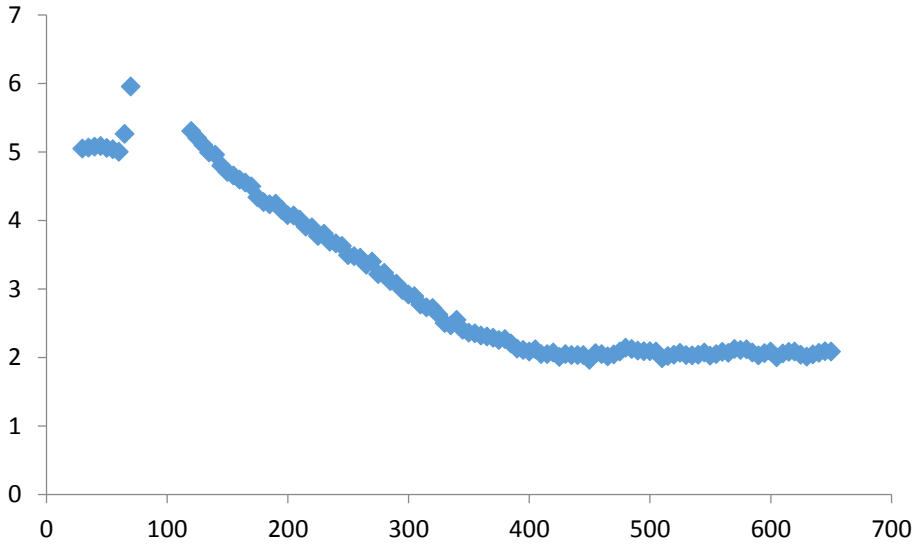

Figure A2.3 Final curve

Appendix A3. Mastersizer Calibration and Calculation Procedure

A3.1 Mastersizer Calibration Procedure

With the methodology for sample analysis previously discussed (Chapter 3) as well as being straight forward, the far more important step is determining the optimal operating conditions. Because of the nature of the experiments, the sample properties vary depending on the batch (therefore moisture content). Drying Victorian brown coal changes the particle strength, with wet coal being relatively soft compared to the dried particles (discussed in Chapter 7).

This is important as the Malvern Mastersizer 2000 uses pressurised air to disperse the particles for the analysis and can result in inaccurate distributions. At low pressures the particles are not adequately dispersed resulting in an artificially high particle sizes through agglomeration and clumping. However, higher pressures have the unwanted effect of particle breakage before analysis occurs. To remove both of these effects calibration runs are employed to prove the consistency and accuracy of the operating conditions.

As the moisture content changes from 60% to 0% the ideal circumstance for the particle size distribution analysis is a single set of operating conditions which does not cause agglomeration or breakage for both wet and dry coals. The determination of the optimal conditions uses both as-received coal and dried coal. With a common stable region found for both conditions an assumption is made that the samples which have a moisture range between these two values do not undergo agglomeration or breakage.

Another variable which can affect the results is the obscurity of the feed. The obscurity indicates the percentage of the coal passing through the beam and again, both too low and too higher obscurity values cause inaccuracies of the recorded values. Because the obscurity is based off the feed conditions in the coal, the feed flow rate along with the moisture content of the coal both affect the obscurity values. Analysed for both wet and dry coals, an obscurity range of 0.5 to 3 % has been targeted.

The general characteristic curve for the dispersive air pressures results in a decreasing size, followed by a level/stable period and finally another decrease in the particle size, with an ideal graph shown in **Figure A3.1**.

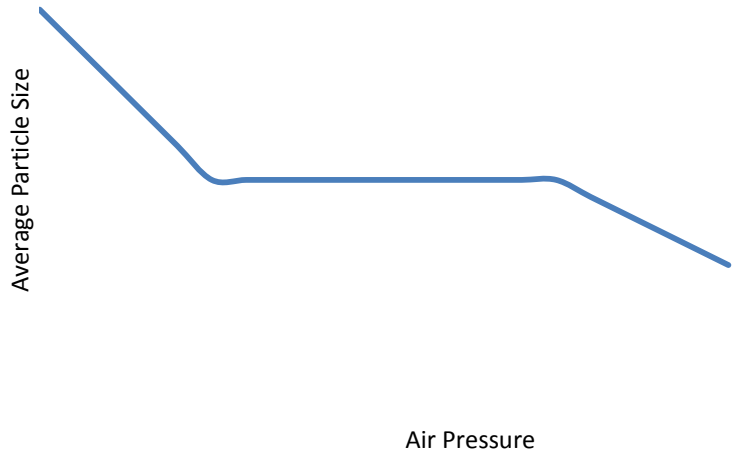

Figure A3.1 Theoretical air pressure trend

Analysing the effect of air pressure **Figure A3.2** and **Figure A3.3** show the increasing effect of air pressure on wet coal. **Figure A3.2** shows the decrease in the volume percentage as pressure increases, while in **Figure A3.3** the d(0.1), d(0.5) and d(0.9) are charted. The d values are used to highlight the change in average particle size of 10%, 50% and 90% volume respectively. In **Figure A3.5** the initial average particle values are shown to be stable, with pressures over 1.5 bar resulting in a continual decrease in particle size.

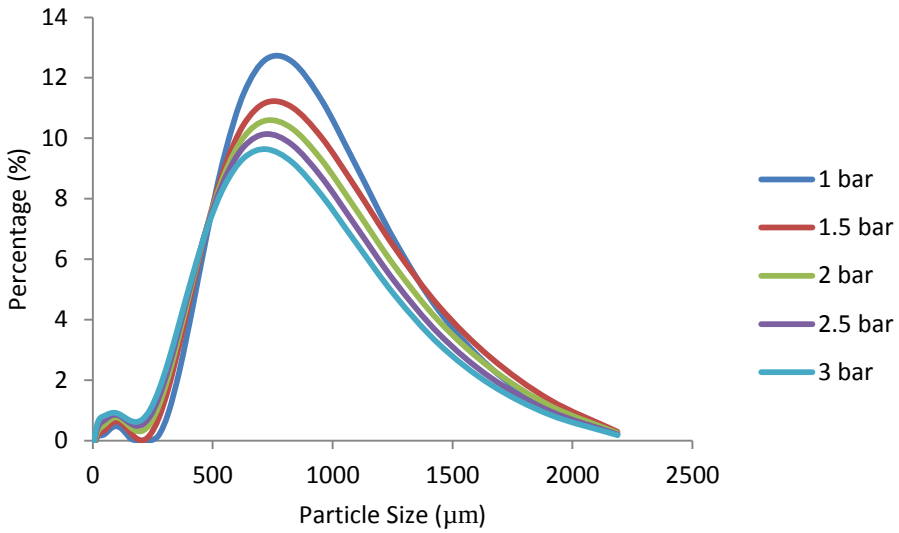

Figure A3.2 Dispersive air pressure calibration of wet coal

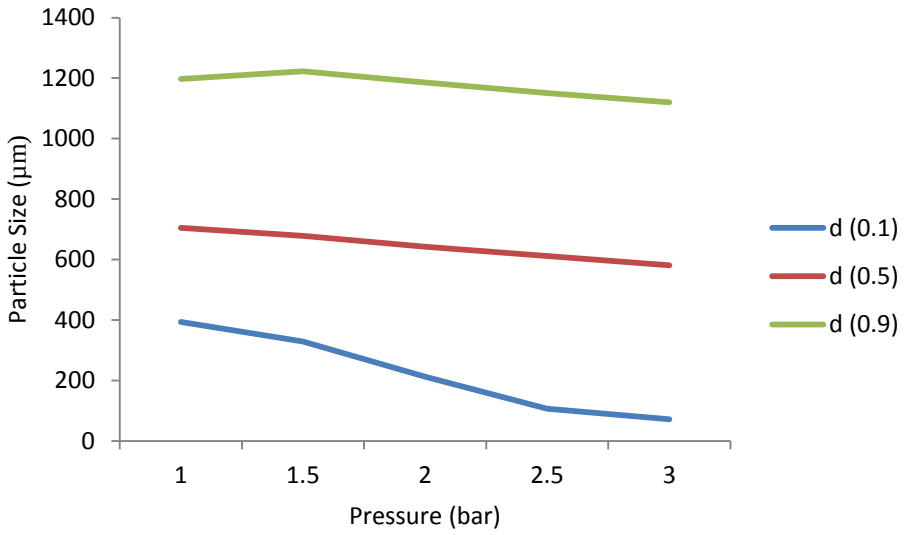

Figure A3.3 Dispersive air pressure calibration of wet coal, particle diameter markers

This method is repeated for dried coal, with similarly showing a stable region from 1 to 3 bar (**Figure A3.4** and **Figure A3.5**). Both these conclusions were qualitatively observed with debris of particle breakage seen in the dispersion tubing at high pressures.

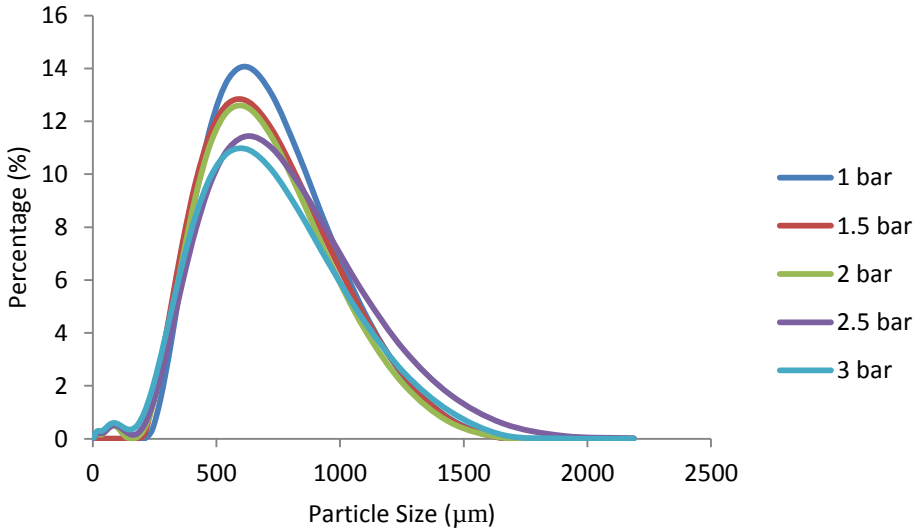

Figure A3.4 Dispersive air pressure calibration of dry coal

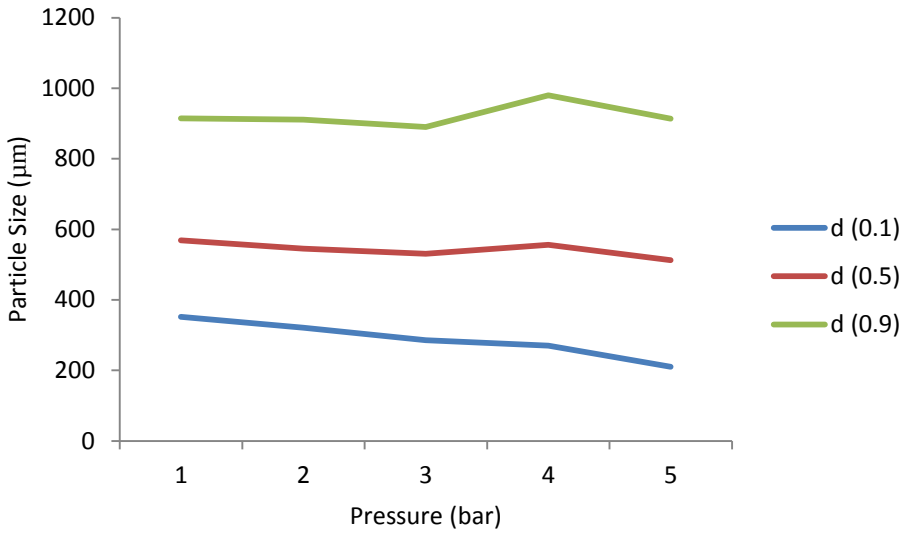

Figure A3.5 Dispersive air pressure calibration of dry coal, particle diameter markers

Based off the previous results, a common region between wet and dry coal was found to be 1.5 bar, and chosen as the particle dispersant pressure.

Using the same methodology for vibration rate, the effect of obscurity ratios were also analysed. The vibration rate, which controls the particle, feed rate, directly effects the obscurity. Based off 70%, 50% and 30% vibrational rates (and obscurity levels of 2.8%, 1.68% and 0.67% respectively) for wet brown coal the variation in particle shows no difference (**Figure A3.6**).

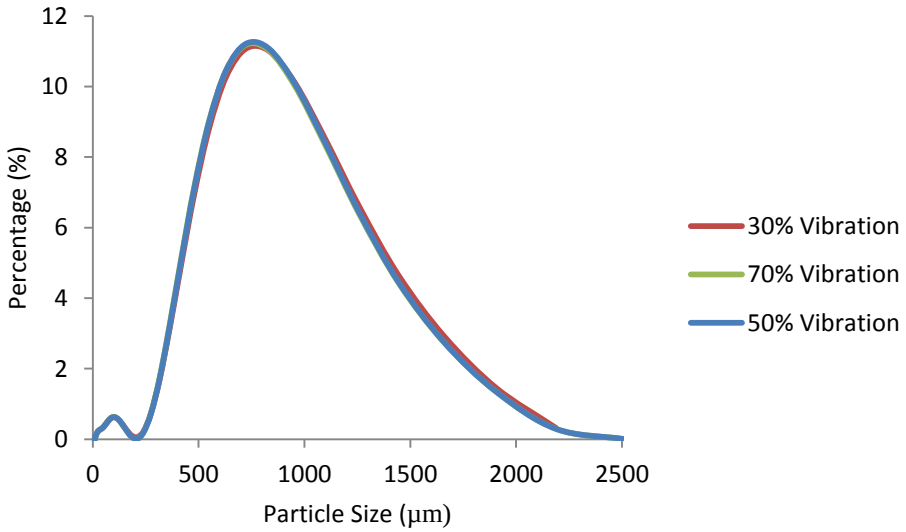

Figure A3.6 Comparisons of Vibrational rate (wet coal)

Comparing this trend to dried coal (**Figure A3.7**) the results show no difference in particle size allowing the conclusion that for both wet and dry particles the vibrational rate has no appreciable impact on the particle size distribution. With this in mind a vibration rate of 50% was chosen as an optimum point for sample analysis.

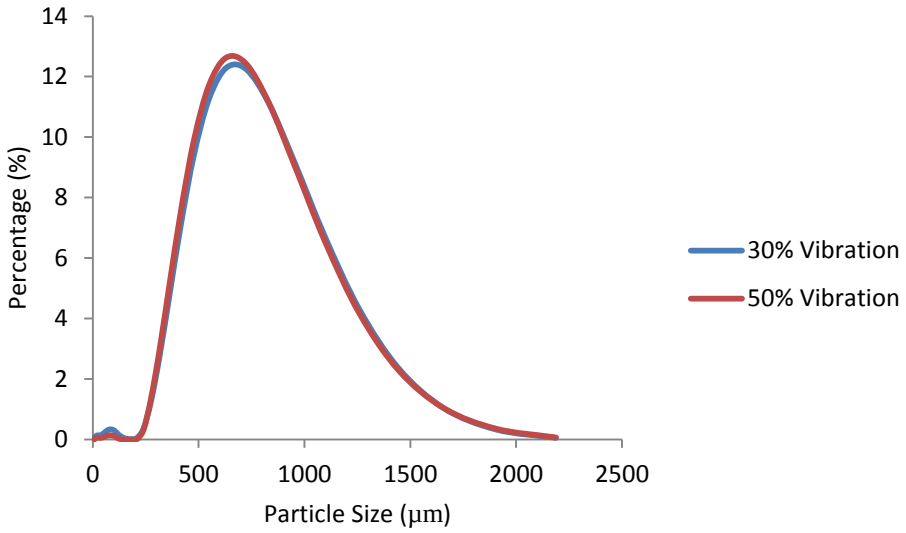

Figure A3.7 Comparisons of Vibrational rate (dry coal)

A3.2 Mastersizer Calculation Methodology

Unlike the previously discussed Mastersizer methodology outlined in Chapter 3, this provides the calculation procedure used to generate the particle size distribution data. This provides detailed, step by step, procedure along with the justifications required for the methodology in order to validate the experimental results.

1. Once the experimental results are obtained, the first step in data processing is to crop and recalculate the results, removing the coal fines from the particle size distribution (below 150 µm)
    a. The elutriated mass represents a small difference in the total distributions mass (approximately 4.4%) however it does present an additional source of error. This is due to the fine collection method. Throughout the experiment it was found to be impossible to collect the total mass of the elutriated materials as well as substantial loss of elutriate was seen through the dry cell procedure.

b. Because the mass was variable, the decision was made to remove elutriate entirely. Elutriate was easy to determine in the raw data because of the smaller secondary peak observed in the raw data (**Figure A3.8**)

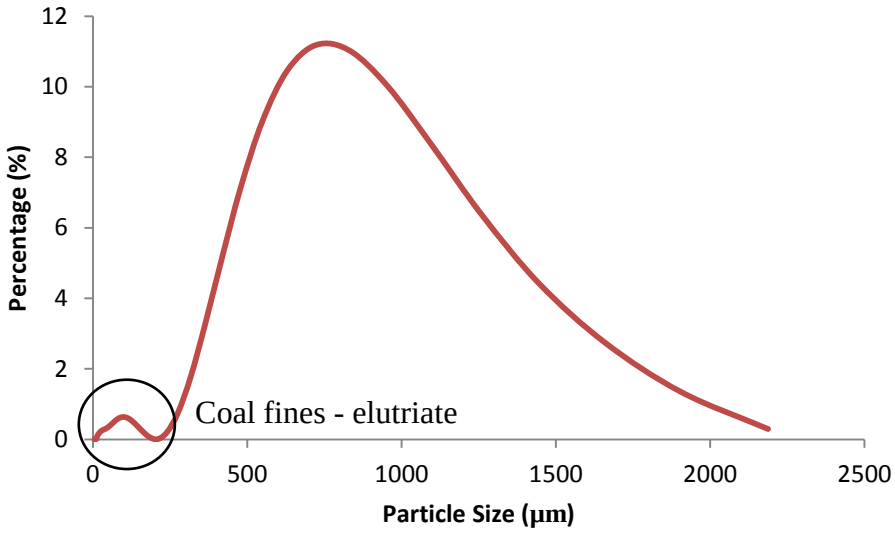

Figure A3.8 Raw Mastersizer 2000 data

2. The individual runs are averaged based off obscurity weighting
    a. Due to the large number of runs required for each condition, the results are required to be averaged.
    b. To accurately average the results based off the relative sample mass the obscurity results were used. The obscurity is a measure of the amount of particles that are crossing the beam line during the analysis, by creating an obscurity percentage of each run the resultant average is more accurately reflects the particle size distribution.
    c. This method does not generate standard deviation or error based off multiple runs as all results are equally valid and the deviation in the particle size distribution is due to particle segregation occurring within the vibrating sample feeder, hence the requirement for the weighted average.

Appendix A4. Fourier Transform Infrared Spectroscopy (FTIR) Calculation Methodology

With the Fourier Transform Infrared Spectroscopy (FTIR) operational methodology already outlined in Chapter 3, further work is required to process the raw data into accurately quantifiable functional group composition.

The relative breakdown of oxygen functional groups can be observed though the use of FTIR analysis and a commercially available data processing program (OriginPro 7.5). Using infrared spectrum from 400-4000 cm^{-1} the bands relating to relevant functional groups was chosen according to literature [272-279]. To approximate the number of bands and peak positions, the second derivative of the spectral data was taken and examined [272, 273].

To interpret the FTIR peaks, the calculations required looking at a range of absorbance peaks, from 1850 – 1500 cm^{-1}, 3000 - 2800cm^{-1}, and 3500 - 3000cm^{-1}. Using Gaussian curve fitting the individual absorbance peaks are fitted to the specific bands, with the area of the curves compared.

The fitted curve's shown in **Figure A4.1**, **Figure A4.2** and **Figure A4.3** highlight three separate regions where important changes occur. Over 1850 – 1500 seven separate peaks are seen, with five shown in the 3000 - 2800 and two in the 3500 – 3000 range. Each peak is indicative of a separate functional group, with a list of the observed functional groups shown in **Table A4.1**, **Table A4.2** and **Table A4.3**. The peaks in question are from Loy Yang coal, dried in a Steam Fluidized Bed at 130°C.

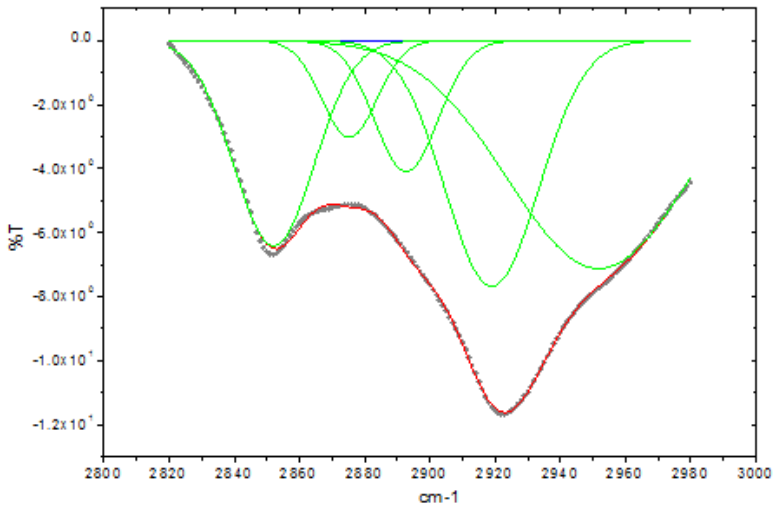

Figure A4.1 FTIR data 130°C Loy Yang coal, range 2800 - 3000 cm^{-1}

Table A4.1 Functional group wavelengths 3000 - 2800cm^{-1}

2800-3000 cm^{-1}	
2958 cm^{-1}	methyl (–CH3)
2922 cm^{-1}	methylene (–CH2–)
2870 cm^{-1}	symmetric methyl (–CH3)
2850 cm^{-1}	methylene (–CH2–)
2896 cm^{-1}	methane (C–H)

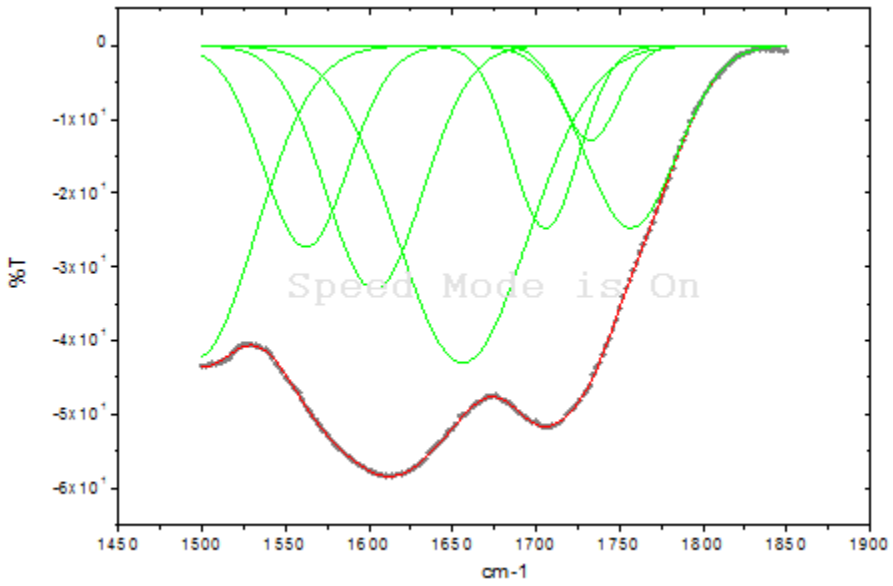

Figure A4.2 FTIR data 130°C Loy Yang coal, range 1850 - 1500 cm^{-1}

Table A4.2 Functional group wavelengths 1850 – 1500 cm^{-1}

1500-1800 cm^{-1}	
1772 cm^{-1}	esters, aliphatic COOH
1738 cm^{-1}	esters, aliphatic COOH
1705 cm^{-1}	aromatic COOH
1652 cm^{-1}	highly conjugated C=O
1611 cm^{-1}	aromatic C=C
1561 cm^{-1}	COO- aromatic ring
1488 cm^{-1}	COO- aromatic ring

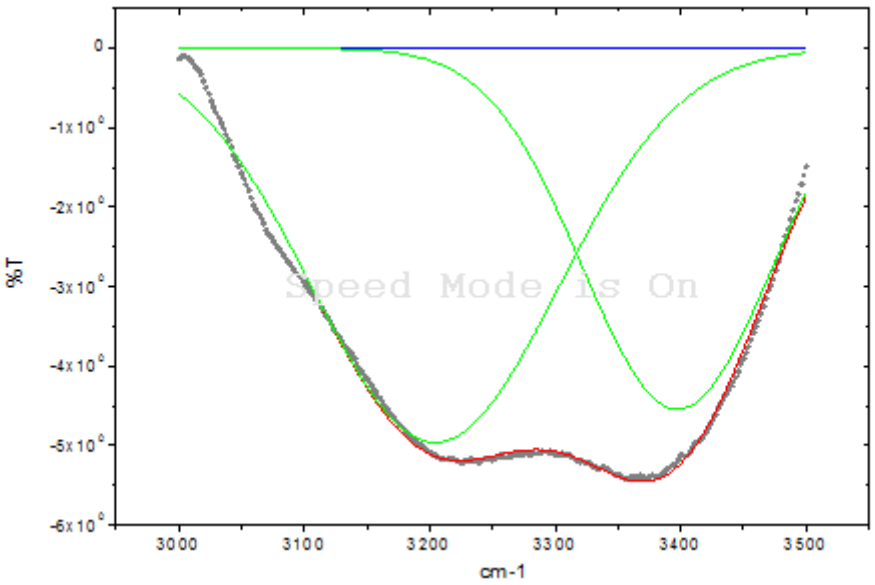

Figure A4.3 FTIR data 130°C Loy Yang coal, range 3000 - 3500 cm^{-1}

Table A4.3 Functional group wavelengths 3500 - 3000cm^{-1}

3000-3500 cm^{-1}	
3230 cm^{-1}	hydrogen bonded water
3425 cm^{-1}	phenolic and carboxylic structures

Using OriginPro 7.5 the specific wavelength band was chosen and plotted. Using the inbuilt curve fitting tool the steps for determining the functional group area is to:

1. Place a baseline for the curves to originate from and subtract it, re-zeroing the curve
    a. This define the fitted peaks origin point, and allows the best fit of peaks along with the accurate measure of peak area for comparison
2. Choose the number of peaks present within the graph
    a. Depending on the region analysed (**Table A4.1**, **Table A4.2** or **Table A4.3**) this will be between 2 and 7
3. Add the peak positions
    a. Based on the functional group wavelengths the peak positions are placed on the graph
4. Manually fit the individual curves

    a. An important distinction in using OriginPro 7.5 to OriginPro 8.0 is the ability to manually fit the curves, opposed to the less accurate automatic fit function. Varying the individuals peak with, height and position allows you to find the best available fit
5. Allow the final conversion fit to streamline the manual fit
6. Obtain the peak area information, which can be used in the analysis of function group composition

Due to the low sample masses required for the disc creation (2mg sample mass for 200 mg of potassium bromide) the variation of sample mass is a source of potential error. Minor changes in sample mass results in a change in the stretching of the intensity peaks, making the functional groups inaccurate for comparison across multiple samples. To counteract this, the data obtained through these measurements are normalised based off a peak that remains consistent across all samples.

From literature [65, 188, 189], carbon to carbon bonds (C=C) are shown to be unchanged during the temperature range used. Using the carbon to carbon curves area (Wavelength 1611 cm^{-1}) to normalise the other functional group areas allow the comparison of ratios, in effect charting the presence of individual functional groups.

Appendix A5. Ceramic Model Extracted Data, Hager et. al. [179]

This data has been used in the formation of the single particle ceramic drying model, found in Chapter 9.

Table A5.1-3 Case A–C – Ceramic model extracted data

Time (s)	Temperature (°C)	Drying rate ($\times 10^4$) kg/kg db	Moisture kg/kg db
0.0	100.00	1.07	0.15
98.8	100.27	1.07	0.14
193.7	100.27	1.07	0.13
285.6	100.20	1.09	0.12
399.0	100.58	1.04	0.11
503.1	100.50	1.08	0.10
588.9	100.69	1.06	0.09
674.6	100.69	1.07	0.08
778.8	101.07	1.04	0.07
870.7	101.25	0.99	0.06
981.1	102.08	0.95	0.05
1091.6	103.62	0.83	0.04
1180.8	106.25	0.67	0.03
1279.4	110.30	0.47	0.02
1359.7	114.74	0.31	0.02
1452.2	119.18	0.16	0.02
1541.4	121.36	0.08	0.01
1642.6	122.77	0.03	0.01

Time (s)	Temperature (°C)	Drying rate ($\times 10^4$) kg/kg db	Moisture kg/kg db
0.0	101.46	2.87	0.15
61.5	101.71	2.87	0.13
101.3	101.70	2.96	0.12
162.5	101.83	2.96	0.10
220.7	102.08	2.90	0.09
283.5	102.71	2.67	0.07
341.8	104.25	2.47	0.05
401.5	107.72	2.08	0.04
461.4	115.43	1.55	0.03
521.3	126.37	0.89	0.02
604.3	139.88	0.17	0.01
684.0	146.05	0.05	0.01
746.8	147.20	(–0.006) 0	0.01
824.9	148.22	(–0.011) 0	0.01

Time (s)	Temperature (°C)	Drying rate ($\times 10^4$)	Moisture kg/kg db

		kg/kg db	
0.0	100.00	5.39	0.15
38.4	101.59	5.39	129.00
69.9	101.78	5.43	0.11
108.6	102.18	5.19	0.09
159.6	103.82	4.42	0.07
197.7	109.16	3.70	0.05
238.6	117.18	2.95	0.03
278.4	128.71	2.11	0.02
319.3	146.41	1.13	0.01
358.1	160.62	0.28	0.01
400.0	167.81	0.14	0.01
439.8	171.30	(–0.023) 0	0.01
479.5	173.35	0.07	0.01
520.3	174.78	(–0.097) 0	0.01
560.1	175.18	0.04	0.01
600.9	175.79	0.00	0.01
640.6	175.98	(–0.025) 0	0.01

Appendix A6. Coal Model Extracted Data, Kiriyama et. al. [256]

This data has been used in the formation of the single particle coal drying model, found in Chapter 9.

Table A6.1-8 Case A - H– Coal model extracted data

Time *(min)*	Moisture content *(kg/kg total)*	Temperature *(℃)*
3.24	0.59	100.46
3.73	0.58	100.46
5.03	0.56	100.45
6.62	0.53	100.45
8.44	0.50	100.41
10.09	0.47	100.41
12.03	0.44	100.89
13.39	0.42	100.82
15.16	0.39	100.91
16.74	0.36	100.99
18.57	0.34	101.21
20.16	0.32	101.40
21.87	0.30	101.61
23.69	0.28	101.62
25.46	0.26	102.32
27.10	0.25	104.20
28.75	0.24	107.61
30.40	0.23	118.23
32.22	0.23	141.87
33.75	0.22	155.81
35.52	0.22	163.12
37.05	0.22	166.48
38.93	0.22	168.80
40.34	0.22	169.33
42.40	0.22	169.69
43.75	0.22	169.68
45.63	0.22	169.67
47.11	0.22	169.66
48.93	0.22	169.66
50.40	0.22	169.65
52.28	0.22	169.64

Time *(min)*	Moisture content *(kg/kg total)*	Temperature *(℃)*
1.08	0.07	99.72
1.17	0.07	99.74

1.65	0.07	99.84
2.13	0.07	99.96
2.70	0.07	100.07
3.18	0.06	100.06
3.84	0.06	100.05
4.43	0.06	100.38
5.12	0.05	100.93
5.76	0.05	101.14
6.37	0.05	101.32
7.02	0.04	102.03
7.66	0.04	102.74
8.25	0.04	103.42
8.92	0.04	104.93
9.67	0.03	108.50
10.37	0.03	118.83
11.04	0.03	135.32
12.01	0.03	157.14
12.88	0.03	164.38
13.62	0.03	167.57
14.56	0.03	168.88
15.26	0.03	168.87
16.09	0.03	169.09
16.95	0.03	169.19
17.58	0.03	169.34
18.26	0.03	169.23
19.04	0.03	169.06
19.68	0.03	168.91

Time *(min)*	Moisture content *(kg/kg total)*	Temperature *(℃)*
5.05	0.59	100.67
5.43	0.58	100.70
7.00	0.56	100.64
8.80	0.54	100.47
10.45	0.52	100.47
12.32	0.50	100.46
13.67	0.49	100.46
15.47	0.46	100.45
17.04	0.45	100.45
18.99	0.43	100.55
20.26	0.41	100.66
22.29	0.39	100.82
23.78	0.37	100.93
25.51	0.35	100.92
27.08	0.34	101.11
29.03	0.32	101.37

30.53	0.31	101.21
32.17	0.29	101.46
33.67	0.28	101.87
35.84	0.27	102.32
37.19	0.26	102.87
39.21	0.25	103.88
40.64	0.24	105.92
42.66	0.24	111.07
44.08	0.23	119.83
46.10	0.23	132.03
47.45	0.23	137.62
49.32	0.23	142.74
50.67	0.23	145.34
53.22	0.23	147.58
54.19	0.23	147.97
56.51	0.23	148.64
60.40	0.23	148.90
63.55	0.22	148.94
66.69	0.23	149.31

Time *(min)*	Moisture content *(kg/kg total)*	Temperature *(℃)*
1.32	0.07	100.28
1.55	0.07	100.28
2.13	0.07	100.46
2.73	0.07	100.38
3.38	0.07	100.43
4.09	0.06	100.54
4.66	0.06	100.54
5.24	0.06	100.54
5.89	0.06	100.54
6.49	0.05	100.46
6.84	0.05	100.36
7.44	0.05	100.41
8.05	0.05	100.63
8.60	0.05	100.82
9.25	0.04	100.98
9.95	0.04	101.31
10.80	0.04	101.84
11.43	0.04	102.38
12.06	0.04	102.96
12.71	0.03	103.79
13.41	0.03	104.92
14.16	0.03	106.87
14.86	0.03f	111.27
15.56	0.03	119.96

16.19	0.03	130.61
16.84	0.03	139.16
17.52	0.03	143.68
18.30	0.03	147.07
18.95	0.03	148.77
19.77	0.03	149.30
20.30	0.03	149.61
20.90	0.03	149.79
21.65	0.03	149.79
22.36	0.03	149.92

Time *(min)*	Moisture content (kg/kg total)	Temperature (°C)
5.58	0.61	100.32
7.81	0.59	100.24
11.65	0.57	100.23
15.24	0.54	100.22
19.47	0.52	100.21
23.56	0.49	100.20
27.66	0.47	100.19
30.99	0.44	100.19
35.47	0.41	100.28
38.93	0.39	100.44
43.16	0.37	100.63
47.90	0.34	101.02
51.10	0.33	101.34
55.33	0.31	101.73
59.42	0.29	102.05
63.65	0.28	102.78
68.26	0.27	104.40
72.49	0.25	107.34
76.97	0.25	113.34
81.71	0.24	121.76
86.19	0.24	125.60
90.80	0.24	127.12
95.15	0.24	127.79
99.64	0.24	128.33
104.25	0.24	128.39
108.73	0.24	128.43
113.08	0.24	128.62
117.69	0.24	128.61

Time *(min)*	Moisture content (kg/kg total)	Temperature (°C)
1.63	0.07	100.17
2.39	0.07	100.13

2.60	0.07	100.10
3.91	0.07	99.94
4.96	0.07	99.95
5.96	0.06	99.85
7.27	0.06	99.84
7.49	0.06	99.92
8.32	0.06	100.22
9.10	0.06	100.23
10.68	0.05	100.24
11.59	0.05	100.24
12.46	0.05	100.27
13.90	0.05	100.46
15.00	0.05	100.76
15.87	0.04	101.07
17.31	0.04	101.41
18.31	0.04	101.54
19.36	0.04	102.01
20.62	0.04	102.68
21.80	0.03	103.80
23.03	0.03	105.68
24.03	0.03	108.35
25.21	0.03	112.98
26.17	0.03	117.33
27.48	0.03	122.85
28.57	0.03	125.98
29.62	0.03	127.89
30.67	0.03	128.82
31.98	0.03	129.58
33.11	0.03	129.62
34.16	0.03	129.86
35.21	0.03	130.14
36.34	0.03	130.15
37.48	0.03	129.87
38.61	0.03	129.80

Time *(min)*	Moisture content (kg/kg total)	Temperature (°C)
7.53	0.59	100.20
16.19	0.57	100.20
24.53	0.55	100.20
33.19	0.53	100.21
40.89	0.52	100.21
49.87	0.49	100.21
58.20	0.48	100.23
66.86	0.46	100.31
75.84	0.44	100.39

83.22	0.43	100.39
92.20	0.41	100.42
100.85	0.40	100.50
109.19	0.38	100.65
118.49	0.36	100.85
126.19	0.35	101.04
136.13	0.34	101.44
145.10	0.33	101.96
155.04	0.31	102.45
164.02	0.31	103.05
173.96	0.30	103.87
183.57	0.29	104.68
192.55	0.29	105.50
203.13	0.28	106.55
212.10	0.28	107.38
222.04	0.28	108.15
231.34	0.27	108.72
241.59	0.27	109.35
250.25	0.27	109.64
259.86	0.27	109.74
271.08	0.27	109.92
278.77	0.27	109.90
287.75	0.27	109.89

Time *(min)*	Moisture content (kg/kg total)	Temperature (°C)
6.29	0.07	99.80
7.95	0.07	99.80
9.69	0.07	99.79
11.87	0.07	99.79
13.73	0.07	99.79
15.47	0.07	99.79
17.54	0.07	99.83
19.50	0.06	99.87
21.35	0.06	99.90
23.20	0.06	99.94
25.49	0.06	99.95
26.91	0.06	99.95
28.98	0.06	99.95
30.83	0.06	99.95
32.79	0.06	99.97
34.53	0.05	100.09
36.06	0.05	100.19
38.45	0.05	100.19
40.20	0.05	100.22
42.27	0.05	100.35

44.55	0.05	100.51
46.30	0.05	100.66
47.93	0.05	100.79
51.96	0.04	101.26
53.70	0.04	101.55
55.99	0.04	102.03
58.39	0.04	102.51
59.91	0.04	102.79
61.66	0.04	103.12
63.29	0.04	103.48
65.36	0.04	103.97
67.10	0.04	104.44
69.17	0.04	104.98
71.02	0.04	105.37
73.09	0.04	105.83
74.84	0.03	106.23
76.03	0.03	106.50
78.32	0.03	107.02
79.96	0.03	107.45
82.03	0.03	107.97
84.42	0.03	108.49
86.17	0.03	108.84
87.91	0.03	109.11
90.20	0.03	109.35
92.16	0.03	109.50
93.79	0.03	109.60
95.42	0.03	109.69
97.39	0.03	109.79
99.24	0.03	109.85

Appendix A7. References

1. International Energy Agency, *Key World Energy Statstics*. 2013, International Energy Agency.
2. Economic Commission for Europe. Committee on Sustainable Energy *Low-Rank Coal Utilization. Internation Codification System*. 2002, United Nations: New York and Geneva.
3. Zhu, Q., *Update on Lignite Firing*. 2012, IEA Clean Coal Centre.
4. Burnard, K. and S. Bhattacharya, *Power Generation from Coal - Ongoing Developments and Outlooks*. 2011, International Energy Agency.
5. Yu, J., A. Tahmasebi, Y. Han, F. Yin, and X. Li, *A review on water in low rank coals: The existence, interaction with coal structure and effects on coal utilization.* Fuel Processing Technology, 2013. **106**: p. 9-20.
6. Karthikeyan, M., J.V.M. Kuma, C.S. Hoe, and D.L.Y. Ngo, *Factors Affecting Quality of Dried Low-Rank Coals.* Drying Technology, 2007. **25**(10): p. 1601 -1611.
7. Allardice, D.J., L.M. Clemow, G. Favas, W.R. Jackson, M. Marshall, and R. Sakurov, *The characterisation of different forms of water in low rank coals and some hydrothermally dried products.* Fuel, 2003. **82**: p. 661 - 557.
8. Karthikeyan, M., W. Zhonghua, and A.S. Mujumdar, *Low-Rank Coal Drying Technologies—Current Status and New Developments.* Drying Technology, 2009. **27**(3): p. 403 — 415.
9. Mills, S.J., *Global perspective on the use of low quality coals*. 2011, IEA Clean Coal Centre.Fr
10. Bhattacharya, S., K.B. Kabir, and K. Hein, *Dimethyl ether synthesis from Victorian brown coal through gasification – Current status, and research and development needs.* Progress in Energy and Combustion Science
11. Emami Taba, L., M.F. Irfan, W.A.M. Wan Daud, and M.H. Chakrabarti, *The effect of temperature on various parameters in coal, biomass and CO-gasification: A review.* Renewable and Sustainable Energy Reviews 2012. **16**(8): p. 5584-5596.
12. Song, C., A.K. Saini, and Y. Yoneyama, *A new process for catalytic liquefaction of coal using dispersed MoS2 catalyst generated in situ with added H2O.* Fuel, 2000. **79**(3–4): p. 249-261.
13. Thakur, D.S. and M.G. Thomas, *Catalyst deactivation during direct coal liquefaction: a review.* Industrial & Engineering Chemistry Product Research and Development, 1984. **23**(3): p. 349-360.
14. Board, I.C.I.A., *Power generation from coal: measuring and reporting efficiency performance and CO2 emissions*. 2010: OECD/IEA.
15. Campisi, A. and F. Woskoboenko, *Brown Coal R&D Scoping Study*. 2009, HRL.
16. World Coal Association, *Coal Matters 3/ Coal and Electricity Generation*, World Coal Association, Editor. 2012. p. 1-6.
17. Global CCS Institute, *Post Combustion Carbon Capture - Thermodynamic modelling*. 2013, Global CCS Institute.
18. Fei, Y., A.A. Aziz, S. Nasir, W.R. Jackson, M. Marshall, J. Hulston, and A.L. Chaffee, *The spontaneous combustion behaviour of some low rank coals and a range of dried products.* Fuel, 2009. **88**(9): p. 1650-1655.
19. Greensmith, T.J., *Petrology of the Sedimentary Rocks* Vol. 5th edition. 1971: Thomas Murby and Co., London.

20. Allardice, D.J., A.L. Chaffee, R.W. Jackson, and M. Marshall, *Water in Brown Coal and Its Removal*, in *Advances in the Science of Victorian Brown Coal*, C.-Z. Li, Editor. 2004, Elsevier. p. 85 - 133.
21. Hayashi, J.-I. and C.Z. Li, *Structure and Properties of Victorian Brown Coal*, in *Advances in the Science of Victorian Brown Coal*, C.Z. Li, Editor. 2004, Elsevier. p. 11 - 84.
22. Willson, W.G., D. Walsh, and B. Irwinc, *Overview of Low-Rank Coal (LRC) Drying.* International Journal of Coal Preparation and Utilization, 1997. **18**(1): p. 1 - 15.
23. Lett, R.G. and T.C. Ruppel, *Coal, Chemical and Physical Properties*, in *Encyclopedia of Energy*. 2004.
24. Schobert, H.H., *Structural Features of Low-Rank Coals.* Resources, Consevation and Recycling, 1990. **3**: p. 111-123.
25. Meyers, R.A., *Coal Structure*, ed. R.A. Meyers. 1992, Harcourt Brace Javanovich: Academic press.
26. Potter, O.E., C.J. Beeby, W.J.N. Fernando, and P. Ho, *Drying Brown Coal in Steam-Heated, Steam-Fluidized beds.* Drying Technology, 1983. **2**(2): p. 219 - 234.
27. Muhammad Aziz, Y.K., and Atsushi Tsutsumi, *Self-Heat Recuperative Fluidized Bed Drying of Brown Coal.* Chemical Engineering and Processing, 2011.
28. Trommelen, A. and E. Crosby, *Evaporation and drying of drops in superheated vapors.* AIChE Journal 1970. **16**(5): p. 857-867.
29. Messai, S., J. Sghaier, D. Lecomte, and A. Belghith, *Drying Kinetics of a Porous Spherical Particle and the Inversion Temperature.* Drying Technology, 2008. **26**(2): p. 157 - 167.
30. Brockway, D.J., A.L. Ottrey, and R.S. Higgins, *The Science of Victorian Brown Coal* The Science of Victorian Brown Coal Vol. 2. 1991. 129.
31. Charrière, D. and P. Behra, *Water sorption on coals.* Journal of Colloid and Interface Science, 2010. **344**: p. 460-467.
32. Karr, C., *Analytical Methods for Coal and Coal Products*. Vol. 1. 1978, New York: Academic Press.
33. Osman, H., S.V. Jangam, J.D. Lease, and A.S. Mujumdar, *Drying of Low-Rank Coal (LRC)—A Review of Recent Patents and Innovations.* Drying Technology, 2011. **29**(15): p. 1763-1783.
34. Mraw, S.C. and D.F. O'Rourke, *Water in Coal Pores: The Enthalpy of Fusion Reflects Pore Size Distribution.* Journal of Colloid and Interface Science, 1982. **89**(1): p. 268-271.
35. Vorres, K.S., *Effect of Temperature, Sample Size, and Gas Flow Rate on Drying on Beulah-Zap Lignite and Wyodak Subbituminous Coal.* Energy and Fuels, 1994. **8**: p. 320-323.
36. Norinaga, K., H. Kumagai, J.i. Hayashi, and C. T., *Types of Water Associated with Coal*, M. Saki, Editor., Hokkaido National Industrial Research Institute: Japan.
37. Allardice, D.J. and D.G. Evans, *The brown coal/water system. Part 2. Water sorption isotherms on bed moist Yallourn brown coal.* Fuel, 1971. **50**(3): p. 236-253.
38. Allardice, D.J. and D.G. Evans, *The brown-coal/water system: Part 1. The effect of temperature on the evolution of water from brown coal.* Fuel, 1971. **50**(2): p. 201-210.
39. Norinaga, K., H. Kumagai, J.-i. Hayashi, and T. Chiba, *Classification of Water Sorbed in Coal on the Basis of Congelation Characteristics.* Energy and Fuels, 1998. **12**: p. 574 - 579.
40. Fei, Y., A.L. Chaffee, M. Marshall, and W.R. Jackson, *Lignite–water interactions studied by phase transition—differential scanning calorimetry.* Fuel, 2005. **84**: p. 1557.

41. Mahajan, O.P. and P.L. Walker Jr, *Water Adsorption on Coals.* Fuel, 1971. **50**(3): p. 308-317.
42. Švábová, M., Z. Weishauptová, and O. Pribyl, *Water vapour adsorption on coal.* Fuel, 2011. **90**: p. 1892-1899.
43. Ma, S., J.O. Hill, and S. Heng, *DSC determination of coal specific energy.* Thermochemeca Acta, 1991. **190**: p. 291 - 297.
44. Mayoral, M.C., M.T. Izquierdo, M.J. Blesa, J.M. Andres, B. Rubio, and J.L. Miranda, *DSC study of curing in smokeless briquetting.* Thermochimica Acta, 2001. **371**: p. 41-44.
45. Kim, H.-S., Y. Nishiyama, K. Ideta, J. Miyawaki, Y. Matsushita, J.-I. Park, I. Mochida, and S.-H. Yoon, *Analysis of water in Loy Yang brown coal using solid-state 1H NMR.* Journal of Industrial and Engineering Chemistry, 2013. **19**(5): p. 1673-1679.
46. Lynch, L.J. and D.S. Webster, *An n.m.r. study of the water associated with brown coal.* Fuel, 1979. **58**(6): p. 429-432.
47. Ramli, W. and W. Daud, *Fluidized Bed Dryers — Recent Advances.* Advanced Powder Technology, 2008. **19**: p. 403 - 418.
48. Bullinger, C.W., *Apparatus and Method of Enchancing the Quality of High-Moisture Materials and Separating and Concentrating Organic and/or Non-Organic Material Contained Therein*, G.R. Energy, Editor. 2008: US. p. 172.
49. Shelton, W.W., *Method for drying particulate law rank coal in a fluidized bed*, A.R. Company, Editor. 1986: United States.
50. Cha, C.Y., *Inclined Fluidized Bed System for Drying Fine Coal*. 1992, Western Research Institue: US. p. 16.
51. Jeon, D., T. Kang, H. Kim, S. Lee, and S. Kim, *Investigation of drying characteristics of low rank coal of bubbling fluidization through experiment using lab scale.* Science China, 2011. **54**(7): p. 1680-1653.
52. Looi, A.Y., K. Golonka, and M. Rhodes, *Drying kinetics of single porous particles in superheated steam under pressure.* Chemical Engineering Journal, 2002: p. 329–338.
53. Syahrul, S., F. Hamdullahpur, and I. Dincer, *Thermal analysis in fluidized bed drying of moist particles.* Applied Thermal Engineering, 2002. **22**: p. 1763-1775.
54. Kim, H.-S., Y. Matsushita, M. Oomori, T. Harada, J. Miyawaki, S.-H. Yoon, and I. Mochida, *Fluidized bed drying of Loy Yang brown coal with variation of temperature, relative humidity, fluidization velocity and formulation of its drying rate.* Fuel, 2012. **105**: p. 415-424.
55. Wang, W.-C., *Laboratory investigation of drying process of Illinois coals.* Powder Technology, 2012. **225**(0): p. 72-85.
56. Rudisuli, M., T.J. Schildhauer, S.M.A. Biollaz, and J.R. van Ommen, *Scale-up of bubbling fluidized bed reactors – A review.* Powder Technology, 2011.
57. Potter, O.E. and C. Beeby, *Scale up of Steam Drying.* Drying Technology: An International Journal, 1994. **12**(1-2): p. 179-215.
58. Dong, N.S., *Utilisation of Low Rank Coals*. 2011, IEA Clean Coal Centre.
59. Stokie, D., J. Yu, A. Auxilio, and S. Bhattacharya. *Coal Drying and Dewatering for power generation – Current Status, Research and Development Needs, International Conference on Coal Science and Technology*. in *International Conference on Coal Science & Technology* 2011. Oviedo, Spain
60. Klutz, H.-J., C. Moser, and N. von Bargen, *The RWE Power WTA Process (Fluidized Bed Drying) as a Key for Higher Efficiency.* Mining and Geoengineering 2011. **35**(3).

61. Klutz, H.-J., C. Moser, and D. Block, *Development status of WTA fluidized-bed drying for lignite at RWE Power AG.* Power plant technology - Secure and sustainable energy supply, 2010. **2**.
62. Hoehne, O., S. Lechner, M. Schreiber, and H.J. Krautz, *Drying of Lignite in a Pressurized Steam Fluidized Bed—Theory and Experiments.* Drying Technology, 2010. **28**(1): p. 5-19.
63. Brandenburgische Technische Universität Cottbus, L.K., *Pressurized Steam Fluidized Bed Drying of Lignite*.
64. Olaf Hoehne, S.L., Matthias Schreiber, and Hans Joachim Krautz, *Drying of Lignite in a Pressurized Steam Fluidized Bed—Theory and Experiments.* Drying Technology, 2009. **28**(1): p. 5 - 19.
65. Tahmasebi, A., J. Yu, and S. Bhattacharya, *Chemical Structure Changes Accompanying Fluidized-Bed Drying of Victorian Brown Coals in Superheated Steam, Nitrogen, and Hot Air.* Energy and Fuels, 2012.
66. Ness, M. and C. Bullinger, *Pre-Drying the Lignite to GRE's Coal Creek Station*. 2005.
67. Chen, Z., W. Wu, and P.K. Agarwal, *Steam drying of coal. Part 1. Modeling the behavior of a single particle.* Fuel, 2000. **79**: p. 961–973.
68. H. Osman, S.V.J., J. D. Lease and Arun S. Mujumdar, *Drying of low-rank coal (LRC) – A review of recent patents and innovations*. 2011, M3TC: Singapore.
69. *Superheated Steam Drying*, in *Advanced Drying Technologies*. 2009, Taylor and Francis Group.
70. Jangam, S.V., M. Karthikeyan, and A.S. Mujumdar, *A Critical Assessment of Industrial Coal Drying Technologies: Role of Energy, Emissions, Risk and Sustainability.* Drying Technology, 2011. **29**(4): p. 395-407.
71. *WTA Technology - A modern process for treating and drying lignite*, R. Power, Editor. 2009: Essen Cologne.
72. Porsche, T., L. Thannhauser, O. Hohne, B. Jentzschm, T. Rauerm, and J. Martin, *Pressurised Fluidized Bed Drying (PFBD) of Lignite; Progress of the PFBD technology*, Vattenfall, Editor.
73. Ross, D., S. Doguparthy, D. Huynh, and M. McIntosh, *Pressurised flash drying of Yallourn lignite.* Fuel, 2005. **84**: p. 47–52.
74. McIntosh, M.J., *Mathematical model of drying in a brown coal mill system. 2. Testing of model.* Fuel, 1976. **55**: p. 53-58.
75. McIntosh, M.J., *Mathematical model of drying in a brown coal mill system. 1. Formation of Model.* Fuel, 1976. **55**: p. 47 - 52.
76. D. Ross, S.D., D. Huynh, and M. McIntosh, *Pressurized Flash Drying of Yallourn Lignite.* Fuel, 2005. **84**(1): p. 47-52.
77. Doguparthy, S., D. Huynh, D. Ross, and H. Ellis, *High Pressure and High temperature Flue Gas Coal Drying*. 2001.
78. Godfrey, B., *Recent Developments in Innovative Drying Technologies*, in *Low Rank Coal International Symposium*. 2010: Melbourne.
79. Tanselle, J., *Investor Presentation*. 2009, White Energy Company Limited.
80. Sarunac, N., M. Ness, and M. Coughlin. *Beneficiation of High-Moisture Coals for Improved Performance and Reduced Emissions*. in *37th International Technical Conference on Clean Coal and Fuel Systems*. 2012. Clearwater.
81. Bergins, C., J. Hulston, K. Strauss, and A.L. Chaffee, *Mechanical/thermal dewatering of lignite. Part 3: Physical properties and pore structure of MTE product coals.* Fuel, 2007. **86**: p. 3-16.
82. McIntosh, M.J. and D.Q. Huynh, *Coal dewatering system and method*. 2008.

83. Wibberley, L., A. Cottrell, D. Palfreyman, P. Scaife, and P. Brown, *Techo-Economic Assessment of Power Generation Options for Australia*. 2006, Cooperative Research Centre for Coal in Sustainable Development. p. 247.
84. Katalambula, H. and R. Gupta, *Low-Grade Coals: A Review of Some Prospective Upgrading Technologies.* Energy and Fuels, 2009. **23**: p. 3392 - 3405.
85. Butler, C.J., A.M. Green, and A.L. Chaffee, *MTE water remediation using Loy Yang brown coal as a filter bed adsorbent.* Fuel, 2008. **87**: p. 894-904.
86. Artanto, Y., E. McDonnell, T.V. Verheyen, S. Adeloju, and A.L. Chaffee, *The remediation of MTE water by combined anaerobic digestion and chemical treatment.* Fuel, 2009. **88**: p. 1786-1792.
87. Clayton, S.A., O.N. Scholes, A.F.A. Hoadley, R.A. Wheeler, M.J. McIntosh, and D.Q. Huynh, *Dewatering of Biomaterials by Mechanical Thermal Expression.* Drying Technology: An International Journal, 2006. **24**(7): p. 819-834.
88. Clayton, S.A., O.N. Scholes, A.F.A. Hoadley, R.A. Wheeler, M.J. McIntosh, and D.Q. Huynh, *Dewatering of Biomaterials by Mechanical Thermal Expression.* Drying Technology, 2006. **24**(7): p. 819-834.
89. Sherman, M.I., *Hot Water Drying of Low Rank Coal*. 1983, Kamyr Inc: United States Patent.
90. Lee, S., *Technology for Low Rank Coal Utilization in Korea*, in *4th Low Rank Coal Workshop*. 2012.
91. Favas, G. and W.R. Jackson, *Hydrothermal Dewatering of lower rank coals 1. Effects of process conditions on the properties of dried product.* Fuel, 2003. **82**: p. 53-57.
92. Allardice, D.J., *The Water in Brown Coal*, in *The Science of Victorian Brown Coal*. 1991, Butterworth-Heinemann: Oxford. p. 102-150.
93. Favas, G., W.R. Jackson, and M. Marshall, *Hydrothermal dewatering of lower rank coals. 3. High-concentration slurries from hydrothermally treated lower rank coals.* Fuel, 2003. **82**: p. 71-79.
94. Favas, G. and W.R. Jackson, *Hydrothermal dewatering of lower rank coals. 2. Effects of coal characteristics for a range of Australian and international coals.* Fuel, 2003. **82**: p. 59-69.
95. Resources, I.E. *Pilot Plant*. 2011 [cited 2013 28/05].
96. Ignite Energy Resources. *The Catalytic Hydrothermal Reactor Technology, Cat-HTR.* 2013; Available from: http://igniteer.com/technology.html.
97. Dimitris, M.-K., K. Magdalini, and S.M. Arun, *Rotary Drying*, in *Handbook of Industrial Drying, Third Edition*. 2006, CRC Press.
98. Butler, T.G., *Method and apparatus of rotatable drum dryer with flights releasably secured in different orientations* 1996, Gencor Industries: US.
99. Yamoto, Y., *Aeration-Type Rotary Dryer*. 1999, Yamoto Sanko: US.
100. Kudra, T. and A.S. Mujumdar, *Special drying technologies*, in *Advanced Drying Technologies*. 2009.
101. Jangam, S.V. and A.S. Mujumdar, *Coal Dehydration - A compilation of relevant publications and technical reports*, S.V.J.a.A.S. Mujumdar, Editor. 2010.
102. Jing, C., *Best Practices and Perspectives of Energy Efficiency Technologies for Utilization of Low Rank Coal within APEC Economies*. 2012, APEC Energy Working Group: Beijing, P. R. China.
103. ZEMAG. *Tubular Dryers*. 2013; Available from: http://www.mindac.com/en/display.aspx?id=1.
104. Kinoshita, S., S. Yamamoto, T. Deguchi, and T. Shigehisa, *Demonstration of Upgraded Brown Coal (UBC) Process by 600 tonnes/day Plant.* Kobelco Technology Review, 2010. **29**.

105. Ohm, T.-I., J.-S. Chae, J.-H. Lim, and S.-H. Moon, *Evaluation of a hot oil immersion drying method for the upgrading of crushed low-rank coal.* Journal of Mechanical Science and Technology, 2012. **26**(4): p. 1299-1303.
106. Fujitsuka, H., R. Ashida, and K. Miura, *Upgrading and dewatering of low rank coals through solvent treatment at around 350C and low temperature oxygen reactivity of the treated coals.* Fuel, 2013.
107. Miura, K., K. Mae, R. Ashida, T. Tamura, and T. Ihara, *Dewatering of coal through solvent extraction.* Fuel, 2002. **81**: p. 1417-1422.
108. Kanda, H., H. Shirai, and Y. Hiei. *Dewatering process for high moisture coal using liquid DME as extracting solvent*. in *AIChE Annual Meeting*. 2003. San Francisco.
109. Kanda, H. and H. Makino, *Energy-efficient coal dewatering using liquefied dimethyl ether.* Fuel, 2010. **89**: p. 2104-2109.
110. Graham, J., *Microwaves for Coal Quality Improvement: The Drycol Project*, in *SACPS/International Pittsbrugh Coal Conference*. 2007: Johannesburg, South Africa.
111. Tahmasebi, A., J. Yu, Y. Han, H. Zhao, and S. Bhattacharya, *A kinetic study of microwave and fluidized-bed drying of a Chinese lignite.* Chemical Engineering Research and Design, 2013.
112. Gao, F., *Comparison of Microwave Drying and Convential Drying of Coal*, in *Department of Mining Engineering*. 2010, Queen's University: Kingston Ontario.
113. Tahmasebi, A., J. Yu, X. Li, and C. Meesri, *Experimental study on microwave drying of Chinese and Indonesian low-rank coals.* Fuel Processing Technology, 2011. **92**: p. 1821 - 1829.
114. Learey, T.R., *Microwave Drying of Coal*. 2010, Industrial Microwave Sstems: US. p. 10.
115. Latchum, J.W., *Apparatus and Method for Drying Solid Materials*. 1986, Phillips Petroleum Company: US. p. 8.
116. Smith, F.J., *Microwave Fluidized Bed Dryer*. 1968, Crypdry Coporation: US. p. 6.
117. Doelting, M.K., *Microwave Assisted Fluidized Bed Processor*. 1990, Glatt GmnH: US. p. 15.
118. CoalTek. *CoalTek - Overview*. 2013; Available from: http://coaltek.com/clean-coal-overview/.
119. Johns, R.B., A.L. Chaffee, and K.F. Harvey, *The Conversion of Brown Coal to Dense, Dry, Hard Materials.* Fuel Processing Technology, 1989. **21**: p. 209-221.
120. Helmer, W. and F. Hasheminejad, *Secondary Coal Recovery from Slurry Ponds Utilizing Solar Drying.* Powder Technology, 1984. **40**: p. 247-255.
121. Pandolfo, A.G. and R.B. Johns, *Physical and chemical charateristics of densified low rank coals.* Fuel, 1992. **72**(6): p. 7550761.
122. Moore, A., *Coldry Technology in the Latrobe Valley*. 2010.
123. Limited, E.C.T. *Coldry Overview*. 2012 [cited 2012 09/01/2012]; An overview of the Coldry process]. Available from: http://www.ectltd.com.au/coldry/the-coldry-process/.
124. Environmental Clean Technologies Limited *Tincom re-engagement*. 2011 [cited 2012 09/01/2012]; Available from: http://media.abnnewswire.net/media/en/docs/ASX-ESI-362658.pdf.
125. Skripchenko, G.B. and M.Y. Shpirt, *Explosion Free Flash Drying of Coal in a Vortex Flow of Heat Transfer Gas.* Solid Fuel Chemistry, 2011. **45**(2): p. 14-22.
126. LFP, *Upgrading Low Value Coals with LFP systems*. 2012.
127. Schwartze, J.P. and S. Bröcker, *A theoretical explanation for the inversion temperature.* Chemical Engineering Journal, 2002. **86**(1–2): p. 61-67.

128. Kucuk, H., A. Midilli, A. Kilic, and I. Dincer, *A Review on Thin-Layer Drying-Curve Equations.* Drying Technology 2014. **32**(7): p. 757-773.
129. Yucel, U., H. Alpas, and A. Bayindirli, *Evaluation of high pressure pretreatment for enhancing the drying rates of carrot, apple, and green bean.* Journal of Food Engineering, 2010. **98**(2): p. 266-272.
130. Srinivasakannan, C. and N. Balasubramanian, *An Analysis on Modeling of Fluidized Bed Drying of Granular Material.* Advanced Powder Technology, 2008. **19**: p. 73-82.
131. Erbay, Z. and F. Icier, *A review of thin layer drying of foods: theory, modeling, and experimental results.* Critical Reviews in Food Science and Nutrition 2010. **50**(5): p. 441-464.
132. Midilli, A., H. Kucuk, and Z. Yapar, *A New Model for Single-Layer Drying.* Drying Technology: An International Journal, 2002. **20**(7): p. 1503-1513.
133. Agarwal, P.K., W.E. Genetti, Y.Y. Lee, and S.N. Prasad, *Model for drying during fluidized-bed combustion of wet low-rank coals.* Fuel, 1984. **63**.
134. Komatina, M., V. Manovic, and A. Saljnikov, *A Model of Coal Particle Drying in Fluidized Bed Combustion Reactor.* Energy Sources, Part A: Recovery, Utilization, and Environmental Effects, 2007. **29**(3): p. 239-250.
135. Kovenskii, V.I., V.A. Borodulya, Y.S. Teplitskii, G.I. Pal'chenok, and D.S. Slizhuk, *Modeling of superheated-steam drying of biofuel in a fluidized bed.* Journal of Engineering Physics and Thermophysics, 2010. **83**(4): p. 764-769.
136. Olufemi, B.A. and I.F. Udefiagbon, *Modelling the Drying of Porous Coal Particles in Superheated Steam.* Chemical & Biochemical Engineering Quarterly, 2010. **24**(1): p. 29-34.
137. Fyhr, C. and I.C. Kemp, *Mathematical modelling of batch and continuous wel-mixed fluidised bed dryers.* Chemical Engineering and Processing, 1999. **38**: p. 11-18.
138. Gu, F., *Coal Drying in a Bubbling Fluidized Bed*, in *Mechanical Engineering and Mechanics*. 2004, Lehigh University.
139. Levy, E.K., N. Sarunac, H. Bilirgen, and H. Caram, *Use of Coal Drying to Reduce Water Consumed in Pulverized Coal Power Plants*. 2006, Energy Research Center Lehigh University: United States Department of Energy.
140. Levy, E.K., H.S. Caram, Z. Yao, Z. Wei, and N. Sarunac. *Kinetics of coal drying in bubbling fluidised beds* in *Proceedings Fifth World Congress on Particle Technology*. 2006. Orlando, Florida.
141. Wang, Q., Z.-y. Gu, J.-r. Bai, J. Liu, and H.-p. Liu, *Comparative Study of the Characteristics of Oil Shale with Hot Air Drying and Microwave Drying.* Energy Procedia, 2012. **17, Part A**(0): p. 884-891.
142. Chen, Z., P.K. Agarwal, and J.B. Agnew, *Steam drying of coal. Part 2. Modeling the operation fluidized bed drying unit.* Fuel, 2001. **80**: p. 209-223.
143. Tahmasebi, A., J. Yu, Y. Han, H. Zhao, and S. Bhattacharya, *Thermogravimetric study and modeling for the drying of a Chinese lignite.* Asia-Pacific Journal of Chemical Engineering, 2013.
144. Blake, J.H., *Process and system for drying coal in a fluidized bed by partial combustion*. 1980, FMC Corporation: US. p. 9.
145. Ottoson, J.D., *Method for stablizing particulate low rank coal in a fluidized bed*. 1985, Atlantic Richfield Company: US. p. 5.
146. Ladt, M.A., *Method of Drying Fine Coal Particles*. 1984, Lecorp: US. p. 6.
147. Dunlop, D.D., *Process for Drying Coal*. 2009, EMI Newcoal, Inc: US. p. 12.
148. Stone, L.H., *Circular Vibratory Fluid Bed Dryer*. 2004, Kason Coporation: US. p. 6.
149. Pikon, J. and A.S. Mujumdar, *Drying of Coal*, in *Handbook of Industrial Drying*. 2006, Taylor & Francis Group, LLC.

150. Heinrich, S., M. Ihlow, M. Henneberg, M. Peglow, E. Machnow, and L. Mörl, *Studies of Steam Drying in a Fluidized Bed.* Drying Technology, 2002. **20**(1): p. 175-194.
151. Hamilton, C.J., *Steam Fluidised Bed Drying of Coal*, in *International Coal Engineering Conference*. 1990: Sydney.
152. Bergins, C., *Kinetics and mechanism during mechanical/thermal dewatering of lignite*. Fuel, 2003. **82**: p. 355 - 364.
153. *Mechanical Thermal Expression*, in *Advanced Drying Technologies*. 2009.
154. Jentzsch, B., O. Höhne, and T. Porsche, *Experiences with drying of lignite in a pressurized steam fluidized bed pilot plant*, in *Oxyfuel Combustion Conference*.
155. Systems, B.P., *Pressurized Steam Fluidized Bed Drying*, B.B.S. GmbH, Editor.
156. *DryFining Fuel Enchancement Process*, G.R. Energy, Editor. 2013.
157. Sarunac, N., M. Ness, and C. Bullinger, *One Year of Operating Experience with a Prototype Fluidized Bed Coal Dryer at Coal Creek Generating Station*, in *Third International Conference on Clean Coal Technologies*. 2007: Cagliari, Sardinia, Italy.
158. Bullinger, C., M. Ness, and N. Sarunac. *Coal Creek Prototype Fluidized Bed Coal Dryer: Performance Improvement, Emissions Reduction, and Operating Experience Coal Experience*. in *31st International Technical Conference on Coal Utilization and Fuel Systems,*. 2006. Clearwater FL.
159. Giles, A., *Drying Out*, E.C.T. Ltd, Editor. 2012. p. 6.
160. Flannery, B. and I. Maras, *White Energy Company - Company Presentation*. 2013.
161. Coal, W. *History of the White Coal Technology*. 2013 [cited 2013 29/05].
162. Flannery, B. and I. Maras, *White Energy Company - Company Presentation*. 2012.
163. Atkinson, J., *White Energy's Coal Upgrading Plant in Indonesia 77% Complete*, W.E.C. Limited, Editor. 2008.
164. Exergen. *Projects*. 2013 [cited 2013 28/05].
165. Kraemer, I. *Exergen's Continuous HydroThermal Dewatering (CHTD) of Brown Coal*. in *Sustainable Development Conference SD07*. 2007. Cairns.
166. Exergen. *Technology*. 2013 [cited 28/05 2013].
167. Resources, I.E. *Cat-HTR Products*. 2011 [cited 2013 28/05].
168. Hancock, L., *New life for K-Fuel*, in *The Gillette News Record*. 2011.
169. Burton, T., *NYSE Arca: EEE*, in *Coal Upgrading and Conversion Conference*. 2011, EverGreen Energy Inc: Sheraton Towers, Singapore.
170. Bailey, J., *Step forward for briquette plant*, in *Mining NZ*. 2013.
171. *Upgrading the Future - UBC Process*, Kobelco, Editor. 2013.
172. Developments, L.T.L., *La Trobe Lignite Developments*. 2008.
173. Pacific Edge Holdings. *About Us*. 2013; Available from: http://www.latrobelignite.com.au/pages/view/about_us_1.
174. Agarwal, P.K., W.E. Genetti, and Y.Y. Lee, *Coupled Drying and Devolatilization of Wet Coal in Fluidized Beds.* Chemical Engineering Science, 1986. **41**(9): p. 2373-2383.
175. Garnavi, L., N. Kasiri, and S.H. Hashemabadi, *Mathematical modeling of a continuous fluidized bed dryer.* International Journal in Heat and Mass Transfer, 2006. **33**: p. 666-675.
176. Woo, M.W., D. Stokie, W.L. Choo, and S. Bhattacharya, *Master curve behaviour in superheated steam drying of small porous particles.* Applied Thermal Engineering, 2013. **52**: p. 460-467.
177. Zhang, K. and C. You, *Experimental and Numerical Investigation of Lignite Particle Drying in a Fixed Bed.* Energy and Fuels, 2011.

178. Kittiworrawatt, S. and S. Devahastin, *Improvement of a mathematical model for low-pressure superheated steam drying of a biomaterial.* Chemical Engineering Science, 2009. **64**: p. 2644 0 2650.
179. Hager, J., M. Hermansson, and R. Wimmerstedt, *Modelling steam drying of a single porous ceramic sphere: experiments and simulations.* Chemical Engineering Science, 1997. **52**(8): p. 1253-1264.
180. Hyun-Seok Kim, Y.M., Motohira Oomori, Tatsuro Harada, Jin Miyawaki, Seong-Ho Yoon, Isao Mochida, *Fluidized bed drying of Loy Yang brown coal with variation of temperature, relative humidity, fluidization velocity and formulation of its drying rate.* Fuel, 2012.
181. *Electricity generation, consumption and greenhouse gas emissions in Victoria*. 2006, The Office of the Commissioner for Environmental Sustainability: Melbourne.
182. Soponronnarit, S., S. Prachayawarakorn, W. Rordprapat, A. Nathakaranakula, and W. Tia *A Superheated-Steam Fluidized-Bed Dryer for Parboiled Rice: Testing of a Pilot-Scale and Mathematical Model Development*. Drying Technology, 2006. **24**, 1457-1467.
183. Singh, P., N. Choudhury, A. Sarkar, P. Sarkar, and T. Das, *Reactivity assessment of non-coking coal by oxidative thermogravimetric studies.* Indian Journal of Chemical Technology 2005. **12**(1): p. 30-34.
184. Karthikeyan, M., *Minimization of Moisture Readsorption in Dried Coal Samples.* Drying Technology, 2008. **26**(7): p. 948 - 955.
185. Zhang, D.-k., T.F. Wall, D.J. Harris, I.W. Smith, J. Chen, and B.R. Stanmore, *Experimental studies of ignition behaviour and combustion reactivity of pulverized fuel particles.* Fuel, 1992. **71**(11): p. 1239-1246.
186. Chao, J., H. Yang, Y. Chen, J. Luv, H. Zhang, and Q. Liu, *The Investigation of the Coal Ignition Temperature in Oxygen-Enriched Atmosphere by TGA.* Cleaner Combustion and Sustainable World (Journal), 2013: p. 589-593.
187. Crawford, R.J., D.W. Guy, and D.E. Mainwaring, *The influence of coal rank and mineral matter content on contact angle hysteresis.* Fuel, 1994. **73**(5): p. 742-746.
188. Tahmasebi, A., J. Yu, Y. Han, F. Yin, S. Bhattacharya, and D. Stokie, *Study of Chemical Structure Changes of Chinese Lignite upon Drying in Superheated Steam, Microwave, and Hot Air.* Energy & Fuels, 2012. **26**(6): p. 3651-3660.
189. Tahmasebi, A., J. Yu, Y. Han, and X. Li, *A study of chemical structure changes of Chinese lignite during fluidized-bed drying in nitrogen and air.* Fuel Processing Technology, 2012. **101**: p. 85-93.
190. Kirtania, K., J. Tanner, K.B. Kabir, S. Rajendran, and S. Bhattacharya, *< i> In situ</i> synchrotron IR study relating temperature and heating rate to surface functional group changes in biomass.* Bioresource Technology 2014. **151**: p. 36-42.
191. Huber, U., *A Generalization of the Dubinin-Radushkevich Equation for the Filling of Heterogeneous Micropore Systems in Strongly Activated Carbons.* Journal of Colloid and Interface Science, 1978. **67**(2): p. 195-203.
192. Sakurovs, R., S. Day, S. Weir, and G. Duffy, *Application of a Modified Dubinin-Radushkevich Equation to Adsorption of Gases by Coals under Supercritical Conditions.* Energy and Fuels, 2007. **21**: p. 992-997.
193. McEnaney, B., *Estimation of the Dimensions of the Micropores in Active Carbons Using the Dubinin-Radushkevich Equation.* Carbon, 1987. **25**(1): p. 69-75.
194. Ry, Y.-C., T.-S. Jiang, and C.Y. Wen, *Particle Attrition Phenomena in a Fluidized Bed.* Powder Technology, 1987. **49**: p. 193-206.

195. D.J. Allardice, L.M.C., G. Favas, W.R. Jackson, M. Marshall, and R. Sakurov, *The characterisation of different forms of water in low rank coals and some hydrothermally dried products.* Fuel, 2003. **82**: p. 661 - 557.
196. David J. Allardice, A.L.C., W. Roy Jackson, and Marc Marshall, *Water in Brown Coal and Its Removal*, in *Advances in the Science of Victorian Brown Coal*, C.-Z. Li, Editor. 2004, Elsevier. p. 85 - 133.
197. D. J. Allardice, a.D.G.E., *The brown-coal/water system: Part 1. The effect of temperature on the evolution of water from brown coal.*
198. Martina Švábová , Z.W., and Oldrich Pribyl, *Water vapour adsorption on coal.* Fuel, 2011. **90**: p. 1892-1899.
199. K. Norinaga, H.K., J.i. Hayashi, and T. Chiba, *Types of Water Associated with Coal*, M. saki, Editor., Hokkaido National Industrial Research Institute: Japan.
200. Jun-ichiro Hayashi, K.N., Norihide Kudo, and Tadatoshi Chiba, *Estimation of Size and Shape of Pores in Moist Coal Utilizing Sorbed Water as a Molecular Probe.* Energy & Fuels, 2001. **15**: p. 903-909.
201. Jun-ichiro Hayashi, a.C.-Z.L., *Structure and Properties of Victorian Brown Coal*, in *Advances in the Science of Victorian Brown Coal*, C.-Z. Li, Editor. 2004, Elsevier. p. 11 - 84.
202. Jianglong Yu, A.T., Yanna Han, Fengkui Yin, and Xianchun Li, *A review on water in low rank coals: The existence, interaction with coal structure and effects on coal utilization.* Fuel Processing Technology, 2012.
203. Koyo Norinaga, H.K., Jun-ichiro Hayashi, and Tadatoshi Chiba, *Classification of Water Sorbed in Coal on the Basis of Congelation Characteristics.* Energy & Fuels, 1998. **12**: p. 574 - 579.
204. Yi Fei, A.L.C., Marc Marshall, and W. Roy Jackson, *Lignite–water interactions studied by phase transition—differential scanning calorimetry.* Fuel, 2005. **84**: p. 1557.
205. Tahmasebi, A., J. Yu, H. Su, Y. Han, J. Lucas, H. Zheng, and T. Wall, *A differential scanning calorimetric (DSC) study on the characteristics and behavior of water in low-rank coals.* Fuel, (0).
206. Homshaw, L.G., *High resolution heat flow DSC: Application to study of phase transitions, and pore size distribution in saturated porous materials* Journal of Thermal Analysis, 1980. **19**: p. 215 - 234.
207. S. Ma, J.O.H., and S. Heng, *DSC determination of coal specific energy.* Thermochemeca Acta, 1991. **190**: p. 291 - 297.
208. Stephen C. Mraw, a.D.F.O.R., *Water in Coal Pores: The Enthalpy of Fusion Reflects Pore Size Distribution.* Journal of Colloid and Interface Science, 1982. **89**(1): p. 268-271.
209. Stokie, D., M.W. Woo, and S. Bhattacharya, *Comparison of Superheated Steam and Air Fluidized-Bed Drying Characteristics of Victorian Brown Coals.* Energy & Fuels, 2013. **27**(11): p. 6598-6606.
210. Stokie, D., S. Bhattacharya, and J. Tanner. *Physical and Chemical Properties of Steam Fluidized Bed Dried Coal*. in *The 38th International Technical Conference on Clean Coal & Fuel Systems* 2013. Clearwater, Florida, USA.
211. Yang, D., Z. Wang, X. Huang, Z. Xiao, and X. Liu, *Numerical Simulation on Superheated Steam Fluidized Bed Drying: I. Model Construction.* Drying Technology, 2011. **29**(11): p. 1325-1331.
212. Shi, Y., Z. Xiao, Z. Wang, X. Liu, and D. Yang, *Numerical Simulation on Superheated Steam Fluidized Bed Drying: II. Experiments and Numerical Simulation.* Drying Technology, 2011. **29**(11): p. 1332-1342.

213. Pata, J., M. Carsky, M. Hartman, and V. Vesely, *Minimum Fluidization Velocities of Wet Coal Particles.* American Chemical Society, 1988.
214. Jiliang, M., C. Xiaoping, and L. Daoyin, *Minimum fluidization velocity of particles with wide size distribution at high temperatures.* Powder Technology, 2013. **235**: p. 271-278.
215. Evans, D.G., *The brown-coal/water system: Part 4. Shrinkage on drying*. Fuel, 1973. **52**(3): p. 186-190.
216. Murray, J.B. and D.G. Evans, *The brown-coal/water system: Part 3. Thermal dewatering of brown coal.* Fuel, 1972. **51**(4): p. 290-296.
217. Liu, X., B. Li, and K. Miura, *Analysis of pyrolysis and gasification reactions of hydrothermally and supercritically upgraded low-rank coal by using a new distributed activation energy model.* Fuel Processing Technology, 2001. **69**(1): p. 1-12.
218. Perry G, J., J. Allardice D, and T. Kiss L, *The Chemical Characteristics of Victorian Brown Coal*, in *The Chemistry of Low-Rank Coals*. 1984, American Chemical Society. p. 3-14.
219. Ibarra, J.V., E. Munoz, and R. Moliner, *FTIR study of the evolution of coal structure during the coalification process.* Organic Geochemistry, 1996. **24**(6): p. 725-735.
220. Fagerna, L., V. Arpiainen, and E. Kuoppala, *Organic compounds released in fluidized-bed drying of peat, bark and lignite.* Fuel Processing Technology, 1991. **29**: p. 107-118.
221. Buckley, A.N. and R.N. Lamb, *Surface chemical analysis in coal preparation research: complementary information from XPS and ToF-SIMS.* International Journal of Coal Geology, 1996. **32**: p. 87-106.
222. Yurum, Y. and N. Altuntas, *Air oxidation of Beypazari lignite at 50C, 100C and 150C.* Fuel, 1998. **77**(15): p. 1808-1814.
223. Ma, S., J.O. HIll, and S. Heng, *A Thermal Analysis Study of the Pyrolysis of Victorian Brown Coal.* Journal of Thermal Analysis, 1989. **35**: p. 977 - 988.
224. Gómez-de la Cruz, F.J., F. Cruz-Peragón, P.J. Casanova-Peláez, and J.M. Palomar-Carnicero, *A vital stage in the large-scale production of biofuels from spent coffee grounds: The drying kinetics.* Fuel Processing Technology 2015. **130**(0): p. 188-196.
225. Miura, K., K. Mae, W. Li, T. Kusakawa, F. Morozumi, and A. Kumano, *Estimation of Hydrogen Bond Distribution in Coal through the Analysis of OH Stretching Bands in Diffuse Reflectance Infrared Spectrum Measured by in-Situ Technique.* Energy & Fuels, 2001. **15**(3): p. 599-610.
226. Liu, X., T. Hirajima, M. Nonaka, A.T. Mursito, and K. Sasaki, *Use of FT-IR Combined with Forms of Water to Study of the Changes in Hydrogen Bonds during Low-Temperature Heating of Lignite.* Drying Technology, 2015: p. null-null.
227. Baxter, L.L., T.H. Fletcher, and D.K. Ottesen, *Spectral emittance measurements of coal particles.* Energy & Fuels, 1988. **2**(4): p. 423-430.
228. Silverstein, R.M., F.X. Webster, and D. Kiemle, *Spectrometric Identification of Organic Compounds*. Vol. 7th Edition. 2005.
229. Coates, J., *Interpretation of infrared spectra, a practical approach.* Encyclopedia of analytical chemistry, 2000.
230. *Appendix C: Contact Angle Goniometry*, in *Surface Design: Applications in Bioscience and Nanotechnology*. 2009, Wiley-VCH Verlag GmbH & Co. KGaA. p. 471-473.
231. Shafrin Elaine, G. and A. Zisman William, *Upper Limits to the Contact Angles of Liquids on Solids*, in *Contact Angle, Wettability, and Adhesion*. 1964, AMERICAN CHEMICAL SOCIETY. p. 145-157.

232. Keller Jr, D.V., *The contact angle of water on coal.* Colloids and Surfaces, 1987. **22**(1): p. 21-35.
233. Gosiewska, A., J. Drelich, J.S. Laskowski, and M. Pawlik, *Mineral Matter Distribution on Coal Surface and Its Effect on Coal Wettability.* Journal of Colloid and Interface Science, 2002. **247**(1): p. 107-116.
234. He, Y.B., *Contact Angle Measurments on Fine Coal Particles*, in *Department of Mining and Mineral Process Engineering*. 1989, The University of Brithish Columbia.
235. Androutsopoulos, G.P. and T.J. Linardos, *Effects of Drying upon Lignite Macro-Pore Structure.* Powder Technology, 1986. **47**(9-15).
236. Hayashi, J.-i., K. Norinaga, N. Kudo, and T. Chiba, *Estimation of Size and Shape of Pores in Moist Coal Utilizing Sorbed Water as a Molecular Probe.* Energy and Fuels, 2001. **15**: p. 903-909.
237. Linge, H.G., *The Surface Area of Coal Particles.* Fuel, 1989. **68**(111 -113).
238. Marsh, H., *Adsorption methods to study microporosity in coals and carbons—a critique.* Carbon, 1987. **25**(1): p. 49-58.
239. Gil, A. and P. Grange, *Application of the Dubinin-Radushkevich and Dubinin-Astakhov equations in the charaterization of microporous solids.* Collids and Surfaces A : Physicochemical and Engineering Aspects, 1996. **113**: p. 39-50.
240. Zhang, H., K. Cen, J. Yan, and M. Ni, *The fragmentation of coal particles during the coal combustion in a fluidized bed.* Fuel, 2002. **81**: p. 1835-1840.
241. Lin, L., J.T. Sears, and C.Y. Wen, *Elutriation and attrition of char form a large fluidized bed.* Powder Technology, 1980. **27**(1): p. 105-115.
242. Colakyan, M. and O. Levenspiel, *Elutriation from fluidized beds.* Powder Technology, 1984. **38**(3): p. 223-232.
243. Brookes, K. and D. Glasser, *A Simplified Model of Spontaneous Combustion in Coal Stockpiles.* Fuel, 1986. **65**: p. 1035-1041.
244. Salantino, P. and L. Massimilla, *A descriptive Model of Carbon attrition in the Fluidized Combustion of Coal Char.* Chemical Engineering Science, 1985. **40**(10): p. 1905-1916.
245. Senneca, O., M. Urciuolo, R. Chirone, and D. Cumbo, *An experimental study of fragmentation of coals during fast pyrolysis at high temperature and pressure.* Fuel, 2011. **90**: p. 2931-2938.
246. Vleeskens, J.M. and M. Roos, *Attrition of chars in fluidized bed combustion.* Fuel, 1989. **68**: p. 825-828.
247. Ammendola, P. and F. Scala, *Attrition of lignite char during fluidized bed gasification.* Experimental Thermal and Fluid Science, 2012. **43**: p. 9-12.
248. Sundback, C.A., J.M. Beer, and A.F. Sarofim. *Fragmentation Behaviour of Single Coal Particles in a Fluidized Bed*. in *Twentieth Symposium (International) on Combustion/The Combustion Institute*. 1984.
249. Senneca, O., M. Urciuolo, and R. Chirone, *A semidetailed model of primary fragmentation of coal.* Fuel, 2013. **104**: p. 253-261.
250. Jiang, X., L. Zhou, J. Liu, and X. Han, *A model on attrition of quartzite particles as a bed material in fluidized beds.* Powder Technology, 2009. **195**: p. 44-49.
251. Tooyserkani, Z., *Hydrothermal Pretreatment of Softwood Biomass and Bark for Pelletization*, in *Chemical and Biological Engineering*. 2013, The University of British Columbia: Vancouver. p. 157.
252. Hasibuan, R. and W.R. Wan Daud, *Quality Changes of Superheated Steam–Dried Fibers from Oil Palm Empty Fruit Bunches.* Drying Technology 2009. **27**(2): p. 194-200.

253. Monazam, E.R., S.L. J., R. Evans, and K. Schroeder, *Water Adsorption and Desorption by Coals and Chars.* Energy and Fuels, 1998. **12**: p. 1299-1304.
254. Li, X., H. Song, Q. Wang, C. Meesri, T. Wall, and J. Yu, *Experimental study on drying and moisture re-adsorption kinetics of an Indonesian low rank coal.* Journal of Environmental Sciences, 2009: p. S127-S130.
255. Perry, R. and D. Green, *Perry's Chemical Engineers' Handbook, Eighth Edition*. 2008: McGraw-Hill Education.
256. Kiriyama, T., H. Sasaki, A. Hashimoto, S. Kaneko, and M. Maeda, *Size Dependence of the Drying Characteristics of Single Lignite Particles in Superheated Steam.* Metallurgical and Materials Transactions E, 2014: p. 1-15.
257. Komatsu, Y., A. Sciazko, M. Zakrzewski, S. Kimijima, A. Hashimoto, S. Kaneko, and J.S. Szmyd, *An experimental investigation on the drying kinetics of a single coarse particle of Belchatow lignite in an atmospheric superheated steam condition.* Fuel Processing Technology 2015. **131**: p. 356-369.
258. Di Blasi, C., *Combustion and gasification rates of lignocellulosic chars.* Progress in Energy and Combustion Science, 2009. **35**(2): p. 121-140.
259. Haykiri-Açma, H., A. Ersoy-Meriçboyu, and S. Küçükbayrak, *Combustion reactivity of different rank coals.* Energy Conversion and Management, 2002. **43**(4): p. 459-465.
260. Li, C.-Z., *Some recent advances in the understanding of the pyrolysis and gasification behaviour of Victorian brown coal.* Fuel, 2007. **86**(12–13): p. 1664-1683.
261. Jenkins, R.G., S.P. Nandi, and P.L. Walker Jr, *Reactivity of heat-treated at 500°C.* Fuel, 1973. **52**: p. 288-293.
262. Cai, H.Y., A.J. Güell, I.N. Chatzakis, J.Y. Lim, D.R. Dugwell, and R. Kandiyoti, *Combustion reactivity and morphological change in coal chars: Effect of pyrolysis temperature, heating rate and pressure.* Fuel, 1996. **75**(1): p. 15-24.
263. Messenböck, R.C., D.R. Dugwell, and R. Kandiyoti, *CO2 and steam-gasification in a high-pressure wire-mesh reactor: the reactivity of Daw Mill coal and combustion reactivity of its chars.* Fuel, 1999. **78**(7): p. 781-793.
264. Chan, Y., Z. Zhang, M. Zhu, C. Luan, C. You, and D. Zhang, *A Preliminary High-Pressure Thermogravimetric Study of Combustion Reactivity of a Collie Coal Char*, in *Cleaner Combustion and Sustainable World*, H. Qi and B. Zhao, Editors. 2013, Springer Berlin Heidelberg. p. 121-125.
265. Adanez, J., A. Abad, F. Garcia-Labiano, P. Gayan, and L.F. de Diego, *Progress in Chemical-Looping Combustion and Reforming technologies.* Progress in Energy and Combustion Science, 2012. **38**(2): p. 215-282.
266. Ye, D.P., J.B. Agnew, and D.K. Zhang, *Gasification of a South Australian low-rank coal with carbon dioxide and steam: kinetics and reactivity studies.* Fuel, 1998. **77**(11): p. 1209-1219.
267. Radovic, L.R., K. Steczko, P.L. Walker Jr, and R.G. Jenkins, *Combined effects of inorganic constituents and pyrolysis conditions on the gasification reactivity of coal chars.* Fuel Processing Technology, 1985. **10**(3): p. 311-326.
268. Zeng, C., S. Clayton, H. Wu, J.-i. Hayashi, and C.-Z. Li, *Effects of Dewatering on the Pyrolysis and Gasification Reactivity of Victorian Brown Coal.* Energy and Fuels, 2007. **21**: p. 399-404.
269. Tognotti, L., A. Malotti, L. Petarca, and S. Zanelli, *Measurement of Ignition Temperature of Coal Particles Using a Thermogravimetric Technique.* Combustion Science and Technology, 1985. **44**(1-2): p. 15-28.
270. Mortari, D.A., I. Ávila, A.M. dos Santos, and P.M. Crnkovic, *Study of Thermal Decomposition and Ignition Temperature of Bagasse, Coal and their Blends.* Engenharia Térmica (Thermal Engineering), 2010. **9**(1): p. 81-88.

271. Omega Point Laboratories, *ASTM D1929-96 (reapproved 2001) Standard Test Method for Determining Ignition Properties of Plastics*. 2004.
272. Arash Tahmasebi, J.Y., Xianchun Li, and Chatphol Meesri, *Experimental study on microwave drying of Chinese and Indonesian low-rank coals.* Fuel Processing Technology, 2011. **92**: p. 1821 - 1829.
273. Arash Tahmasebi, J.Y., Yanna Han, and Xianchun Li, *A study of chemical structure changes of Chinese lignite during fluidized-bed drying in nitrogen and air*. Fuel Processing Technology, 2012. **101**: p. 85-93.
274. Carol A. Rhoads, P.C.P., and P.H. Given, *FTIR Studies of the Contributions of Plant Polymers to Coal Formation.* International Journal of Coal Geology, 1987. **8**: p. 69-83.
275. Chong Chen, J.G., and Yongjie Yan, *Observation of the Type of Hydrogen Bonds in Coal by FTIR.* Energy & Fuels, 1998. **12**: p. 446-449.
276. Jose V. Ibarra, E.M., and Rafael Moliner, *FTIR study of the evolution of coal structure during the coalification process.* Organic Geochemistry, 1996. **24**(6): p. 725-735.
277. J.V. Ibarra, J.L.M., *Detection of weathering in stockpiled coals by Fourier transform infrared spectroscopy.* Vibrational Spectroscopy, 1996. **10**: p. 311-318.
278. Solomon, P.R. and R.M. Carangelo, *FTI R analaysis of coal. I. Techniques and determination of hydroxyl concentrations.* Fuel, 1982. **61**: p. 663-669.
279. Solomon, P.R. and R.M. Carangelo, *FT-i.r. analysis of coal 2. Aliphatic and aromatic hydrogen concentration.* Fuel, 1988. **67**: p. 949-959.